VOL. 693 NO. 1 17 FEBRUARY 1995

JOURNAL OF CHROMATOGRAPHY A

INCLUDING ELECTROPHORESIS AND OTHER SEPARATION METHODS

ELSEVIER

JOURNAL OF CHROMATOGRAPHY A

INCLUDING ELECTROPHORESIS AND OTHER SEPARATION METHODS

Scope. The *Journal of Chromatography A* publishes papers on all aspects of **chromatography, electrophoresis** and related methods. Contributions consist mainly of research papers dealing with chromatographic theory, instrumental developments and their applications. In the *Symposium volumes*, which are under separate editorship, proceedings of symposia on chromatography, electrophoresis and related methods are published. *Journal of Chromatography B: Biomedical Applications* —This journal, which is under separate editorship, deals with the following aspects: developments in and applications of chromatographic and electrophoretic techniques related to clinical diagnosis or alterations during medical treatment; screening and profiling of body fluids or tissues related to the analysis of active substances and to metabolic disorders; drug level monitoring and pharmacokinetic studies; clinical toxicology; forensic medicine; veterinary medicine; occupational medicine; results from basic medical research with direct consequences in clinical practice.

Submission of Papers. The preferred medium of submission is on disk with accompanying manuscript (see *Electronic manuscripts* in the Instructions to Authors, which can be obtained from the publisher, Elsevier Science B.V., P.O. Box 330, 1000 AH Amsterdam, Netherlands). Manuscripts (in English; *four* copies are required) should be submitted to: Editorial Office of *Journal of Chromatography A*, P.O. Box 681, 1000 AR Amsterdam, Netherlands, Telefax (+31-20) 485 2304, or to: The Editor of *Journal of Chromatography B: Biomedical Applications*, P.O. Box 681, 1000 AR Amsterdam, Netherlands. Review articles are invited or proposed in writing to the Editors who welcome suggestions for subjects. An outline of the proposed review should first be forwarded to the Editors for preliminary discussion prior to preparation. Submission of an article is understood to imply that the article is original and unpublished and is not being considered for publication elsewhere. For copyright regulations, see below.

Publication information. *Journal of Chromatography A* (ISSN 0021-9673): for 1995 Vols. 683–714 are scheduled for publication. *Journal of Chromatography B: Biomedical Applications* (ISSN 0378-4347): for 1995 Vols. 663–674 are scheduled for publication. Subscription prices for *Journal of Chromatography A*, *Journal of Chromatography B: Biomedical Applications* or a combined subscription are available upon request from the publisher. Subscriptions are accepted on a prepaid basis only and are entered on a calendar year basis. Issues are sent by surface mail except to the following countries where air delivery via SAL is ensured: Argentina, Australia, Brazil, Canada, China, Hong Kong, India, Israel, Japan, Malaysia, Mexico, New Zealand, Pakistan, Singapore, South Africa, South Korea, Taiwan, Thailand, USA. For all other countries airmail rates are available upon request. Claims for missing issues must be made within six months of our publication (mailing) date. Please address all your requests regarding orders and subscription queries to: Elsevier Science B.V., Journal Department, P.O. Box 211, 1000 AE Amsterdam, Netherlands. Tel.: (+31-20) 485 3642; Fax: (+31-20) 485 3598. Customers in the USA and Canada wishing information on this and other Elsevier journals, please contact Journal Information Center, Elsevier Science Inc., 655 Avenue of the Americas, New York, NY 10010, USA, Tel. (+1-212) 633 3750, Telefax (+1-212) 633 3764.

Abstracts/Contents Lists published in Analytical Abstracts, Biochemical Abstracts, Biological Abstracts, Chemical Abstracts, Chemical Titles, Chromatography Abstracts, Current Awareness in Biological Sciences (CABS), Current Contents/Life Sciences, Current Contents/Physical, Chemical & Earth Sciences, Deep-Sea Research/Part B: Oceanographic Literature Review, Excerpta Medica, Index Medicus, Mass Spectrometry Bulletin, PASCAL-CNRS, Referativnyi Zhurnal, Research Alert and Science Citation Index.

US Mailing Notice. *Journal of Chromatography A* (ISSN 0021-9673) is published weekly (total 52 issues) by Elsevier Science B.V., (Sara Burgerhartstraat 25, P.O. Box 211, 1000 AE Amsterdam, Netherlands). Annual subscription price in the USA US$ 5389.00 (US$ price valid in North, Central and South America only) including air speed delivery. Second class postage paid at Jamaica, NY 11431. **USA POSTMASTERS**: Send address changes to *Journal of Chromatography A*, Publications Expediting, Inc., 200 Meacham Avenue, Elmont, NY 11003. Airfreight and mailing in the USA by Publications Expediting.

See inside back cover for Publication Schedule, Information for Authors and information on Advertisements.

0021-9673/95/$09.50

Printed in the Netherlands

CONTENTS

(Abstracts/Contents Lists published in Analytical Abstracts, Biochemical Abstracts, Biological Abstracts, Chemical Abstracts, Chemical Titles, Chromatography Abstracts, Current Awareness in Biological Sciences (CABS), Current Contents/Life Sciences, Current Contents/Physical, Chemical & Earth Sciences, Deep-Sea Research/Part B: Oceanographic Literature Review, Excerpta Medica, Index Medicus, Mass Spectrometry Bulletin, PASCAL-CNRS, Referativnyi Zhurnal, Research Alert and Science Citation Index)

REGULAR PAPERS

Column Liquid Chromatography

Series of homologous displacers for preparative chiral displacement chromatographic separations on Cyclobond-II columns
by G. Quintero, M. Vo, G. Farkas and G. Vigh (College Station, TX, USA) (Received 14 November 1994) . . . 1

High-performance liquid chromatographic determination of the rhamnolipids produced by *Pseudomonas aeruginosa*
by T. Schenk, I. Schuphan and B. Schmidt (Aachen, Germany) (Received 8 November 1994) . . . 7

Further examination of a "concerted cluster" model of multivalent affinity. Heterogeneous adsorption of lactate dehydrogenase to Cibacron Blue immobilised on cellulose
by V. Dowd and R.J. Yon (London, UK) (Received 25 October 1994) . . . 15

Characterization of the protein binding of chiral drugs by high-performance affinity chromatography. Interactions of *R*- and *S*-ibuprofen with human serum albumin
by D.S. Hage (Lincoln, NE, USA) and T.A.G. Noctor and I.W. Wainer (Montreal, Canada) (Received 14 October 1994) . . . 23

Tryptic peptide mapping of sequence 299–585 of human serum albumin by high-performance liquid chromatography and fast atom bombardment mass spectrometry
by S. Fisichella, S. Foti, G. Maccarrone and R. Saletti (Catania, Italy) (Received 25 October 1994) . . . 33

High-performance liquid chromatographic determination of active ingredients in cough–cold syrups with indirect conductometric detection
by O.-W. Lau and C.-S. Mok (Shatin, Hong Kong) (Received 25 October 1994) . . . 45

Separation of geometrical *syn* and *anti* isomers of obidoxime by ion-pair high-performance liquid chromatography
by U. Spöhrer and P. Eyer (Munich, Germany) (Received 18 October 1994) . . . 55

Direct high-performance liquid chromatographic resolution of planar chiral tricarbonyl (η^6-arene)–chromium(0) complexes
by C. Villani and W.H. Pirkle (Urbana, IL, USA) (Received 24 October 1994) . . . 63

Gas Chromatography

Comparison of four homologous retention index standard series for gas chromatography of basic drugs
by I. Rasanen, I. Ojanperä and E. Vuori (Helsinki, Finland) (Received 15 November 1994) . . . 69

Preparation of 4-vinylpyridine and divinylbenzene porous-layer open tubular columns by in situ copolymerization
by Z. Ruan and H. Liu (Lanzhou, China) (Received 4 October 1994) . . . 79

Analysis of a mixture of linear and cyclic siloxanes by cryo-gas chromatography–Fourier transform infrared spectroscopy and gas chromatography–mass spectrometry
by S. Wachholz, F. Keidel, U. Just and H. Geissler (Berlin, Germany) and K. Käppler (Dresden, Germany) (Received 1 November 1994) . . . 89

Supercritical Fluid Extraction

Influence of ageing on the supercritical fluid extraction of pollutants in soils
by V. Camel (Paris, France), A. Tambuté (Vert-le-Petit, France) and M. Caude (Paris, France) (Received 30 September 1994) . . . 101

Electrophoresis

Combined effects of non-linear electrophoresis and non-linear chromatography on concentration profiles in capillary electrophoresis
by M.S. Bello, M.Y. Zhukov and P.G. Righetti (Milan, Italy) (Received 26 July 1994) . . . 113

(Continued overleaf)

Contents (continued)

Enhancement of selectivity and concentration sensitivity in capillary zone electrophoresis by on-line coupling with column liquid chromatography and utilizing a double stacking procedure allowing for microliter injections
by S. Pálmarsdóttir and L.-E. Edholm (Lund, Sweden) (Received 25 October 1994) 131

Monitoring of a conjugation reaction between fluorescein isothiocyanate and myoglobin by capillary zone electrophoresis
by P.R. Banks and D.M. Paquette (Montreal, Canada) (Received 1 November 1994) 145

Analysis of oxalate in Bayer liquors: a comparison of ion chromatography and capillary electrophoresis
by P.E. Jackson (Lane Cove, Australia) (Received 2 November 1994) 155

SHORT COMMUNICATIONS

Column Liquid Chromatography

Simultaneous structure–activity determination of disulfiram photolysis products by on-line continuous-flow liquid secondary ion mass spectrometry and enzyme inhibition assay
by L.M. Benson, K.A. Veverka, D.C. Mays, A.N. Nelson, Z.H. Shriver, J.J. Lipsky and S. Naylor (Rochester, MN, USA) (Received 1 November 1994) 162

Use of narrow-bore high-performance liquid chromatography–diode array detection for the analysis of intermediates of the biological degradation of 2,4,6-trinitrotoluene
by F. Ahmad and D.J. Roberts (Houston, TX, USA) (Received 4 November 1994) 167

Determination of chlorophylls by reversed-phase high-performance liquid chromatography with isocratic elution and the column-switching technique
by K. Saitoh, I. Awaka and N. Suzuki (Sendai, Japan) (Received 25 November 1994) 176

Gas Chromatography

Prediction of gas chromatographic retention indices of 2,4-dinitrophenylhydrazones
by M. Görgényi (Szeged, Hungary), H. Van Langenhove (Ghent, Belgium) and Z. Király (Szeged, Hungary) (Received 16 August 1994) 181

JOURNAL OF CHROMATOGRAPHY A

VOL. 693 (1995)

JOURNAL OF CHROMATOGRAPHY A

INCLUDING ELECTROPHORESIS AND OTHER SEPARATION METHODS

ELSEVIER

Amsterdam – Lausanne – New York – Oxford – Shannon – Tokyo

J. Chromatogr. A, Vol. 693 (1995)

0021-9673/95/$09.50

ELSEVIER

Journal of Chromatography A, 693 (1995) 1–5

JOURNAL OF CHROMATOGRAPHY A

Series of homologous displacers for preparative chiral displacement chromatographic separations on Cyclobond-II columns

Gilberto Quintero[1], Matthew Vo, Gyula Farkas[2], Gyula Vigh*

Department of Chemistry, Texas A & M University, College Station, TX 77843-3255, USA

First received 23 August 1994; revised manuscript received 14 November 1994; accepted 14 November 1994

Abstract

A series of homologous displacers have been synthesized to aid the development of chiral displacement chromatographic separations on Cyclobond-II cyclodextrin silica stationary phases. The displacers contain an anchor group, derived from mandelic acid, a H-bonding mid-section (carboxyl and C = O groups) and a solubility adjusting tail section (*n*-alkanoate groups). The capacity factors and the individual excess adsorption isotherms of these displacers were measured in acetonitrile–citrate buffer eluents. Both the k' values and the isotherm parameters vary regularly with both the acetonitrile concentration of the eluent and the length of the alkanoate chain. Because the capacity factors and the adsorption strengths of these compounds cover a sufficiently broad range, they can serve as displacers in a variety of displacement chromatographic separations on Cyclobond-II columns.

1. Introduction

In earlier papers we demonstrated that preparative displacement chromatographic separations of geometrical isomers, positional isomers and enantiomers can be achieved using columns packed with commercially available cyclodextrin silica stationary phases operated in the reversed-phase mode [1–5], and on Pirkle-type naphthylalanine silica stationary phases operated in the normal-phase mode [6,7]. One of the most serious impediments to the development of a displacement chromatographic separation is the lack of readily available displacers. Traditionally, displacers are selected by trial-and-error, using previous experience with similar analytes and potential displacer as guides. On cyclodextrin silicas, operated in the reversed-phase mode, ionic detergents, alkylphenols, nitrophenols and cyclic alcohols have been used successfully as displacers [1–5].

The displacers must satisfy divergent demands: they must be highly soluble in the carrier solvent to form concentrated displacer solutions, they must adsorb competitively on the stationary phase and must do so more strongly than the solutes, yet they must allow easy and fast regeneration of the column once the separation is complete. Unfortunately, no single compound

* Corresponding author.

[1] Present address: Tennessee Valley Authority, Chattanooga, TN, USA.

[2] Present address: Chinoin Pharmaceutical Company, Budapest, Hungary.

0021-9673/95/$09.50
SSDI 0021-9673(94)01123-0

class possesses all these characteristics. However, in the case of Pirkle-type stationary phases, a generic displacer structure could be identified and three series of homologous compounds were synthesized and studied in detail: the 3,5-dinitrobenzoyl esters of alcohols, the 3,5-dinitrophenylcarbamates of alcohols, and the N-3,5-dinitrophenylamidoethyl-1-alkanoates [6]. These displacer families are based on a common core structure and can be synthesized using inexpensive reagents and simple preparative methods.

Based on the success of the above approach to displacer selection, we attempted to identify generic displacer structures for cyclodextrin silica stationary phases operated in the reversed-phase mode, and to synthesize several homologous displacers using a simple reaction scheme. The objective of this paper is to describe such a family of closely related displacers, intended for use on the Cyclobond-II α-cyclodextrin silica stationary phases [8,9].

The proposed generic displacers for α-cyclodextrin silica stationary phases contain an anchor group which fits the cavity of α-cyclodextrin (phenyl group), a section that can form multiple hydrogen bonds with the secondary hydroxyl groups of α-cyclodextrin (carboxyl and carbonyl groups), and a solubility-adjusting tail section which regulates displacer solubility (alkanoate group of variable chain length).

2. Experimental

Three 250 mm × 4.6 mm I.D. Cyclobond-II columns, packed with a 5-μm α-cyclodextrin (CD) silica stationary phase, were obtained from Astec (Whippany, NJ, USA). One of the columns was used for the retention studies, the adsorption isotherm determinations and the fraction analysis work to obtain the reconstructed displacement chromatograms. The other two columns, connected in series, were used for the actual displacement chromatographic separations.

HPLC-grade acetonitrile (ACN) and tetrahydrofuran (THF) were purchased from J.T. Baker (Phillipsburg, NJ, USA). Water was obtained from a Milli-Q unit (Millipore, Bedford, MA, USA). All chemicals used for the synthesis of the displacers were obtained from Aldrich (Milwaukee, WI, USA), and used as received, without further purification.

The ester type displacers were synthesized [10] according to the general Schotten–Baumann reaction scheme (Fig. 1). Briefly, 8 mmol acid halide, dissolved in 10 ml tetrahydrofuran (THF), was added dropwise over a period of 30 min to a 50-ml round-bottom flask containing 4 mmol of mandelic acid, 10 ml of THF and 2 ml of pyridine. While stirred, the mixture was refluxed for 2 h. Subsequently, THF was removed using a Buchi RotaVapor-R (Fisher Scientific, Pittsburgh, PA, USA), 30 ml of 0.1 *M* HCl solution was added to the residue and extracted three times with 10-ml portions of CH_2Cl_2. The combined CH_2Cl_2 extracts were washed three times with 10-ml portions of 0.01 *M* HCl solution, dried over magnesium sulfate, and allowed to evaporate slowly to obtain a crystalline product. Finally, the product was purified by recrystallizing it twice from CH_2Cl_2. The structure of the final product was verified by ^1H NMR spectroscopy (XL-200E; Varian, Palo Alto, CA, USA) and its purity was checked by HPLC using the Cyclobond-II column.

The retention measurements and adsorption isotherm determination methods were described in detail in Ref. [6]. The custom-built, multi-

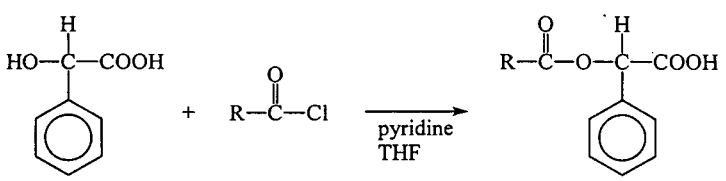

Fig. 1. Reaction scheme for the synthesis of the mandelic acid-based displacers.

purpose liquid chromatographic system [1–5] was used for the displacement chromatographic separations. All measurements were made at 30°C. The columns were regenerated after the isotherm determinations and the displacement chromatographic separations by running a 5%/min solvent gradient starting with the carrier solvent composition and ending with pure ACN. Finally, ACN was pumped through the column until the UV absorbance of the effluent became equal to that of the wash ACN.

3. Results

The capacity factors (k') of the potential displacers were determined in several ACN–citrate buffer eluents as shown in Fig. 2. The log k' values increase regularly with the length of the alkanoate chain in the displacers, as usual in reversed-phase HPLC.

The adsorption isotherms of the synthesized displacers were also measured in eluents of increasing ACN concentration. As an example, the individual excess adsorption isotherms measured in a 3% (v/v) acetonitrile in 40 m*M* citrate buffer (pH 6) are shown in Fig. 3. In the concentration ranges tested, the isotherms can

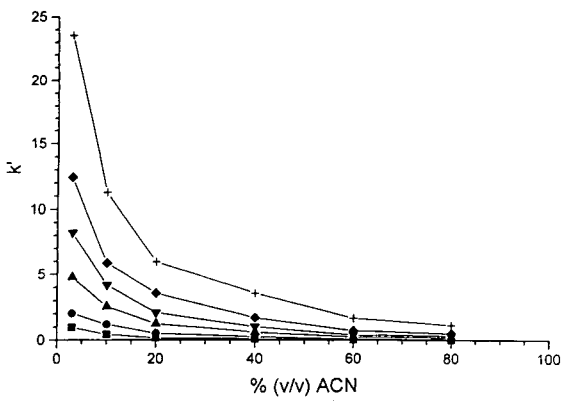

Fig. 2. Capacity factors of the mandelic acid-based displacers as a function of the ACN concentration in the pH 6, acetonitrile: 1 m*M* citrate eluents on the Cyclobond-II column at 30°C. □ = Mandelic acid; ○ = acetate derivative; ▲ = butyrate derivative; ▼ = pentanoate derivative; ◆ = hexanoate derivative; + = octanoate derivative.

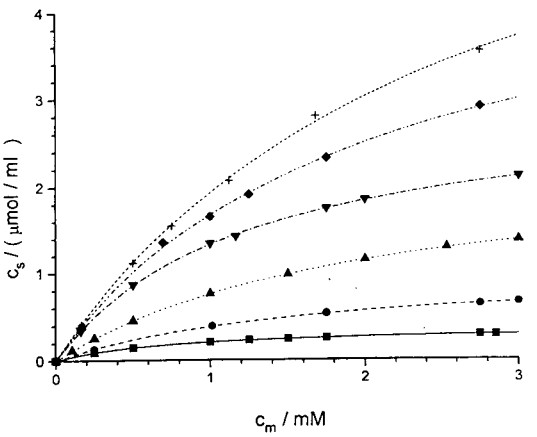

Fig. 3. Adsorption isotherms of the mandelic acid-based displacers in the pH 6, acetonitrile–1 m*M* citrate (3:97, v/v) eluents on the Cyclobond-II column at 30°C. □ = Mandelic acid; ○ = acetate derivative; ▲ = butyrate derivative; ▼ = pentanoate derivative; ◆ = hexanoate derivative; + = octanoate derivative. The lines show the isotherms calculated with the Langmuir isotherm equation and the parameters shown in Table 1. c_s = Stationary phase concentration; c_m = mobile phase concentration.

be described adequately with the simple Langmuir isotherm equation [6]. The isotherm parameters, determined by the Origin Version 3 software package, are listed in Table 1. The *b* parameters do not change regularly with the carbon number as was the case with the 3,5-dinitrobenzamido-type displacers developed for the Pirkle-type chiral stationary phases [6]. The *a* parameters increase as the chain length is increased, indicating that the adsorption behavior of these homologous displacers on Cyclobond-II is similar, and that their adsorption strengths cover a broad enough range to be of use for

Table 1
Langmuir isotherm parameters for the mandelic acid-based displacers of increasing side-chain length

C_n	*a*	*b*
0	0.482 ± 0.001	1.317 ± 0.004
2	0.62 ± 0.02	0.60 ± 0.03
4	1.137 ± 0.005	0.490 ± 0.005
5	2.40 ± 0.04	0.80 ± 0.02
6	2.55 ± 0.07	0.52 ± 0.03
8	2.70 ± 0.06	0.39 ± 0.02

Acknowledgement

Partial financial support by the National Science Foundation (CH-8919151), the Texas Coordinating Board of Higher Education TATR Program (Grant Number 3376) and the Dow Chemical Company, Midland, MI, USA as well as the gift of the Cyclobond-II columns by Astec are gratefully acknowledged.

References

[1] Gy. Vigh, G. Quintero and Gy. Farkas, *J. Chromatogr.*, 484 (1989) 237.
[2] Gy. Vigh, G. Quintero and Gy. Farkas, *J. Chromatogr.*, 484 (1989) 251.
[3] Gy. Vigh, G. Quintero and Gy. Farkas, *J. Chromatogr.*, 506 (1990) 481.
[4] Gy. Farkas, L.H. Irgens, G. Quintero, M.D. Beeson, A. Al-Saeed and Gy. Vigh, *J. Chromatogr.*, 645 (1993) 67.
[5] L.H. Irgens, Gy. Farkas and Gy. Vigh, *J. Chromatogr. A*, 666 (1993) 603.
[6] P.L. Camacho, Gy. Vigh and D.H. Thompson, *J. Chromatogr.*, 641 (1993) 31.
[7] P.L. Camacho, M.D. Beeson, Gy. Vigh and D.H. Thompson, *J. Chromatogr.*, 646 (1993) 259.
[8] D.W. Armstrong, *US Pat.*, 4 539 399 (1985).
[9] *Cyclobond Handbook*, Astec, Whippany, NJ, 1990.
[10] G. Quintero, *Ph.D. Thesis*, Texas A & M University, College Station, TX, 1990.

ELSEVIER

Journal of Chromatography A, 693 (1995) 7–13

JOURNAL OF CHROMATOGRAPHY A

High-performance liquid chromatographic determination of the rhamnolipids produced by *Pseudomonas aeruginosa*

Torsten Schenk*, Ingolf Schuphan, Burkhard Schmidt

Rheinisch-Westfälische Technische Hochschule Aachen, Institut für Biologie V (Ökologie/Ökotoxikologie/Ökochemie), Worringer Weg 1, D-52056 Aachen, Germany

First received 23 August 1994; revised manuscript received 8 November 1994; accepted 15 November 1994

Abstract

The bacterial biosurfactants 3-[3′-(L-rhamnopyranosyloxy)decanoyloxy]decanoic acid (RL-1) and 3-[3′-(2″-O-α-L-rhamnopyranosyl-α-L-rhamnopyranosyloxy)decanoyloxy]decanoic acid (RL-2) were isolated from *Pseudomonas aeruginosa* DSM 2659 cultures. An HPLC method was developed for the *p*-bromophenacyl esters of the rhamnolipids. Separation was obtained within 25 min on a RP C_{18} column using a linear gradient of water–acetonitrile (30:70 to 0:100) and UV detection (265 and 320 nm). Linearity of response existed for 1.2–25 μg of the RL-1- and 1.8–25 μg of the RL-2-*p*-bromophenacyl ester (0.9–19.2 μg RL-1 and 1.3–18.0 μg RL-2). The reproducibility of the entire analytical method (extraction, derivatisation) was tested.

1. Introduction

In recent years, interest in microbial surfactants has been increasing, because these natural products are considered both an alternative and addition to synthetic surfactants. The advantages of biosurfactants compared to synthetic products are their biodegradability, low toxicity, and simple production by microbial fermentation processes [1]. Biosurfactants show a wide range of applications, such as clean-up of oil spills, secondary and tertiary oil recovery. It is also possible to use biosurfactants as additives in cosmetics, foodstuffs, beverages and pharmaceutical products [2].

Aerobic bacteria of the species of *Pseudomonas aeruginosa* are known to produce as biosurfactants four chemically closely related glycolipids, when grown on glucose, glycerol or *n*-alkanes. These compounds are rhamnolipids composed of rhamnose and β-hydroxycarboxylic acid subunits, and are excreted into the culture medium [3–6]. Structural characterization of the compounds has been achieved [6,7]. The *P. aeruginosa* glycolipids play an important and crucial role during cultivation of the bacteria, especially when *n*-alkanes are used as sole carbon source [8]. Consequently, the glycolipids are also known to enhance the biodegradation of some hydrocarbons in soil [9]. The strain *P. aeruginosa* DSM 2659 primarily produces two of the four rhamnolipids. These are 3-[3′-(α-L-rhamnopyranosyloxy)decanoyloxy]decanoic acid (RL-1) and 3-[3′- (2″-O-α-L-rhamnopyranosyl-α-L-rhamnopyranosyloxy)decanoyloxy]decanoic acid (RL-2; Fig. 1). Rhamnolipids RL-3 [3-(α-L-rhamnopyranosyloxy)decanoic acid] and RL-4 [3-(2′-O-α-L-rhamnopyranosyl-α-L-rhamnopyra-

* Corresponding author.

0021-9673/95/$09.50
SSDI 0021-9673(94)01127-3

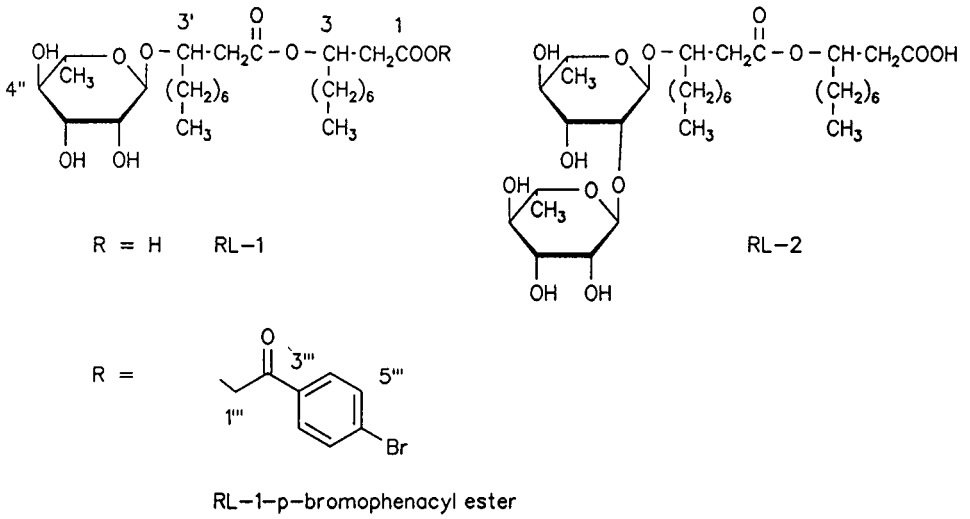

Fig. 1. Chemical structures of the rhamnolipids RL-1 and RL-2.

nosyloxy)decanoic acid] are biosynthesized under certain cultivation conditions only.

During our investigations concerning the biodegradation of *n*-alkanes, and the enhancing effects exerted by glycolipids, the need for a rapid and sensitive analytical method to determine the individual rhamnolipid concentrations has emerged. So far, rhamnolipids in the culture medium of bacteria have been determined quantitatively either indirectly by determination of F_{cmc} values [10], or directly by determination of rhamnose concentrations after hydrolysis of the rhamnolipids according to Hodge and Holreiter [11], and Chandrasekaran and Bemiller [12]. Both methods have the disadvantage that only the total amount of the glycolipids, but not the concentrations of the individual rhamnolipids can be determined quantitatively. In addition, interfering substances present in the culture broth of the bacteria may affect the determination of the F_{cmc} values. The objectives of the present study were to (1) isolate the individual rhamnolipids of *P. aeruginosa* DSM 2659, (2) develop an HPLC method for the rhamnolipids including derivatisation, and (3) apply the method for the examination of the rhamnolipid concentrations in authentic bacterial culture media.

2. Experimental

2.1. Microorganism and cultivation conditions

P. aeruginosa DSM 2659 (Rsan-ver strain) was obtained from DSM (Deutsche Sammlung von Mikroorganismen, Braunschweig, Germany), and used throughout this work. Originally, the strain was isolated from soil samples in the vicinity of an oil refinery located in Mexico [10]. The freeze-dried microorganisms were rehydrated with 1 ml of standard I medium (Merck, Darmstadt, Germany) and inoculated onto standard I agar plates. The optimized medium 3M (18.2 g l^{-1} glucose) for the liquid cultivation of *P. aeruginosa* and production of the rhamnolipids was as described by Guerra-Santos et al. [10], except that $FeSO_4$ was omitted, and H_3PO_4 was replaced by KH_2PO_4 and K_2HPO_4 (4 and 5 g l^{-1}, respectively). The pH of the medium was adjusted to 6.8. A liquid culture was started by adding a loopful of cells from a standard I agar plate to a 250-ml Erlenmeyer flask containing 100 ml medium. *P. aeruginosa* was grown at 37°C with gyratory shaking at 133 rpm. After 18 h, 8 ml of this culture were inoculated into a 1000-ml fernbach flask, containing 400 ml medium and

cultivated as described for another 7 days. The latter culture was used for the preparative isolation of the rhamnolipids RL-1 and RL-2. In order to follow analytically the production of the glycolipids during the growth of the bacterial culture, *P. aeruginosa* was cultivated in 100 ml medium contained in a 250-ml Erlenmeyer flask as described above for 7 days.

2.2. Isolation of the rhamnolipids

For preparative isolation, bacteria and medium were separated by centrifugation (10 000 *g* for 10 min at 4°C). An 8-g amount of $Al_2(SO_4)_3$ was added to the supernatant, and the rhamnolipids were precipitated by stirring for 1 h. The precipitate was collected by centrifugation at 5000 *g* for 10 min, and resuspended in water. Then, the slurry was acidified with 1 *M* HCl (pH 2), extracted 3 × with 50 ml EtOAc, and the combined extracts were dried over anhydrous Na_2SO_4. The resulting yellowish, oily rhamnolipids were analysed by TLC on silica gel plates (Macherey–Nagel, Düren, Germany) using the solvent system $CHCl_3$–MeOH–AcOH (65:15:2, v/v/v). Localisation of the separated zones was performed with a thymol spray reagent {0.5 g thymol in EtOH–conc. H_2SO_4 (95:5, v/v); after spraying, plates were heated to 120°C for 20 min [13] }; R_F values of RL-1 and RL-2 were 0.74 and 0.36, respectively. The rhamnolipids were purified by ion-exchange chromatography on a 100-ml DEAE-Sepharose CL 6B (Fluka, Buchs, Switzerland) column (50 × 2.5 cm) equilibrated with a mixture of 10 m*M* Tris · HCl (pH 8; Sigma, Deisenhofen, Germany) and EtOH (8:2, v/v). After application to the column, the biosurfactants were washed (until the yellow pigment was totally removed) and eluted with 0.4 *M* NaCl in 10 m*M* Tris · HCl (fractions 1–65, 12 ml each), and then 0.6 *M* NaCl in the same buffer (66–120). Fractions containing the purified rhamnolipids (50–85) were combined, acidified with 1 *M* HCl (pH 2), and the glycolipids were recovered as described. Subsequently, the rhamnolipids were separated chromatographically, or were subjected to the preparative derivatisation procedure.

For separation, the purified rhamnolipids were chromatographed on a column (40 × 3.00 cm) of 110 g silica gel 60 (Merck) with a gradient of $CHCl_3$–MeOH (85:15 to 65:35, v/v). After evaporation of the solvents of the respective fractions and lyophylisation, pure RL-1 and RL-2 were obtained in crystalline form. RL-1: ^1H NMR (Varian VXR 300; 300 MHz, $C^2H_3O^2H$): δ 0.9 [t, 6H, $J = 7$ Hz, H–C (10, 10′)], 1.22 [d, 3H, $J = 6$ Hz, H–C (6″)], 1.27–1.36 [m, 20H, H–C (5, 6, 7, 8, 9, 5′, 6′, 7′, 8′, 9′)], 1.5–1.65 [m, 4H, H–C (4, 4′)], 2.4–3.9 [m, 7H, H–C (2″, 3″, 4″, 5″), HO–C (2″, 3″, 4″)], 3.97 [m, 1H, H–C (3′)], 4.05 [m, 1H, H–C (3)], 4.89 [d, 1H, $J = 2$ Hz, H–C (1″)]. ^{13}C NMR (Varian VXR 300; 75 MHz, $C^2H_3O^2H$): δ 14.5 (C-10, C-10′), 18.0 (C-6″), 23.7 (C-9, C-9′), 25.8 and 26.2 (C-5, C-5′), 30.3 and 30.4 (C-6, C- 6′), 30.7 (C-7, C-7′), 32.9 and 33.0 (C-8, C-8′), 39.9 and 41.2 (C-2, C-2′), 70.1 (C-5″), 71.9 (C-3″), 72.2 (C-2″), 73.8 (C-3, C-3′), 74.3 (C-4″), 99.1 (C-1″), 172.4 and 174.2 (C-1, C-1′). IR (Perkin-Elmer Fourier transform IR 1700 S; KBr): 3368 (COOH, OH), 2956 (CH), 2926 (CH), 2858 (CH), 1733 (CO) cm^{-1}. Identical spectra were obtained for RL-2, excepting the integrals of the ^1H NMR spectrum.

For analytical purposes, 2 ml were aseptically withdrawn from the bacterial culture (100 ml medium in 250-ml Erlenmeyer flask). After centrifugation in order to remove the microorganisms, the supernatant was acidified with 1 *M* HCl (pH 2) and extracted 3 × with 5 ml EtOAc. The extract was dried over Na_2SO_4. After evaporation of the solvent, the partly purified rhamnolipids were obtained, which were directly subjected to the analytical derivatisation procedure.

2.3. Preparative derivatisation of the rhamnolipids

Generally, the synthesis was performed as described by Jupille [14], and modified by Syldatk [5]. A 100-mg amount of the purified rhamnolipid mixture, 125 μl Et_3N and 75 mg *p*-bromoacetophenone (Aldrich, Steinheim, Ger-

many) in 2 ml acetone (freshly distilled, kept over molecular sieve 4 Å) were stirred for 16 h at 20°C. After filtration and evaporation of the solvent, the resulting residue was chromatographed on silica gel 60 (85 g; 40 × 3.00 cm) with $CHCl_3$–MeOH (94:6, v/v). After evaporation of the solvents of the respective fractions, pure RL-1 and RL-2 phenacyl ester derivatives were obtained. RL-1-*p*-bromophenacyl ester: ^1H NMR (300 MHz, C^2HCl_3): δ 0.87 [t, 6H, $J = 7$ Hz, H–C (10, 10′)], 1.25–1.29 [m, 20H, H–C (5, 6, 7, 8, 9, 5′, 6′, 7′, 8′, 9′)], 1.26 [m, 3H, H–C (6″)], 1.5–1.65 [m, 4H, H–C (4, 4′)], 2.4–3.9 [m, 7H, H–C (2″, 3″, 4″, 5″), HO–C (2″, 3″, 4″)], 3.82 [m, 1H, H–C (3′)], 4.14 [m, 1H, H–C (3)], 4.88 [br. s, 1H, H–C (1″)], 5.31 [d, 2H, $J = 2.7$ Hz, H–C (1‴)], 7.63 [d, 2H, $J = 9$ Hz, H–C (5‴, 7‴)], 7.78 [d, 2H, $J = 9$ Hz, H–C (4‴, 8‴)]. ^{13}C NMR (75 MHz, C^2HCl_3): 14.0 and 14.1 (C-10, C-10′), 17.4 (C-6″), 22.6 and 24.7 (C-9, C-9′), 25.1 and 29.1 (C-5, C-5′), 29.2 and 29.3 (C-6, C-6′), 29.5 and 29.6 (C-7, C-7′), 31.7 and 31.8 (C-4, C-4′), 32.7 and 34.0 (C-8, C-8′), 38.7 and 39.9 (C-2, C-2′), 66.3 (C-1‴), 66.2 (C-1‴), 68.3 (C-5″), 70.6 (C-3, C-3′), 71.3 (C-2″), 71.8 (C-3″), 73.5 (C-4″), 129.3 (C-6‴, C-4‴, C-8‴), 132.3 (C-5‴, C-7‴), 132.7 (C-3‴), 170.4 and 171.1 (C-1, C-1′), 191.1 (C-2‴). IR ($CHCl_3$): 3419 (COOH and OH), 2955 (CH), 2929 (CH), 2858 (CH), 1738 (CO), 1708 (CO), 1588 (ArC) cm^{-1}. The substance gave a single peak when analysed by HPLC. The RL-2-*p*-bromophenacyl ester was similarly analysed spectroscopically, and showed identical spectra, excepting the ^1H NMR integrals. Both RL-1 and RL-2 derivatives were used as reference compounds in the analytical experiments.

2.4. Analytical derivatisation of the rhamnolipids

For routine analysis of the rhamnolipid concentrations in the culture broth, the partly purified rhamnolipids (usually 0–5 mg/ml) were dissolved in 1 ml CH_3CN in a screw cap vial. Molar ratios of approximately 1:4:2 (glycolipid:*p*-bromoacetophenone:Et_3N) were used for maximal derivatisation rates of ca. 95% [14,15]; the reaction was carried out at 60°C for 1 h. The product was directly used for the HPLC analysis, or was otherwise stored at −20°C.

2.5. Reagents and solvents

CH_3CN (distilled successively over P_2O_5 and CaH_2) and water (double distilled) were used exclusively as HPLC eluents. Both were filtered (0.45 μm; Schleicher & Schuell, Dassel, Germany) and degassed before use. All other solvents and reagents were commercially available and used without further purification.

2.6. HPLC apparatus and chromatographic conditions

The HPLC instrument consisted of a System Gold Beckman chromatograph, equipped with an Altex 210A valve injector joined to a 100-μl loop, a Beckman System Gold diode array detector 168 and a Beckman System Gold programmable solvent module 126. The chromatography was carried out on an ET 250/8/4 Nucleosil 5 C_{18} (5 μm; Macherey–Nagel) column (250 mm × 4.6 mm). Water (solvent A) and CH_3CN (solvent B) were used as mobile phase: 4 min, A:B, 3:7 (v:v); 10 min, gradient from 3:7 to 0:10; 9 min 0:10; 2 min, return to 3:7. Chromatography was performed at 25°C with a flow-rate of 0.8 ml/min and an injection volume of 100 μl. The column effluent was monitored at 265 and 320 nm.

3. Results and discussion

3.1. Extraction of rhamnolipids

Different extraction methods for the isolation of the rhamnolipids from aqueous media have been reported. These include solvent systems such as EtOAc [6], $CHCl_3$–MeOH (2:1, v/v) [7] and Et_2O [9]. Preliminary experiments (see below) demonstrated that EtOAc was most efficacious. An almost quantitative extraction of the glycolipids was achieved, which was regarded as crucial for the subsequent HPLC analysis.

Generally, the procedure used in the present study was a modification of the method described by Pang [16]. In the preparative experiment, the rhamnolipids were precipitated from the medium by addition of 2% $Al_2(SO_4)_3$ and were separated from the supernatant, in order to reduce the large volume of the aqueous phase. In the case of the analytical assays (2-ml samples), the glycolipids were directly extracted with EtOAc after acidification of the aqueous phase.

3.2. Chromatography

Complete separation of the RL-1- and RL-2-*p*-bromophenacyl esters was achieved in 25 min using a RP C_{18} column. Typical HPLC runs for the reference compounds are shown in Fig. 2. Additional peaks appeared in the chromatograms, but according to their respective UV spectra, were not identified with other rhamnolipids. Presumably, they were produced by other microbial products present in the culture medium, which could not removed completely by a single run on a silica gel column. In the authentic nutrient solutions, the derivatised RL-1 and RL-2 were identified by cochromatography (retention times) with the reference compounds. A typical run (Fig. 3) shows that the RL-1- and RL-2-*p*-bromophenacyl esters could be sufficiently separated from other compounds present in the bacterial media. Additional proof for the identity of RL-1 and RL-2 was derived from the UV spectra of their respective *p*-bromophenacyl ester derivatives (Fig. 4). The detection limits were 1.2 μg for the RL-1- and 1.8 μg for the RL-2-*p*-bromophenacyl ester (0.9 μg and 1.3 μg RL-1 and RL-2, respectively).

The underivatised rhamnolipids RL-1 and RL-2 could also be chromatographed and separated by ion chromatography on a ET 250/8/4 Nucleosil 5 C_{18} (5 μm) column (250 mm × 4.6 mm I.D.). The mobile phase was CH_3CN–phosphate buffer [0.02 *M*, containing $5 \cdot 10^{-3}$ *M* tetrabutylammonium hydrogensulfate, TBA (Sigma); pH 7.5] (65:35, v/v). Chromatography was performed as described, and the rhamnolipids were detected at 215 and 254 nm. The detection limit of the underivatised RL-1 and RL-2 was 200 mg.

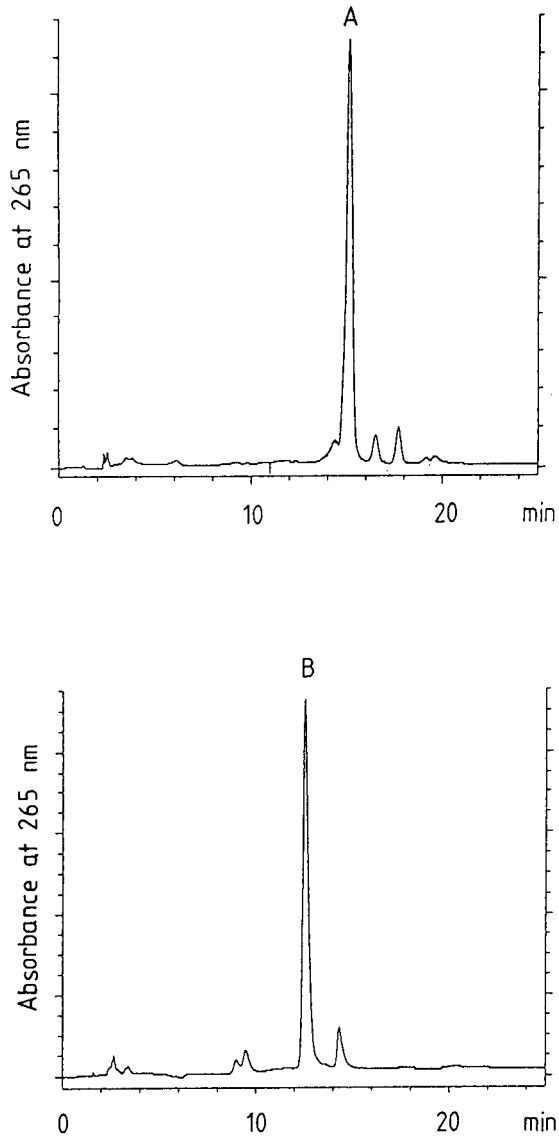

Fig. 2. HPLC chromatograms of the reference compounds RL-1-*p*-bromophenacyl ester (A) and RL-2-*p*-bromophenacyl ester (B).

3.3. Linearity and reproducibility of the method

External standardization by peak area was used for the quantitative determination of the rhamnolipids. The calibration graphs were linear over the ranges 1.2–25 μg for the RL-1- and 1.8–25 μg for the RL-2-*p*-bromophenacyl ester

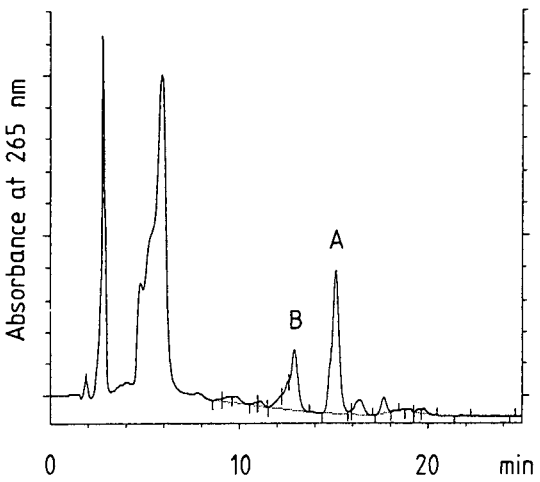

Fig. 3. Typical chromatogram of the derivatised rhamnolipids (A = RL-1; B = RL-2) from the culture medium of *Pseudomonas aeruginosa* DSM 2659.

(correlation coefficients, r, 0.998 and 0.999, respectively). In order to determine the recovery of the entire method, 50 μg, 500 μg and 5 mg RL-1 were dissolved in 10 ml culture medium, extracted and derivatised as described. The results shown in Table 1 demonstrate that ca. 74% of RL-1 were recovered; this was regarded as adequate with regard to the physico-chemical properties of the biosurfactants. Similar experiments using Et_2O for extraction gave considerably poorer recoveries of about 13%.

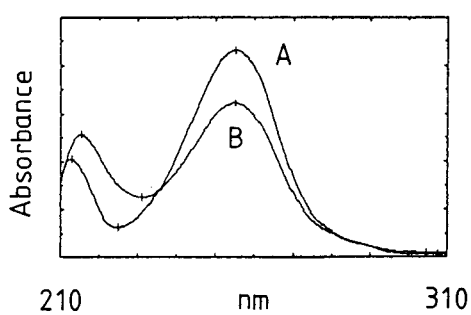

Fig. 4. UV spectra of the RL-1 (A) and RL-2 (B) derivatives in CH_3CN (77 μg/ml).

Table 1
Recovery of the reference compound RL-1 added to the autoclaved culture medium

RL-1 added (μg)	RL-1 derivative recovered	
	μg	%
50	44.6	64.6
500	548.7	78.9
5000	5362.3	77.1

Extraction and derivatisation were performed as outlined in the Experimental section.

3.4. Application of the method to the rhamnolipid analysis in authentic culture media

The production of the rhamnolipids RL-1 and RL-2 in the course of a cultivation cycle of *P. aeruginosa* as monitored by the HPLC method described above is depicted in Fig. 5. The concentrations determined in the culture medium ranged from 0.050 to 1.689, and 0.015 to 0.869 g l^{-1} in the case of RL-1 and RL-2, respectively. Fig. 5 shows that after a lag phase of about 24 h, an intense production of the biosurfactants occurred up to 60 h of cultivation.

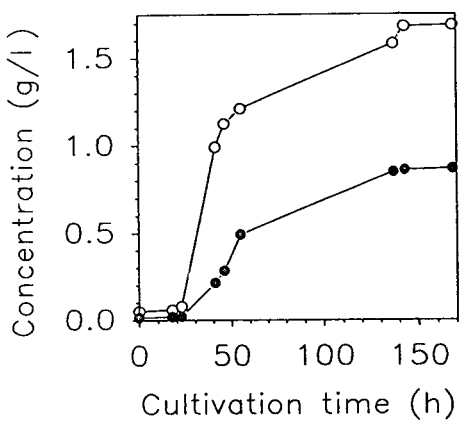

Fig. 5. Concentrations of the rhamnolipids RL-1 (○) and RL-2 (●) in the culture medium of *Pseudomonas aeruginosa* DSM 2659 during one growth cycle.

Then, the cells entered the stationary phase and production ceased. On the whole, these results are in agreement with previously published data on the rhamnolipid production by *P. aeruginosa* DSM 2659 (2.25 g l^{-1} total rhamolipids at the end of the cultivation period [17]) which were determined using F_{cmc} values. The advantages of the present method have been discussed above. In addition, it may be assumed that the rapid and precise determination of the individual rhamnolipids will help getting a better insight into the processes occurring in *P. aeruginosa* cultures, especially when *n*-alkanes are used as carbon source. Future experiments will demonstrate whether the procedure is suitable for the quantitative analysis of the rhamnolipids in soils, in order to evaluate the effects of the compounds in a natural environment. It is hoped that analogous methods will be developed for other classes of (glycolipid) biosurfactants.

Acknowledgements

The authors appreciate the help of Mr. R. Aglaster for the introduction into the HPLC techniques and Mrs. G. Kessels for preliminary experiments with the isolation and derivatisation of the rhamnolipids. We thank the Deutsche Forschungsgemeinschaft, Bonn–Bad Godesberg, Germany for financial support of this work.

References

[1] D.F. Gerson and J.E. Zajic, *Proc. Biochem.*, 14 (1979) 20.
[2] N. Kosaric, W.L. Cairns and N.C.C. Gray (Editor), *Biosurfactants and Biotechnology*, Marcel Dekker, New York, Basle, 1987, Ch. 1, p. 2.
[3] S. Itoh, H. Honda, F. Tomita and T. Suzuki, *J. Antibiot.*, 24 (1971) 855.
[4] G. Hauser and M.L. Karnowsky, *J. Biol. Chem.*, 229 (1957) 91.
[5] C. Syldatk, *Ph.D. Thesis*, University of Braunschweig, Braunschweig, 1984.
[6] C. Syldatk, S. Lang and F. Wagner, *Z. Naturforsch. C*, 49 (1985) 51.
[7] J.L. Parra, J. Pastor, F. Comelles, M.A. Manresa and M.P. Bosch, *Tenside Surf. Det.*, 27 (1990) 302.
[8] K. Hisatsuka, T. Nakahara, N. Sano and K. Yamada, *Agric. Biol. Chem.*, 35 (1971) 686.
[9] D.K. Jain, H. Lee and J.T. Trevors, *J. Ind. Microbiol.*, 10 (1992) 87.
[10] L. Guerra-Santos, O. Käppeli and A. Fiechter, *Appl. Environ. Microbiol.*, 48 (1984) 301.
[11] J.D. Hodge and B.T. Holreiter, *Methods Carbohydr. Chem.*, 1 (1962) 380.
[12] E.V. Chandrasekaran and J.N. Bemiller, *Methods Carbohydr. Chem.*, 8 (1980) 89.
[13] *Anfärbereagenzien für Dünnschicht- und Papier- Chromatographie*, Merck, Darmstadt, 1984.
[14] J. Jupille, *J. Chromatogr. Sci.*, 17 (1979) 160.
[15] S. Lam and E. Grushka, *Sep. Purif. Methods*, 14 (1985) 67.
[16] X. Pang, *Ph.D. Thesis*, University of Bonn, Bonn, 1992.
[17] H.E. Reiling, U. Thanei-Wyss, L.H. Guerra-Santos, R. Hirt, O. Käppeli and A. Fiechter, *Appl. Environ. Microbiol.*, 51 (1986) 985.

ELSEVIER

Journal of Chromatography A, 693 (1995) 15–21

JOURNAL OF CHROMATOGRAPHY A

Further examination of a "concerted cluster" model of multivalent affinity Heterogeneous adsorption of lactate dehydrogenase to Cibacron Blue immobilised on cellulose

V. Dowd[1], R.J. Yon*

School of Biological and Chemical Sciences, University of Greenwich, Woolwich Campus, Wellington Street, London SE18 6PF, UK

First received 24 August 1994; revised manuscript received 25 October 1994; accepted 25 October 1994

Abstract

A multivalent affinity model, termed the "concerted cluster" model, envisages interactions between a multisite protein and discrete and permanent sets of single and paired immobilised ligands, requiring a rigid support matrix. Extensive data on the binding of rabbit muscle lactate dehydrogenase to Cibacron Blue immobilised on cellulose, collected at several immobilised-dye concentrations, gave biphasic Scatchard plots, and were interpreted quantitatively in terms of single and paired ligands. The data were fitted by a least-squares method to model equations. The concentrations of single and paired ligands, and the stoichiometric association constant for single ligands, were in agreement with literature values and model predictions. However, the stoichiometric association constant for ligand pairs was considerably smaller than predicted, indicating less cooperativity within a ligand pair than expected. Nevertheless these results support the hypothesis that cellulose (unlike agarose) provides a sufficiently rigid matrix for permanent ligand clusters to exist.

1. Introduction

The interactions of multisite proteins (i.e. proteins having several identical ligand binding sites) with ligands immobilised on insoluble stationary phases have been analysed by the use of several theoretical models [1–7]. Multivalent interaction (interaction of a single protein molecule with several immobilised ligands) requires a pair (or higher-order cluster) of ligands to exist in an accessible geometry for the time required by the protein molecule to make two or more contacts. If the strands of the supporting matrix are highly motile (e.g. hydrophilic and infrequently cross-linked long-chain polymers), such clusters may form only transitorily, reducing the probability of multivalent encounters. If the support matrix is rigid, however, immobilised ligands would be incapable of translatory motion relative to each other, allowing perma-

* Corresponding author.
[1] Present address: Affinity Chromatography Ltd., 307 Huntingdon Road, Girton, Cambridge CB3 0JX, UK.

0021-9673/95/$09.50
SSDI 0021-9673(94)01045-5

nent clusters to exist. Proximity and entropic considerations suggest that there should then be strong cooperativity between ligands within an accessible cluster. Compared with binding to an isolated, single ligand, a multisite protein molecule should bind extremely tightly to a permanent accessible cluster.

To model this behaviour quantitatively, it was proposed [6,7] that (a) concentrations of singlets, pairs and higher-order clusters may be obtained by assuming a localised Poisson distribution of ligands, (b) a factor may be introduced to account for macroscopic non-uniformity and (c) the cooperativity within a cluster is so high that protein-to-cluster binding is concerted. Equations derived from this "concerted cluster" model were tested on the binding of aldolase to phosphocellulose, which showed at least two sets of adsorption sites. Numerical analysis led to realistic estimates of the concentrations of single and accessible paired ligands, the microscopic association constant for ligand binding, and hence the conclusion that cellulose is a sufficiently rigid matrix for the "concerted cluster" model to hold [7].

A difficulty in analysing this and similar systems is the low concentration of paired ligands to be expected, detection of which requires binding data at very low protein concentrations. In the aldolase–phosphocellulose case, there was a relative paucity of such data. In search of supporting evidence, we examined the binding of rabbit muscle lactate dehydrogenase to the biomimetic dye Cibacron Blue immobilised on cellulose. Using a sensitive enzyme assay, we studied the interaction at very low protein concentrations where, in addition to the expected single-ligand binding, at least one additional population of high-affinity adsorption sites is clearly evident. To cover both populations of adsorption sites, we present binding data covering nearly four orders of magnitude of soluble protein. Additionally, the effect of varying the overall concentration of immobilised ligand is examined. These results permit a more thorough examination of the clustering hypothesis than has hitherto been possible.

2. Materials and methods

2.1. Materials

Rabbit muscle lactate dehydrogenase and Reactive Blue 2 were from Sigma, Poole, UK. Cellulose (microcrystalline) was from Whatman, Maidstone, UK. Sephadex G-25 was from Pharmacia-LKB, Milton Keynes, UK. All other reagents and buffers were from Sigma or from BDH, Poole, UK.

Blue celluloses, with varying amounts of immobilised dye, were prepared according to the salting-in method of Dean and Watson [8] with modifications suggested by Stead [9]. The concentrations of immobilised dye were determined after acid hydrolysis [10]. Although there was slow leakage of dye from the darker blue celluloses, the loss during the time course of a partitioning experiment was negligible.

2.2. Enzyme assay

Lactate dehydrogenase was assayed by spectrophotometric monitoring of the oxidation of β-NADH (0.1 mM) in sodium phosphate buffer (20 mM, pH 7.4) containing 2 mM sodium pyruvate. The reaction was monitored at 340 nm in a Pye-Unicam SP500 spectrophotometer interfaced with a BBC Model B microcomputer for computation of reaction rate and enzyme concentration. The reaction rate was linearly proportional to enzyme concentration down to 0.2 nM of lactate dehydrogenase.

2.3. Partitioning experiments

Partitioning experiments were performed in imidazole–chloride buffer, pH 7.5 (0.04 M imidazole and 0.39 M NaCl adjusted with HCl). Immediately prior to these experiments, lactate dehydrogenase (supplied as an ammonium sulphate suspension) was desalted by passage through a Sephadex G-25 column equilibrated with imidazole–chloride buffer. Initially, partitioning of the enzyme between the immobilised dye and free solution was determined by the

column recycling method [11] which allowed continuous monitoring of the unbound protein during the approach to equilibrium. From these experiments an appropriate equilibration time was selected for the remainder of the partitioning experiments, which were performed by the mix-centrifuge method [7,12]. The enzyme concentration in free solution was determined by protein absorbance at 280 nm or by enzyme assay.

3. Data treatment

For statistical and accessibility reasons we consider only single and paired ligands, ignoring higher-order clusters [6,7]. Protein binding to two independent sets of immobilised adsorption sites may be shown [7] to be governed by the following equation, which assumes equilibrium binding:

$$[P_b] = \frac{K_1[X_1][P_s]}{K_1[P_s]+1} + \frac{K_2[X_2][P_s]}{K_2[P_s]+1} \quad (1)$$

$[P_b]$ and $[P_s]$ are the experimental variables; $[P_b]$ is the molar concentration of adsorbed protein at equilibrium and $[P_s]$ is the molar concentration of soluble (unadsorbed) protein. The other symbols are model parameters whose values are estimated by least-squares fitting. $[X_1]$ and $[X_2]$ are the molar concentrations of two populations of immobilised protein-binding sites, which in the present analysis are taken to be single and paired ligands, respectively. K_1 and K_2 are the corresponding stoichiometric association constants.

We have fitted the experimental data to Eq. 1 in two ways:

(1) Three-parameter fit: data were fitted to the unchanged concerted-cluster model as detailed in Ref. [7]. The values of $[X_1]$, $[X_2]$, K_1 and K_2 are dependent on three independent parameters: [M] (total accessible ligand), K_M (microscopic or site binding constant) and F (reciprocal of accessible fraction of total reaction volume). Of particular relevance to the present discussion is the dependence of K_2 on these parameters:

$$K_2 = 0.00134 \cdot \frac{K_M^2}{([M]F)^2} \quad (2)$$

This and other relevant equations are given in Ref. [7].

(2) Four-parameter fit: in a second fit to the concerted cluster model we relaxed the constraint on K_2 imposed by Eq. 2, i.e. K_2 was fitted as a fourth independent parameter. Otherwise the procedure was the same as in (1).

The fitting procedure generates parameter values and standard errors by non-linear regression using the simplex method on proportional errors in $[P_b]$ as described previously [7].

4. Results

4.1. Characterisation of blue cellulose

The five dyed cellulose samples used were dark blue and contained 1.62, 3.16, 4.76, 9.46 and 14.3 mM immobilised dye (average concentrations relative to the packed wet volume). These values were determined immediately after the partitioning experiments described below. Although the samples were thoroughly washed prior to use, on storage over several days a slow leakage of dye was observed; however the rate of loss was negligible over the time period of a partitioning experiment, and the leaked dye had negligible affect on the enzyme assay. Partitioning experiments (below) showed that the dye accessible to the enzyme was generally about 0.1% of the total immobilised, in line with previous reports of low accessibility [13,14].

4.2. Evidence for two sets of adsorption sites from Scatchard plots

In tests with unmodified cellulose, no binding of lactate dehydrogenase could be detected with the enzyme at 1 nM and at 5 μM, confirming that binding to the modified (blue) cellulose

involved the immobilised dye. At each of five concentrations of immobilised dye, 30–35 measurements of $[P_s]$ and $[P_b]$ were taken covering total protein concentrations from about 0.2 nM to about 5 μM. The results for three dye concentrations are shown as Scatchard plots in Fig. 1 (two of the five sets are omitted for clarity). The pronounced biphasic curvature is clear evidence of at least two sets of adsorption sites for protein in each case. The set with higher affinity was invariably present at low concentrations, and was only evident at protein concentrations below 10^{-7} M.

4.3. Model fitting and error distribution

The experimental data were fitted to Eq.1 by the simplex method which generates estimates of the model parameters. The quality of fit was assessed by examining the distribution of proportional errors {proportional error = (experimental value of $[P_b]$ − fitted value of [Pb])/fitted value of [Pb]}. The complete set of experimental data covered nearly four orders of magnitude for both $[P_b]$ and $[P_s]$ (Fig. 2A). In Fig. 2B and C the error distributions are shown for two modes of fitting to Eq. 1, as follows:

(1) Data were fitted to the unmodified concerted-cluster model. This fit required only three

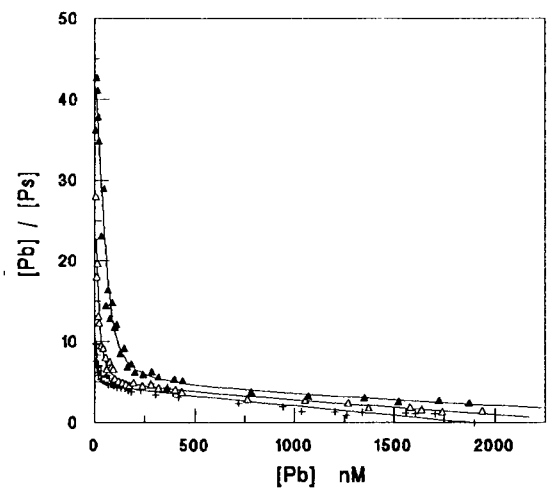

Fig. 1. Scatchard representation of lactate dehydrogenase binding to Cibacron Blue immobilised on cellulose. Data are shown for protein interacting with Cibacron Blue immobilised at total concentrations of 1.62 mM (+), 3.16 mM (△) and 14.3 mM (▲). Data at other dye concentrations are omitted for clarity. The continuous lines represent the best four-parameter fits to Eq. 1.

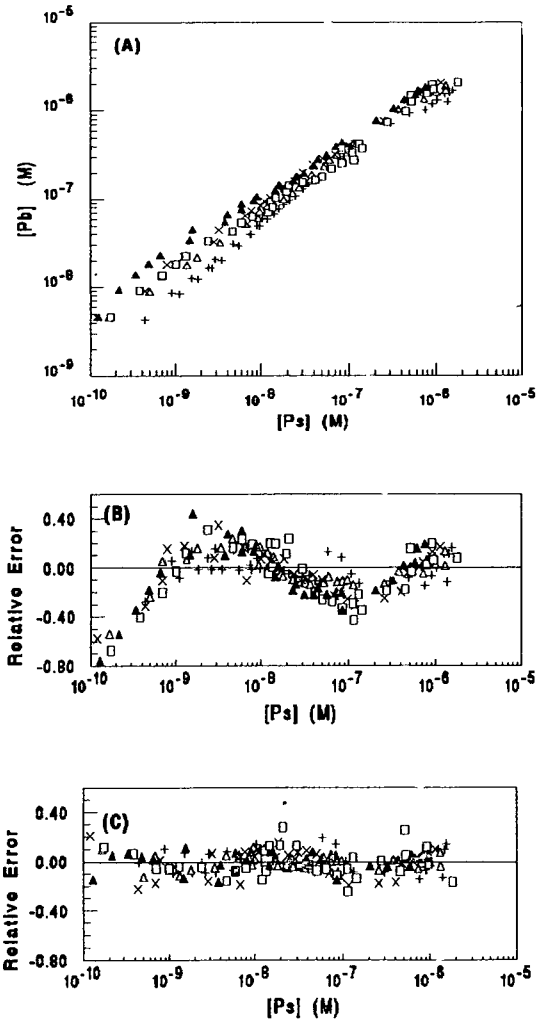

Fig. 2. Experimental data and error distributions. (A) Double-logarithmic plot showing the full range of partitioning data for lactate dehydrogenase interacting with immobilised Cibacron Blue. (B) Error distribution for the best fit of the experimental data to the model, including all constraints (three-parameter fit). (C) Error distribution for the best fit to the model, with constraint on K_2 relaxed (four-parameter fit; see text). Partitioning data are shown for total immobilised dye concentrations of 1.62 mM (+), 3.16 mM (△), 4.76 mM (□), 9.46 mM (×) and 14.3 mM (▲).

parameters, [M], K_M and F. The error distribution is shown in Fig. 2B. The fit is relatively poor; errors are not only non-uniformly distributed, but are worst at the lowest protein concentrations, signifying that the fit to the second (high-affinity) set of sites is particularly bad. The deteriorating fit was very largely due to the extremely high values of K_2 generated by Eq. 2.

(2) The data were refitted to Eq. 1 but the constraint on K_2 (Eq. 2) was omitted. This fit therefore had four independent parameters, [M], K_M, F and K_2. The error distribution is much more uniform (Fig. 2C), and represents a much better fit. This procedure is equivalent to an unrestricted fit to Eq. 1 with $[X_1]$, K_1, $[X_2]$ and K_2 as independent parameters, since there are four independent parameters in each case. Such an unrestricted fit generated identical values for the parameters of Eq.1, and an identical error distribution.

The fitted values of K_2 are generally of the order $10^8\ M^{-1}$, which is much smaller than predicted by Eq. 2 (which predicts $K_2 \geq 10^{14}\ M^{-1}$, i.e. essentially irreversible binding). It is clear therefore that, although a high-affinity set of sites exists such as is predicted by the cluster model, the extremely high level of site–site cooperativity predicted by Eq. 2 does not exist in this system. This arguably signifies that, within an accessible ligand pair, there are interfering factors (possibly steric) that reduce the intrinsic site constant K_M for protein interaction with the second member of the pair compared with that for the first.

4.4. Effects on model parameters of varying the dye concentration

For the remainder of this section we discuss only the four-parameter fit and the associated values of $[X_1]$, $[X_2]$, K_1 and K_2. The best-fit values of these parameters and their standard errors were determined at each of the five total-dye concentrations, and are shown in Fig. 3.

The concentrations of both the single ($[X_1]$) and paired ($[X_2]$) ligands increase hyperbolically with the total-dye concentration, showing a tendency to saturation, as expected (Fig. 3A and B). Depending on total-dye concentration, $[X_1]$ is 50–200 times greater than $[X_2]$. However the *relative* increase in $[X_2]$ is greater than that in $[X_1]$; for example, the increase in total-dye from 1.5 to 15 mM approximately doubles the value of $[X_1]$ but increases $[X_2]$ seven-fold. This observation is consistent with a Poissonian distribution of ligands within the volume-space accessible to the protein, as proposed in the model (see Fig. 1 of Ref. [6]).

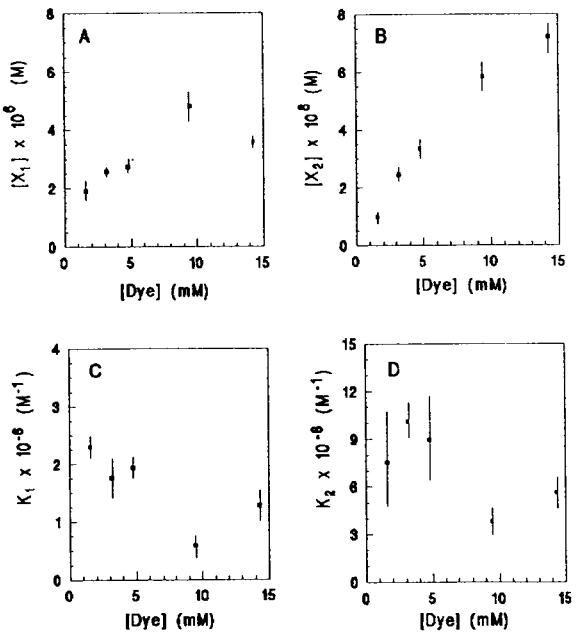

Fig. 3. Dependence of (A) $[X_1]$, (B) $[X_2]$, (C) K_1 and (D) K_2 on the total concentration of immobilised Cibacron Blue. Parameter values are shown with standard error range (vertical bars).

The fitted values of K_1 and K_2 in general have larger standard errors than the estimates of $[X_1]$ and $[X_2]$, hence trends in these parameters are discussed with lower confidence (Fig. 3C and D). Fig. 3C gives K_1 values that are all in the range $(0.6–2.3)\cdot 10^6\ M^{-1}$. These compare favourably with published values (given as dissociation constants, here converted to association constants) of $4.3\cdot 10^6\ M^{-1}$ [15] and $2.2\cdot 10^6\ M^{-1}$ [16] for monovalent binding of lactate dehydrogenase to Cibacron Blue immobilised on Sepharose, and $2\cdot 10^6\ M^{-1}$ for binding the dye in free solution

[17]. In terms of the cluster model we would expect K_1 and K_2 to be independent of total dye concentration. In fact both K_1 and K_2 appear to decrease with increasing total-dye concentration, suggesting that at higher dye concentrations there is interference from effects such as dye adsorption to the matrix [16] or dye stacking [18].

5. Discussion

Lactate dehydrogenase has four coenzyme-binding sites [19]; these sites bind the free dye with identical microscopic binding constants, and the interaction of the enzyme with the free dye has been characterised [17,20,21]. Monovalent interaction of the enzyme with the dye immobilised on beaded agarose (Sepharose) has also been characterised [11,14–16]. For the present theory, the enzyme was treated as a sphere of radius 4 nm.

The results reported in the present paper confirm the existence in Cibacron Blue cellulose of a small proportion of high-affinity sites, in addition to the major proportion of lower-affinity sites for binding lactate dehydrogenase. In terms of the concerted-cluster model [6], we interpret these as ligand pairs and single ligands, respectively (the concentrations of three- and four-ligand clusters we assume to be negligible both on statistical and accessibility grounds; see discussion in Ref. [6]). The concentrations of these sites are compatible with the concerted-cluster model which suggests a Poisson distribution of ligands within the matrix space that is accessible to the protein (necessarily less than the total reaction volume [7]). The association constants for single ligands ("monovalent" binding) are close to published figures for both the immobilised and free dye. However the association constants for the presumed ligand pairs are only about 100-fold greater than the constants for single ligands; the model requires that they be at least 10^7 times greater, i.e. it postulates a much higher degree of cooperativity between sites than is observed. The extremely high model value for K_2 is calculated by assuming that only two factors are important in determining this value, namely (1) the intrinsic association constant K_M, assumed to be the same for each member of the ligand pair and for an isolated ligand, and (2) the "apparent local concentration" of ligand within the cluster, which is very much greater than the accessible dye concentration. The calculation ignores the geometrical/steric constraints on the protein achieving a good fit to both ligands simultaneously, and this is the most likely reason for the model failing in its estimate of K_2.

The present results support the suggestion, based originally on studies with aldolase and phosphocellulose [6], that cellulose provides the degree of rigidity in a matrix that is essential for permanent ligand clusters to exist. We speculate that this is a consequence of the micro-crystalline structure of cellulose. In contrast, studies on the lactate dehydrogenase–Cibacron Blue system, at similar low protein concentrations, but with agarose (Sepharose) and other "soft" materials as the support matrix, show no evidence of the low-concentration, high-affinity adsorption sites observed in the present case [14,22], arguably indicating the transient nature of clustering on these "soft" matrices.

Acknowledgement

This work was supported by a grant from the Biotechnology/Chemical Engineering Directorate of the Science and Engineering Council, UK.

References

[1] I.M. Chaiken, *Anal. Biochem.*, 97 (1979) 1–10.
[2] L.W. Nichol, L.D. Ward and D.J. Winzor, *Biochemistry*, 20 (1981) 4856–4860.
[3] P. Kyprianou and R.J. Yon, *Biochem. J.*, 207 (1982) 549–556.
[4] H.W. Hethcote and C. DeLisi, in I.M. Chaiken, M. Wilchek and I. Parikh (Editors), *Affinity Chromatography and Biological Recognition*, Academic Press, London, 1983, pp. 119–134.
[5] A.I. Liapis, *J. Biotech.*, 11 (1989) 143–160.

[6] R.J. Yon, *J. Chromatogr.*, 457 (1988) 13–23.
[7] V. Dowd and R.J. Yon, *J. Chromatogr.*, 627 (1992) 145–151.
[8] P.D.G. Dean and D.H. Watson, *J. Chromatogr.*, 165 (1979) 301–319.
[9] C.V. Stead, in M.A. Vijayalakshmi and O. Bertrand (Editors), *Protein–Dye Interactions: Developments and Applications*, Elsevier Applied Science, London, New York, 1989, pp. 21–32.
[10] G.K. Chambers, *Anal. Biochem.*, 83 (1977) 551–557.
[11] P.J. Hogg and D.J. Winzor, *Arch. Biochem. Biophys.*, 234 (1984) 55–60.
[12] S.J. Harris and D.J. Winzor, *Biochim. Biophys. Acta*, 999 (1989) 95–99.
[13] Y.C. Liu, R. Ledger, C. Bryant and E. Stellwagen, in I.M. Chaiken, M. Wilchek and I. Parikh (Editors), *Affinity Chromatography and Biological Recognition*, Academic Press, London, 1983, pp. 135–142.
[14] R.J. Yon and M.J. Easton, in M.A. Vijayalakshmi and O. Bertrand (Editors), *Protein–Dye Interactions*, Elsevier Applied Science, London, New York, 1988, pp. 72–79.
[15] Y.C. Liu, R. Ledger and E. Stellwagen, *J. Biol. Chem.*, 259 (1984) 3796–3799.
[16] Y.C. Liu and E. Stellwagen, *J. Biol. Chem.*, 262 (1987) 583–588.
[17] S.T. Thompson and E. Stellwagen, *Proc. Natl. Acad. Sci. U.S.A.*, 73 (1976) 361–365.
[18] A.G. Mayes, J. Hubble and R. Eisenthal, *Biotech. Bioeng.*, 40 (1992) 1263–1270.
[19] J.J. Holbrook, A. Liljas, S.J. Steindel and M.G. Rossmann, in P.D. Boyer (Editor), *The Enzymes*, Vol. 11, Academic Press, London, 3rd ed., 1975, pp. 191–292.
[20] A.R. Ashton and G.M. Polya, *Biochem. J.*, 175 (1978) 501–506.
[21] R.A. Edwards and R.W. Woody, *Biochem. Biophys. Res. Commun.*, 79 (1977) 470–476.
[22] V. Dowd and R.J. Yon, unpublished results.

ELSEVIER

Journal of Chromatography A, 693 (1995) 23–32

JOURNAL OF CHROMATOGRAPHY A

Characterization of the protein binding of chiral drugs by high-performance affinity chromatography Interactions of *R*- and *S*-ibuprofen with human serum albumin

David S. Hage[a,*], Terence A.G. Noctor[b], Irving W. Wainer[b]

[a]*Department of Chemistry, University of Nebraska, Lincoln, NE 68588-0304, USA*
[b]*Department of Oncology, McGill University, Montreal, Quebec H3G 1A4, Canada*

First received 24 August 1994; revised manuscript received 14 October 1994; accepted 18 October 1994

Abstract

Zonal elution and high-performance affinity chromatography were used to study the different binding characteristics of *R*- and *S*-ibuprofen with the protein human serum albumin (HSA). This was done by injecting small amounts of *R*- and *S*-ibuprofen onto an immobilized HSA column in the presence of a mobile phase that contained a known concentration of *R*- or *S*-ibuprofen as a competing agent. These studies indicated that *R*- and *S*-ibuprofen had one common binding site on the immobilized HSA column. In addition, *S*-ibuprofen had at least one other major binding region. The association equilibrium constant for *R*-ibuprofen with HSA was found to be $5.3 \cdot 10^5\ M^{-1}$ at pH 6.9 and 25°C. Under the same conditions, the association constants for *S*-ibuprofen at its two sites were $1.1 \cdot 10^5\ M^{-1}$ and $1.2 \cdot 10^5\ M^{-1}$. The *S*-ibuprofen sites were present in about a 1:1 ratio and appeared to exhibit some allosteric interactions at high *S*-ibuprofen concentrations. The chromatographic technique used in this work is a general one which can be adapted for use in studying the interactions of other chiral compounds with either HSA or additional proteins.

1. Introduction

Protein binding in blood is a significant factor in the transport and release of many drugs and hormones. These interactions can influence the biological distribution of these compounds as well as their excretion, therapeutic activity and toxicity [1]. One protein that is involved in such binding processes is human serum albumin (HSA). HSA is the major protein in serum and is known to bind to a wide range of small organic and inorganic compounds [2]. This binding is believed to occur at two major sites on HSA (i.e., the warfarin–azapropazone site and the indole–benzodiazepine site) plus a number of minor binding regions [3–6].

In characterizing the interactions of a chiral compound with HSA, it is important to consider the behavior of each individual form of the solute since the binding of HSA can be stereoselective in nature [7–14]. One way in which this stereoselectivity can be produced is by the chiral forms of a compound having different binding strengths for HSA. For example, *R*- and *S*-warfarin bind to the same site on HSA but have significantly different association constants

* Corresponding author.

0021-9673/95/$09.50
SSDI 0021-9673(94)01009-9

for this region [10–12]. In addition, stereoselectivity may be produced by the various forms of a chiral compound having different binding regions. Examples of this latter case include the binding of HSA with D- and L-tryptophan [13] or *R*- and *S*-oxazepam hemisuccinate [14].

Ibuprofen is one chiral drug which may exhibit different binding to HSA for its individual enantiomeric forms. Ibuprofen [i.e., 2-(4-isobutylphenyl)-propionic acid] is a common nonsteroidal, anti-inflammatory agent used in the treatment of rheumatoid arthritis and related conditions [15]. This compound exists in two forms, *R*- and *S*-ibuprofen, which differ in their therapeutic and pharmacological properties [16]. Racemic ibuprofen is 99% protein bound in human plasma at normal therapeutic levels [17]. Most or all of this binding is believed to occur with HSA.

A large number of studies have been performed examining the binding of ibuprofen to HSA; however, the actual strength of this binding and number of sites involved in this interaction are still areas of controversy. Most studies agree that ibuprofen has a primary binding site on HSA with an association equilibrium constant in the range of 10^5 to 10^6 M^{-1} [17–25]. However, it is not yet clear whether there is only one ibuprofen binding region on HSA [20–23] or additional, weaker binding sites [17,19,24,25]. One potential problem with most of these earlier studies is that the experiments were performed using racemic ibuprofen mixtures [17–25]. Recent work using the individual enantiomers of ibuprofen suggests that there are different numbers of sites and/or affinities involved in the interactions of HSA with *R*- and *S*-ibuprofen [26,27].

This work will use an immobilized HSA column and high-performance affinity chromatography (HPAC) to examine the binding of HSA to the *R*- and *S*-enantiomers of ibuprofen. In this case, a column that contains HSA immobilized to a silica-based support will be used as the basis for the experiment. Previous studies have shown that the properties of this type of column show good correlation with the properties of HSA in solution [12–14,27–31]. For example, equilibrium constant measurements performed on HSA columns with *R*- and *S*-warfarin or D- and L-tryptophan have resulted in binding affinities that differ by less than 20% from solution values measured by equilibrium dialysis [12,13,29]. Displacement phenomena and allosteric interactions observed on the same types of HSA columns have also been shown to agree with the behavior of HSA in solution [14,27–31]. Similar conclusions have been reached by other workers, who have used columns containing HSA (or other types of serum albumin) immobilized to agarose-based supports [8,10].

The binding of *R*- and *S*-ibuprofen to HSA will be examined in this work by injecting small amounts of each enantiomer onto an HSA column while a known concentration of *R*- or *S*-ibuprofen is applied to the column in the mobile phase. By examining how the mobile phase concentration of the ibuprofen additive affects the retention of the injected solute, information will be gained on the type of competition which is occurring between these two species. This, in turn, will be used to determine the number of binding regions for each enantiomer and the corresponding association constants for these sites. These results will then be compared with those of previous studies which have examined the binding of ibuprofen with HSA.

2. Theory

The binding of *R*- and *S*-ibuprofen to HSA was examined by using the technique of zonal elution. In this method, a known concentration of a competing agent (I) is continuously applied to a column that contains an immobilized ligand (L) while injections of a small amount of analyte (A) are made. If I and A compete at a single site on L, then the following equation can be used to describe the retention of A on the column [28]:

$$\frac{1}{(k' - X)} = \frac{V_m K_I [I]}{K_A m_L} + \frac{V_m}{K_A m_L} \quad (1)$$

In the above equation, V_m is the void volume of the column (i.e., the elution volume of a non-retained solute), m_L is the moles of binding sites in the column involved in the competition

of A with L, and [I] is the concentration of the competing agent in the mobile phase. K_A is the association equilibrium constant for the binding of A to L at the site of competition and K_I is the association equilibrium constant for the interaction of I at the same site. The term k' is the capacity factor for the injected solute, or $k' = (t_R/t_m - 1)$, where t_R is the measured retention time of the solute and t_m is the void time of the column. The term X is a constant that represents the portion of k' due to the binding of A to sites at which I does not compete or due to sites for which the contribution to k' is already known through independent measurements. If no additional binding sites are present in the column (i.e., $X = 0$), then Eq. 1 reduces to the same form as derived in other previous studies [29,32,33].

If the amount of injected analyte is sufficiently small (i.e., linear elution conditions are present), then Eq. 1 predicts that a plot of $1/(k' - X)$ versus [I] for a system with single-site competition will give a linear relationship with a slope of $V_m K_I/K_A m_L$ and an intercept of $V_m/K_A m_L$. The value of K_I can be determined directly from this plot by calculating the ratio of the slope to the intercept. If the concentration of binding sites in the column is known (i.e., m_L/V_m), then the value of K_A can also be obtained from the intercept.

If multisite binding or allosteric interactions are present, then deviations from the linear behavior predicted by Eq. 1 will be seen. This makes plots of $1/(k' - X)$ versus [I] useful in detecting such interactions [12,13,28,29]. Eq. 1 can also be used to monitor competition or allosteric interactions at specific sites on a ligand, even when one of the agents (A or I) has multisite binding with L. This is possible since the value of $1/(k' - X)$ is affected only by changes in those sites at which both A and I bind. By using an analyte or a competing agent that is known to have single-site interactions with the ligand, the binding of other compounds at the same site can be examined [29,34].

In the situation where single-site binding is present and the same compound is used as both the competing agent and the injected analyte, Eq. 1 reduces to the following form:

$$\frac{1}{k'} = \frac{V_m[I]}{m_L} + \frac{V_m}{K_A m_L} \quad (2)$$

This expression is obtained by setting X equal to zero (i.e., by assuming that there are no sites that do not interact with both A and I) and by setting K_A equal to K_I (i.e., by assuming that the binding strengths for A and I are identical at each site). This new relationship predicts that a plot of $1/k'$ vs. [I] will yield a linear relationship for a system with single-site competition. In this case, the ratio of the slope to the intercept gives K_A and the inverse of the slope gives m_L/V_m, or the effective concentration of binding sites in the column. As noted with Eq. 1, non-linear behavior in a plot made according to Eq. 2 might be observed if the interactions of A and L take place at more than one type of site. However, if the contributions to k' are known for these additional sites, then a linear plot can still be obtained by using Eq. 1 and a value for X that corresponds to the portion of k' that is due to these regions.

3. Experimental

3.1. Reagents

The individual enantiomers of *R*- and *S*-ibuprofen were kindly supplied by Upjohn Labs. (Kalamazoo, MI, USA). Racemic ibuprofen (>98% pure) was obtained from Sigma (St. Louis, MO, USA). The immobilized HSA column was obtained from Shandon Scientific (Runcorn, UK). Other chemicals and solvents used were of the purest grades available. All buffers and aqueous solutions in this study were prepared using water from a Milli-Q water system (Millipore, Milford, MA, USA).

3.2. Apparatus

The chromatographic system consisted of one Spectroflow Model 400 pump, a Model 480 injector and a Model 783 programmable absorbance detector from ABI Analytical (Ramsey, NJ, USA). The immobilized HSA column was 15 cm × 4.6 mm I.D. and was thermostated

at 25 ± 0.1°C using a CH-30 temperature-regulated jacket from FIAtron Laboratory Systems (Oconomowoc, WI, USA).

3.3. Chromatography

The immobilized HSA column was prepared using diol-bonded Nucleosil 300-7 (Machery-Nagel, Düren, Germany) activated with 1,1'-carbonyldiimidazole (CDI) [30]. The final protein content of this support was estimated to be 95 ± 2 mg HSA per gram of support, as determined by the supplier [30].

All mobile phases were prepared by adding 0 to 30 μM of the desired competing agent to 0.05 M sodium phosphate buffer (pH 6.90) containing 15% (v/v) acetonitrile. All mobile phases containing ibuprofen were prepared using the individual enantiomers of this compound. Prior to their use, the mobile phases were degassed by ultrasonication and passed through 0.45-μm Millipore HV filters. Mobile phases were applied to the immobilized HSA column at a flow-rate of 0.8 ml/min. In each experiment, a 20-μl sample was injected which contained 0.5 μg of analyte dissolved in 1-propanol–water (50:50, v/v). The sample solution generally contained only R- or S-ibuprofen. However, injections of samples containing racemic ibuprofen could also be made when the chromatographic conditions were sufficient to produce baseline resolution of the individual ibuprofen enantiomers.

Elution of the injected ibuprofen was detected by monitoring the absorbance of the column eluent at 265 nm. Because this study used an ibuprofen enantiomer as both the injected solute and mobile phase additive, there was an increase in the background signal due to the mobile phase as higher concentrations of competing agent were used. This did not create any significant problems under the range of ibuprofen concentrations studied in this work (i.e., 0–30 μM). However, a decrease in the sensitivity and precision of the absorbance measurements was noted at higher mobile phase levels of ibuprofen.

The capacity factor (k') was determined in duplicate or triplicate for each injected compound by comparing the analyte's mean retention time (t_R) to the retention time of water (t_m). The mean retention time of each peak was determined by the modified B/A half-height method [35]. In plots of $1/(k' - X)$ versus [I], the value of X for sites with no competition between I and A was assigned a value of zero when A and I represented the same compound. When A and I were not identical, the value of X was determined by iterative testing, as described previously [28].

Data on the second binding site for S-ibuprofen were obtained by using the calculated capacity factor for S-ibuprofen at its first binding site (i.e., the site shared by R- and S-ibuprofen) as the value of X in a plot of $1/(k' - X)$ for the S-/S-ibuprofen competitive binding studies. The capacity factor for the first site was determined by using the relationship $X = (Km_L/V_m)/(K[I] + 1)$, where m_L/V_m and K represent the concentration and association constant of the first S-ibuprofen site, as measured in R-/S-ibuprofen competitive binding experiments. After calculating the value of X at each level of competing agent used, the results obtained were subtracted from the overall experimentally measured capacity factors. A plot of $1/(k' - X)$ versus [I] was then made and analyzed according to Eq. 1, as discussed earlier.

All experiments in this study were performed on a single HSA column over the course of three weeks and approximately 50 injections. The binding properties of the immobilized HSA column were stable throughout this time period, as indicated by a total variation of only 4–14% in the measured retention of R- and S-ibuprofen when no competing agent was present. Similar stability has been noted in previous work with other HSA columns [12,13,29].

4. Results and discussion

4.1. Competitive binding studies using R-ibuprofen as a mobile phase additive

Initial studies were performed by injecting small amounts of R- or S-ibuprofen onto the immobilized HSA column in the presence of

Table 1
Influence of the mobile phase concentration of *R*-ibuprofen on the capacity factors of injected *R*-ibuprofen (k'_R) and *S*-ibuprofen (k'_S)

[*R*-Ibuprofen] (μM)	k'_R	k'_S
0.0	75.66	23.20
0.5	56.86	20.11
1.0	43.37	17.74
2.0	31.73	15.70
3.0	24.79	14.80
4.0	20.94	13.89
5.0	19.55	12.65
6.0	15.52	12.49
8.0	11.96	11.49
10.0	10.92	11.09

The values shown for k'_R and k'_S represent the mean results of duplicate or triplicate injections. The quantity [*R*-ibuprofen] represents the mobile phase concentration of *R*-ibuprofen that was applied to the column during each experiment.

mobile phases containing different concentrations of *R*-ibuprofen as a competing agent. For both enantiomers, a decrease in retention was observed as increasing amounts of *R*-ibuprofen were added to the mobile phase. The capacity factors measured for the injected solutes are shown in Table 1. The corresponding graphs of $1/(k' - X)$ versus [*R*-ibuprofen] are given in Fig. 1.

The plot shown in Fig. 1 for the injections of *R*-ibuprofen was obtained by using a value of zero for X in Eq. 1. This X value was chosen since the analyte and competing agent were identical, and thus had no sites on the column for which they did not compete. The *R*-ibuprofen plot in Fig. 1 was linear over the entire concentration range studied. The correlation coefficient was 0.9956 for the 10 data points shown. This linear relationship indicated that *R*-ibuprofen had one major class of binding sites on the column. By taking the ratio of the slope to the intercept for this plot, an association equilibrium constant of 5.5 $(\pm 1.0) \cdot 10^5$ M^{-1} was calculated for *R*-ibuprofen at its binding site, where the number in parentheses represents a range of ± 1 S.D. Although the exact location of this binding region was not examined in this work, data from earlier competition studies indicate that this is probably located at the indole–benzodiazepine site of HSA [27].

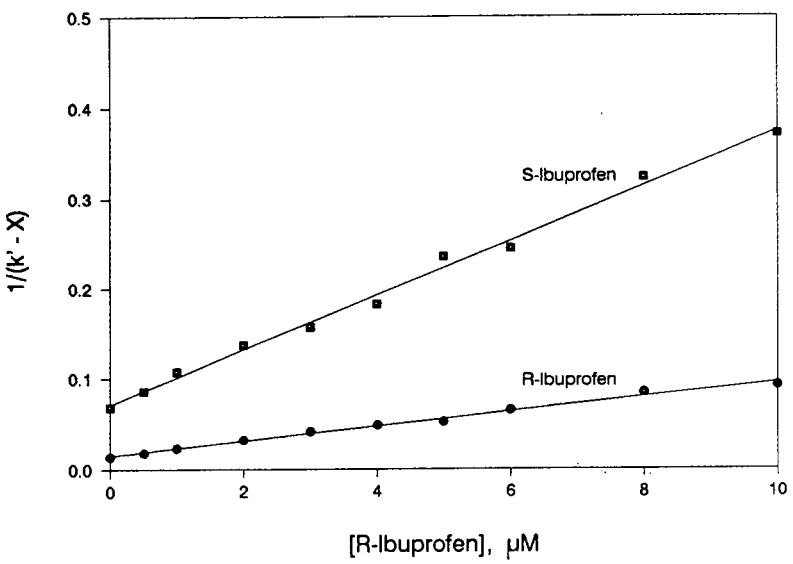

Fig. 1. Change in $1/(k' - X)$ with mobile phase concentration of applied *R*-ibuprofen as injections of *R*-ibuprofen (●) and *S*-ibuprofen (□) were made onto an immobilized HSA column. The equations of the best-fit lines were $y = (8100 \pm 300\ M^{-1})x + (0.015 \pm 0.003)$ for *R*-ibuprofen and $y = (30\,500 \pm 800\ M^{-1})x + (0.071 \pm 0.008)$ for *S*-ibuprofen. The values of X used for the *R*- and *S*-ibuprofen plots were 0.00 and 8.40, respectively.

As mentioned in the Theory section, one unique feature of using the same compound as both the injected analyte and the competing agent, as was done in this study with *R*-ibuprofen, is that this causes the association constants for the two agents to be identical (i.e., $K_I = K_A$). As shown in Eq. 2, the slope obtained for a plot of $1/k'$ vs. [I] should then be equal to V_m/m_L, from which the concentration of binding sites in the column (m_L/V_m) can be easily obtained. Based on this approach, the concentration of *R*-ibuprofen sites in the HSA column was calculated to be $1.24\ (\pm 0.04) \cdot 10^{-4}\ M$.

From the protein content and packing density of the immobilized HSA support, it was possible to estimate the total amount of HSA that was present in the column. A final value of 1.6 μmol HSA, or an effective concentration of $8.0 \cdot 10^{-4}$ M, was obtained by this approach. If it is assumed, as indicated by Fig. 1, that *R*-ibuprofen has only one binding site on HSA, then a comparison of this amount of HSA with the measured concentration of *R*-ibuprofen sites indicates that only about 15% of these sites were active in the column. Similar values have been reported for the binding of immobilized HSA to other solutes [12,13,29]. This relatively low activity is probably due to denaturation, steric hindrance or improper orientation of the HSA as a result of the immobilization process [12,13,29]. Fortunately, the approach used in this work to study ibuprofen–HSA interactions was not affected to any major extent by these non-binding regions, because only those sites that showed competition between the injected and applied ibuprofen were monitored [29].

A comparison of the concentration of *R*-ibuprofen sites in the column with the applied concentrations of *R*-ibuprofen, as given in Table 1, shows that the binding sites were present in a large excess during these studies. In this case, the mobile phase levels of *R*-ibuprofen ranged from 0 to 8% of the effective binding site concentration. This represents a very different situation from that present in other methods used to study solute–protein binding (e.g., ultrafiltration or equilibrium dialysis), in which solute concentrations often approach or exceed the amount of binding protein. Although the lower solute levels used here may make the detection of weak binding sites difficult, these same conditions would also tend to make the chromatographic approach more selective in the analysis of higher affinity sites.

As was found for injections of *R*-ibuprofen, the graph shown in Fig. 1 for the competition of injected *S*-ibuprofen with *R*-ibuprofen in the mobile phase also gave a linear relationship. The best-fit line had a correlation coefficient of 0.9971 over the ten data points shown. This behavior suggested that *R*- and *S*-ibuprofen had a single class of sites for which they competed in the column. Protein binding interactions between *R*- and *S*-ibuprofen have been suggested in earlier studies [36], but the number of sites involved in these interactions has been examined only recently [27].

From the slope and intercept of the plot for *S*-ibuprofen in Fig. 1, the association equilibrium constant for *R*-ibuprofen at the site of competition was determined to be $4.3\ (\pm 0.5) \cdot 10^5\ M^{-1}$. This value was statistically identical to the association constant obtained in the *R*-ibuprofen/*R*-ibuprofen study. This indicated that the same binding site for *R*-ibuprofen was being sampled in both experiments.

By using the concentration of *R*-ibuprofen binding sites that was determined earlier and by assuming that *R*- and *S*-ibuprofen had equal access to this site [12], it was possible to use the slope of the *S*-ibuprofen curve in Fig. 1 to calculate the association constant for *S*-ibuprofen at the site of competition. An association constant of $1.1\ (\pm 0.1) \cdot 10^5\ M^{-1}$ was obtained for *S*-ibuprofen by this procedure.

The plots in Fig. 1 for both *R*- and *S*-ibuprofen gave good agreement between the experimental intercepts (i.e., k' when no competing agent was present) and the intercepts which were determined by linear regression of the entire data set. For example, the experimental and best-fit intercepts for *R*-ibuprofen were 0.013 and 0.015 (± 0.003), respectively. For *S*-ibuprofen, these values were 0.067 and 0.070 (± 0.008). The agreement between these values is significant since it indicates that the displacement of either

Table 2
Influence of the mobile phase concentration of *S*-ibuprofen on the capacity factors of injected *R*-ibuprofen (k'_R) and *S*-ibuprofen (k'_S)

[*S*-Ibuprofen] (μM)	k'_R	k'_S
0.0	80.86	27.37
2.0	72.97	22.22
4.0	70.73	16.56
6.0	61.94	16.07
8.0	49.05	13.91
10.0	45.21	12.45
15.0	41.51	11.81
20.0	34.60	10.88
30.0	Not done	10.86

The values shown for k'_R and k'_S represent the mean results of duplicate or triplicate injections. The quantity [*S*-ibuprofen] represents the mobile phase concentration of *S*-ibuprofen that was applied to the column during each experiment.

R- or *S*-ibuprofen by *R*-ibuprofen was through a direct, rather than an allosteric, mechanism of competition [29].

4.2. Competitive binding studies using *S*-ibuprofen as a mobile phase additive

Studies similar to those described for *R*-ibuprofen were also performed using *S*-ibuprofen as a mobile phase additive. A decrease in the retention of *R*- and *S*-ibuprofen was seen as higher mobile phase concentrations of *S*-ibuprofen were applied to the column. Table 2 lists the capacity factors that were obtained for *R*- and *S*-ibuprofen during this study. The corresponding plots of $1/(k' - X)$ versus [*S*-ibuprofen] are given in Fig. 2.

The data in Fig. 2 for the injections of *R*-ibuprofen gave a linear relationship with a correlation coefficient of 0.9850 over the eight data points shown. This confirmed that *S*- and *R*-ibuprofen had single-site competition on HSA, as indicated earlier in Fig. 1. One difference between these results and those in Fig. 1 was that the slope/intercept ratio of Fig. 2 gave the association constant for *S*-ibuprofen, rather than

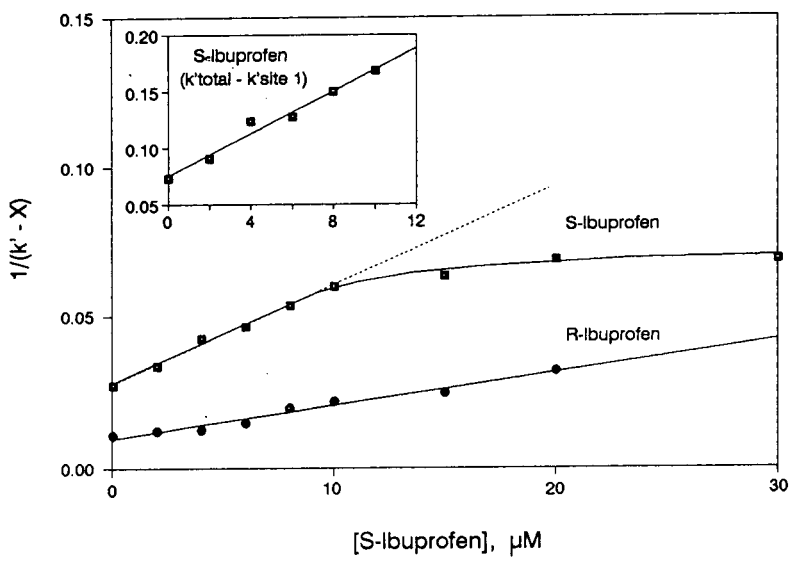

Fig. 2. Change in $1/(k' - X)$ with mobile phase concentration of applied *S*-ibuprofen as injections of *R*-ibuprofen (●) and *S*-ibuprofen (■) were made onto an immobilized HSA column. The equation of the best-fit line shown for the first five points of the *S*-ibuprofen data was $y = (4400 \pm 300\ M^{-1})x + (0.013 \pm 0.002)$. The best-fit line shown for *R*-ibuprofen was $y = (1400 \pm 100\ M^{-1})x + (0.013 \pm 0.002)$. The values of X used for the *R*- and *S*-ibuprofen plots were 11.04 and 0.00, respectively. The insert shows the *S*-ibuprofen data after subtracting out the calculated contribution to k' from the *S*-/*R*-ibuprofen common binding site. The best-fit line for the five points in the insert was $y = (9400 \pm 700\ M^{-1})x + (0.076 \pm 0.006)$ and the correlation coefficient was 0.9873.

for *R*-ibuprofen, at their common binding site. The equilibrium constant calculated from Fig. 2 for *S*-ibuprofen at the site of competition was 1.1 $(\pm 0.2)\cdot 10^5\ M^{-1}$. This value was the same as the previous estimate made from Fig. 1.

The association constant for *R*-ibuprofen with HSA was determined from Fig. 2 by using the slope of the *S*-ibuprofen plot and the concentration of *R*-ibuprofen binding sites measured earlier. A result of 6.2 $(\pm 0.9)\cdot 10^5\ M^{-1}$ was obtained. This value was in good agreement with the association constant values that were determined for *R*-ibuprofen from Fig. 1.

The competition of injected *S*-ibuprofen with *S*-ibuprofen in the mobile phase was the only case in this work which produced any type of non-linear behavior. The *S*-ibuprofen plot in Fig. 2 gave a linear response up to a competing agent concentration of 8 μM. This was followed by a leveling off of the *S*-ibuprofen curve at higher competing agent concentrations. This behavior indicated that at least two separate sites were involved in the binding of *S*-ibuprofen to the immobilized HSA column. Multisite binding was also indicated by the inverse slope of this plot (i.e., m_L/V_m), which was twice the value predicted by the number of *R*-ibuprofen sites that were measured on the column. The properties of these additional sites were studied by correcting the overall capacity factor for the contribution due to the interactions of *S*-ibuprofen at the shared *R*-/*S*-ibuprofen binding site. The resulting graph is shown in the inset of Fig. 2.

The plot obtained for the adjusted capacity factors was similar in shape to the original graph shown in Fig. 2, but with higher values for $1/(k' - X)$. By applying Eq. 1 to the linear portion of this graph, the concentration of the additional *S*-ibuprofen binding sites was estimated to be 1.06 $(\pm 0.09)\cdot 10^{-4}\ M$ and the apparent association constant for these sites was determined to be 1.2 $(\pm 0.1)\cdot 10^5\ M^{-1}$. The ratio of the concentration of these additional sites vs. the concentration of sites shared by *S*-ibuprofen and *R*-ibuprofen was 0.9:1.0. From this data the contribution to the capacity factor for *S*-ibuprofen that was due to the additional sites, where $k' = K_A m_L/V_m$, was estimated to be 13 (± 2). This agreed with the X value of 11.04 that was determined in Fig. 1 for the competition of injected *S*-ibuprofen with *R*-ibuprofen in the mobile phase. All of this information indicated that there were probably only two major classes of sites involved in the binding of *S*-ibuprofen to the immobilized HSA column. The exact location of these sites currently remains unknown.

The similarity of the association constants measured for *S*-ibuprofen at the two binding sites explains why a linear region was initially observed for the *S*-ibuprofen data in Fig. 2. The non-linearity of this data at high *S*-ibuprofen levels indicates that there is probably some allosteric or indirect competition between the *S*-ibuprofen sites at high concentrations. One reason that similar behavior was not noted for the *R*-ibuprofen results in Fig. 2 may be that the stronger binding of *R*-ibuprofen minimized or prevented allosteric effects from being seen under the experimental conditions used. Alternatively, only the second site for *S*-ibuprofen may have been altered or the binding of *R*- and *S*-ibuprofen at the first site may have been sufficiently different that only the *S*-enantiomer was affected by the interactions of *S*-ibuprofen at the second site. A similar difference in allosteric effects for enantiomers binding to the same region on HSA has been reported for *R*- and *S*-warfarin [31].

4.3. Comparison of data with previous models for ibuprofen–HSA binding

The results presented in this work indicate that there is one major binding site on HSA for *R*-ibuprofen and two or more major sites on HSA for *S*-ibuprofen. The average association constants measured for these sites are summarized in Table 3. These averages are based on the three estimates obtained for the association constant of *R*-ibuprofen at its major binding region, (site A), the two estimates obtained for *S*-ibuprofen at the same site, and a single measurement made for the binding of *S*-ibuprofen at its second site (site B).

The association constants obtained in this study show good agreement with previous values

Table 3
Binding of *R*- and *S*-ibuprofen to immobilized HSA

Binding region	Association equilibrium constant (M^{-1})	
	R-Ibuprofen	*S*-Ibuprofen
Site A	$5.3 (\pm 0.9) \cdot 10^5$	$1.1 (\pm 0.1) \cdot 10^5$
Site B	–	$1.2 (\pm 0.1) \cdot 10^5$

The given values were measured at 25°C in 0.05 *M* sodium phosphate buffer containing 15% (v/v) acetonitrile. The numbers in parentheses represent ± 1 S.D.

reported for the primary binding regions of ibuprofen on HSA. For example, Sollene and Means [20] measured an association constant of $1.4 \cdot 10^5\ M^{-1}$ at 25°C and pH 8.0 for the main binding site of racemic ibuprofen on HSA. Kober and Sjöholm [21] determined a primary binding constant of $1 \cdot 10^6$–$1.3 \cdot 10^6\ M^{-1}$ at 20–22°C and pH 7.4 for racemic ibuprofen mixed with human serum, HSA in solution and HSA immobilized onto microparticles. Similar association constants, ranging from $1 \cdot 10^5$ to $2.7 \cdot 10^6\ M^{-1}$, have been reported for racemic ibuprofen in studies performed at pH 7.4 and 37°C [17,18,22–25]. The individual association constants given in Table 3 for *R*- and *S*-ibuprofen are larger than those determined recently by microcalorimetry [37]. However, the binding constant for *R*-ibuprofen does agree with the results of earlier chromatographic experiments that examined the competition of this enantiomer with various benzodiazepines [27].

The presence of at least one common binding site for *R*- and *S*-ibuprofen, as shown in Table 3, has been suggested by Lee et al. [36]. Furthermore, the existence of at least two ibuprofen binding regions on HSA has been proposed in a recent report by Noctor et al. [27]. In this latter study, it was found that *R*- and *S*-ibuprofen gave different types of behavior when allowed to compete with benzodiazepines on an immobilized HSA column. It was concluded that two stereoselective binding regions were present, each having preferential binding to a different ibuprofen enantiomer [27]. The same trend was observed in the present study, with site A binding most tightly to *R*-ibuprofen and site B having interactions with only *S*-ibuprofen. From these results, it is proposed that sites A and B are the same as the IBU_R and IBU_S binding regions noted in the earlier report [27].

The fact that *R*- and *S*-ibuprofen share one binding site plus the fact that sites A and B have similar binding constants for *S*-ibuprofen may explain why there have been apparent discrepancies in past studies concerning ibuprofen–HSA binding. For example, the use of a racemic ibuprofen mixture would make it impossible to detect the different affinities of *R*- and *S*-ibuprofen for site A. Work based on racemic ibuprofen would also make it difficult to detect the presence of an additional site for one of the enantiomers, unless a large number of replicates and a wide range of experimental conditions are used. Even with the use of the pure enantiomeric samples, the similarity of the association constants for *S*-ibuprofen at sites A and B would make it hard to distinguish between these two sites unless competitive binding studies are performed, such as described in this work, that use agents with different binding affinities to these regions (e.g., *R*- or *S*-ibuprofen).

The different association constants and number of sites observed in this work for *R*- and *S*-ibuprofen indicate the importance of considering individual enantiomers in developing an accurate picture of drug–protein binding. Similar conclusions have been reached in previous studies which have examined the protein binding of other chiral compounds [12,13,27,28]. It was also found in this work that HPAC was a useful tool in examining the protein binding of the ibuprofen enantiomers. For example, by examin-

ing the changes in the capacity factors for *R*- and *S*-ibuprofen during the competitive binding studies, it was possible to determine whether or not the two forms of the drug had any common binding sites with the competing agent present in the mobile phase. By treating the data further, it was possible to determine the number of sites on HSA which were binding to each enantiomer and to estimate the association constants for these sites. The technique used in this work is not limited to ibuprofen or HSA, but can also be applied to the study of other chiral drugs or binding proteins.

Acknowledgements

D.S.H. was supported in part by the National Institutes of Health under grant No. GM44931. The provision of the CDI-immobilized HSA column by Shandon Scientific is also gratefully acknowledged.

References

[1] G.A.J. van Os, E.J. Ariens and A.M. Simonis, in E.J. Ariens (Editor), *Molecular Pharmacology*, Vol. 1, Academic Press, New York, 1964, p. 29.
[2] C.F. Chignell, in G.D. Fasman (Editor), *Handbook of Biochemistry and Molecular Biology*, Vol. 2, CRC Press, Cleveland, OH, 3rd ed., 1976, pp. 554–582
[3] W.E. Müller, K.J. Fehske and S.A.C. Schläfer, in M.M. Reidenberg and S. Erill (Editors), *Drug-Protein Binding*, Praeger Publishers, New York, 1986, Ch. 2.
[4] I. Sjöholm, in M.M. Reidenberg and S. Erill (Editors), *Drug-Protein Binding*, Praeger Publishers, New York, 1986, Ch. 4.
[5] J.-P. Tillement, G. Houin, R. Zini, S. Urien, E. Albengres, J. Barrè, M. Lecomte, P. D'Athis and B. Sebille, *Adv. Drug Res.*, 13 (1984) 59.
[6] W.E. Müller and U. Wollert, *Nauyn-Schmiedeberg's Arch. Pharmacol.*, 288 (1975) 17.
[7] W.E. Müller and U. Wollert, *Pharmacology*, 19 (1979) 59.
[8] C. Lagercrantz, T. Larsson and H. Karlsson, *Anal. Biochem.*, 99 (1979) 352.
[9] R.H. McMenamy and F. Watson, *Comp. Biochem. Physiol.*, 26 (1968) 329.
[10] C. Lagercrantz, T. Larsson and I. Denfors, *Comp. Biochem. Physiol.*, 69C (1981) 375.
[11] J.H.M. Miller and G.A. Smail, *J. Pharm. Pharmacol.*, 29 (1977) 33.
[12] B. Loun and D.S. Hage, *Anal. Chem.*, 66 (1994) 3814.
[13] J. Yang and D.S. Hage, *J. Chromatogr.*, 645 (1993) 241.
[14] E. Domenici, C. Bertucci, P. Salvadori, S. Motellier and I.W. Wainer, *Chirality*, 2 (1992) 263.
[15] S.S. Adams and J. Warwick-Butler, *Clin. Rheum. Dis.*, 5 (1979) 359.
[16] A.M. Evans, *Eur. J. Clin. Pharmacol.*, 42 (1992) 237.
[17] R.F.N. Mills, S.S. Adams, E.E. Cliffe, W. Dickinson and J.S. Nicholson, *Xenobiotica*, 3 (1973) 589.
[18] M. Gibaldi, G. Levy and P.J. McNamara, *Clin. Pharmacol. Ther.*, 24 (1978) 1.
[19] J.B. Whitlam, M.J. Crooks, K.F. Brown and P.V. Pedersen, *Biochem. Pharmacol.*, 28 (1979) 675.
[20] N.P. Sollenne and G.E. Means, *Mol. Pharmacol.*, 15 (1979) 754.
[21] A. Kober and I. Sjöholm, *Mol. Pharmacol.*, 18 (1980) 421.
[22] L. Aarons, D.M. Grennan and M. Siddiqui, *Eur. J. Clin. Pharmacol.*, 25 (1983) 815.
[23] G.L. Lockwood, K.S. Albert, S.J. Szpunar and J.G. Wagner, *J. Pharmacokin. Biopharm.*, 11 (1983) 469.
[24] B. Honoré and R. Brodersen, *Mol. Pharmacol.*, 25 (1984) 137.
[25] M.T. Montero, J. Estelrich and O. Valls, *Int. J. Pharmaceut.*, 62 (1960) 21.
[26] J.K. Paliwal, D.E. Smith, S.R. Cox, R.R. Berardi, V.A. Dunn-Kucharski and G.H. Elta, *J. Pharmacokin. Biopharmaceut.*, 21 (1993) 145.
[27] T.A.G. Noctor, C.D. Pham, R. Kaliszan, and I.W. Wainer, *Mol. Pharmacol.*, 42 (1992) 506.
[28] T.A.G. Noctor, I.W. Wainer and D.S. Hage, *J. Chromatogr.*, 577 (1992) 305.
[29] B. Loun and D.S. Hage, *J. Chromatogr.*, 579 (1992) 225.
[30] E. Domenici, C. Bertucci, P. Salvadori, G. Félix, I. Cahagne, S. Motellier and I.W. Wainer, *Chromatographia*, 29 (1990) 170.
[31] E. Domenici, C. Bertucci, P. Salvadori and I.W. Wainer, *J. Pharm. Sci.*, 80 (1991) 164.
[32] A.J. Muller and P.W. Carr, *J. Chromatogr.*, 284 (1984) 33.
[33] D.J. Anderson and R.R. Walters, *J. Chromatogr.*, 331 (1985) 1.
[34] B. Loun and D.S. Hage, *J. Chromatogr. B*, in press.
[35] D.J. Anderson and R.R. Walters, *J. Chromatogr. Sci.*, 22 (1984) 353.
[36] E.J.D. Lee, K. Williams, R. Day, G. Graham and D. Champion, *Br. J. Clin. Pharmacol.*, 19 (1985) 669.
[37] V.K. Cheruvallath, S.R. Narayanan and S. Lindenbaum, *Pharmaceut. Res.*, 10 (1993) S27.

ELSEVIER

Journal of Chromatography A, 693 (1995) 33–44

JOURNAL OF CHROMATOGRAPHY A

Tryptic peptide mapping of sequence 299–585 of human serum albumin by high-performance liquid chromatography and fast atom bombardment mass spectrometry

Salvatore Fisichella, Salvatore Foti*, Giuseppina Maccarrone, Rosaria Saletti

Dipartimento di Scienze Chimiche, Università di Catania, V.le A. Doria, 6, 95125-Catania, Italy

First received 3 August 1994; revised manuscript received 25 October 1994

Abstract

The determination of the tryptic peptide mapping of sequence 299–585 (cyanogen bromide fragment A) of human serum albumin (HSA) by chemical and enzymatic cleavages and combined use of HPLC and FAB-MS is described. Reduction and carboxymethylation of A gave four subfragments which were separated by HPLC and digested with trypsin. Tryptic fragments were separated by HPLC and identified by FAB-MS. A total coverage of about 95% of the entire sequence was obtained. Tryptic fragments not identified include mostly single amino acids and very hydrophilic peptides which were absent in the chromatograms. The high reproducibility of the experiments and the satisfactory yield of the tryptic fragments identified demonstrate the great potential of the combined use of HPLC separation and FAB-MS analysis for the structural investigation of HSA.

1. Introduction

Human serum albumin (HSA) is the most abundant protein in the circulatory system. It consists of a single, non-glycosilated, polypeptide chain containing 585 amino acid residues and has many physiological functions. However, the most peculiar property of this protein is its unique ability to bind many endogenous and exogenous ligands, which range from inorganic cationic species to a large variety of organic molecules [1].

Peptide mapping of HSA appears of interest in view of several possible applications, which include the structural characterization of genetic variants, the characterization of chemical modifications, and the determination of the nature and topology of binding sites of HSA for ligands. Different approaches involving various methodologies have been reported [2–6].

Over recent years direct fast atom bombardment mass spectrometry (FAB-MS) of proteolytic mixtures of peptides (FAB mapping) and the combination of FAB-MS with reversed-phase high-performance liquid chromatography (RP-HPLC) have proved to be powerful tools for peptide mapping of proteins [7–12].

A CNBr fragment of bovine serum albumin was partially mapped using these techniques [13], but applications of such procedures to HSA have not yet been reported.

As a part of a research programme concerning the investigation of the interaction of HSA with textile dyes used as ligands for dye–protein

* Corresponding author.

0021-9673/95/$09.50
SSDI 0021-9673(94)01042-0

affinity chromatography [14,15], we have undertaken the determination of tryptic peptide mapping of HSA by combined use of HPLC and FAB-MS and have previously reported the results relative to the sequence 1–298 [16]. We describe here the determination of the tryptic map of the remaining sequence 299–585.

2. Experimental

HSA (Cohn Fraction V), dithiothreitol (DTT), iodoacetic acid and trypsin TPCK treated were purchased from Sigma (Milan, Italy), Spectra Por 6 dialysis membrane was obtained from Roth (Karlsruhe, Germany), trifluoroacetic acid (TFA) was provided by Janssen (Beerse, Belgium), HPLC grade H_2O and CH_3CN were obtained from Carlo Erba (Milan, Italy). All other chemicals were of the highest purity commercially available and were used without further purification. A, B and C cyanogen bromide fragments of unreduced HSA were obtained as described elsewhere [14].

HPLC separations were performed on a Varian 9010 equipped with a Varian 9050 detector and a Varian 4400 integrator. Amino acid analyses were carried out by ion-exchange chromatography with post-column ninhydrin derivatization according to Moore and Stein [17] on a Carlo Erba 3A30 automatic amino acid analyser.

Peptide samples were hydrolysed in 6 *M* hydrochloric acid for 24 h at 105°C in evacuated sealed tubes.

2.1. Reduction and carboxymethylation of fragment A

1 μmol of fragment A was dissolved in 1 *M* Tris–HCl containing 6 *M* guanidine, at a concentration of 10 mg/ml. The pH was adjusted to 8.5 by HCl and a 10-fold molar excess of DTT over the SH concentration, dissolved in 2 ml of the same buffer, was added. The mixture was allowed to react for 3 h at 25°C in the dark under nitrogen atmosphere. Iodoacetic acid (0.95-fold molar excess over total thiols), dissolved in 3 ml of 1 *M* Tris–HCl containing 6 *M* guanidine, was then added and the pH raised to 8.5 by addition of NaOH. The mixture was kept in the dark at room temperature for 1 h maintaining the pH above 8. At the end of the reaction time, excess of iodoacetic acid was eliminated by addition of 10 μl of 2-mercaptoethanol to the reaction mixture. The solution was then dialysed against water and freeze-dried.

2.2. HPLC separation of the subfragments of A

The freeze-dried residue from the reduction and carboxymethylation reaction was dissolved in aqueous 0.05% TFA, filtered on Millex-HV (Millipore, Milan, Italy) and applied onto a RP-Vydac C18 (25 × 1.0 cm) column. About 3 mg of mixture were injected for each run. The column was eluted at room temperature with a linear gradient of solvent B [CH_3CN–isopropanol (2:1) containing 0.08% TFA] in A (H_2O–TFA 0.05%) from 20% to 50% in 35 min. Flow rate was 4 ml min^{-1}. Peaks were detected by their absorption at 224 nm. Four fractions were collected and freeze-dried.

2.3. Tryptic cleavage of reduced and carboxymethylated subfragments of A

Each reduced and carboxymethylated subfragment of A (1 μmol) was dissolved in 20 m*M* ammonium acetate, pH 8.3, containing 1 m*M* calcium chloride, at a concentration of 1 mg/ml. Trypsin was dissolved in the same buffer and added at an enzyme:substrate ratio of 1:50 (mol/mol). The solution was incubated at 37°C for 4 h. The digestion was stopped by cooling in liquid nitrogen and the mixture was immediately freeze-dried.

2.4. HPLC separation of the tryptic peptide mixture of subfragments of A

Lyophilized tryptic peptide mixture of each subfragment of A was dissolved in aqueous 0.1% TFA, filtered on Millex-HV and applied onto a reversed-phase Vydac C18 (1.0 × 25 cm) column. The column was eluted at room temperature with 95% of solvent A (H_2O–TFA 0.1%) and

5% of solvent B (95% CH_3CN–5% H_2O containing 0.08% TFA) for 5 min, and then with a linear gradient of B in A to a final concentration of 47% of B in A in 55 min. Flow rate was 3 ml min^{-1}. Peaks were detected by their absorption at 224 nm. Peaks were collected manually, freeze-dried and subjected to FAB analysis.

2.5. FAB mass spectrometry

FAB mass spectra were recorded on a ZAB-2SE mass spectrometer, equipped with a standard FAB source and a caesium ion gun. The sample was deposited by evaporation from methanol solution onto the probe tip and 2 μl of a 80:20 glycerol–thyoglicerol mixture containing 1% HCl were added. To increase MH^+ signal intensities for peptides containing multiple carboxylic groups, *p*-toluenesulphonic acid was added to the matrix. The sample was bombarded with a beam of 35 KeV caesium ions.

3. Results and discussion

Because HSA consists of a single polypeptide chain of 585 amino acids, its direct digestion with trypsin would give rise to a complex mixture of 79 peptides, which would be difficult to separate by HPLC. In order to obtain a better separation and therefore an extended reproducibility of the tryptic fragments, a combination of chemical and enzymatic cleavages was employed.

Unreduced HSA was initially blocked at the free thiol group of Cys 34 by iodoacetic acid and cleaved by cyanogen bromide. This treatment gives rise to three large fragments which, according to the naming convention of McMenamy et al. [18] are called A, B and C. The mixture of these fragments was separated by gel permeation and ion-exchange chromatography [14].

Tryptic peptide mapping of sequence 1–298 (cyanogen bromide fragments B and C) has been reported previously [16].

Fragment A has a molecular weight of 32 391 and, due to the presence of three methionine residues in its sequence, it is composed of four subfragments held together by disulphide bonds (Table 1). Reduction of the disulphide bridges and carboxymethylation of the resulting free thiol groups produces four independent subfragments.

Table 1
Molecular mass and sequence position of the four subfragments of A

Fragment	Sequence	M_r
A1	299–329	3372
A2	330–446	13905
A3	447–548	11959
A4	549–585	4168

Because of the relatively high molecular weight of fragment A, separation of these component subfragments, prior to tryptic digestion, was carried out. Attempts to separate the four subfragments by ion-exchange chromatography [18] produced unsatisfactory homogeneous fractions. HPLC separation [19,20], instead, resulted in the isolation of pure fractions of the four subfragments, as demonstrated by amino acid analyses and subsequent enzymatic cleavages. HPLC separation of the four subfragments of A is shown in Fig. 1.

The first fraction in the chromatogram (Fig. 1), corresponding to subfragment A1, is formed by two peaks, probably due to the presence of both the free homoserine and homoserine lactone as C-terminal amino acid residue in the peptide. Thus two peptides, slightly differing in retention times, are formed [21]. A2 and A3 may also occur in both forms, but these subfragments appear as single peaks in the chromatogram. It is likely that, because of the higher molecular weight of these peptides, the difference in the retention time of the two forms is smaller so that they are not separated. Peaks not labelled in Fig. 1 are due to partial cleavages at methionine residues and were not further characterized.

The tryptic peptides which should be produced by a completely specific cleavage of the four reduced and carboxymethylated subfragments with trypsin, were predicted using the sequence reported by several authors, obtained from direct sequence analysis [22,23] or from com-

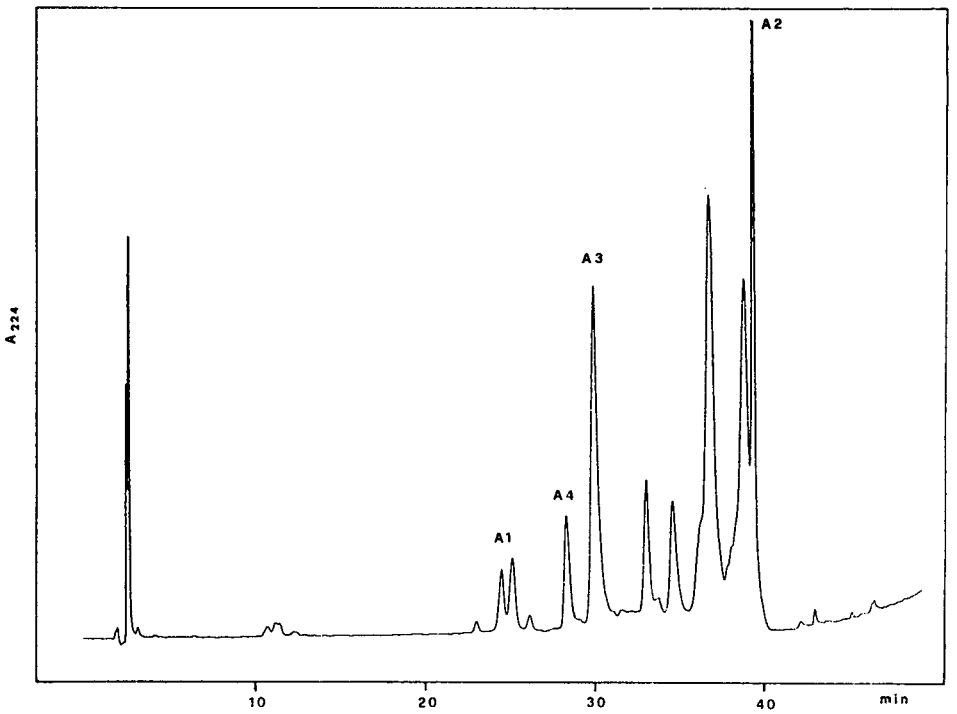

Fig. 1. HPLC separation of the four subfragments of fragment A.

plementary DNA studies [24,25]. These sequences are all coincident within fragment A with the exception of that reported by Lawn et al. [24] in which Glu 396 is substituted by Lys. As will be seen in the following, our results are consistent with the presence of Glu as residue 396. Tryptic fragments derived from A are numbered progressively starting from the N-terminal residue of the whole HSA chain. The tryptic peptides containing methionine result divided in two parts. These are named adding (1) and (2) to the number which identifies the tryptic peptide to indicate the N-terminal and C-terminal moiety, respectively.

Separation of the tryptic peptide fragments was achieved by RP-HPLC. Since FAB-MS identification of the fragments does not require complete separation of the peptides, optimization of the chromatographic conditions was not attempted and the same gradient programme was used in all cases. Retention times of the expected tryptic peptides, as well as retention times of additional peptides identified by FAB-MS in the HPLC of the tryptic mixtures, were calculated according to the equation

$$t_R = a\ln(1 + H) + c$$

where H indicates the hydrophobicity of the peptides, calculated using for the constituent amino acids the weighted retention constants reported by Sasagawa et al. [26,27], and adopting 19.3 and −5.3 for a and c, respectively. The calculated curves are reported in Fig. 2, together with the experimental retention time values. Calculated retention times were in general in good agreement with the experimental values with the notable exception of carboxymethylcysteine containing peptides, for which calculated values were systematically higher than the experimental ones, possibly because the retention constant reported for the carboxymethylcysteine is higher than the real value. Comparison of the experimental retention times of the peptides with the calculated values simplifies and further substantiates the FAB-MS

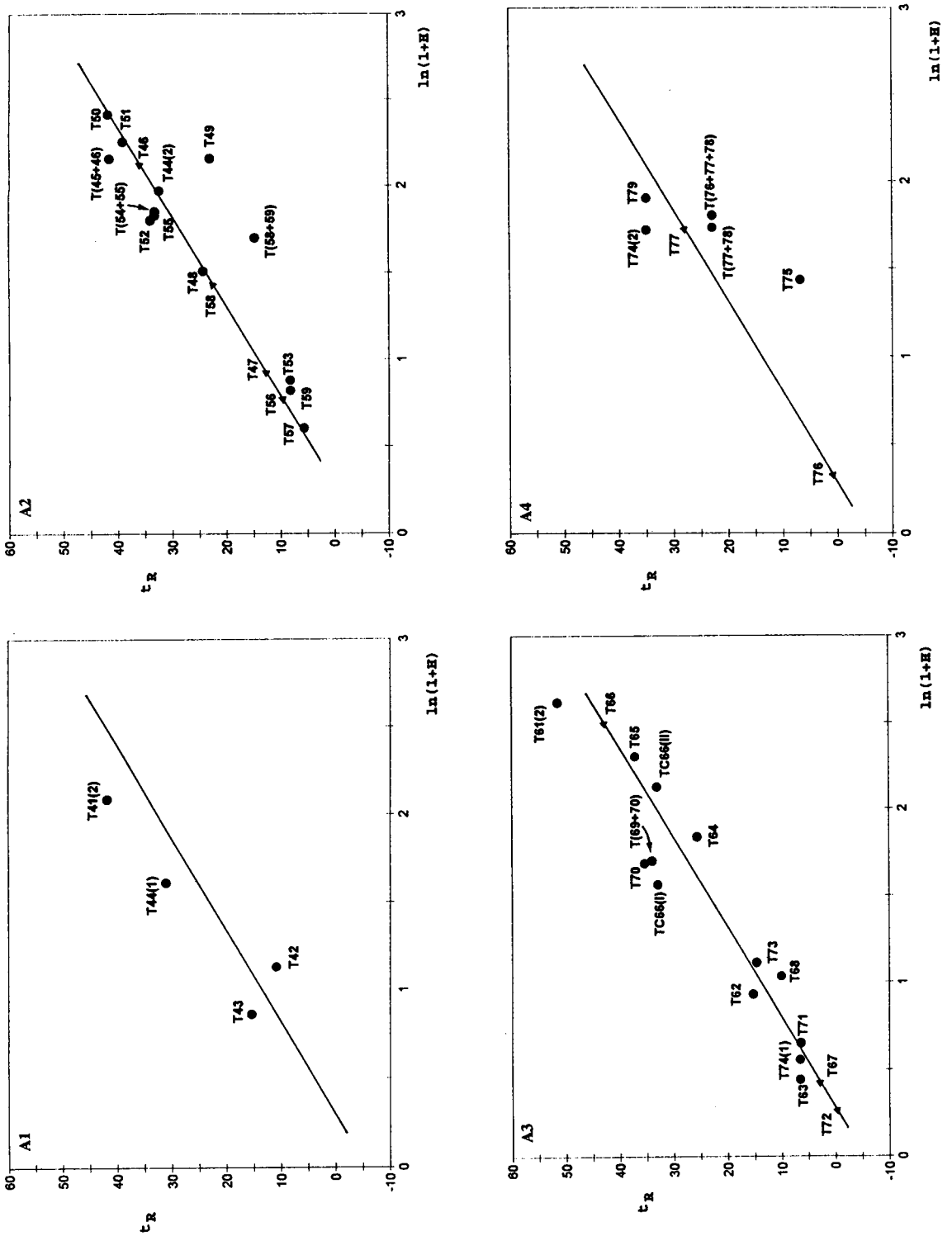

Fig. 2. Experimental (●) and calculated (◀) retention times for the tryptic peptides of A1, A2, A3, and A4. Experimental retention times of unpredicted peptides identified are also included.

Table 2
Sequence, position and identification by HPLC–FAB-MS of the expected tryptic peptides of subfragment A1

Fragment	Position in the sequence	Sequence	M_r	Identification (+) by HPLC–FAB-MS
T41(2)	299–313	PRO–ALA–ASP–LEU–PRO–SER–LEU–ALA–ALA–ASP–PHE–VAL–GLU–SER–LYS	1558.8	+
T42	314–317	ASP–VAL–CMCYS–LYS	521.2	+
T43	318–323	ASN–TYR–ALA–GLU–ALA–LYS	694.3	+
T44(1)	324–329	ASP–VAL–PHE–LEU–GLY–OMO	650.3[a]	+

[a] Free homoserine.

Table 3
Sequence, position and identification by HPLC–FAB-MS of the expected tryptic peptides of subfragment A2

Fragment	Position in the sequence	Sequence	M_r	Identification (+) by HPLC–FAB-MS
T44(2)	330–336	PHE–LEU–TYR–GLU–TYR–ALA–ARG	960.5	+
T45	337	ARG	174.1	as T(45 + 46)
T46	338–348	HIS–PRO–ASP–TYR–SER–VAL–VAL–LEU–LEU–LEU–ARG	1310.7	as T(45 + 46)
T47	349–351	LEU–ALA–LYS	330.2	–
T48	352–359	THR–TYR–GLU–THR–THR–LEU–GLU–LYS	983.5	+
T49	360–372	CMCYS–CMCYS–ALA–ALA–ALA–ASP–PRO–HIS–GLU–CMCYS–TYR–ALA–LYS	1554.5	+
T50	373–389	VAL–PHE–ASP–GLU–PHE–LYS–PRO–LEU–VAL–GLU–GLU–PRO–GLN–ASN–LEU–ILE–LYS	2044.1	+
T51	390–402	GLN–ASN–CMCYS–GLU–LEU–PHE–GLU–GLN–LEU–GLY–GLU–TYR–LYS	1657.7	+
T52	403–410	PHE–GLN–ASN–ALA–LEU–LEU–VAL–ARG	959.5	+
T53	411–413	TYR–THR–LYS	410.2	+
T54	414	LYS	146.1	asT(54 + 55)
T55	415–428	VAL–PRO–GLN–VAL–SER–THR–PRO–THR–LEU–VAL–GLU–VAL–SER–ARG	1510.8	+ also as T(54 + 55)
T56	429–432	ASN–LEU–GLY–LYS	430.2	–
T57	433–436	VAL–GLY–SER–LYS	389.2	+
T58	437–439	CMCYS–CMCYS–LYS	468.1	as T(58 + 59)
T59	440–444	HIS–PRO–GLU–ALA–LYS	580.3	+ also as T(58 + 59)
T60	445	ARG	174.1	–
T61(1)	446	OMO	119.1[a]	–

[a] Free homoserine.

identification of the HPLC peaks in many instances. Moreover, calculated retention times account for the absence of some very hydrophilic peptides in the chromatograms.

HPLC separation of the tryptic peptides of subfragment A1 is illustrated in Fig. 3. Since A1 contains 3 Lys, the formation of 4 tryptic fragments can be anticipated (Table 2). Three chromatographic peaks are identified as T42, T43, and T41(2).

In accordance with previous observation [21], peptide T44(1), which has homoserine as C-terminal amino acid, gives two different HPLC peaks, a faster eluting one, corresponding to the peptide ending in free homoserine, and a second slower eluting peak due to the same peptide with the homoserine in the lactone form. Furthermore the chromatogram (Fig. 4) shows an additional peak at a retention time slightly lower than that corresponding to the free homoserine ending peptide. The FAB spectrum of this peak presents an intense MH^+ signal at m/z 754 which differs by 121 from the MH^+ of the T44(1) peptide containing homoserine in the lactone form. As illustrated previously [16], this signal corresponds to the MH^+ of the product produced by the chemical reaction of tris(hydroxymethyl)aminomethane with the terminal homoserine lactone of the peptide T44(1), in the disulphide reduction step. The fragments identified constitute 100% of the sequence of subfragment A1.

HPLC separation of the tryptic peptides mixture of subfragment A2 is shown in Fig. 4. A2 contains 12 Lys and 6 Arg residues. Because the bond between Lys (378) and Pro (379) is not cleaved by trypsin, 18 tryptic peptides can be predicted. Four fragments [T45, T54, T60, and T61(1)] consist of free amino acids and therefore it is not possible to detect them by HPLC (Table 3).

Ten of the potential tryptic fragments were identified by FAB-MS. Two of them (T53 and T59) are eluted at the same retention time and were collected and identified in one fraction. Peptides T46 and T58 are not found, but two peaks were identified as peptides T(45 + 46) and T(58 + 59). These fragments are produced by incomplete cleavage of Arg (337)–His (338) and Lys (439)–His (440). Incomplete cleavage of the

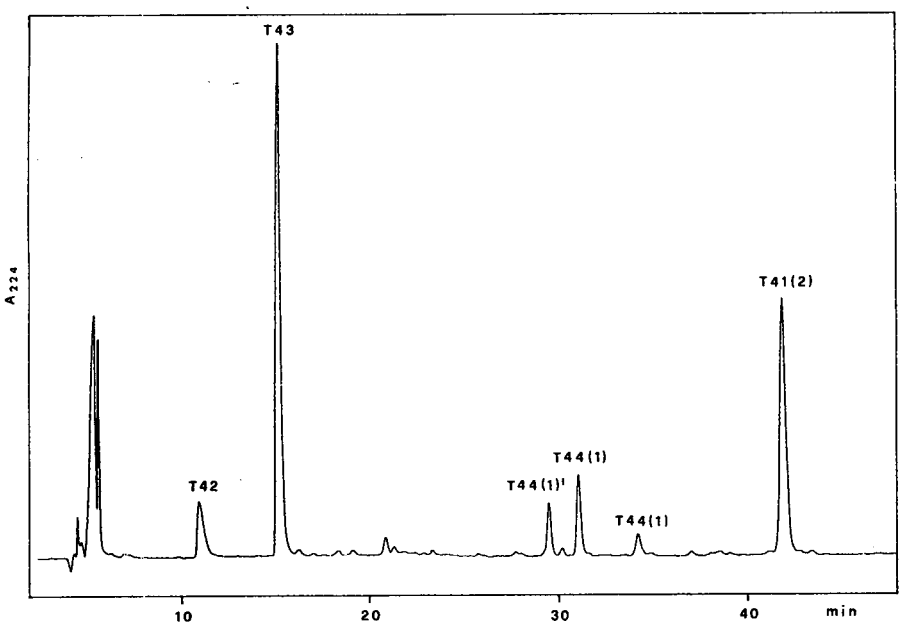

Fig. 3. HPLC separation of the tryptic digest of subfragment A1.

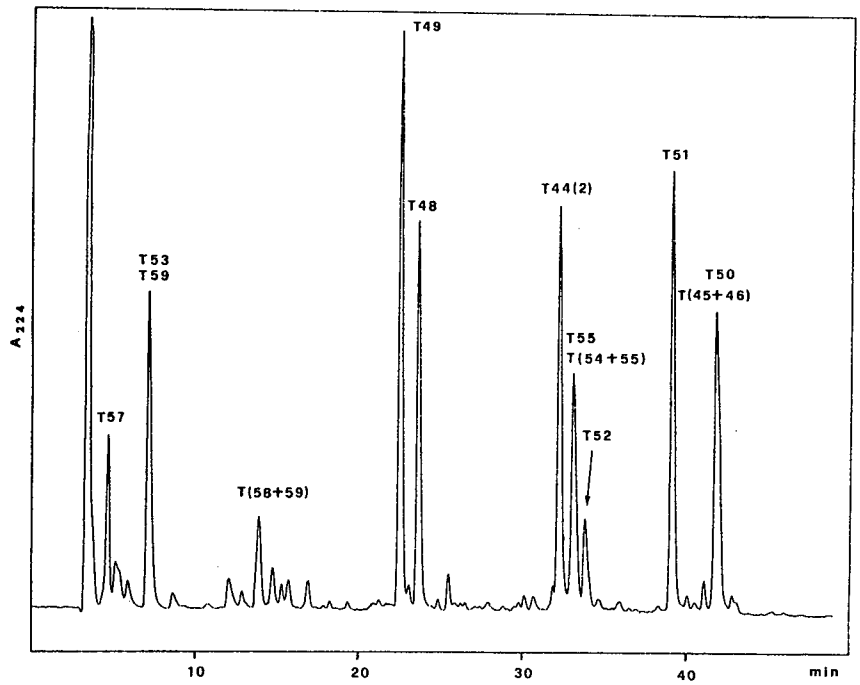

Fig. 4. HPLC separation of the tryptic digest of subfragment A2.

Lys (414)–Val (415) bond accounts for the presence of peptide T(54 + 55), which coelutes with peptide T55. Peptide T51 contains the amino acid in which the sequence reported by Lawn [24] differs from that reported by other authors [22,23,25]. In fact, in the sequence of Lawn the amino acid 396 is a Lys residue, whereas in the others the amino acid residue in this position is Glu. The presence of the peptide T51, found in the present work, confirms the correctness of Glu as residue 396. In all, 92% of the sequence of subfragment A2 was identified.

HPLC separation of the tryptic peptides mixture of subfragment A3 is shown in Fig. 5. This subfragment possesses 10 Lys and 3 Arg, so that a potential yield of 14 tryptic peptides is expected. T69 is a free amino acid and therefore it does not appear in the HPLC chromatogram. Ten of the expected tryptic peptides were identified by FAB-MS (Table 4).

Three of them [T63, T71, and T74(1)], which are very hydrophilic, are eluted at the same retention time. They were collected in one fraction and identified as mixture of peptides. The lactone form of the T74(1) peptide gives a small HPLC peak at 8.20 min. One unexpected peptide was identified as T(69 + 70) originating from incomplete cleavage of Lys (525)–Gln (526) sequence. T70 is also found separately at a slightly higher retention time. The highly hydrophilic peptides T67 and T72 were not found, very likely because of their extremely low retention times (Fig. 2). Peptide T66 does not appear in the chromatogram. However, FAB-MS analysis of a minor peak at 32.95 min indicates that it is composed of two peptides which are produced from peptide T66 by chymotryptic cleavage of Phe (507). The fragments identified constitute about 95% of the sequence of A3.

The chromatographic pattern of the tryptic digest of subfragment A4 is reported in Fig. 6. Subfragment A4 contains 5 Lys giving rise to a potential yield of 6 tryptic fragments, one of which is a single lysine (T78) that is not detected

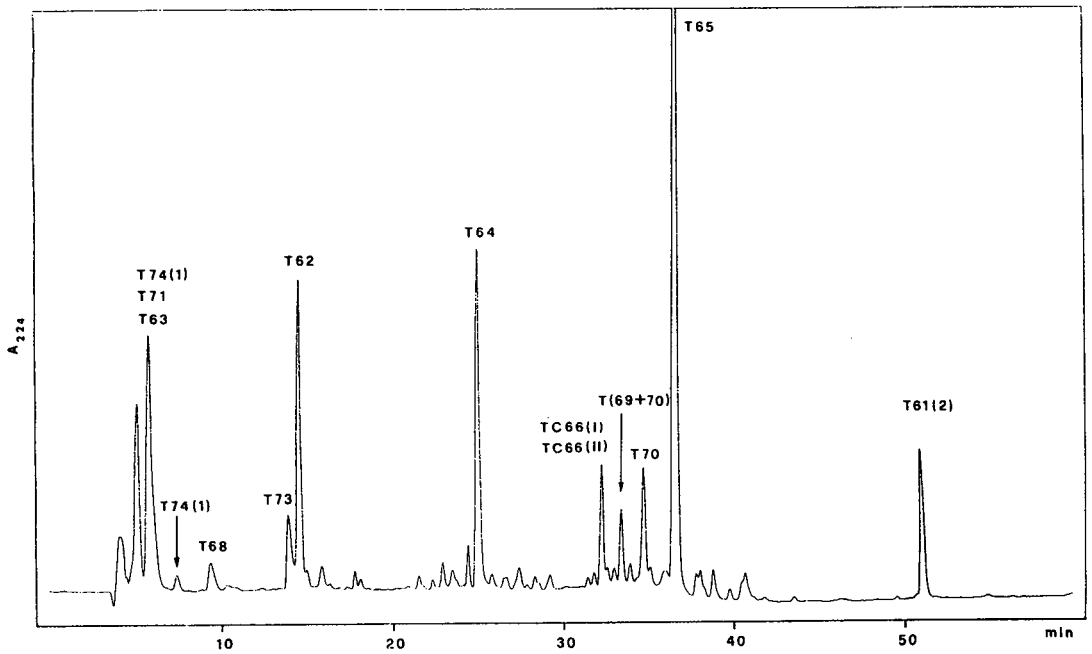

Fig. 5. HPLC separation of the tryptic digest of subfragment A3.

in the HPLC chromatogram. Of the remaining 5 potential peptides, 3 [T74(2), T75, and T79] were identified by FAB-MS (Table 5).

Peptides T74(2) and T79 appear as two almost unresolved peaks at the end of the chromatogram. Peptides T76 and T77 are not detected as such, but the FAB spectrum of an intense HPLC peak eluting at ~23 min shows two intense signals at m/z 1199 and 1628 corresponding to the MH^+ of T(77 + 78) and T(76 + 77 + 78), respectively. These fragments are obviously produced by lack of cleavage of the consecutive Lys

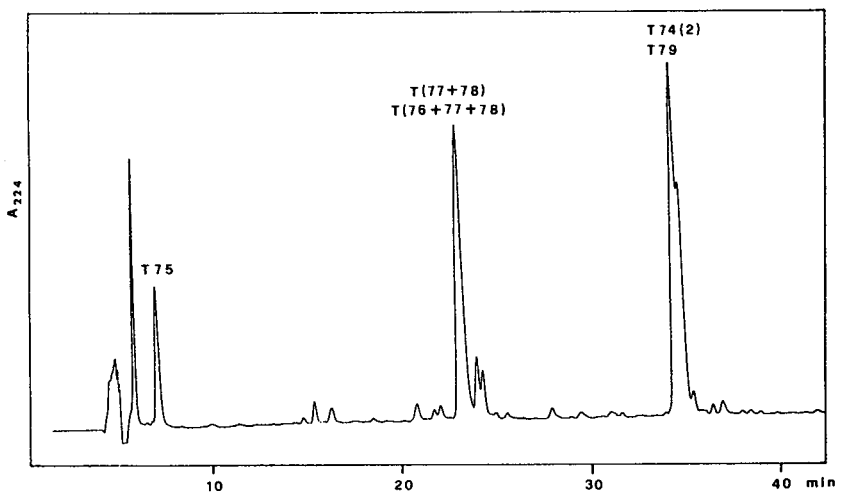

Fig. 6. HPLC separation of the tryptic digest of subfragment A4.

Table 4
Sequence, position and identification by HPLC–FAB-MS of the expected tryptic peptides of subfragment A3

Fragment	Position in the sequence	Sequence	M_r	Identification (+) by HPLC–FAB-MS
T61(2)	447–466	PRO–CMCYS–ALA–GLU–ASP–TYR–LEU–SER–VAL–VAL–LEU–ASN–GLN–LEU–CMCYS–VAL–LEU–HIS–GLU–LYS	2388.1	+
T62	467–472	THR–PRO–VAL–SER–ASP–ARG	673.3	+
T63	473–475	VAL–THR–LYS	346.2	+
T64	476–484	CMCYS–CMCYS–THR–GLU–SER–LEU–VAL–ASN–ARG	1139.5	+
T65	485–500	ARG–PRO–CMCYS–PHE–SER–ALA–LEU–GLU–VAL–ASP–GLU–THR–TYR–VAL–PRO–LYS	1910.9	+
T66	501–519	GLU–PHE–ASN–ALA–GLU–THR–PHE–THR–PHE–HIS–ALA–ASP–ILE–CMCYS–THR–LEU–SER–GLU–LYS	2260	as TC66(I) and TC66(II)
T67	520–521	GLU–ARG	303.1	–
T68	522–524	GLN–ILE–LYS	387.2	+
T69	525	LYS	146.1	as T(69 + 70)
T70	526–534	GLN–THR–ALA–LEU–VAL–GLU–LEU–VAL–LYS	999.6	+ also as T(69 + 70)
T71	535–538	HIS–LYS–PRO–LYS	508.3	+
T72	539–541	ALA–THR–LYS	318.2	–
T73	542–545	GLU–GLN–LEU–LYS	516.3	+
T74(1)	546–548	ALA–VAL–OMO	289.2[a]	+

[a] Free homoserine.

Table 5
Sequence, position and identification by HPLC–FAB-MS of the expected tryptic peptides of subfragment A4

Fragment	Position in the sequence	Sequence	M_r	Identification (+) by HPLC–FAB-MS
T74(2)	549–557	ASP–ASP–PHE–ALA–ALA–PHE–VAL–GLU–LYS	1040.5	+
T75	558–560	CMCYS–CMCYS–LYS	468.1	+
T76	561–564	ALA–ASP–ASP–LYS	447.2	as T(76 + 77 + 78)
T77	565–573	GLU–THR–CMCYS–PHE–ALA–GLU–GLU–GLY–LYS	1070.4	as T(76 + 77 + 78) and T(77 + 78)
T78	574	LYS	146.1	as T(76 + 77 + 78) and T(77 + 78)
T79	575–585	LEU–VAL–ALA–ALA–SER–GLN–ALA–ALA–LEU–GLY–LEU	1012.6	+

(573)–Lys (574) bond and of Lys (564) which is surrounded by three acidic amino acid residues. Considering these latter peptides originating from lack of cleavage at lysine residues, the sequence of subfragment A4 results completely covered.

4. Conclusions

Tryptic peptide mapping of sequence 299–585 (cyanogen bromide fragment A) of HSA has been obtained by chemical and enzymatic cleavage and combination of HPLC and FAB-MS. Reduction of A and carboxymethylation of the resulting free thiol groups gave four subfragments which were separated by HPLC and digested with trypsin. Tryptic fragments were separated by HPLC and identified by FAB-MS. A total coverage of about 95% of the entire sequence was achieved. The method allowed easy identification of unexpected peptides originating from chymotryptic or incomplete tryptic cleavage, and also permitted identification of chemically modified peptides produced by reactions with buffer components. Calculated retention times of the peptides simplified and further substantiated the FAB-MS identification of the HPLC peaks in many, but not in all cases. Most importantly, the calculated retention times enabled explanation of the absence of some tryptic fragments in the chromatograms in terms of their extreme hydrophilicity. The reproducibility of the experiments was excellent and the yield of the tryptic fragments identified satisfactory, thus indicating the great potential of the combined use of HPLC and FAB-MS for the structural investigation of HSA.

Acknowledgement

Partial financial support of Ministero dell' Università e della Ricerca Scientifica e Tecnologica (MURST) is gratefully acknowledged. We also thank Michael Balthasar (University of Kaiserslautern, Germany) for his contribution to this work during his EC Erasmus stage at the Chemistry Department, University of Catania.

References

[1] T. Peters, Jr, in C.B. Anfisen, J.T. Edsall and F.M. Richards (Editors), *Advances in Protein Chemistry*, Vol. 37, Academic Press, London, 1985, p. 161.
[2] L. Minchiotti, M. Galliano, M.C. Zapponi and R. Tenni, *Eur. J. Biochem.*, 214 (1993) 437.
[3] P. Iadarola, L. Minchiotti and M. Galliano, *FEBS Lett.*, 180 (1985) 85.
[4] M. Galliano, L. Minchiotti, P. Iadarola, M. Stoppini, G. Ferri and A.A. Castellani, *FEBS Lett.*, 208 (1986) 364.
[5] L. Minchiotti, M. Galliano, P. Iadarola, E. Zepponi and G. Ferri, *Biochim. Biophys. Acta*, 1039 (1990) 204.
[6] N. Takahashi, Y. Takahashi, N. Ishioka, B.S. Blumberg and F.W. Putnam, *J. Chromatogr.*, 359 (1986) 181.
[7] K. Biemann and S.A. Martin, *Mass Spectrom. Rev.*, 6 (1987) 1.
[8] H.R. Morris and F.M. Grier, *Trends in Biotechnol.*, 6 (1988) 140.
[9] S.A. Carr, M.E. Hemling, M.F. Bean and G.D. Roberts, *Anal. Chem.*, 63 (1991) 2802.
[10] V. Amico, S. Foti, R. Saletti, A. Cambria and G. Petrone, *Biomed. Environ. Mass Spectrom.*, 16 (1988) 431.
[11] M. Svoboda, M. Przybylski, J. Schreurs, A. Miyajima, K. Hogeland and M. Deinzer, *J. Chromatogr.*, 562 (1991) 403.
[12] D. Suckau, M. Mák and M. Przybylski, *Proc. Natl. Acad. Sci. USA*, 89 (1992) 5530.
[13] V. Ling and A.L. Burlingame, in A.L. Burlingame and N. Castagnoli, Jr. (Editors), *Mass Spectrometry in the Health and Life Sciences*, Elsevier, London, 1985, p. 11.
[14] A. Compagnini, M. Fichera, S. Fisichella, S. Foti and R. Saletti, *J. Chromatogr.*, 639 (1993) 341.
[15] S.B. McLoughlin and C.R. Lowe, *Rev. Prog. Coloration*, 18 (1988) 16.
[16] A. Compagnini, S. Fisichella, S. Foti, L. Sardo and R. Saletti, *Rapid Commun. Mass Spectrom.*, 8 (1994) 459.
[17] S. Moore and W. Stein, *J. Biol. Chem.*, 211 (1954) 893.
[18] R.H. McMenamy, H.M. Dintzis and F. Watson, *J. Biol. Chem.*, 246 (1971) 4744.
[19] P. Iadarola, G. Ferri, M. Galliano, L. Minchiotti and M.C. Zapponi, *J. Chromatogr.*, 298 (1984) 336.
[20] P. Iadarola, M.C. Zapponi, M. Stoppini, M.L. Meloni, L. Minchiotti, M. Galliano and G. Ferri, *J. Cromatogr.*, 443 (1988) 317.
[21] P. Pucci, R. Borgia and G. Marino, *J. Chromatogr.*, 331 (1985) 425.
[22] P.Q. Behrens, A.M. Spiekerman and J.R. Brown, *Fed. Proc. Fed. Am. Soc. Exp. Biol.*, 34 (1975) 591.
[23] B. Meloun, L. Moravek and V. Kostka, *FEBS Lett.*, 58 (1975) 134.

[24] R.M. Lawn, J. Adelman, S.C. Bock, A.E. Franke, C.M. Houck, R.C. Najarian, P.H. Seeburg and K.I. Wion, *Nucleic Acids Res.*, 9 (1981) 6103.
[25] A. Dugaiczyk, S.W. Law and O.E. Dennison, *Proc. Natl. Acad. Sci. U.S.A.*, 79 (1982) 71.
[26] T. Sasagawa, T. Okuyama and D.C. Teller, *J. Chromatogr.*, 240 (1982) 329.
[27] T. Sasagawa and D.C. Teller, in W.S. Hancock, (Editor), *CRC Handbook of HPLC for the Separation of Amino Acids, Peptides and Proteins*, Vol. II, CRC Press, Boca Raton, FL, 1984, p. 53.

ELSEVIER

Journal of Chromatography A, 693 (1995) 45–54

JOURNAL OF CHROMATOGRAPHY A

High-performance liquid chromatographic determination of active ingredients in cough–cold syrups with indirect conductometric detection

Oi-Wah Lau*, Chuen-Shing Mok

Department of Chemistry, The Chinese University of Hong Kong, Shatin, Hong Kong

First received 1 March 1994; revised manuscript received 25 October 1994

Abstract

An HPLC method using indirect conductometric detection is proposed for the simultaneous determination of eight active ingredients in cough–cold syrups. It involves the use of an Ultrasphere 5 μm Spherical 80 Å Pore CN analytical column (250 mm × 4.6 mm) as the stationary phase with a mixture of water, acetonitrile and ethanol (38:60:2) containing 1 m*M* perchloric acid as the mobile phase. The active ingredients included bromhexine hydrochloride, chlorpheniramine maleate, codeine phosphate, dextromethorphan hydrobromide, diphenhydramine hydrochloride, ephedrine hydrochloride, papaverine hydrochloride and phenylephrine hydrochloride. Derivatization of the drugs is not required.

The effect of background conductance on detector response, and the factors affecting column separation of the ingredients were studied. The detector responses for all the drugs are similar. The calibration graphs exhibited a wide linear concentration range of 0–500 μg/ml for a sample size of 20 μl with correlation coefficients of better than 0.999 for all the drugs under study. The relative standard deviation for 10 replicate measurements of the content of each drug in cough–cold syrups was always less than 3%. The method has been applied to determine the active ingredients in a number of cough–cold syrups.

1. Introduction

Cough–cold syrups usually contain a number of active ingredients to cater for the therapeutic needs of cough and common cold. The action, properties, and the structures of these ingredients have been detailed in various references [1–5]. Liquid chromatography (HPLC) is the commonest approach to assay the drugs because the method is accurate, simple and does not require prior conversion of the drugs to the base form as needed in the gas–liquid chromatographic (GLC) methods. The HPLC methods have been investigated by many workers [6–12], and most of them were based on ion-pair formation, and the detection method typically based on measuring the UV absorbance of the analytes. The methods cannot be applied to drugs without UV absorbing character.

Other analytical techniques such as derivative spectrophotometric methods [13–15] and GLC methods [7,8,16] have also been reported but the

* Corresponding author.

0021-9673/95/$09.50
SSDI 0021-9673(94)01044-7

spectrophotometric methods could only determine two to three components simultaneously, and the GLC methods involve more tedious sample preparation steps than the HPLC methods.

The present work proposes to employ indirect conductometric detection to determine the active ingredients in cough–cold syrups after HPLC separation. The advantages of the proposed detection method are: (1) the method works equally well for drugs without UV absorptivity; (2) the detector responses for all the drugs are similar, and (3) it can reduce the number of dilution steps required in the current HPLC methods. The effect of background conductance on detector response, and the factors affecting column separation of the ingredients were studied. The results of analysis were compared with those obtained by HPLC methods using UV detection [11,12].

2. Experimental

2.1. Apparatus

The HPLC system used consisted of a Waters 510 HPLC pump (Millipore Corporation, Waters Chromatography Division, Milford, MA, USA) with an Alltech Free-Flow pulse dampener (Alltech Associates, Deerfield, IL, USA), a Wescan Model 21511001 conductivity detector with Model 24020001 temperature controller and Model 26650051 column compartment (Alltech), a Rheodyne injection valve with a 20-μl sample loop (Rheodyne, Berkeley, CA, USA), and a Beckman 427 signal integrator (Beckman Instruments, Altex Division, San Ramon, CA, USA). An analytical column from Beckman, Ultrasphere 5 μm Spherical 80 Å Pore CN analytical column (250 mm × 4.6 mm) was used. The proposed mobile phase was water–acetonitrile–ethanol (38:60:2) containing 1 m*M* $HClO_4$. Other mobile phases with different acetonitrile contents and perchloric acid strength were also used as indicated in the Results and Discussion section.

Instrumental settings were: flow rate, 1 ml/min; column temperature, 30°C; detector zero suppression, 2; detector range, 1 or 10; and chart speed, 0.5 cm/min.

Peaks were detected as negative changes in conductance, and the detector–integrator connections were reversed in polarity to give positive display of peaks on the integrator.

2.2. Reagents

All the drugs were of BP or USP quality and were used without further purification. HPLC grade solvents were used to prepare the mobile phase. All other chemicals were of analytical reagent grade. Water used was distilled and deionized by passing through Millipore Milli-Q 50 ultra pure water system (Millipore, Molsheim, France).

2.3. Standard solutions

Standard solutions of the drugs used for HPLC measurements were prepared by dissolving the drugs in the mobile phase and diluting to the desired concentrations.

2.4. Determination

Each syrup was diluted with the mobile phase to give a final concentration of the analyte in the range of 5 to 100 μg per ml, and a single dilution in the ratio of 1 to 25 or 1 to 50 usually sufficed. The solution was homogenized by shaking, filtered and then injected into the chromatograph.

2.5. The counter-check HPLC method

The active ingredients in the cough–cold syrups were counter checked by HPLC methods with UV detection as proposed by Koziol et al. [11] and Chao et al. [12] but with slight modification in the composition of the mobile phase to optimise column separation.

The HPLC system consisted of a Beckman 110B Solvent Delivery Module, a Waters Lambda-Max Model 481 LC UV Detector and a Beckman 427 integrator. The injection port was

a Rheodyne injector with sample loop size of 20 μl. An Alltech 5 μm Econosphere C_{18} stainless steel column (250 mm × 4.6 mm) was used.

3. Results and discussion

3.1. Characteristics of the chromatogram

Retention of the drugs

The retention times (t_R) and capacity factors of the drugs using different mobile phases are listed in Table 1.

There was baseline resolution of all the drugs with the exception of codeine–ephedrine, where the resolution was about 0.9. In general, all the above drugs could be determined simultaneously in a single chromatographic run, provided that the concentration of each drug is not so high as to produce a very large peak obscuring a neighbouring one.

Solvent peak intensity and analyte concentration

The chromatogram was found to exhibit a negative solvent peak at about 2.5 min. As the polarity of the conductivity detector was reversed, the solvent peak was actually caused by an increase in conductance of the eluent. The peak area or peak height of the solvent peak was found to be directly proportional to the analyte concentration, and the correlation coefficient was better than 0.99 for both peak area and peak height.

3.2. Effect of the composition of mobile phase on the retention time

Changing the water:acetonitrile ratio

It can be seen from Table 1 that the retention times decreased with increase in acetonitrile content, where there was a parallel decrease in the polarity of the mobile phase. Moreover, the rate of decrease was higher for drugs with higher molecular mass, such as bromhexine and chlorpheniramine, which are also more bulky and less polar in nature, compared with those having lower molecular mass and being more polar, such as ephedrine and phenylephrine. The results indicate that hydrophobic interaction of the drugs with the column was one of the essential

Table 1
Effect of acetonitrile content on the retention times (t_R) of the drugs

Drug	t_R(min) in mobile phase			Capacity factor k' (Mobile phase B)
	A	B	C	
Phenylephrine hydrochloride	11.9	8.0	7.4	2.20
Ephedrine hydrochloride	12.7	9.4	7.6	2.76
Codeine phosphate	14.3	9.0	8.1	2.62
Papaverine hydrochloride	19.6	12.1	8.0	3.84
Dextromethorphan hydrobromide	25.5	13.1	8.7	4.24
Diphenhydramine hydrochloride	26.2	14.2	8.3	4.67
Bromhexine hydrochloride	34.8	17.4	8.8	5.96
Chlorpheniramine maleate	35.7	21.2	14.3	7.48

Mobile phases: (A) water–acetonitrile–ethanol (58:40:2) with 1 m*M* $HClO_4$; (B) water–acetonitrile–ethanol (38:60:2) with 1 m*M* $HClO_4$; (C) water–acetonitrile–ethanol (18:80:2) with 1 m*M* $HClO_4$.

operating mechanism for the above column separation.

The mobile phase B shown in Table 1 was chosen as the solvent system for the proposed method as it gave well resolved peaks within about 20 minutes or less for all the drugs under study. Note that two percent of ethanol was added to the above mobile phase to improve column separation efficiency and to enable better degassing of the solvents.

Changing the concentration of the conducting species

The role of perchloric acid in the mobile phase is to create a conducting background to enable detection. Our study on the retention behaviour of the drugs indicated that the retention time decreased with increase in the concentration of perchloric acid. For example, the retention time of the drugs at 1 m*M* $HClO_4$ was found to be only about 0.6 of that at 0.5 m*M* of the acid. A plot of log t_R versus the concentration of perchloric acid, from 0.5 m*M* to 2.0 m*M*, was found to give a correlation coefficient (r) in the range of $-1 < r < -0.9$ for all the drugs under study.

A similar trend in retention time was also observed when the conducting species used was potassium sulphate.

As a similar trend in retention times was observed for different conducting species, the change in retention was unlikely to be caused by the reaction of the eluent conducting species with the drugs. Although protonation of the drugs may, to a certain extent, increase the polarity of the drugs and hence decrease their hydrophobic interaction with the column, this is unlikely to be significant, as replacement of hydronium ion with potassium ion resulted in similar changes. A more plausible explanation is that the higher concentration of the conducting species results in their higher competing power for the active sites on the column and hence the eluting power for the drugs is greater. Moreover, the higher concentration of the conducting species would also increase the polarity of the column surface and hence reduce the hydrophobic interaction of the column with the drugs, resulting in reduction in retention. The decrease in column capacity due to decrease in resin pore size as a result of an increase in ionic content of the mobile phase as proposed by some authors [17] may also be another explanation for the observation.

3.3. Detector response

Effect of molecular mass of the drugs

When the drugs were dissolved in the mobile phase and loaded onto the chromatograph, the counter anions of the drugs being very soluble in the mobile phase were little retained and would be eluted from the column, and hence the detector response of each drug was entirely due to the drug irrespective of the counter anion. It follows that in the discussion below, only the

Table 2
Detector response of ingredients in cough–cold syrups with mobile phase B in Table 1

Ingredient[a]	Detector response[b] ($A \times M$)
Bromhexine hydrochloride (376.1)	8.36
Chlorpheniramine maleate (274.8)	10.08
Codeine phosphate (299.4)	8.15
Dextromethorphan hydrobromide (271.4)	7.75
Diphenhydramine hydrochloride (255.4)	8.19
Ephedrine hydrochloride (165.2)	8.04
Papaverine hydrochloride (339.4)	8.52
Phenylephrine hydrochloride (167.2)	8.10
Average	8.4 (R.S.D. 8.6%)

[a] Molecular mass (M) of the drugs (base form) in parentheses.
[b] A = Area counts per μg.

respective molecular mass (M) of each drug in the base form was considered.

The area response per μg (A) (arbitrary unit) of each drug multiplied by the respective molecular mass (M), ($A \times M$), is shown in column 2 of Table 2. It can be seen that $A \times M$ is essentially constant and has an average value of 8.4 (R.S.D. 8.6%) and six out of the eight values cluster around the value 8.2. $A \times M$ relates the detector response to the same number of molecules as shown below:

$$A \times M = (\text{Area count}/\mu\text{g}) \times M$$
$$= \text{Area count}/(\mu\text{g}/M), \text{ and}$$
$$\mu\text{g}/M \propto \text{no. of molecules per } \mu\text{g}$$

The above result implies that the detector response is directly proportional to the number of molecules, and not dependent on the nature of the analyte.

Effect of the concentration of the conducting species

The peak area response per μg of the drugs eluted with mobile phases having perchloric acid concentrations from 0.5 mM to 2.0 mM were found to be essentially constant and with values within 10% of those given in Table 2. This observation is consistent with our discussion on detection theory that displacement of the background conducting species was quantitative and proportional to the number of analyte species.

3.4. Detection theory

When a solution of the drug was loaded onto the column, the drug in the protonated form was retained by the column while the counter anion was eluted at almost the same time as the solvent. The eluent conducting species, E, which is $HClO_4$ in the present system, dissociates to give anions and cations. Under column equilibrium conditions, the background conductance of the eluent, G_B, as indicated by the conductivity detector of the system can be deduced according to Fritz et al. [18,19] as follows:

$$G_B = \frac{(\lambda_{o,E^+} + \lambda_{o,E^-})\, C_E I_E}{10^{-3} K} \quad (1)$$

where K is the cell constant, λ_{o,E^+} and λ_{o,E^-} are respectively the limiting ionic conductance of the cation and anion of the eluent conducting species, and C_E and I_E are respectively the

Table 3
Results of recovery test and precision study

Ingredient	% Recovery[a]	Precision[b] (R.S.D., %)
Bromhexine hydrochloride	99.6	2.2
Chlorpheniramine maleate	99.8	2.8
Codeine phosphate	103.5	2.0
Dextromethorphan hydrobromide	99.1	1.9
Diphenhydramine hydrochloride	99.5	1.9
Ephedrine hydrochloride	95.1	1.7
Papaverine hydrochloride	98.2	2.6
Phenylephrine hydrochloride	97.7	1.7

[a] Average value of three determinations.
[b] The relative standard deviation of ten replicate determinations of the drugs in cough–cold syrups.

Table 4
Assay results of active ingredients in cough–cold syrups

Sample	Ingredient	Label value, mg per 5 ml	Percentage of label claim	
			Proposed method[a]	HPLC with UV detection[b]
1	Bromhexine hydrochloride	2.5	78 (3.9)	79
	Codeine phosphate	4.5	100 (0.8)	102
	Diphenhydramine hydrochloride	4.5	100 (2.5)	101
	Ephedrine hydrochloride	4.5	104 (1.1)	107
	Papaverine hydrochloride	1.25	100 (2.0)	100
2	Chlorpheniramine maleate	1	100 (5.0)	97
	Dextromethorphan hydrobromide	5	101 (1.3)	101
	Phenylephrine hydrochloride	5	121 (0.3)	122
3	Chlorpheniramine maleate	1	102 (3.1)	95
	Dextromethorphan hydrochloride	5	104 (0.9)	101
	Phenylephrine hydrochloride	5	99 (0.6)	99
4	Codeine phosphate	9	101 (2.6)	100
	Ephedrine hydrochloride	7.2	104 (0.5)	109
5	Chlorpheniramine maleate	4	101 (0.9)	101
	Phenylephrine hydrochloride	5	96 (0.5)	96
6	Chlorpheniramine maleate	2	99 (2.2)	101
	Ephedrine hydrochloride	5	97 (2.5)	105
7	Chlorpheniramine maleate	4	100 (0.8)	103
8	Bromhexine hydrochloride	2.5	101 (1.9)	100
	Codeine phosphate	4.5	99 (1.1)	101
	Diphenhydramine hydrochloride	7.5	100 (0.8)	100
	Ephedrine hydrochloride	7.5	101 (1.9)	100

Table 4 (*Continued*)

Sample	Ingredient	Label value, mg per 5 ml	Percentage of label claim	
			Proposed method[a]	HPLC with UV detection[b]
9	Bromhexine hydrochloride	4	99 (0.7)	102
	Codeine phosphate	4.5	94 (1.1)	101
	Diphenhydramine hydrochloride	4	100 (2.0)	100
	Ephedrine hydrochloride	4	101 (0.9)	102
	Papaverine hydrochloride	1.25	100 (1.2)	102
10	Diphenhydramine hydrochloride	14	97 (3.0)	[c]

[a] Average of three determinations and the relative standard deviation of the triplicate results in percent is shown in parentheses.
[b] Average value of two determinations.
[c] Sample insufficient for measurement.

concentration of the eluent conducting species and the fraction of these species present in the ionic form.

The drug would displace from the column active sites an equivalent number of eluent cations so as to maintain electroneutrality. The eluted eluent cations would cause an instantaneous increase in detector signal and result in the solvent peak the intensity of which, as described above, was found to be proportional to the analyte concentration. Further, when the sample band passes through the detector, the eluent cation concentration is given by:

$$[E^+]_{\text{At sample elution}} = C_E I_E - C_S I_S \quad (2)$$

where C_S is the concentration of the drug in the sample, and I_S is the degree of ionization of the drug. The conductance measured at the detector during sample elution is therefore given by:

$$G_{\text{Elution}} = \frac{\lambda_{o,E^+}(C_E I_E - C_S I_S)}{10^{-3} K} + \frac{\lambda_{o,E^-} C_E I_E}{10^{-3} K} + \frac{\lambda_{o,S^+} C_S I_S}{10^{-3} K} \quad (3)$$

where λ_{o,S^+} is the limiting ionic conductance of the drug. Note that the first term in Eq. 3 is the conductance due to the eluent cation, whose concentration is given by Eq. 2; the second term is the conductance due to the eluent anion, and the third term is the conductance due to the drug itself. The change in conductance (ΔG) associated with the elution of the sample solute is obtained by subtracting the background conductance (Eq. 1) from the conductance during sample elution (Eq. 3). Assuming $I_s = 1$, and $\lambda_{o,S^+} \ll \lambda_{o,E^+}$, since the drugs are bulky and their conductances are much smaller than that of H^+, ΔG takes the form:

$$\Delta G = -\frac{\lambda_{o,E^+} C_S}{10^{-3} K} \quad (4)$$

which indicates that (1) the detector response will be proportional to C_s, the concentration of the drug, and the limiting ionic conductance of the eluent cation, and (2) the signal would be a decrease in conductance. This explains the negative conductance signal as well as the linear relationship of the detector response with the drug concentration.

3.5. Calibration graphs

The calibration graphs were obtained by plotting the peak area (integrator count, unit arbitrary) against the corresponding concentrations of the drug in the mobile phase. In quantitative determination of the active ingredients in cough–cold syrups the results were calculated from the linear regression equations of the calibration graphs, which were found to be linear from 0 to 500 μg/ml at least for a sample size of 20 μl, with correlation coefficients of better than 0.999 for all the plots of peak area vs concentration.

The smallest quantity of each drug that can be measured with an accuracy of within ± 20% of the actual quantity by the proposed system was about 10 nanograms.

3.6. Recovery and precision

The accuracy of the method was studied by adding known amount of each drug separately to a cough–cold syrup where it was known to be absent, and then determining it using the proposed method. Most drugs have recoveries of around 98–99%. Only codeine and ephedrine have poorer recoveries of 103.5 and 95.1 respectively.

The precision of the method was studied by determining the concentration of each drug in cough–cold syrups ten times by the proposed method.

The results of recovery and precision study as shown in Table 3 indicate that the method is reliable and precise.

3.7. Determination of active ingredients in cough–cold syrups

The contents of the eight drugs in nine cough–cold syrups were determined by the proposed method and the results are presented in Table 4. The chromatograms of two cough–cold syrups are shown in Figs. 1 and 2, respectively. Apart from slightly high deviations from spectrophotometric detection observed for some of the results of codeine and ephedrine, which were mainly due to their incomplete baseline resolution by the cyano column and their closeness to the excipient peak, there were in general close agreements between the results obtained using the proposed method and those using the HPLC

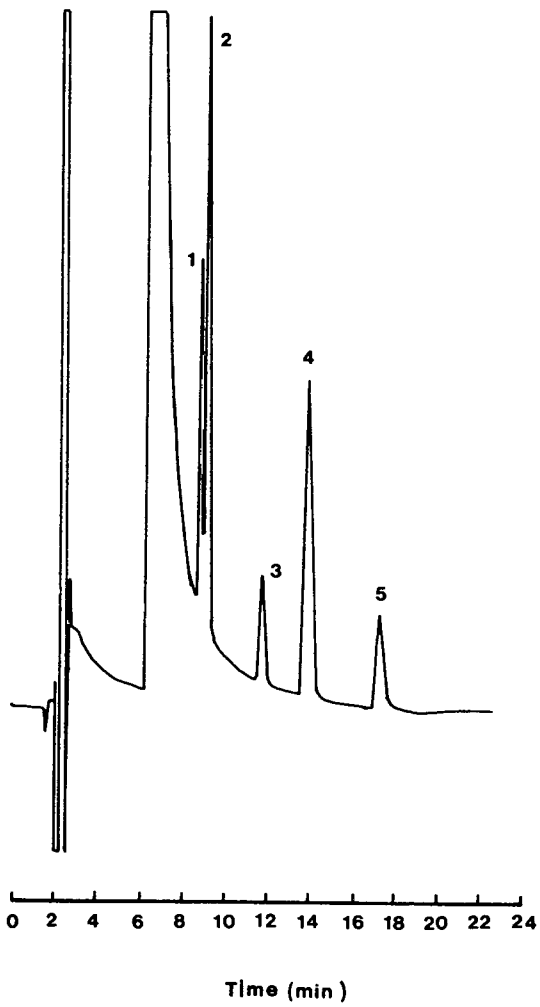

Fig. 1. Indirect conductometric detection of ingredients in cough–cold syrup No. 1. Peaks: 1 = codeine phosphate (0.36 μg); 2 = ephedrine hydrochloride (0.36 μg); 3 = papaverine hydrochloride (0.1 μg); 4 = diphenhydramine hydrochloride (0.36 μg) and 5 = bromhexine hydrochloride (0.2 μg). Excipient peak at about 7 min.

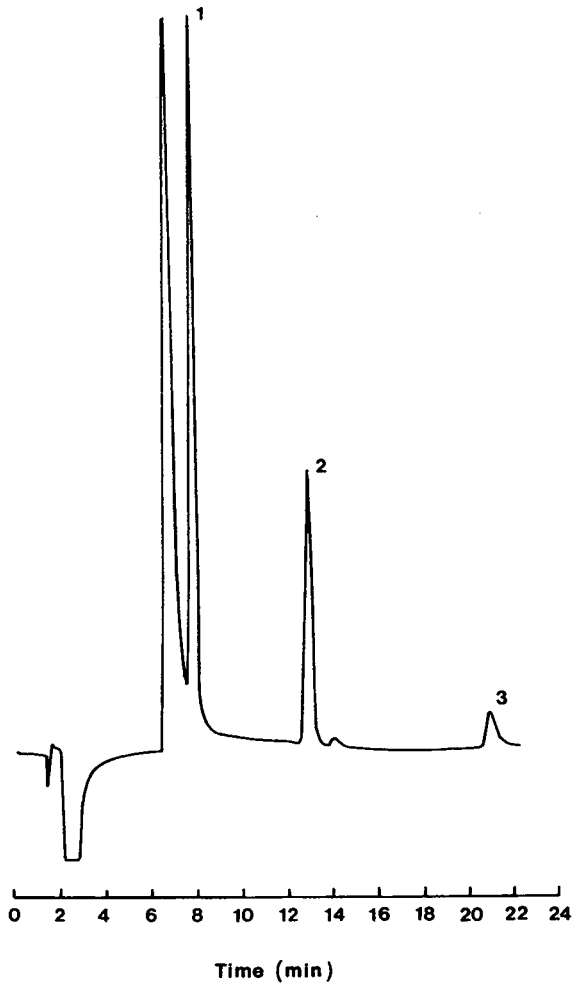

Fig. 2. Indirect conductometric detection of ingredients in cough–cold syrup No. 3. Peaks: 1 = phenylephrine hydrochloride (0.4 μg); 2 = dextromethorphan hydrobromide (0.4 μg) and 3 = chlorpheniramine maleate (0.08 μg). Excipient peak at about 7 min.

method with spectrophotometric detection, the deviations being generally less than 5%.

4. Conclusion

The present study has shown that indirect conductometric detection is a sensitive, reliable and accurate method for the determination of active ingredients in cough–cold syrups. A similar approach can be applied to determine other drugs in pharmaceutical preparations. The proposed detection method is sensitive, as it can detect the drugs down to nanogram levels, with a wide linear range of detector response, which covers most analytical applications on drugs analysis. The beauty of the method is that it does not rely on any specific functional group for detection, and hence, that drugs and other organic compounds which could not be detected previously because of the lack of specific functional group can now be detected.

The detector responses of all the drugs are similar and are proportional to the number of molecules, which enables the ingredients in many pharmaceutical preparations to be analysed in a single chromatographic run, and dilutions necessary to for the concentrations of the analytes to fall within the detector ranges can be greatly reduced. The method is straightforward and simpler than the commonly used HPLC methods involving ion pairing or derivatization.

References

[1] *British Pharmacopoeia 1993*, Her Majesty's Stationery Office, London, 1993.
[2] J.E.F. Reynolds (Editor), *Martindale, The Extra Pharmacopoeia*, The Pharmaceutical Press, London, 29th ed., 1989.
[3] E.G.C. Clarke (Editor), *Isolation and Identification of Drugs*, Vols. 1 and 2, The Pharmaceutical Press, London, 1975.
[4] M. Windholz (Editor), *The Merck Index*, Merck, Rahway, N.J., 11th ed., 1989.
[5] *The United States Pharmacopeia*, XXIInd Revision, United States Pharmacopeial Convention, Rockville, MD, 1990.
[6] O.W. Lau, K. Chan, Y.K. Lau and W.C. Wong, *J. Pharm. Biomed. Anal.*, 7 (1989) 725, and references cited therein.
[7] E.V. Rao, G.R. Rao, S. Raghuveer and P. Khadgapathi, *Analyst*, 112 (1987) 871.
[8] V. Gibbs and Z. Zaide, *J. Pharm. Sci.*, 73 (1984) 1248.
[9] L. Carnevale, *J. Pharm. Sci.*, 72 (1983) 196.
[10] E.J. Kubiak and J.W. Munson, *J. Pharm. Sci.*, 69 (1980) 152.

[11] T.R. Koziol, J.T. Jacob and R.G. Achari, *J. Pharm. Sci.*, 68 (1979) 1135.
[12] M.K. Chao, I.J. Holcomb and S.A. Fusari, *J. Pharm. Sci.*, 68 (1979) 1463.
[13] C.P. Leung and C.K. Law, *Analyst*, 114 (1989) 241.
[14] J.L. Murtha, T.N. Julian and G.W. Radebaugh, *J. Pharm. Sci.*, 77 (1988) 715.
[15] J.M. Hoover, R.A. Soltero and P.C. Bansal, *J. Pharm. Sci.*, 76 (1987) 242.
[16] O.W. Lau and Y.M. Cheung, *Analyst*, 115 (1990) 1349.
[17] J.Å. Jönsson (Editor), *Chromatographic Theory and Basic Principles*, Marcel Dekker, New York, 1987, p. 325 and references cited therein.
[18] D.T. Gjerde and J.S. Fritz, *Anal. Chem.*, 53 (1981) 2324.
[19] J.S. Fritz, D.T. Gjerde and R.M. Becker, *Anal. Chem.*, 52 (1980) 1519.

ELSEVIER

Journal of Chromatography A, 693 (1995) 55–61

JOURNAL OF CHROMATOGRAPHY A

Separation of geometrical *syn* and *anti* isomers of obidoxime by ion-pair high-performance liquid chromatography☆

U. Spöhrer, P. Eyer*

Walther-Straub-Institut für Pharmakologie und Toxikologie, Ludwig-Maximilians-Universität München, Nussbaumstrasse 26, D-80336 Munich, Germany

First received 12 July 1994; revised manuscript received 18 October 1994; accepted 18 October 1994

Abstract

Obidoxime chloride (Toxogonin) is one of the fastest reactivating oximes to restore acetylcholinesterase activity after intoxication with organophosphates. Reversed-phase HPLC analysis with ion-pairing reagents revealed the existence of three geometrical isomers, both in solid obidoxime dichloride monohydrate and in solution (Toxogonin ampoules). The *syn–syn* isomer prevails, the asymmetric *syn–anti* isomer amounts to 5% (solid) and 3% (solution) and the symmetric *anti–anti* isomer less than 0.1%. The structure of the *syn–anti* isomer isolated by ion-exchange chromatography was confined by ^{1}H NMR spectroscopy. The acidity of the oxime protons decreased from the *syn–syn* isomer (mean pK_a 8.0) to the *syn–anti* (mean pK_a 8.3) and the *anti–anti* form (mean pK_a 8.6). In addition, the absorption maximum of the oximate was shifted from 356 (*syn–syn*) to 360 (*syn–anti*) and 367 nm (*anti–anti*). Analysis of outdated Toxogonin ampoules that had been stored at about 20°C for up to 19 years indicated a shelf-life (10% decomposition) of ca. 20 years, which is less than predicted earlier from advanced decomposition studies. Cyanide formation was negligible, and the ratio of *syn–syn*- to *syn–anti*-obidoxime still remained at 3%.

1. Introduction

Mono- and bispyridinium aldoximes have been shown to be effective adjuncts to atropine in the treatment of organophosphate intoxications. Obidoxime (Toxogonin) [1] is used therapeutically in insecticide poisonings in Germany, Israel, Netherlands, South Africa, Sweden, Switzerland and in various developing countries. Obidoxime (Fig. 1) is one of the fastest reactivating oximes [2–8], although not effective in soman poisoning [9,10].

To improve the therapeutic effectiveness of obidoxime treatment in patients with intoxications by long-residing thiono organophosphate insecticides, e.g., parathion, we considered continuous infusion of obidoxime to be more appro-

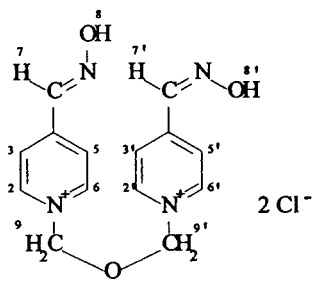

Fig. 1. Structure of *syn–anti*-obidoxime (obidoxime-I).

* Corresponding author.

0021-9673/95/$09.50
SSDI 0021-9673(94)01012-9

priate than a single injection. Similar recommendations have recently been published for treatment with pralidoxime (2-PAM) [11]. To follow the plasma concentrations reliably, we adopted a reversed-phase HPLC method using ion-pairing reagents, as previously applied for quantitative determination of other pyridinium oximes [12–15].

When we succeeded in an improved HPLC separation of obidoxime without tailing, we became aware of a by-product (3–5%) that was found in solid obidoxime, in freshly manufactured Toxogonin ampoules and in outdated batches. Such a compound has already been noted by Benschop et al. [12], who considered it to be a decomposition product of the obidoxime bulk. More recently it has been reported that freshly prepared obidoxime solutions also contain a compound (about 4%) that was suggested to be a regioisomer of obidoxime [16].

Oximes can possess two isomeric configurations, *syn* and *anti*. Poziomek et al. [17] succeeded in isolating the two geometrical isomers of 4-PAM [4-(hydroxyiminomethyl) pyridinium methochloride], which were characterized by ^{1}H NMR spectroscopy. Interestingly, the *syn* isomer of 4-PAM has a higher reactivity towards inhibited acetylcholinesterase than the *anti* isomer: sarin-inhibited electric eel enzyme was reactivated about three times faster by the *syn* isomer.

The structure of 2-PAM as the *syn* isomer has been unequivocally proved by X-ray crystallography [18]. Until now, the pure *anti* isomer of 2-PAM has not been prepared, probably because the *anti* isomer rapidly isomerizes to give the *syn* isomer or decomposes into the nitrile and carboxamido derivative. Utley [14] was probably the first to detect small amounts of the *anti* isomer in solutions of 2-PAM by HPLC. This isomer is hardly detected in freshly prepared 2-PAM solutions but gradually increases to an equilibrium concentration of approximately 3% [14,19]. It has been suggested that the major degradation reactions proceed from the more unstable *anti* isomer of 2-PAM [20].

In the description of obidoxime synthesis, Lüttringhaus and Hagedorn [1] already mentioned that two isomers of obidoxime can be obtained which are interconvertible. During storage the more stable *syn–syn* isomer is formed. Later, preparation of the pure obidoxime isomers was claimed [21] with the *syn* isomer being twice as effective as the *anti* isomer in organophosphate-poisoned mice. Whether the mentioned *anti* isomer of obidoxime possesses a symmetrical *anti–anti* or an asymmetric *syn–anti* configuration has not been reported.

In this study, we describe the isolation and properties of a major by-product of commercial obidoxime preparations that was identified as an asymmetric *syn–anti* isomer of obidoxime. A minor by-product was tentatively described as the *anti–anti* isomer. In addition, we analysed Toxogonin ampoules that had been stored at ambient temperature for up to 19 years to determine the chemical stability and the degradation products in pharmaceutical preparations of obidoxime.

2. Experimental

Solid obidoxime dichloride monohydrate was obtained from Duphar (Amsterdam, Netherlands; batch 058646-FOA 009090). According to the analysis certificate this preparation contained 94.5% obidoxime dichloride and 4.5% water (Karl Fischer) with 4-pyridinealdoxime below 0.1%.

Toxogonin ampoules (1 ml containing 250 mg of obidoxime dichloride, 0.65 mg of methyl 4-hydroxybenzoate and 0.35 mg of propyl 4-hydroxybenzoate) were purchased from Merck (Darmstadt, Germany) and stored for up to 19 years at different places at ambient temperatures averaging between 16 and 21°C.

An attempt to separate obidoxime-I (the *syn–anti* isomer present at about 5% in the solid obidoxime preparation) by fractional crystallization of obidoxime-II, the *syn–syn* isomer, in weakly acidic (pH 4) solution was unsuccessful. However, the separation of the two isomers as monobetaine salts allowed an easy enrichment. Monobetaine formation was carried out as described [1]: about 1 g of obidoxime dichloride monohydrate was dissolved in 3 ml of water at

30°C and mixed with finely ground sodium carbonate (0.27 g) with vigorous stirring (pH 8.1). The colour of the solution changed immediately to red-orange and became turbid. Precipitation was advanced by adding 1 ml of 2-propanol dropwise. After storage in a refrigerator for 1 h, the orange precipitate was centrifuged and the dark supernatant, which had an obidoxime-I to obidoxime-II ratio of about 1:3, was removed. Further crystallizations increased the portion of obidoxime-I in the supernatant only marginally. Therefore, we took advantage of their differences in acidity and separated the two isomers in the supernatant by ion-exchange chromatography.

The monobetaines (12.5 mg of obidoxime-I in 200 ml) were chromatographed on CM_{50}-Sephadex (18 × 5 cm I.D. column; equilibrated with 10 m*M* ammonium acetate, pH 8.5). Obidoxime-II was eluted first when a linear gradient (500 ml of 10 m*M*–500 ml of 20 m*M* ammonium acetate, pH 8.5) was applied, followed by obidoxime-I and a small additional peak eluting last. The first cut, containing obidoxime-II, was pure as judged by HPLC. Cut 2, containing obidomine-I was >99% pure, but tended to isomerize slowly upon lyophilization (5% obidoxime-II). The amount of the material eluting last was too small for NMR analysis but allowed characterization by UV spectroscopic titration (obidoxime-0).

For ^1H NMR spectroscopy, both lyophilized isomers were dissolved in ^2H_2O and measured in a 500-MHz Bruker instrument with H_2O set to 4.80 ppm.

2.1. Analytical procedure

The pK_a values of the oxime functions were investigated by spectroscopic titration at 20°C. Oximate formation was followed at around 360 nm. According to the Henderson–Hasselbalch equation, log ($[A^-]/[HA]$) was plotted versus pH, which gives pK_a at $\log([A]/[HA]) = 0$. On changing the pH, perfect isosbesticity was observed throughout. For spectroscopic determinations of more concentrated solutions (up to 30 m*M*), cuvettes with shorter light paths were used (0.01, 0.1, 1 and 10 mm; Hellma, Freiburg, Germany). Electronic spectra were recorded with a UV-265 spectrophotometer (Shimadzu, Duisburg, Germany).

The obidoxime isomers and some of their decomposition products were determined by HPLC on LiChrospher 60 RP-select B (5 μm) (Merck) with an L-6200A pump (Merck) at a flow-rate of 1.2 ml/min. The mobile phase consisted of methanol–PIC-B7–PIC-A (12:4:0.5 ml, diluted to 100 ml with water). The ion-pairing reagents PIC-B7 and PIC-A were obtained from Waters–Millipore (Eschborn, Germany). PIC-A was included to reduce peak tailing of obidoxime. Peaks were quantified with an SPD-6AV UV–Vis detector or an SPD M6A diode-array detector (Shimadzu) and a D-2500 chromato-integrator (Merck) calibrated with authentic standards. The detection wavelength was set to 285 nm.

Formaldehyde was determined as formaldimedone [22]. Hydrocyanic acid was determined spectrophotometrically by the Zincke–König reaction [23]. The ampoules were cooled on ice before opening and the contents transferred immediately into Fernbach flasks for microdiffusion of hydrocyanic acid [23].

3. Results and discussion

When freshly prepared obidoxime solutions were analysed by HPLC (Fig. 2), several by-products were observed that were also found in Toxogonin ampoules. The major by-product (peak I) and the main compound (peak II) had virtually the same UV spectra (Fig. 3). Rechromatography of the cuts from several HPLC runs showed that the compounds did not change their individual retention times. Hence, the by-product giving peak I was tentatively assumed to be a regioisomer of obidoxime. Similarly, a compound eluting earlier (by-product giving peak 0, Fig. 2) had spectroscopic properties similar to those of the main compound. The material eluting after 2.2 min had an identical retention time (sample spiking) and UV spectrum as 4-pyridinealdoxime and amounted to less than

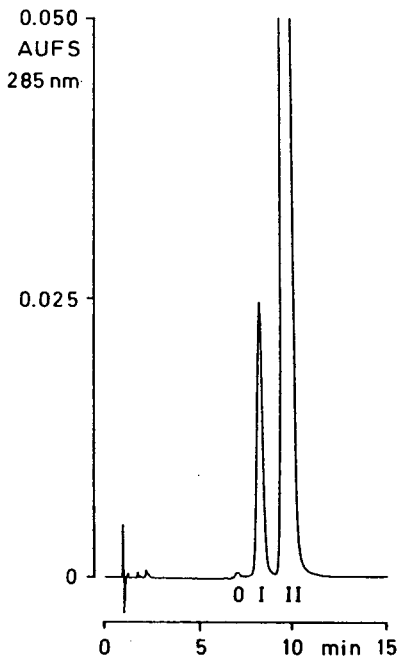

Fig. 2. HPLC analysis of freshly dissolved obidoxime dichloride. Peaks: 6.84 min = *anti–anti*-obidoxime (0.07%); 7.94 min = *syn–anti*-obidoxime (5.1%); 9.32 min = *syn–syn*-obidoxime (94.8%).

0.1%. This material probably originated from obidoxime synthesis.

Spectroscopic titration of the tentative obidoxime isomers that were obtained from several HPLC runs (cf., Fig. 2) showed different pK_a values of the oxime functions. We intentionally exploited this behaviour to separate the compounds on a larger scale by anion-exchange chromatography.

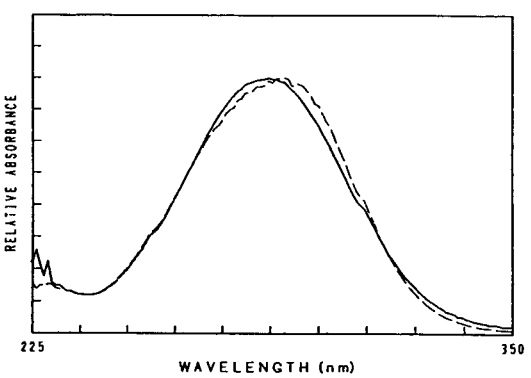

Fig. 3. UV spectra of two obidoxime isomers. Spectra of the HPLC eluate (pH 4) were recorded with a diode-array detector and normalized to the same relative absorbance. Solid line, *syn–syn*-obidoxime; dashed line, *syn–anti*-obidoxime.

The structure (Fig. 1) of the isolated obidoxime-I and obidoxime-II was confirmed by ^1H NMR spectroscopy. The data summarized in Table 1 indicate that obidoxime-II possesses the symmetric *syn–syn* configuration whereas obidoxime-I showed some asymmetry with four different aromatic proton signals, two different methine resonances and two different methylene signals. Particularly striking were the differences in the proton signals 3′ and 5′, which were shifted by 0.39 ppm to lower field in the *anti* configuration, while the signal of the methine proton (7′) was shifted by 0.47 ppm to higher field. Such a behaviour has been repeatedly described in the literature for other oximes [17,24,25]. The reason for this phenomenon might be the missing coplanarity of the aromatic ring and the aldoxime group in the case of the *anti* configuration, while the diamagnetic anisotropy of the oxime group has been suggested to strengthen the outer field at the methine proton in the *syn* configuration [24,25]. The isolated material of obidoxime-0 was too small for ^1H NMR analysis.

UV spectroscopic titration of the three obidoxime isomers indicated a systematic difference in acidity of the oxime function, being highest in the *syn–syn* and lowest in the assumed *anti–anti* configuration (Table 2). Such a phenomenon has been discussed previously [24,25]. Moreover, the absorption maximum of the oximate was shifted to longer wavelengths from *syn–syn* to *anti–anti*. This behaviour has been previously described for *syn–anti* isomerism of other oxime compounds [24,25].

HPLC analysis of outdated Toxogonin ampoules that had been stored up to 19 years indicated several additional products (Fig. 4). The material that eluted first (M-1; 1.89 min) had similar spectroscopic characteristics to obidoxime. The oxime maximum at 284 nm changed to 354 nm on alkalinization. In addition a second maximum was present at 262 nm that

Table 1
^{1}H NMR data for obidoxime isomers

Position	Obidoxime-II (*syn–syn*)			Obidoxime-I (*syn–anti*)		
	δ (ppm)	*J* (Hz)	Relative intensity	δ (ppm)	*J* (Hz)	Relative intensity
2	8.88	6.9	1	8.91	6.5	1
3	8.20	6.9	1	8.22	6.5	1
5	8.20	6.9	1	8.22	6.5	1
6	8.88	6.9	1	8.91	6.5	1
7	8.33		1	8.34		1
9	6.17		2	6.19		2
2′	8.88	6.9	1	9.07	6.6	1
3′	8.20	6.9	1	8.59	6.6	1
5′	8.20	6.9	1	8.59	6.6	1
6′	8.88	6.9	1	9.07	6.6	1
7′	8.33		1	7.86		1
9′	6.17		2	6.24		2

^{1}H NMR spectra were recorded in ^2H_2O (H_2O = 4.80 ppm). For assignments, see Fig. 1.

did not show any pH dependence. These figures indicate that one oxime function had remained whereas the other pyridinium ring probably had a 4-carboxy or carboxamido function [22]. Because of the high polarity of the compound, we favour an isonicotinic acid structure and tentatively assign the compound as 4′-carboxy-4-(hydroxyiminomethyl)-1,1′-oxydimethylenedipyridinium dichloride. Such a degradation pathway has already been described [26,27].

The material eluting at 2.2 min was 4-pyridinealdoxime. The amount of the material eluting at 4.72 min was too small for further analysis. The compounds eluting at 7.55, 8.9 and 10.55 min belong to the regioisomers of obidoxime. As formaldehyde and cyanide can be formed during degradation of obidoxime [26,28], we analysed the different batches accordingly. Table 3 gives the amounts of compounds found in the various batches.

Visual examination of the outdated Toxogonin ampoules that had been stored between 16 and 20°C on average showed that the oldest preparations had the most intense orange colour, whereas freshly prepared solutions were almost colourless. As the pH of the old batches was lower (pH 3.6) than in fresh solutions (pH 4.0) a change in colour due to the formation of the orange betaine form [1] was unlikely. In fact, spectroscopy of the solutions at pH 4 between 800 and 500 nm excluded a charge-transfer complex [1]. Rather, the absorbance gradually increased without the formation of distinct maxima or shoulders in the visible spectrum. All batches revealed the typical obidoxime maximum at 285 nm.

Table 2
UV spectroscopic data and pK_a values for obidoxime isomers

Compound	Obidoxime-II	Obidoxime-I	Obidoxime-0
Tentative structure	*syn–syn*	*syn–anti*	*anti–anti*
Absorption maximum of the betaine (nm)	356	360	367
pK_a	8.0	8.3	8.6

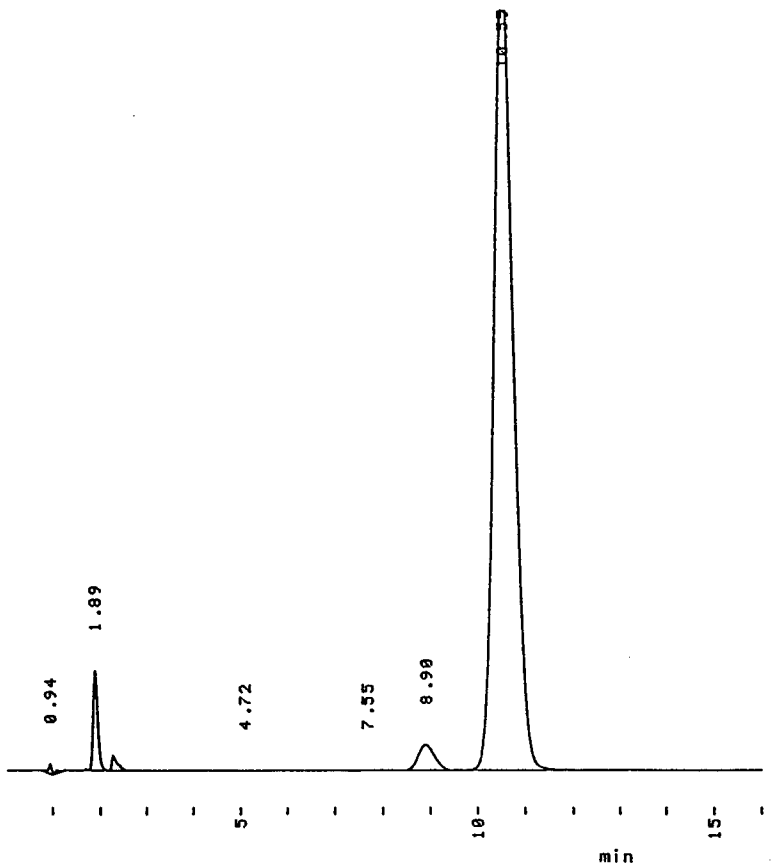

Fig. 4. HPLC analysis of an outdated Toxogonin ampoule. The following products were tentatively assigned: 1.89 min = 4′-carboxy-4-(hydroxyiminomethyl)-1,1′-oxydimethylenedipyridinium dichloride; 2.20 min = 4-pyridinealdoxime; 7.55 min = *anti–anti*-obidoxime; 8.90 min = *syn–anti*-obidoxime; 10.55 min = *syn–syn* obidoxime.

Table 3
Analysis of Toxogonin ampoules

Storage (years)	pH	Colour[a]	M-1 (%)	4-PAO (%)	CH_2O (%)	HCN (10^{-3} %)	Obi-1 (%)	Obi-2 (%)
19	3.57	0.54	2.4	0.83	0.16	0.32	2.90	89.0
14	3.62	0.37	2.3	0.97	0.08	0.27	3.04	88.5
14	3.62	0.41	2.3	0.93	0.10	0.35	3.00	89.3
14	3.70	0.30	1.8	0.63	0.08	0.29	3.03	91.7
14	3.63	0.34	0.8	0.73	0.12	0.29	3.04	90.0
14	3.54	0.16	2.2	0.40	0.06	0.20	3.12	90.9
2	4.00	0.05	0.2	0.06	0.04	0.11	3.04	95.9

Mean values of three determinations per batch. Abbreviations: M-1 = 4′-carboxy-4-(hydroxyiminomethyl)-1,1′-oxydimethylenedipyridinium dichloride; 4-PAO = 4-pyridinealdoxime; Obi-1 = *syn–anti*-obidoxime; Obi-2 = *syn–syn*-obidoxime.
[a] Colour: molar absorptivity of a 1% solution at 400 nm.

It has been mentioned [1] that the molar absorptivity of the oximate did not follow the Lambert–Beer law. This observation was confirmed by Schoene [29], who reported on bathochromic and hypsochromic shifts of the oximate spectra in increasingly concentrated solutions. These experiments were performed in 0.5–50 m*M* obidoxime solutions (pH 7.5). To allow readings at these high concentrations, Schoene used cuvettes with a 1-mm light path and made use of difference spectroscopy, e.g., sample cuvette 50 m*M*, reference cuvette 37.5 m*M* obidoxime [29]. Of course, such measurements are detrimentally falsified by stray light (50 m*M* obidoxime at pH 7.5 has a molar absorptivity at 334 nm of about 100 $l \cdot mol^{-1} \cdot cm^{-1}$ with a 1-mm light path!). When we repeated these measurements using quartz cuvettes with 0.01–10-mm light paths at pH 3, 7.5 and 8.0, the spectra followed the Lambert–Beer law perfectly. No bathochromic shifts were observed. Hence, we cannot confirm spectroscopic anomalies that had been interpreted as indicative of charge-transfer complex formation [29]. Thus, the orange colour probably stems from an unknown decomposition product.

Overall, this study has shown that obidoxime solutions contain about 3% of the asymmetric *syn–anti* isomer and about 96% of the *syn–syn* isomer. Solid obidoxime dichloride contains almost 5% of the *syn–anti* isomer. In addition, we could confirm the high stability of obidoxime solutions with a shelf-life of almost 20 years when stored around 20°C. The stability, however, is less than predicted from advanced decomposition studies (calculated shelf-life of about 100 years at 25°C [30]).

References

[1] A. Lüttringhaus and I. Hagedorn, *Arzneim. Forsch.*, 14 (1964) 1–5.

[2] K. Schoene and E.-M. Strake, *Biochem. Pharmacol.*, 20 (1971) 1041–1051.

[3] W.D. Erdmann and M. v. Clarmann, *Dtsch. Med. Wochenschr.*, 88 (1963) 2201–2206.

[4] E. Heilbronn, and B. Tolagen, *Biochem. Pharmacol.*, 14 (1965) 73–77.

[5] J. Knolle, *Klin. Wochenschr.*, 48 (1970) 1157–1168.

[6] I. Stark, *Thesis*, University, Freiburg, 1971.

[7] I. Stark, *Chem. Unserer Zeit*, 18 (1984) 96–106.

[8] W.L.A.M., De Kort, S.H. Kiestra and B. Sangster, *J. Toxicol. Clin. Toxicol.*, 26 (1988) 199–208.

[9] O.L. Wolthuis and E.M. Cohen, *Biochem. Pharmacol.*, 16 (1967) 361–367.

[10] K. Schoene and H. Oldiges, *Arch. Int. Pharmacodyn. Ther.*, 204 (1973) 110–123.

[11] J.L. Willems, H.C. De Bisschop, A.G. Verstraete, C. Declerck, Y. Christiaens, P. Vanscheeuwyck, W.A. Buylaert, D. Vogelaers and F. Colardyn, *Arch. Toxicol.*, 67 (1993) 79–84.

[12] H.P. Benschop, K.A.G. Konings, S.P. Kossen and D.A. Ligtenstein, *J. Chromatogr.*, 225 (1981) 107–114.

[13] N.D. Brown, M.P. Strickler, H.K. Sleeman and B.P. Doctor, *J. Chromatogr.*, 212 (1981) 361–365.

[14] D. Utley, *J. Chromatogr.*, 265 (1983) 311–322.

[15] P. Eyer, and W. Hell, *Arch. Pharm.* 318 (1985) 938–946.

[16] B.M. Paddle and M.H. Dowling, *J. Chromatogr.*, 648 (1993) 373–380.

[17] E.J. Poziomek, D.N. Kramer, W.A. Mosher and H.O. Michel, *J. Am. Chem. Soc.*, 83 (1961) 3916–3917.

[18] D. Carlström, *Acta Chem. Scand.*, 20 (1966) 1240–1246.

[19] D.G. Prue, R.N. Johnson and B.T. Kho, *J. Pharm. Sci.*, 72 (1983) 751–756.

[20] D. Utley, *J. Chromatogr.*, 396 (1987) 237–250.

[21] L. Leitis, M.V. Shimanskaya and A. Varslavans, *Latv. PSR Zinat. Akad. Vestis, Kim. Ser. (2)*, (1969) 249–250.

[22] P. Eyer, W. Hell, A. Kawan and H. Klehr, *Arch. Toxicol.*, 59 (1986) 266–271.

[23] P. Eyer, A. Kawan and B. Ladstetter, *Arch. Toxicol.*, 61 (1987) 63–69.

[24] I. Pejkovic-Tadic, M. Hranisavljevic-Jakovljevic, S. Nesic, C. Pascual and W. Simon, *Helv. Chim. Acta*, 48 (1965) 1157–1160.

[25] H.P. Lorenz, *Thesis*, University, Freiburg, 1974.

[26] R. Bernasconi, *Pharm. Acta Helv.*, 40 (1965) 564–574.

[27] I. Christenson, *Acta Pharm. Suec.*, 5 (1968) 23–36.

[28] I. Christenson, *Acta Pharm. Suec.*, 9 (1972) 309–322.

[29] K. Schoene, *Arzneim. Forsch.*, 18 (1968) 1350–1351.

[30] I. Christenson, *Acta Pharm. Suec.*, 5 (1968) 249–262.

ELSEVIER

Journal of Chromatography A, 693 (1995) 63–68

JOURNAL OF CHROMATOGRAPHY A

Direct high-performance liquid chromatographic resolution of planar chiral tricarbonyl (η^6-arene)–chromium(0) complexes

Claudio Villani[1], William H. Pirkle*

School of Chemical Sciences, University of Illinois, Urbana, IL 61801, USA

First received 7 September 1994; revised manuscript received 24 October 1994; accepted 24 October 1994

Abstract

Thirty-four disubstituted tricarbonyl (η^6-arene)–chromium complexes having planar chirality were examined by HPLC on a recently developed chiral stationary phase (CSP). This CSP contains "active sites" comprised of clefts formed by the perpendicular disposition of π-acidic 3,5-dinitrobenzamide groups relative to π-basic naphthyl groups. Thirty of the thirty-four show different retention factors for their enantiomers. A mechanistic hypothesis which accounts for the enantiodiscrimination is presented. The arene, using the face *anti* to the tricarbonylchromium, enters the cleft and undergoes simultaneous face-to-face and face-to-edge $\pi-\pi$ interactions with the aromatic "walls" of the cleft. Hydrogen bond formation provides a third attractive interaction, facilitating enantiodiscrimination.

1. Introduction

Disubstituted tricarbonyl (η^6-arene)–chromium complexes are chiral when the substituents are different and either *ortho* or *meta* to each other. Owing to the altered reactivity of the arenes in these chromium complexes, the steric shielding exerted by the bulky metal fragment, and the ease of removal of the chromium moiety, there has been a rapid increase in the use of planar chiral (arene) tricarbonyl–chromium complexes in asymmetric synthesis [1–3]. Although a number of synthetic applications of enantiomerically pure complexes have been described, there are relatively few examples of the chromatographic separation of the enantiomers of these complexes on chiral stationary phases (CSPs). For these few examples, analytical-scale separations have been conducted on stationary phases in which carbohydrate derivatives have been coated on silica [4–6] whereas microcrystalline triacetylcellulose has been used for preparative-scale separations [7–9].

In the present paper, we describe the chromatographic behavior of thirty-four chiral chromium–tricarbonylarene complexes on CSP 1, a new brush-type CSP [10,11]. In 30 of the 34

* Corresponding author.

[1] Present address: Dipartimento di Studi di Chimica e Tecnologia delle Sostanze Biologicamente Attive, Universitá "La Sapienza", P.le A. Moro 5, 00185 Rome, Italy.

0021-9673/95/$09.50
SSDI 0021-9673(94)01041-2

cases, complete or extensive separation of the enantiomers was noted. A recognition model which accounts for the enantioselectivity observed for this class of analytes is presented.

2. Experimental

2.1. Chiral stationary phase

A commercial (*S,S*)-Whelk-O 1 (250 × 4.6 mm; Regis Technologies, Morton Grove, IL, USA) was used for this work.

2.2. Analytes

The racemic chromium complexes were obtained using the standard procedure of thermolysis of $Cr(CO)_6$ in the presence 1–2 mmol of the disubstituted arene in refluxing di-*n*-butyl ether–tetrahydrofuran [12]. As an example, the preparation of (η^6-N-pivaloyl-*o*-toluidine)Cr$(CO)_3$ (**6e**) is described in detail. A mixture of N-pivaloyl-*o*-toluidine (500 mg, 1.72 mmol) and $Cr(CO)_6$ (400 mg, 1.82 mmol) in degassed dibutyl ether (30 ml) and tetrahydrofuran (THF; 3 ml) was heated to reflux for 15 h, cooled, and filtered through a short pad of neutral alumina to remove unreacted $Cr(CO)_6$. Removal of the solvent in vacuo, followed by column chromatography (silica gel, CH_2Cl_2), yielded **6e** (450 mg, 1.37 mmol) as yellow crystals: ^{1}H NMR (C^2HCl_3) δ 1.31 (9 H, s), 2.17 (3 H, s), 5.10–5.20 (1 H, m), 5.35–5.45 (2 H, m), 6.13 (1 H, d, J = 9.0 Hz), 6.88 (1 H, bs); IR (KBr) 3320, 1959, 1888, 1654, 1522 cm^{-1}. Analysis, calculated for $C_{15}H_{17}NO_4Cr$: C, 55.05; H, 5.20; N, 4.28; Cr, 15.90; found: C, 55.35; H, 5.30; N, 4.32; Cr, 15.62. 2-*exo*-Alkylated-1-tetralone complexes [13] (**4d–h**) and N-acylated indole complexes [14] (**5b–f**) were obtained as described in the literature. The chromium complexes were identified by the typical upfield shifts of the aromatic protons of the complexed ring found in the ^{1}H NMR spectra (1–2 ppm relative to the free aromatic ligand) and by the strong CO stretching bands (1990–1880 cm^{-1}) of the $Cr(CO)_3$ group in the Fourier transform (FT) IR spectra.

2.3. Instrumentation

Chromatography was performed using an Anspec-Bischoff Model 2200 isocratic HPLC pump, a Rheodyne 7125 injector with 20-μl sample loop and a Milton Roy LDC UV Monitor D fixed-wavelength detector operating at 254 nm. A Rudolph Autopol III with a 20-cm flow cell was used to monitor the sign of $[\alpha]_D$. A Jasco 500 A spectropolarimeter equipped with a flow cell was used for the on-line recording of circular dichroism (CD) spectra. ^{1}H NMR spectra were obtained using a Varian-XL (200 MHz) spectrometer using tetramethylsilane (δ 0.00 ppm) as an internal reference. FT-IR spectra were obtained (KBr pellets) on a IBM IR-32 spectrometer. Elemental analyses were provided by the University of Illinois microanalytical laboratory.

3. Results and discussion

The data obtained in the resolutions of the racemic $Cr(CO)_3$ complexes on the (*S,S*)-Whelk-O 1 stationary phase are summarized in Table 1. Most of the compounds examined can be baseline-resolved on the (*S,S*)-Whelk-O 1 using 20% 2-propanol in hexane as a mobile phase. These "standard conditions" are used for comparative purposes and are not necessarily optimal for a given analyte. In instances where these conditions afford separation factors of less than 1.1, reduced concentrations of 2-propanol and/or lower temperatures will afford greater resolution values. The use of methylene chloride as a polar modifier gives further improvement in resolutions of the chromium complexes of *ortho*-substituted benzaldehydes **1a** and **b** and acetophenones **2a** and **b**.

Common to the successfully resolved analytes is the presence of an oxygen atom in the arene framework to act as a hydrogen bond acceptor. Non-acylated *ortho*-toluidine or 1,2,3,4-tetrahydroquinoline complexes are not resolved and only marginal separation (observable by polarimetric detection) is obtained for the indole complex, **5a**. In the series of α-tetralone complexes, **4**, enantioselectivity increases with the

Table 1
Chromatographic data for the resolution of tricarbonyl (η^6-arene)–chromium complexes **1–8** on the (*S,S*)-Whelk-O 1

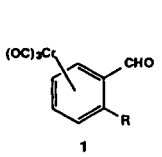

1

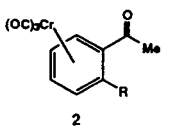

2

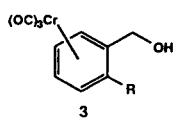

3

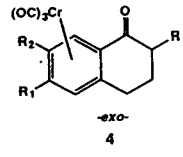

4

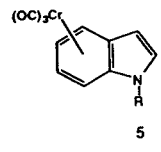

5

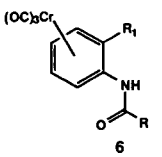

6

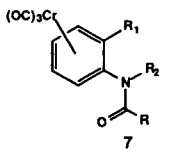

7

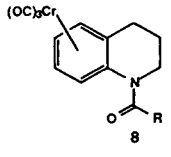

8

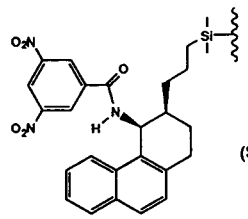

(S,S) Whelk-O 1 CSP

Compound	R	R_1	R_2	k'_1	α	$[\alpha]_D$
1a	CH_3			4.28*	1.07*	+
1b	OCH_3			7.57*	1.09*	+
2a	CH_3			3.57*	1.06*	+
2b	OCH_3			8.00*	1.00*	+
3a	CH_3			1.77	1.11	+
3b	OCH_3			3.22	1.15	+
4a	H	H	H	4.48	1.08	+
4b	H	H	OCH_3	3.82	1.07	+
4c	H	OCH_3	H	5.93	1.18	+
4d	CH_3	H	H	2.25	1.19	+
4e	*n*-C_3H_7	H	H	1.48	1.23	+
4f	Allyl	H	H	1.63	1.21	+
4g	CH_3	OCH_3	H	2.91	1.29	+
4h	Allyl	OCH_3	H	2.07	1.37	+
5a	H			1.57	1.00	+
5b	CO–CH_3			6.79	1.04	+
5c	CO–*n*-C_3H_7			3.36	1.00	−
5d	CO–*n*-C_5H_{11}			2.36	1.09	−
5e	CO–*n*-C_9H_{19}			1.34	1.13	−
5f	CO–*tert.*-C_4H_9			2.28	1.00	−
6a	CH_3	CH_3		4.93	1.62	−
6b	*n*-C_3H_7	CH_3		3.14	1.86	−
6c	*n*-C_5H_{11}	CH_3		2.43	1.88	−
6d	*n*-C_9H_{19}	CH_3		1.79	1.99	−
6e	*tert.*-C_4H_9	CH_3		2.44	1.75	−
6f	*tert.*-C_4H_9	C_2H_5		1.71	1.75	−
6g	*tert.*-C_4H_9	iso-C_3H_7		1.14	1.75	−
6h	*tert.*-C_4H_9	*tert.*-C_4H_9		0.78	1.65	−
6i	*tert.*-C_4H_9	OC_2H_5		1.86	1.69	−
7	*tert.*-C_4H_9	CH_3	CH_3	2.10	1.00	/

(Continued on p. 66)

Table 1 (*continued*).

Compound	R	R_1	R_2	k'_1	α	$[\alpha]_D$
8a	CH_3			11.86	2.08	–
8b	*n*-C_3H_7			3.71	2.50	–
8c	*n*-C_5H_{11}			3.14	2.73	–
8d	*n*-C_9H_{19}			2.30	2.74	–
8e	*tert.*-C_4H_9			2.29	2.46	–

α = Chromatographic separation factor; k'_1 = retention factor of the first-eluted enantiomer using 20% (v/v) 2-propanol in hexane as the mobile phase (asterisk: 30% CH_2Cl_2), flow-rate 2.0 ml/min, temperature 20°C. The $[\alpha]_D$ column gives the sign of $[\alpha]_D$ of the first-eluted enantiomer.

introduction of a *para*-methoxy group and/or an *exo*-alkyl substituent. Elution order, based on polarimetric detection and comparison with literature data [1], is uniform throughout the series, the (1*R*)-enantiomers being more retained on the (*S*,*S*)-CSP. N-Acylindole complexes show reduced enantioselectivity and a change in the sign of rotation of the less retained enantiomer as one passes from **5b** to **5c–f**. The signs of $[a]_D$ have not been related to the absolute configurations of these compounds and while we suspect that there has been an inversion in the order of elution, a change in the sign of rotation cannot be excluded. A change in the order of elution might occur if there is a change in the analyte's conformational preferences (i.e., *E*/*Z* isomerism around the N–CO bond) with an increase in the size of the acyl substituent. Greater enantioselectivities are obtained for the chromium complexes of N-acylated *ortho*-substituted anilines **6a–i** and N-acylated 1,2,3,4-tetrahydroquinolines **8a–e** (Fig. 1).

The elution order for the type **6** and type **8** amide complexes can be established, since (+)-**6a** is known to have the (1*S*)-configuration [15,16]. The on-line recorded CD spectra of the more retained enantiomers of **6a**, **6e** and **8e** are very similar, each having a positive Cotton effect around 320 nm. Since the sign of $[\alpha]_D$ of the least retained enantiomer is always negative, it is believed that each of the more retained enantiomers of the type 6 and type 8 amide complexes listed has the (1*S*)-configuration. Inspection of the data in Table 1 shows that enantioselectivity increases as the steric bulk of the acyl substituent increases. However, the size of the *ortho*-alkyl substituent has little effect on enantioselectivity. On the other hand, no chiral recognition is observed for the corresponding N-methyl derivative, **7**. This can be rationalized by the chiral recognition model depicted in Fig. 2. Here, the chiral selector and each of the analyte enantiomers are shown in stable, highly populated (in solution) conformations. The amide complexes have the carboxamide carbonyl oxygen close to the *ortho*-aromatic hydrogen and the smaller amide hydrogen close to the *ortho* substituent. The aromatic ring is essentially coplanar with the

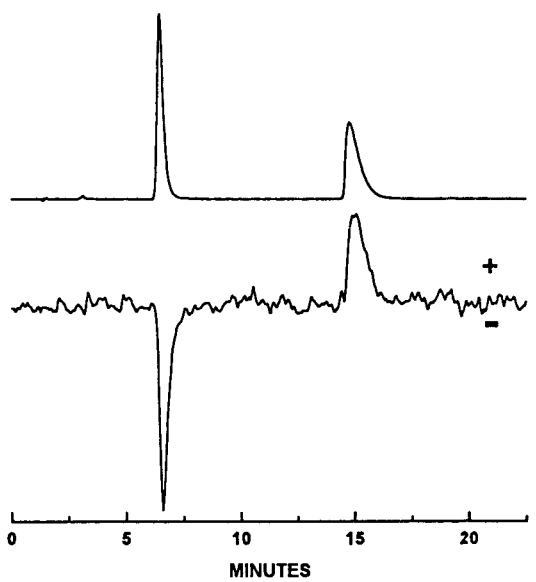

Fig. 1. Resolution of the enantiomers of **8e** on CSP 1, with simultaneous UV (top) and CD (bottom) detection at 320 nm.

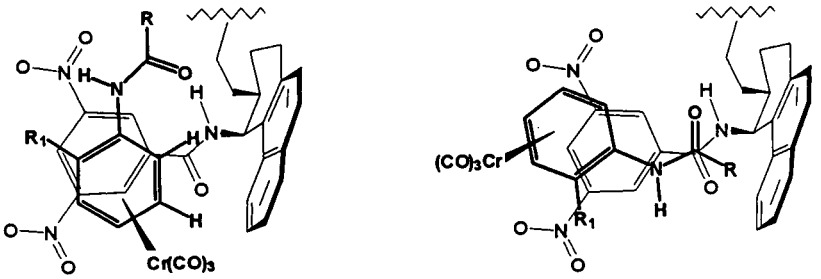

Fig. 2. Proposed recognition model between CSP 1 and the least (left) and most (right) retained enantiomers of amide-type tricarbonyl–chromium complexes.

plane of the carboxamide group. Chemical shifts of the aromatic *ortho*-hydrogens are diagnostic of conformational preferences. In **6a–e** and **8a–e**, they are strongly deshielded (0.6–0.8 ppm) with respect to the remaining aromatic hydrogens. The selector is depicted in the conformation found in the solid state by X-ray diffraction analysis [17].

There are numerous examples of molecular complexes between arenetricarbonyl–chromium compounds and aromatic electron acceptors [18–21]. The principal attractive interactions invoked in the formation of the most stable diastereomeric adsorbate (Fig. 2, left) are a hydrogen bond between the amide N–H of the CSP and the carbonyl oxygen of the analyte and simultaneous face-to-face and face-to-edge $\pi-\pi$ interactions [22] between the aromatic portion of the analyte as it occupies the cleft formed by the 3,5-dinitrobenzamide and the naphthyl group. Even should the less strongly complexed enantiomer enter a cleft, it could not enjoy these three attractive interactions simultaneously. In endeavoring to undergo the hydrogen bonding and face-to-face $\pi-\pi$ interactions, the less strongly complexed enantiomer would, as depicted on the right in Fig. 2, instead of an attractive face-to-edge interaction, encounter a repulsive steric interaction between the alkyl substituent, R, of the analyte and the naphthyl ring of the CSP. The extent of "destabilization" afforded by this interaction would be expected to be related to the effective size of R. In the case of the tertiary amide derivative, **7**, the plane of the carboxamide group is perpendicular to that of the aromatic ring, for all the aromatic hydrogens give a single ^{1}H NMR signal, indicating that they are remote from the carbonyl oxygen. This places the carboxamide oxygen, an essential interaction site, in a different spatial relationship with respect to the other binding sites. This is presumably responsible for the inability of CSP 1 to differentiate between the enantiomers of **7**. Should the carboxamide oxygen be *endo* to the tricarbonyl–chromium portion of the complex, it is evident that neither enantiomer of **7** could utilize this oxygen as a hydrogen bond donor while undergoing a face-to-face $\pi-\pi$ interaction.

The proposed mode of association is consistent with ^{1}H NMR data obtained from mixtures of (*S,S*)-**9**, a soluble analogue, of the selector used in CSP 1, and each of the enantiomers of **8e**. For example, the resonance of the NH hydrogen of (*S,S*)-**9** (0.047 *M* in $C^2H_2Cl_2$, $\delta = 6.65$ ppm) is shifted downfield by 0.20 and 0.10 ppm, respectively, in the presence of equimolar amounts of (1*S*)-**8e** or (1*R*)-**8e**. This indicates more extensive hydrogen bond formation in the former mixture, a mixture containing the enantiomer more strongly retained by CSP 1.

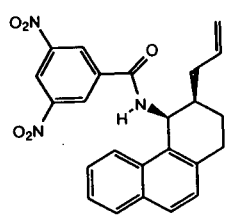

(S,S)-9

Upfield shifts of 0.17 and 0.02 ppm are also observed for the *ortho*-hydrogens of (1*S*)-**8e** and (1*R*)-**8e**, respectively (0.047 *M* in $C^2H_2Cl_2$, $\delta =$

6.32 ppm) in the presence of equimolar amounts of (*S*,*S*)-**9**. This is consistent with more extensive face-to-face $\pi-\pi$ interaction in the former mixture which contains the enantiomer more strongly retained by CSP 1. Alternatively, these shifts could conceivably arise from small but unequal changes in the dihedral angles of the planes of the carboxamide and arene groups on complexation.

Acknowledgements

We thank Professor S. Maiorana of the University of Milan for providing samples of compounds **1a**, **1b**, **2a** and **2b** and Dr. G. Terfloth of the University of Illinois at Urbana–Champaign for providing a sample of (*S*,*S*)-**9**. This work has been supported by the National Science Foundation and by EM Science.

References

[1] A. Solladié-Cavallo, in L. Liebeskind (Editor), *Advances in Metal-Organic Chemistry*, Vol. 1, JAI Press, Greenwich, 1989, pp. 99–133.
[2] S.G. Davies, J.J. Donohoe and J.M.J. William, *Pure Appl. Chem.*, 64 (1992) 379–386.
[3] M. Uemura, T. Minami, M. Shiro and Y. Hayashi, *J. Org. Chem.*, 57 (1992) 5590–5596.
[4] T.E. Bitterwolf, T.L. Hubler and R. Todine, *J. Macromol. Sci., Chem.*, A27 (1990) 1437–1446.
[5] Y. Yamazaki, M. Morohashi and K. Hosono, *J. Chromatogr.*, 542 (1991) 129–136.
[6] G. Carrea, P. Pasta, S. Colonna and N. Gaggero, *J. Chromatogr.*, 600 (1992) 320–322.
[7] K. Schlögl, *J. Organomet. Chem.*, 300 (1986) 219–248.
[8] V. Gajda, S. Toma and M. Widhalm, *Monatsh. Chem.*, 120 (1989) 147–156.
[9] E. Francotte, *J. Chromatogr. A*, 666 (1994) 565–601.
[10] W.H. Pirkle, C.J. Welch and B. Lamm, *J. Org. Chem.*, 57 (1992) 3854–3860.
[11] W.H. Pirkle and C.J. Welch, *J. Liq. Chromatogr.*, 15 (1992) 1947–1955.
[12] C.A.L. Mahaffy and P.L. Pauson, *Inorg. Synth.*, 28 (1990) 136–140.
[13] G. Jaouen and A. Meyer, *J. Am. Chem. Soc.*, 97 (1975) 4667–4672.
[14] C.W. Holzapfel and F.W.H. Kruger, *Aust. J. Chem.*, 45 (1992) 99–107.
[15] S. Rosca and C.D. Nenitzescu, *Rev. Roumaine Chim.*, 15 (1970) 259–263.
[16] J. Paul and K. Schlögl, *Monatsh. Chem.*, 102 (1971) 788–797.
[17] W.H. Pirkle, C.J. Welch and S. Wilson, *Chirality*, in press.
[18] O.L. Carter, A.T. McPhail and G.A. Sim, *J. Chem. Soc. (A)*, (1966) 822–838.
[19] H. Kobayashi, M. Kobayashi and Y. Kaizu, *Bull. Chem. Soc. Jpn.*, 46 (1973) 3109–3116.
[20] R. Lal De, J. Von Seyerl, L. Zsolnai and G. Huttner, *J. Organomet. Chem.*, 175 (1979) 185–191.
[21] P.G. Sennikov, V.A. Kuznetsov, A.M. Egorochkin, N.I. Sirotkin, R.G. Nazarova and G.A. Razuvaev, *J. Organomet. Chem.*, 190 (1980) 167–176.
[22] W.H. Pirkle and C.J. Welch, *Tetrahedron Asymmetry*, 5 (1994) 777–780.

ELSEVIER

Journal of Chromatography A, 693 (1995) 69–78

JOURNAL OF CHROMATOGRAPHY A

Comparison of four homologous retention index standard series for gas chromatography of basic drugs

Ilpo Rasanen*, Ilkka Ojanperä, Erkki Vuori

Department of Forensic Medicine, P.O. Box 40 (Kytösuontie 11), FIN-00014 University of Helsinki, Helsinki, Finland

First received 2 September 1994; revised manuscript received 15 November 1994; accepted 15 November 1994

Abstract

Four homologous retention index standard series with amine structure were evaluated for the screening of blood samples for basic drugs on NB-54 and DB-1701 capillary columns over a six-month period. An index series consisting of actual drug substances was used as a standard of comparison as it produced the most precise index values. The precision differences between the homologous series were generally small. On the intermediate-polarity column NB-1701, the 4-fluoroaniline series produced the most precise index values, whereas on the low-polarity column NB-54 the trialkylamine series was the most precise. These differences were thought to be caused by the polarity and basicity properties of the standards.

1. Introduction

Screening of body fluids or tissues for drugs is an essential part of clinical toxicology, post-mortem forensic toxicology, human-performance forensic toxicology and forensic urine drug testing. In broad-scale drug screening, the technique which has proven to be particularly efficient is capillary gas chromatography with the use of retention indices (*I*) [1–3]. While conventional *n*-alkane based *I* libraries serve well in inter-laboratory exchange of chromatographic data, these standards are not precise enough for daily routine screening for basic drugs, because of the large structural difference between the standards and the analytes. Additionally, *n*-alkanes are not compatible with the selective detectors required in drug screening. In the present study, the precision of identification of seven basic test drugs was investigated on NB-54 and DB-1701 columns using four homologous amine *I* standard series, three of which are new, and with a reference *I* series consisting of basic drugs. The study was performed over a six-month period with continuous loading with autopsy blood extracts.

2. Experimental

2.1. Standards and test drugs

The N,N-dialkyl-4-fluoroanilines (FA series), the N,N-dialkyl-4-fluorobenzylamines (FB series) and the N,N-dialkylbenzylamines (BA series) were prepared by alkylating the corresponding 4-fluoroaniline (Aldrich, Steinheim, Germany), 4-fluorobenzylamine (Aldrich) and

* Corresponding author.

0021-9673/95/$09.50
SSDI 0021-9673(94)01131-1

benzylamine (Aldrich), respectively. The mixture of amine (0.5 mmol), alkyl halide (1 mmol) and potassium carbonate (1.2 mmol) in 7 ml acetone–water (6:1, v/v) was heated under reflux for 24 h. The solvent was removed in vacuo and the residue was partitioned between dichloromethane and water. The dichloromethane phase was concentrated in vacuo, and the crude products were purified by preparative high-performance liquid chromatography (HPLC). The trialkylamines (TA series) were from Eastman-Kodak (Rochester, NY, USA) and the drugs (the DR series and the test drugs) were obtained from various pharmaceutical companies.

2.2. Apparatus

The gas chromatograph was a Micromat HRGC 412 (HNU-Nordion, Helsinki, Finland) with two nitrogen–phosphorus detectors. The Grob type split/splitless injector fitted with a 1-ml quartz liner was operated in the splitless mode. Silanized glass wool was used in the liner. Automated injections were performed with a CTC A200S (CTC Analytics, Zwingen, Switzerland) autosampler using a 1.5-μl apparent injection volume. The autosampler was set to take the *I* standards in butyl acetate from a separate vial prior to the sample.

HPLC was performed with a Waters (Milford, MA, USA) 501 pump, a Rheodyne (Cotati, CA, USA) 7125 injector equipped with a 1-ml loop, and a Waters 481 variable-wavelength UV–Vis absorbance detector.

2.3. Sample preparation

Whole blood (1 ml) was transferred to a centrifuge tube (10 mm I.D.), Tris buffer (1 *M*, pH 11, 0.3 ml) was added, and the mixture was shaken. The sample was extracted with butyl acetate (0.3 ml) in a vortex mixer for 2 min and centrifuged, and an aliquot of the organic phase (100 μl) was transferred to an autosampler vial.

2.4. Chromatographic conditions

The fused-silica capillary columns were NB-54 (5% phenyl, 1% vinylmethylpolysiloxane) (HNU-Nordion) and DB-1701 (7% phenyl, 7% cyanopropylmethylpolysiloxane) (J & W Scientific, Folsom, CA, USA), both 15 m × 0.32 mm I.D. with 0.25 μm film thickness. Uncoated deactivated fused-silica precolumns (HNU-Nordion) of 5 m × 0.32 mm I.D. were connected to the analytical columns. The carrier gas was helium with a flow-rate of about 2.5 ml/min at 70°C for each column. The injector and detector temperatures were 270 and 290°C, respectively. The splitless time was 0.7 min. The oven temperature was initially held at 70°C for 0.7 min, increased by 20°C/min to 140°C, then increased by 10°C/min to 290°C, and held at the final temperature for 9.5 min.

A 300 mm × 7.8 mm μPorasil silica column (Waters) was used in HPLC. For the purification of the FA series standards, the mobile phase was first cyclohexane–dichloromethane–diethylamine (90:10:0.05, v/v), and finally (240:10:0.125, v/v) for the separation of the remaining alkyl halides from FA8-FA14. The FB and BA series standards were purified using first the mobile phase cyclohexane – dichloromethane – diethylamine (360:10:0.2, v/v) and finally (720:0.5:0.2, v/v).

2.5. Measurement of retention indices

The data processing was performed with Micman 5.0 software (HNU-Nordion). The programme was set to automatically identify the retention index standards by pattern recognition and to report the linear (polygonal) retention indices of the identified test drugs. For the FA, FB, BA and TA series standards (Fig. 1), the single alkyl chain carbon number multiplied by

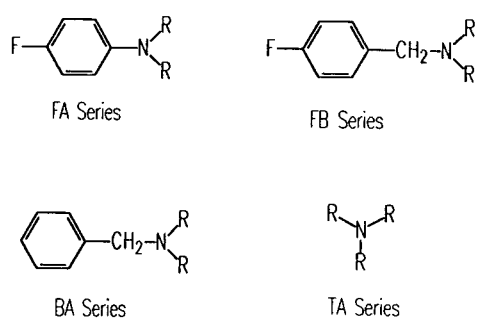

Fig. 1. Structures of the *I* standard series (R = alkyl).

100 was used as the *I* value. The DR series standards' absolute retention times in seconds were used as the *I* values.

3. Results and discussion

The chromatographic behaviour of the seven test drugs extracted from blood and co-injected with the four different *I* standards series is shown in Figs. 2–6. In the design of the FA, FB and BA series, chromatographic properties similar to basic drugs were sought by including amino and phenyl groups in the structures. The FA and FB standards were designed also to be compatible with both nitrogen–phosphorus and electron-capture detection. The TA series had been used earlier in the screening for basic drugs by gas chromatography [4]. The DR series, which acted as a reference, consisted mainly of commercially available drugs and was modified from an earlier study by Franke et al. [5] by choosing four drugs out of fourteen and by adding phenethylamine. The figures show that each homologous series produces well-shaped peaks on NB-54 and DB-1701 columns, and their elution ranges satisfactorily cover the elution range of toxicologically important basic drugs. When a linear temperature programme was used, all the four homologous series showed a fairly linear elution behaviour.

Table 1 shows the precision of identification of the seven test drugs using different *I* methods. The values were obtained from twenty separate runs by each *I* method within a six-month period. During this time, the columns were loaded additionally with fourteen autopsy blood extract injections per day, and two pairs of analytical columns representing different lots were used. Table 1 indicates that the DR series method is more precise than the homologous series methods, as could be expected from the results of earlier investigations [5]. However, according to an established concept, the maximum control of deviations in column performance, temperature programme and carrier gas flow can be obtained by co-injecting the *I* standards with every sample [6,7]. The DR series, consisting mainly of commercially available drugs, is thus unusable for this type of analysis.

The four homologous *I* series methods differed from each other in precision. The FA series method was the best on the intermediate-polarity column DB-1701 and the TA series method on the low-polarity column NB-54. The FB series method was slightly better than the BA method on DB-1701 but the situation was opposite on NB-54. Thus the ability of the present *I* methods to provide precise identification of basic drugs appears to depend on the polarity and basicity of the standards and on column polarity. The FA series standards are fairly polar but essentially non-basic. The FB and BA series standards are less polar than the FA standards, being moderately basic but still less basic than the analytes. The TA series standards are fairly non-polar but they are of the same basicity as the analytes. The DR series fulfils the conditions of both polarity and basicity.

The present retention parameters, although called *I* values, are not strictly based on the retention index theory by Kováts [8]. The values are calculated by linear (polygonal) interpolation with several standards to obtain high intralaboratory precision for a limited group of drugs encountered in daily routine screenings. The absolute *I* values themselves are not aimed to be universally valid but may depend on e.g. the temperature programme used. However, in case of an unidentified compound, the intralaboratory retention parameters can be converted to Kováts *I* values by a simple calibration graph.

4. Conclusions

The drug series (DR series) method proved to be superior to the homologous series methods in terms of precision in the chromatographic identification of basic drugs, as expected. However, due to the DR series standards' usage as drugs, the series can not be co-injected with each sample to obtain the maximum control of chromatographic deviations. Comparison of the four homologous series methods revealed that on

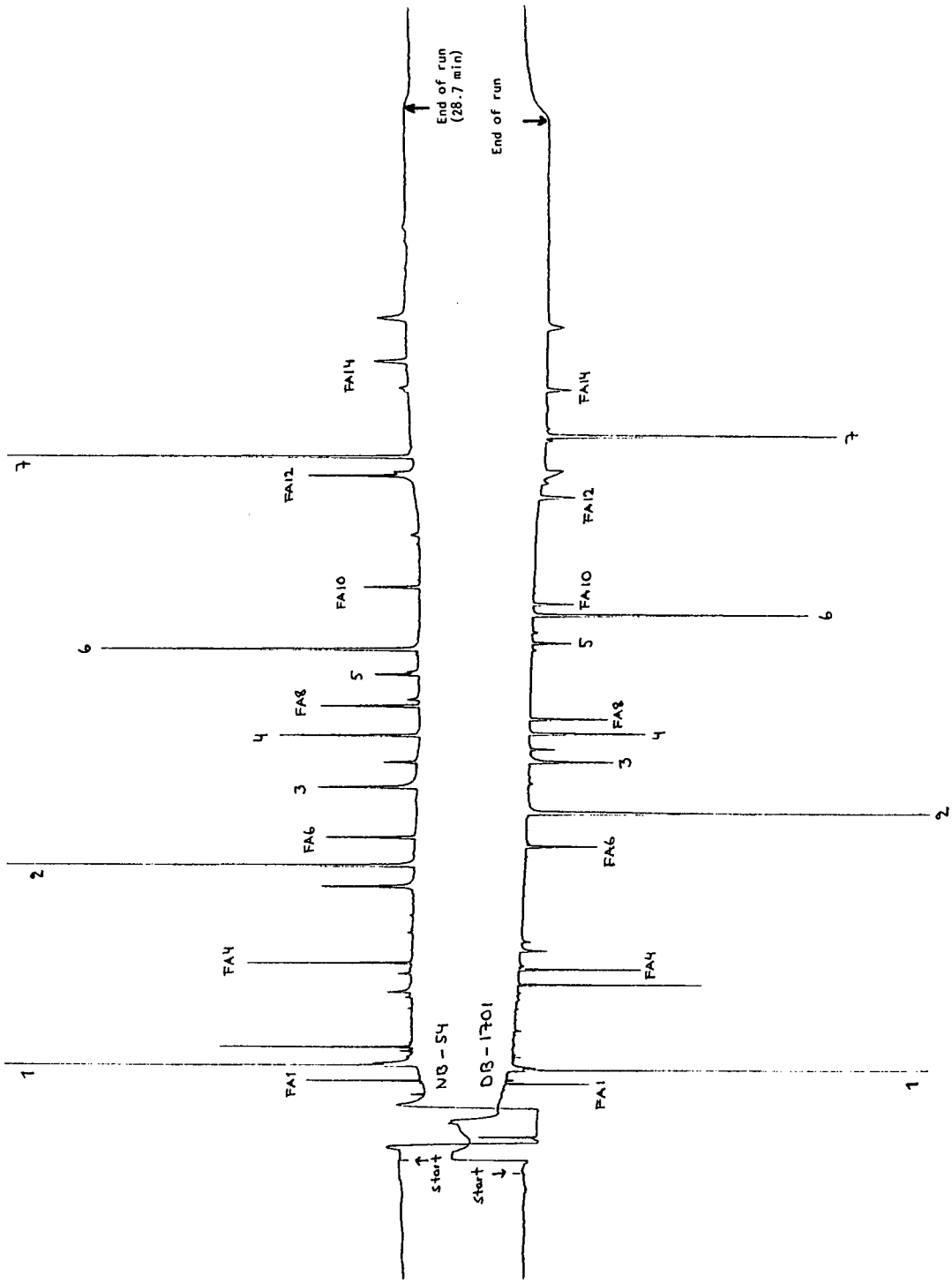

Fig 2. Chromatogram of the test drugs (1–7) co-injected with the FA series *I* standards (FA1: R = methyl etc.). Chart speed, 1 cm/min.

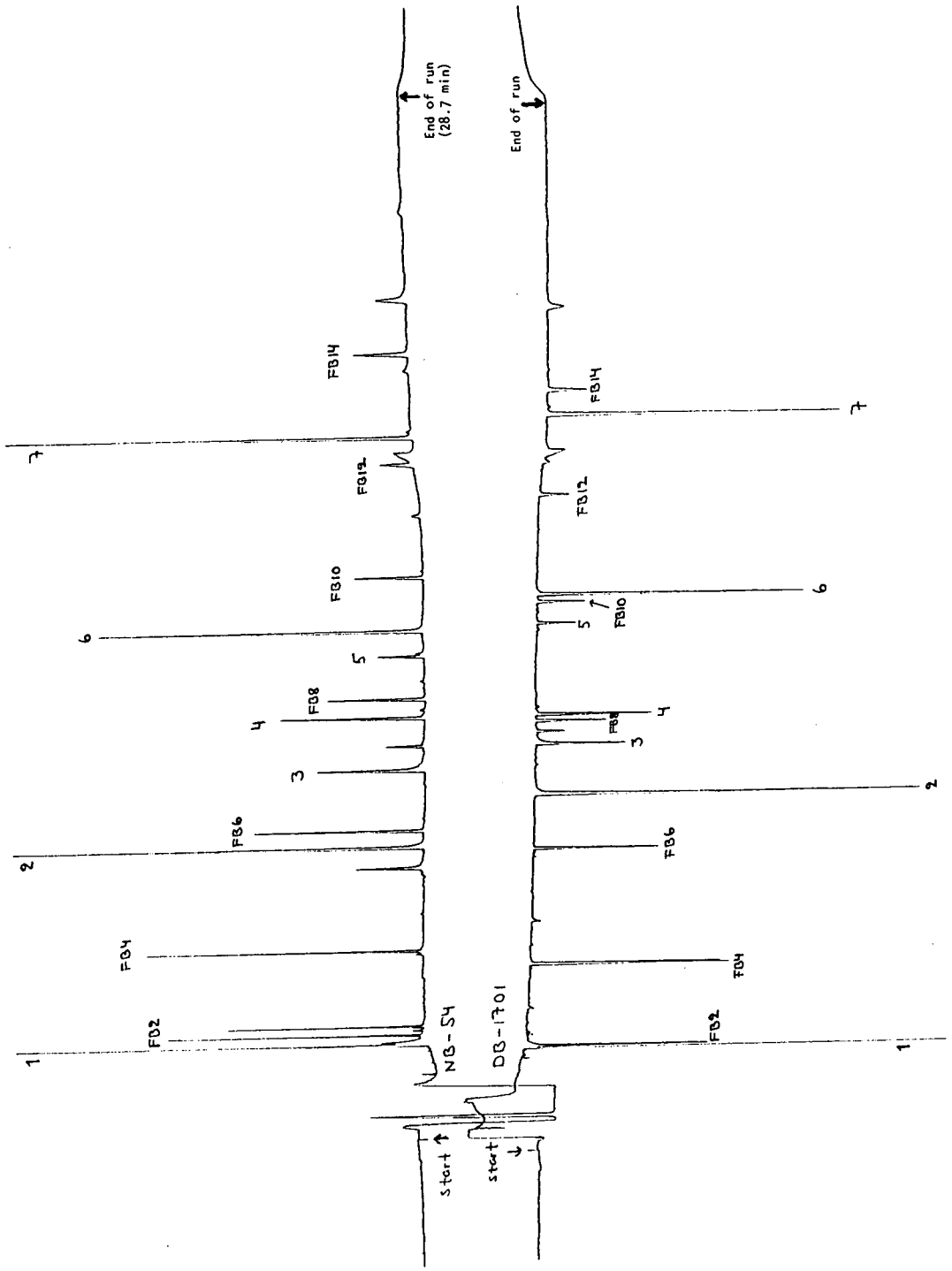

Fig. 3. Chromatogram of the test drugs (1–7) co-injected with the FB series *I* standards (FB2: R = ethyl etc.). Chart speed, 1 cm/min.

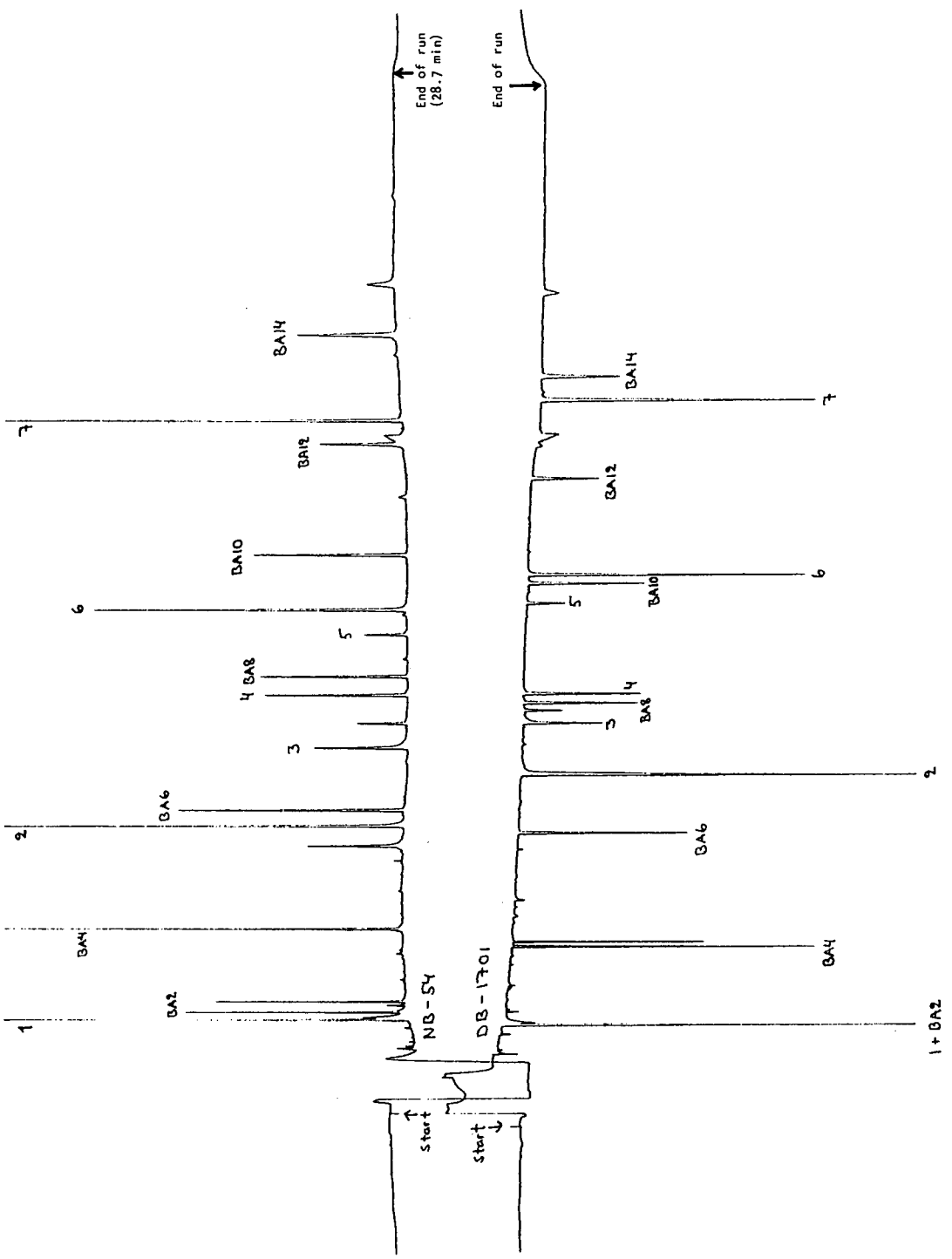

Fig. 4. Chromatogram of the test drugs (1–7) co-injected with the BA series *I* standards (BA2: R = ethyl etc.). Chart speed, 1 cm/min.

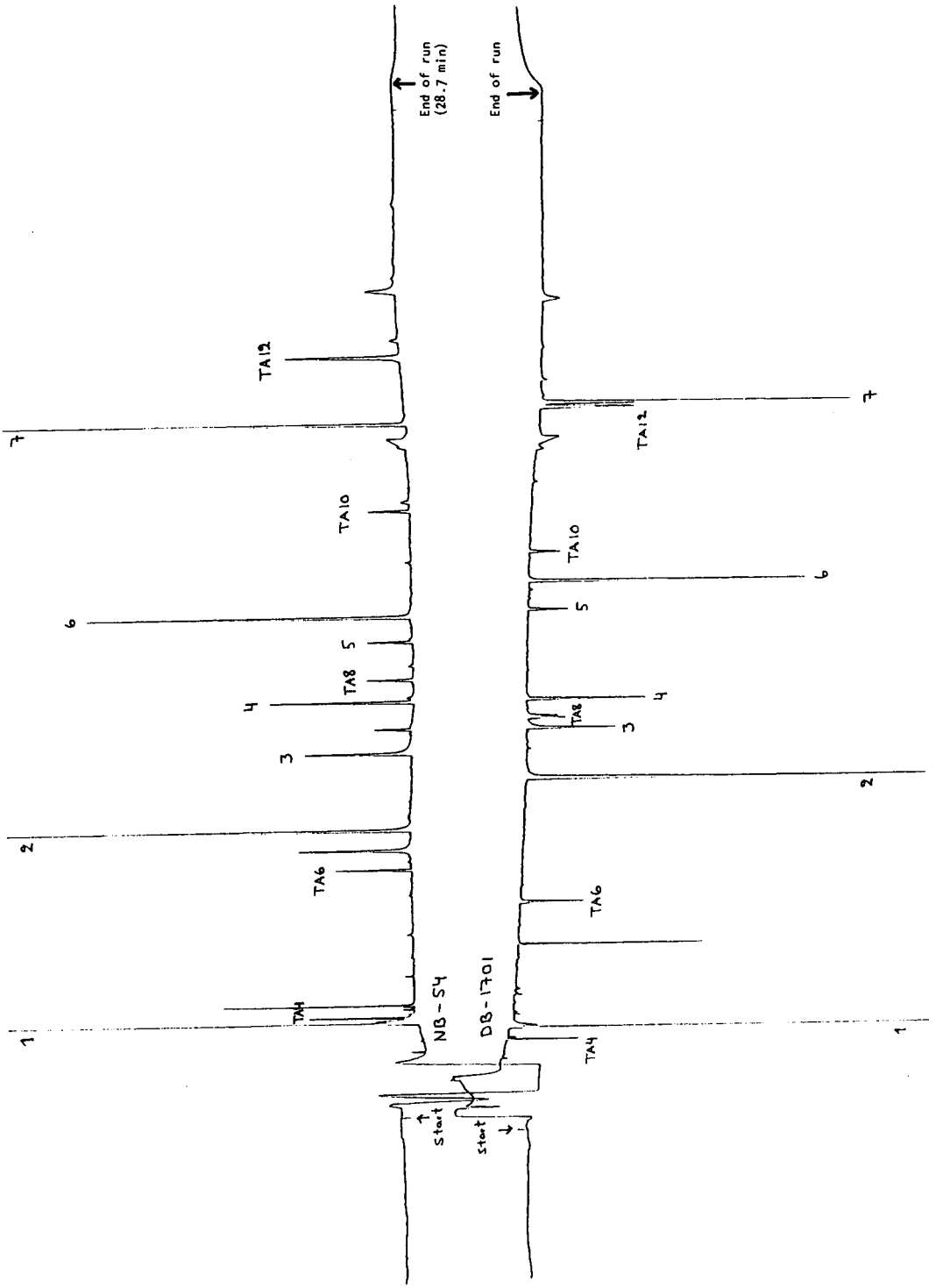

Fig. 5. Chromatogram of the test drugs (1–7) co-injected with the TA series *I* standards (TA4: R = butyl etc.). Chart speed, 1 cm/min.

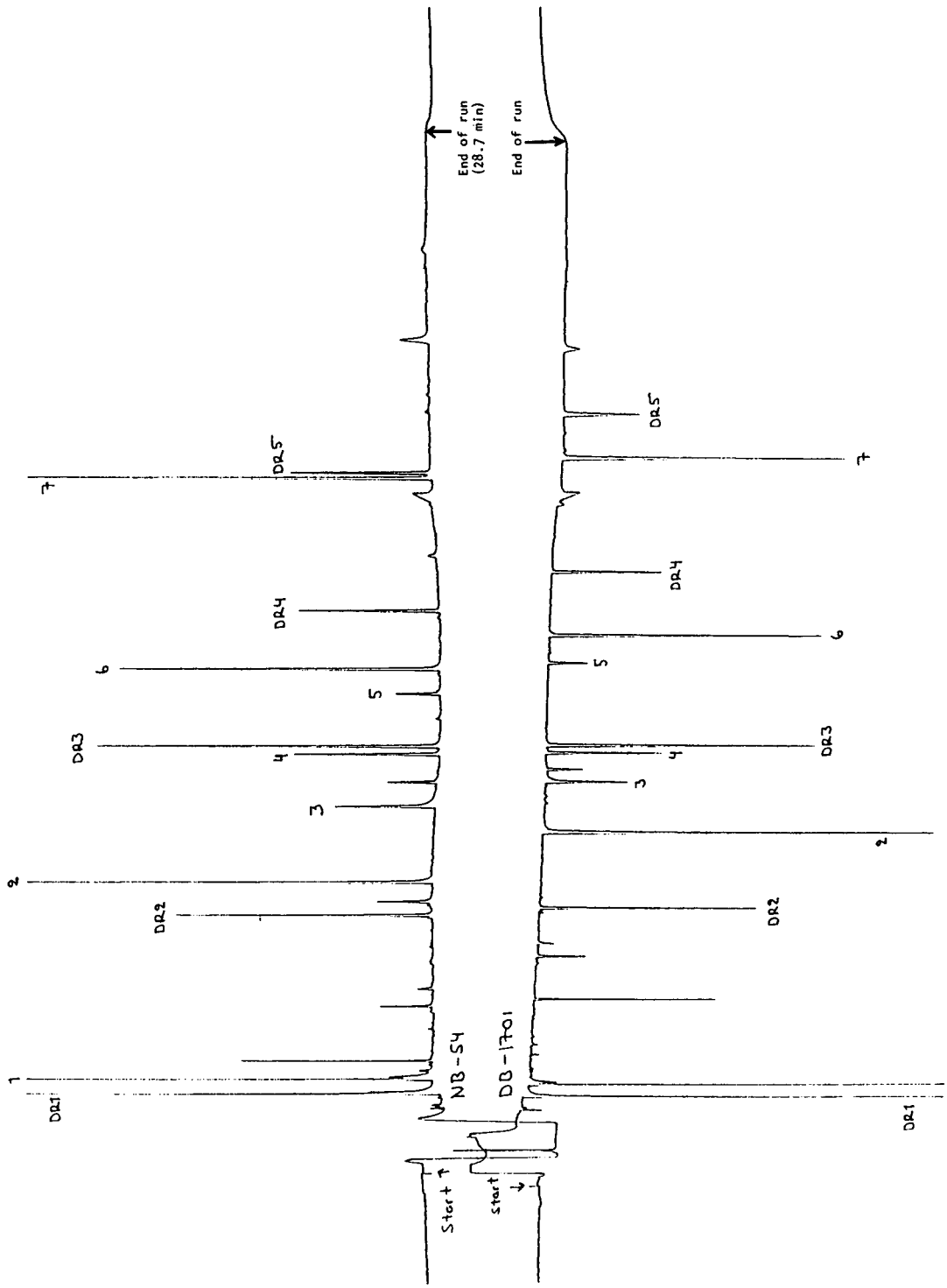

Fig. 6. Chromatogram of the test drugs (1–7) co-injected with the DR series *I* standards (see Table 1, footnote e). Chart speed, 1 cm/min.

Table 1
Precision of identification of test drugs with use of different retention index standard series

Test drug	FA Series[a]		FB Series[b]		BA Series[c]		TA Series[d]		DR Series[e]	
	Mean *I*	R.S.D. (%)	Mean *I*	R.S.D. (%)	Mean *I*	R.S.D. (%)	Mean *I*	R.S.D. (%)	Mean *I*	R.S.D. (%)
(1) Phentermine										
NB-54	138.9	0.431	180.2[f]	0.733	183.8[f]	0.564	372.8[f]	1.190	159.6	0.534
DB-1701	136.5	0.235	195.7[f]	0.201	202.0[g]	0.584	417.6	0.102	188.9	0.209
(2) Caffeine										
NB-54	552.2	0.650	569.6	0.650	571.1	0.615	639.7	0.470	490.1	0.486
DB-1701	653.0	0.339	686.7	0.352	692.0	0.352	735.4	0.376	628.3	0.199
(3) Metoprolol										
NB-54	675.0	0.243	692.3	0.258	692.6	0.247	721.6	0.282	622.1	0.161
DB-1701	733.5	0.257	766.7	0.237	771.4	0.239	790.2	0.308	714.5	0.098
(4) Amitriptyline										
NB-54	753.7	0.323	770.9	0.308	770.5	0.278	775.5	0.303	708.9	0.057
DB-1701	778.3	0.161	812.1	0.164	816.8	0.171	823.4	0.272	762.5	0.021
(5) Codeine										
NB-54	849.7	0.500	867.8	0.478	866.5	0.446	843.4	0.429	809.2	0.179
DB-1701	935.0	0.322	967.5	0.312	970.9	0.324	933.8	0.322	916.9	0.069
(6) Dibenzepine										
NB-54	892.5	0.394	909.9	0.379	908.4	0.349	873.5	0.352	851.6	0.059
DB-1701	984.5	0.327	1017.8	0.363	1021.1	0.371	968.2	0.318	964.9	0.061
(7) Thioridazine										
NB-54	1230.3	0.119	1244.9	0.276	1240.0	0.215	1109.2	0.169	1168.0	0.171
DB-1701	1314.2	0.140	1354.3	0.160	1355.8	0.167	1212.1[h]	0.328	1282.3	0.402
Mean[i]										
NB-54		0.372		0.392		0.358		0.334		0.186
DB-1701		0.258		0.265		0.271		0.321		0.142

Based on 20 measurements of blood extracts over a six-month period.
[a]N,N-Dialkyl-4-fluoroanilines.
[b]N,N-Dialkyl-4-fluorobenzylamines.
[c]N,N-Dialkylbenzylamines.
[d]Trialkylamines.
[e]Drugs: phenethylamine, methyl phenidate, trimipramine, prazepam, strychnine.
[f]Elutes before the first index standard.
[g]Coelutes occasionally with the first index standard.
[h]Elutes after the last index standard.
[i]Excluding the values of phentermine (see footnotes f and g).

DB-1701 the 4-fluoroaniline series (FA series) produces the best results, whereas the trialkylamine series (TA series) is feasible on NB-54. However, the precision differences between the homologous series is small. Obviously, further studies are required to create a non-drug series producing high precision simultaneously on both columns.

References

[1] B. Newton and R.F. Foery, *J. Anal. Toxicol.* 8 (1984) 129.
[2] D.W. Christ, P. Noomano, M. Rosas and D. Rhone, *J. Anal. Toxicol.* 12 (1988) 84.
[3] I. Ojanperä, I. Rasanen and E. Vuori, *J. Anal. Toxicol.* 15 (1991) 204.
[4] V.W. Watts and T.F. Simonick, *J. Anal. Toxicol.* 11 (1987) 210.
[5] J.-P. Franke, J. Wijsbeek and R.A. de Zeeuw, *J. Forensic Sci.* 35 (1990) 813.
[6] A. Kiviranta, *Int. Lab.* 17 (Jan./Feb.) (1987) 58.
[7] I. Rasanen, I. Ojanperä and E. Vuori, *J. High Resolut. Chromatogr.*, in press.
[8] E. sz. Kováts, *Helv. Chim. Acta*, 41 (1958) 1915.

ELSEVIER

Journal of Chromatography A, 693 (1995) 79–88

JOURNAL OF CHROMATOGRAPHY A

Preparation of 4-vinylpyridine and divinylbenzene porous-layer open tubular columns by in situ copolymerization

Zongqin Ruan*, Hanxun Liu

Lanzhou Institute of Chemical Physics, Chinese Academy of Sciences, Lanzhou 730000, China

First received 18 July 1994; revised manuscript received 4 October 1994; accepted 4 October 1994

Abstract

A new type of polar porous polymer glass capillary column, named OPPLOT-S, was prepared by in situ copolymerization of 4-vinylpyridine and divinylbenzene. Its chemical composition was found to be similar to that of Porapak S. The OPPLOT-S columns performed very efficiently in analysing alcohols, hydrocarbons, nitriles, amines, polar and apolar mixtures and permanent gases. They can provide good separations of NH_3–H_2O, CH_3OH–H_2O and CO–CH_4–CO_2 in a relatively short time under general conditions. The polarities of capillary columns were evaluated by using the Rohrshneider and McReynolds constants.

1. Introduction

Organic porous polymers have been extensively utilized as column packing materials, since Hollis [1] reported the development of such polymers as stationary phases for GC. The very specific separation characteristics of the porous polymers were recognised [2–7]. They have the advantage that polar compounds are not absorbed by the column, but eluted as symmetrical peaks in comparison with alumina and molecular sieves. Moreover, they can provide conditions such that the retention of the column is not influenced by water. Porous polymer packings such as the Chromosorb and Porapak series have been commercially used in packed GC columns to analyse volatiles and gases including hydrocarbons, alcohols, ketones, aldehyde, acides, esters, ethers, nitriles, amines and permanent gases.

Recently, the application of porous polymers in capillary GC has been developed owing to their unique separation characteristics [8–14]. It appears that they offer the advantages of porous polymer packings with the high resolution of a capillary column. De Zeeuw et al. [8,9] reported that a capillary column (PoraPLOTQ) coated with styrene and divinylbenzene was prepared by a two-step procedure. In the preparation process a porous polymer was formed and its stabilization on the inside of the capillary columns was achieved. Wang and Liu [13] introduced another apolar porous polymer capillary column coated with ethylvinylbenzene and divinylbenzene by in situ copolymerization and named it OPPLOT-Q, since its chemical composition was found to be similar to that of Porapak Q. The preparation process was a one-step procedure in which

* Corresponding author.

SSDI 0021-9673(94)00951-1

stabilization of the porous polymer coating layer was achieved via a special additional reagent.

It is possible to prepare polar porous polymer capillary columns that possess particular properties and are suitable for the separation of different types of compounds. A suitable choice of monomers with special functional groups make it possible to obtain good separations for particular applications. In this paper, we describe the preparation of a new polar porous polymer polymer capillary column coated with 4-vinylpyridine and divinylbenzene copolymerized in situ, named OPPLOT-S. The reproducibility, thermal stability and retention characteristics of the OPPLOT-S column are discussed in detail.

2. Experimental

2.1. Apparatus

GC measurements were carried out with a Hewlett-Packard (HP) Model 5890A gas chromatograph equipped with a flame ionization detector and an HP 3392 integrator–recorder. Nitrogen was used as the carrier gas at a velocity of ca. 20–25 cm/s. An HP 5880 gas chromatograph equipped with a thermal conductivity detector was used to analyse permanent gases and aqueous compounds and helium was used as the carrier gas.

A Shimadzu GDM-1B glass capillary drawing machine was used to draw glass capillaries with different inner diameters. Electron micrographs of the porous polymer coating materials were obtained with a JEOL JEM-1200EX/S electron microscope. The qualitative analysis of porous polymers was carried out with a Nicolet 10DX Fourier transform IR spectrometer.

2.2. Chemicals

All reagents used for GC were of chemical or analytical-reagent grade and used as received. Divinylbenzene (DVB) and 4-vinylpyridine (4VP) were purified by washing with 10% sodium hydroxide to remove the stabilizer before use.

2.3. Preparation of the OPPLOT-S columns

All glass capillary columns were treated with a special method before use. The leached surface of a glass capillary was dehydrated by filling 90% of its volume with 20% hydrochloric acid and heating at 180°C for 10 h. After heating, the capillary was rinsed with 10 ml of 0.5% hydrochloric acid, 10 ml of water and 10 ml of methanol and dried at 150°C for 5 h under a nitrogen flow. The capillary can acquire a highly active surface via silylation [13].

The OPPLOT-S capillary columns were prepared by in situ copolymerization of 4VP and DVB in a mixed solution of polar and apolar reagents (octanol–heptane solvent system) as diluent and 0.5% azobisisobutyronitrile as initiator. The suspension obtained was forced by nitrogen pressure into a capillary column and the two ends were sealed with a flame, sustaining a pressure of ca. 49 kPa (0.5 kg/cm^2), then reacted at 70°C for 10 h. After completion of the reaction, the capillary columns were washed with 10 ml of methanol and 10 ml of pentane and dried at 150°C for 5 h under a nitrogen flow. The OPPLOT-S columns were evaluated with ethyl acetate at 150°C.

3. Results and discussion

The chromatographic characteristics of porous polymers differ with variation in the kinds of monomers and diluents, the concentration of cross-linking reagent and the reaction conditions. The kind of monomers used was the key factor for the selectivity of the porous polymers. Hollis [3] described the chemical compositions of a series of Porapak porous polymer packings. Porapak S is prepared from vinylpyridine and divinylbenzene. Fig. 1 shows the IR spectra of polymer coatings of OPPLOT-Q and OPPLOT-S columns. The spectrum of OPPLOT-S differs from that of OPPLOT-Q because there is a strong absorption peak at 1600 cm^{-1} on curve 2.

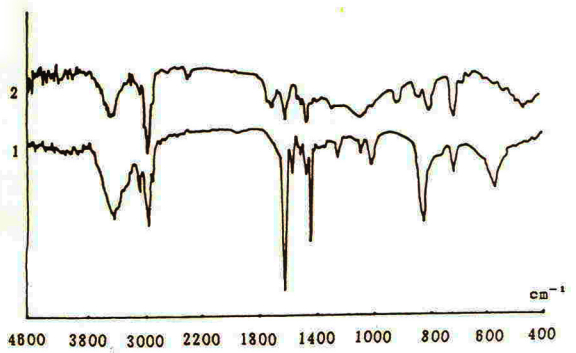

Fig. 1. IR spectra of (2) OPPLOT-Q and (1) OPPLOT-S porous polymer coatings (potassium bromide disc method).

This means that the OPPLOT-S porous polymer has different functional groups to OPPLOT-Q, the former being produced from 4VP.

In order to use optimized flow-rate conditions for practical analyses, we determined Van Deemter curves at different temperatures. The linear velocity of the carrier gas, u, was calculated from the relationship $u = L/t_m$, where L is the length of column and t_m is the retention time of methane. For the solute selected, H was calculated from the classical relationship

$$H = \frac{L}{5.54}\left(\frac{w_{1/2}}{t_R - t_m}\right)^2$$

where t_R is the retention time of the solute and $w_{1/2}$ is the half-width of its chromatographic peak. Curves of the number of theoretical plates (H) versus the mean linear velocity (u) are shown in Fig. 2. Benzene, cyclohexane and 1-butanol were selected as the solutes, because they could provide different effects with the stationary phase, at column temperatures of 130 and 150°C. For benzene, H is not very temperature dependent, at least for u values higher than about 10 cm/s. The curves obtained with 1-butanol differed from those for benzene, H increasing markedly with increase in temperature. The curves for cyclohexane is slightly changed along with increasing of the temperature. For these three solutes the minimum H was obtained at $u \approx 15$–20 cm/s. We therefore select $u \approx 20$–25 cm/s as the optimum flow-rate for practical applications.

The concentration of cross-linking reagent was considered to change the size of the porous polymer bead and the pore structure [3]. Hollis reported that the size and rigidity of the pores of the polymer beads increased with increase in the content of cross-linking reagent. Three electron micrographs of porous polymer coatings with 4VP concentrations of 10, 20 and 30% are shown in Fig. 3. The size of the porous polymer is regular at 1–2 μm. It is concluded that the size of the porous polymer beads decreased with increasing content of 4VP or decreasing content of DVB.

The chromatographic characteristics of the OPPLOT-S column not only changed with variation in the concentration of the monomer, but

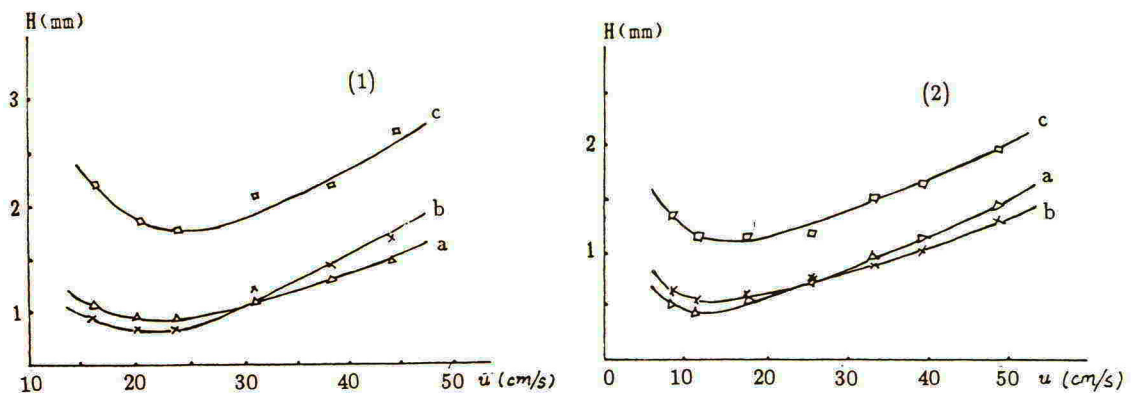

Fig. 2. Variation of H with the linear velocity, u, of the carrier gas (N_2) at (1) 130°C and (2) 150°C for the solutes (a) benzene, (b) cyclohexane and (c) 1-butanol.

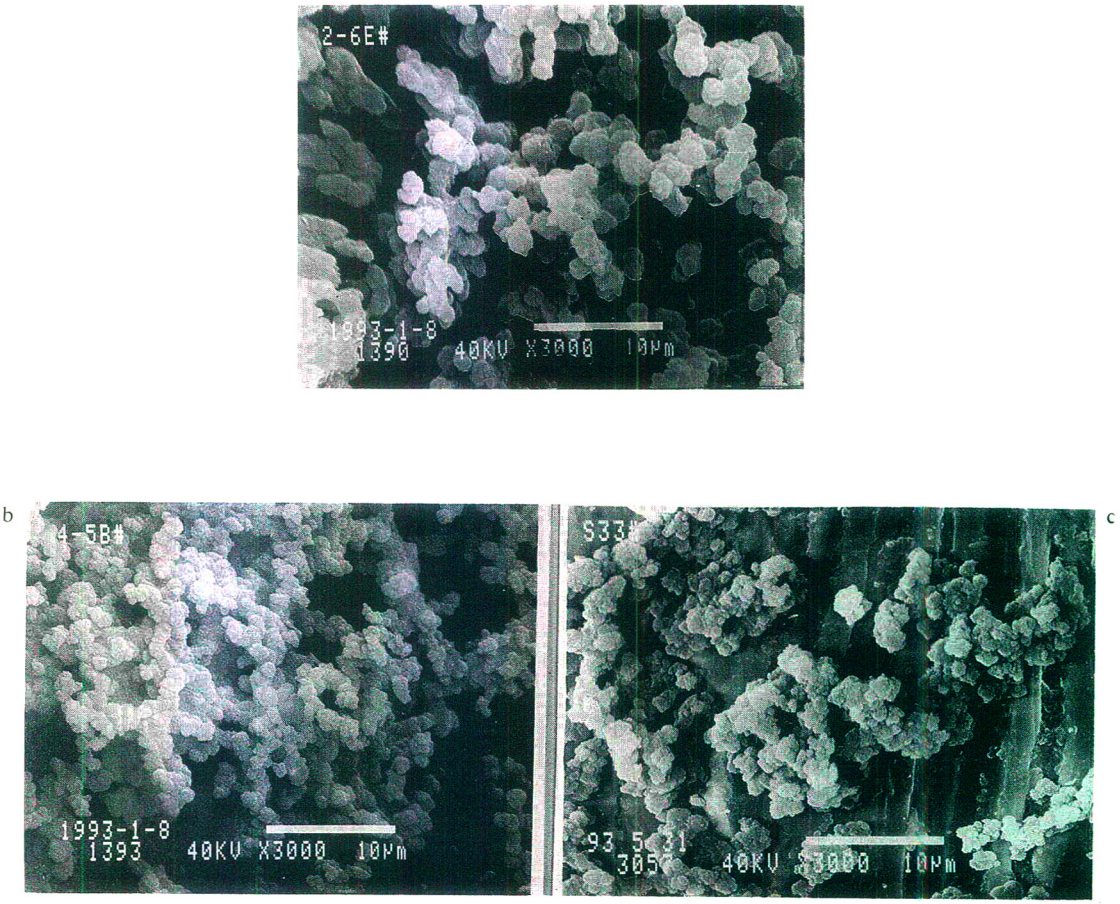

Fig. 3. Electron micrographs of porous polymer coatings with different 4VP concentrations. 4VP : DVB = (a)1 : 9, (b) 1 : 4 and (c) 3 : 7.

was also influenced by the kind of diluent. The diluent used for the suspension solution for situ copolymerization must meet the following conditions: it must form a homogeneous mixture with the reactants and it must not swell the polymer beads after the in situ copolymerization reaction. Hence it is very important to select polar–apolar mixed solutions as diluents in order to produce polar porous polymer PLOT columns with high column efficiency. The OPPLOT-S column was prepared using an octanol–heptane solvent system. The variation of the number of theoretical plates (H) and with the ratio of polar and apolar diluent components (D) is shown in Fig. 4. It was found that the concentration of the polar diluent influenced the chromatographic characteristics of OPPLOT-S. The selected range of polar diluent concentration become narrow with an increase in the content of 4VP.

The polarity of GC stationary phases is usually evaluated by using Rohrshneider and McReynolds constants [15,16]. Table 1 gives the retention indices of five different molecular types measured at 200°C on OPPLOT-S and OPPLOT-Q columns. The polarity of the OPPLOT-S column is higher than that of the OPPLOT-Q column, and the OPPLOT-S column containing 30% 4VP shows the highest polarity because it

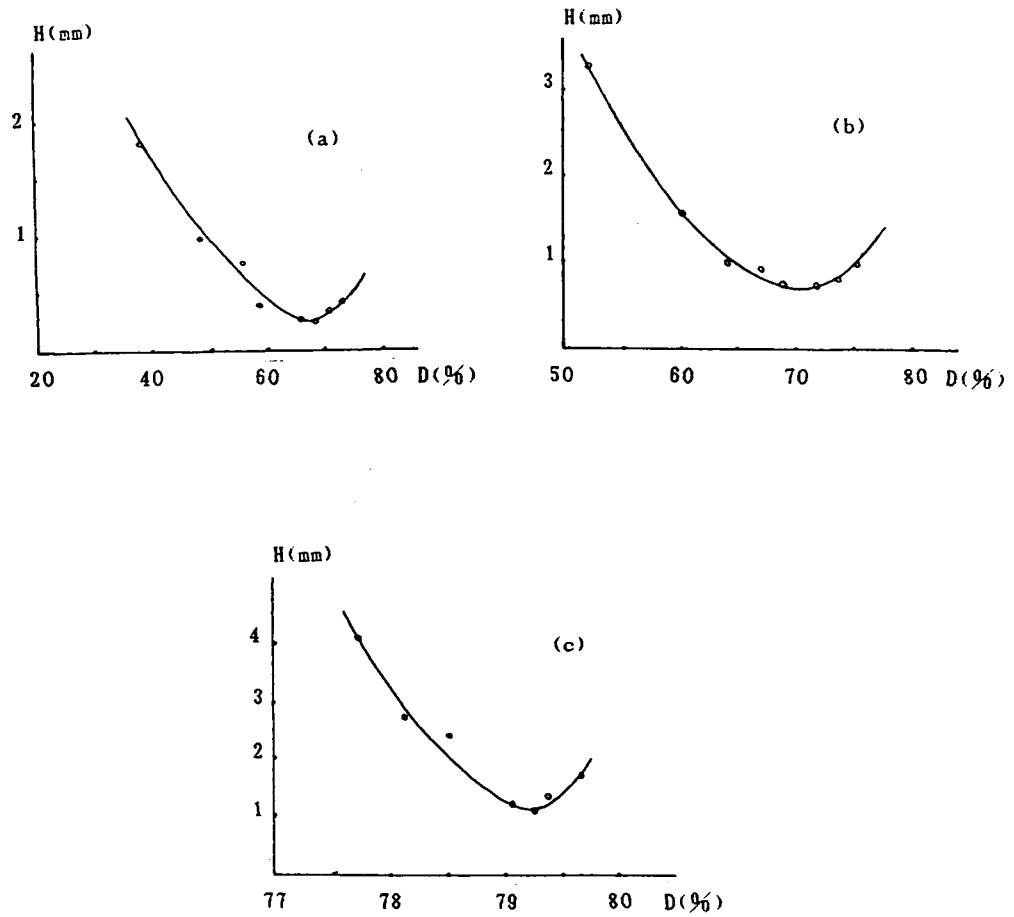

Fig. 4. Curves for selecting polar diluents for OPPLOT-S columns. 4VP : DVB = (a) 1 : 9, (b) 1 : 4 and (c) 3 : 7. Solute = ethyl acetate.

Table 1
Comparison of the retention indices on OPPLOT-Q and OPPLOT-S columns for different molecular types, measured at 200°C

Column	Benzene	1-Butanol	3-Pentanone	2-Nitropropane	Pyridine
OPPLOT-Q	611	555	644	628	640
OPPLOT-S (10% 4VP)	620	597	667	666	684
OPPLOT-S (20% 4VP)	631	625	686	696	704
OPPLOT-S (30% 4VP)	642	649	704	725	724

has the highest 4VP content. This investigation shows that the overall selectivity of the OPPLOT-S column differs from that of the OPPLOT-Q column.

The following equation was used for calculating the retention indices, I:

$$I = 100\left[n + z\left(\frac{\log t'_n - \log t'_x}{\log t'_{n+z} - \log t'_n}\right)\right]$$

where n and $n+z$ correspond to alkanes with n and $n+z$ carbon atoms, respectively, and x corresponds to a solute the retention time of which is between that of n and $n+z$ alkanes and t'_n, t'_x and t'_{n+z} are the relative retention time of n-pentane, solute and n-octane, respectively; the gas hold-up time of the column is obtained using methane.

Table 2 gives the reproducibility of preparing OPPLOT-S columns. It was found that the column efficiencies were all above 1500 theoretical plates per metre as evaluated with ethyl acetate. When the reactant concentration (C) increases, the capacity factor increases. This means that capillary columns with different coating layer thicknesses can be prepared for particular applications by controlling the reactant concentration by in situ copolymerization.

Table 2
Reproducibility of OPPLOT-S columns

No.	Column (m × mm I.D.)	C (w/w)	N/m	k	α
1	15.5 × 0.49	5.98	1675	1.48	1.82
2	15.5 × 0.49	5.98	1653	1.51	1.83
3	15.5 × 0.49	7.08	1698	1.65	1.84
4	15.5 × 0.49	5.98	1682	1.65	1.84
5	15.5 × 0.48	7.68	1818	1.78	1.84
6	15.5 × 0.48	7.68	1875	1.83	1.84
7	15.5 × 0.47	8.38	1781	2.00	1.83
8	15.5 × 0.47	8.38	1774	2.10	1.83
9	15.5 × 0.50	8.45	1856	2.01	1.84
10	15.5 × 0.50	8.45	1856	1.99	1.82
11	15 × 0.49	9.24	1982	2.23	1.82
12	15 × 0.49	9.24	1862	2.23	1.82
13	15 × 0.49	9.24	1845	2.21	1.82
14	15 × 0.49	9.24	1980	2.24	1.83

Column temperature, 150°C. Solutes: ethyl acetate (for N/m and k) and 1-propanol–*sec.*-butanol (for α).

Table 3
Thermal stability data on OPPLOT-S column with 10% 4VP

Heating temperature (°C)	Heating time (h)	N/m	k	α
240	3	1982	2.19	1.78
	6	1924	2.39	1.78
	20	1990	2.55	1.79
250	3	1919	2.49	1.80
	6	1990	2.56	1.81
	20	1724	2.63	1.79
260	3	1724	2.63	1.79
	7	1724	2.63	1.76
270	3	1463	2.66	1.76
	12	1351	2.66	1.76

Conditioner as in Table.
Column temperature 150°C. Solutes: ethyl acetate (for N/m and k) and 1-propanol–*Sec*-butanol (for α).

The thermal stability of OPPLOT-S columns was determined by heating for different times at different temperatures in a nitrogen flow. The results are given in Tables 3–5. It is clear that the OPPLOT-S column can be conditioned at 250, 230 or 210°C when the 4VP concentration is 10, 20 or 30%, respectively.

A number of applications are illustrated in Figs. 5–12. Hydrocarbons can be separated on an OPPLOT-S column (Fig. 5). Temperature programming allows most C_7 hydrocarbons to be separated. Fig. 6 shows the separation of a

Table 4
Thermal stability data on OPPLOT-S column with 20% 4VP

Heating temperature (°C)	Heating time (h)	N/m	k	α
210	3	1742	3.12	1.75
	10	1756	3.15	1.76
220	3	1784	3.13	1.79
	10	1776	3.19	1.80
	20	1758	3.24	1.76
230	3	1772	3.25	1.75
	10	1486	3.29	1.73
	20	1378	3.38	1.70

Conditions as in Table 3.

Table 5
Thermal stability data on OPPLOT-S column with 30% 4VP

Heating temperature (°C)	Heating time (h)	N/m	k	α
190	3	1964	1.85	1.65
	7	2058	1.83	1.66
	20	1993	1.88	1.68
200	3	1908	1.90	1.68
	10	1964	1.94	1.66
	20	1908	1.94	1.66
210	3	1751	1.94	1.66
	10	1658	1.94	1.65

Conditions as in Table 3.

mixture of alcohols. These types of compounds elute with slightly tailing because of the polarity of the stationary phase in comparison with the OPPLOT-Q column [13].

The OPPLOT-S column also can be used

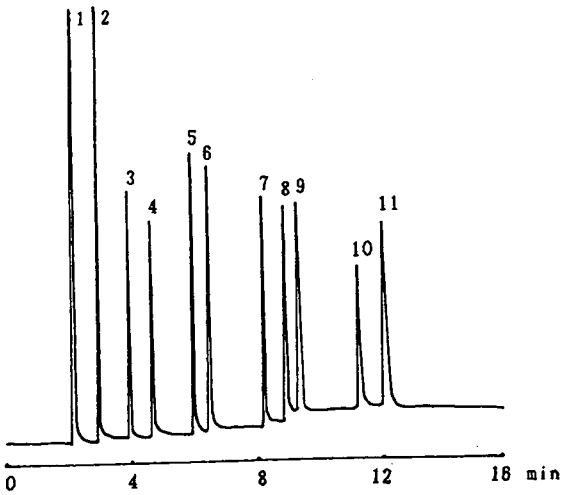

Fig. 6. Separation of a mixture of alcohols. Column, 22 m × 0.35 mm I.D. OPPLOT-S; temperature, increased from 120 to 220°C at 10°C/min. Peaks: 1 = methanol; 2 = ethanol; 3 = 2-propanol; 4 = propanol; 5 = isobutanol; 6 = *sec.*-butanol; 7 = 1-butanol; 8 = isopentanol; 9 = 1-pentanol; 10 = 2,3-dimethyl-3-pentanol; 11 = 2-methylpentanol.

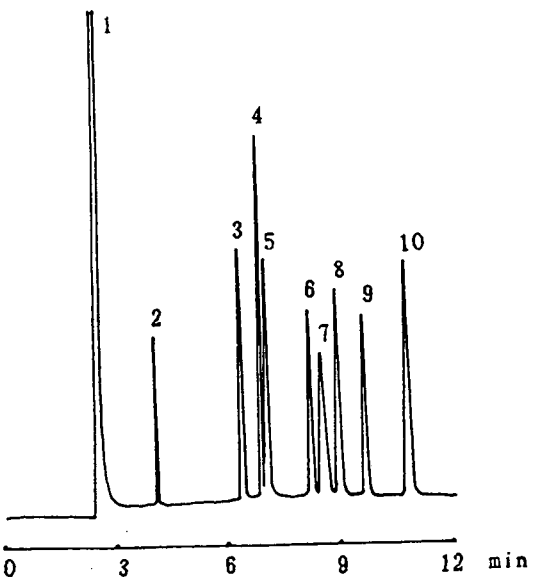

Fig. 5. Separation of a mixture of C_7 hydrocarbons. Column, 25 m × 0.41 mm I.D. OPPLOT-S; temperature, increased from 130 to 180°C at 8°C/min. Peaks: 1 = methanol; 2 = pentane; 3 = hexane; 4 = benzene; 5 = cyclohexane; 6 = 2,4-dimethylpentane; 7 = 2,2,3-trimethylbutane; 8 = 2-methylhexane; 9 = heptane; 10 = toluene.

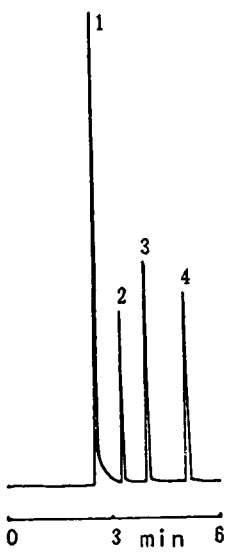

Fig. 7. Separation of a mixture of nitriles. Column, 22 m × 0.35 mm I.D. OPPLOT-S; temperature 150°C. Peaks: 1 = methanol; 2 = acetonitrile; 3 = acrylonitrile; 4 = propionitrile.

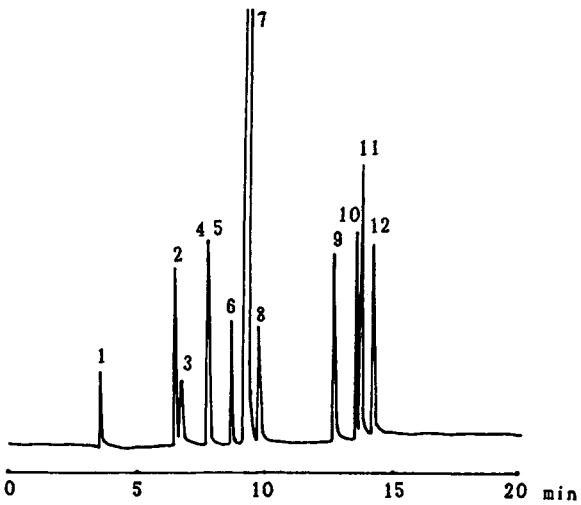

Fig. 8. Separation of a mixture of polar and apolar compounds. Column, 22 m × 0.35 mm I.D. OPPLOT-S; temperature, isothermal for 5 min at 100°C, then increased at 8°C/min to 200°C. Peaks: 1 = methanol; 2 = acetonitrile; 3 = ethanol; 4 = acetone 5 = dichloromethane; 6 = methyl acetate; 7 = pentane; 8 = 2-propanol; 9 = ethyl acetate; 10 = hexane; 11 = benzene; 12 = cyclohexane.

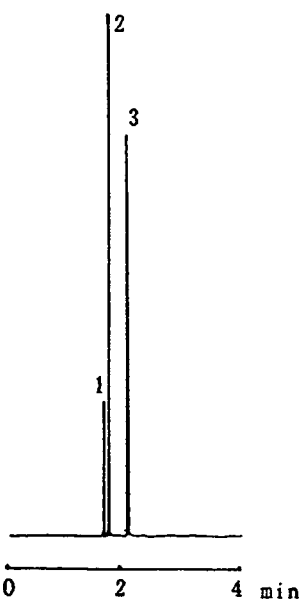

Fig. 9. Separation of CO, CH_4 and CO_2. Column, 36 m × 0.36 mm I.D. OPPLOT-S; temperature, 50°C. Peaks: 1 = CO; 2 = CH_4; 3 = CO_2.

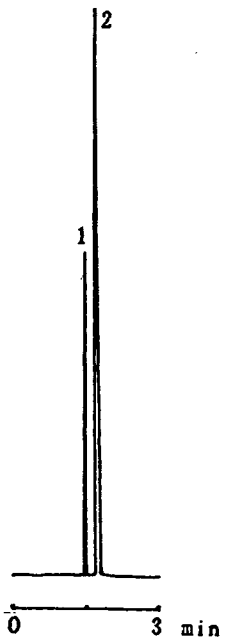

Fig. 10. Separation of water and methanol. Column, 18 m × 0.36 mm I.D. OPPLOT-S; temperature, 130°C. Peaks: 1 = water; 2 = methanol.

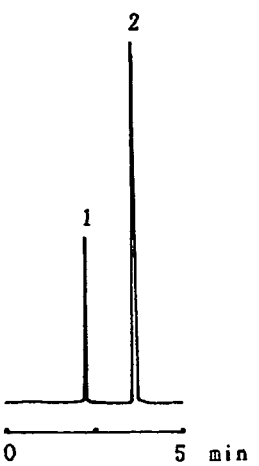

Fig. 11. Separation of ammonia liquor. Column, 18 m × 0.36 mm I.D. OPPLOT-S; temperature, 100°C. Peaks: 1 = ammonia; 2 = water.

advantageously for analysing nitriles with symmetrical peaks (Fig. 7).

One of the unique retention characteristics of the porous polymer is shown in the separation of

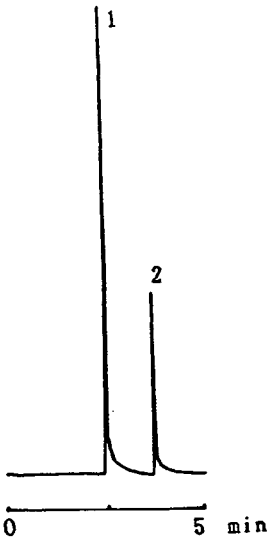

Fig. 12. Separation of amines. Column, 22 m × 0.35 mm I.D. glass OPPLOT-S; temperature, 200°C. Peaks: 1 = diethylamine; 2 = triethylamine.

polar and apolar volatile mixtures, as high-polarity compounds cannot be eluted from alumina and molecular sieves, which means they cannot be analysed together with light hydrocarbons or permanent bases. The OPPLOT-S column can provide a good separation of such mixture (Fig. 8).

Separation of carbon dioxide from air had to be performed with a porous polymer stationary phase as CO_2 is absorbed by alumina and molecular sieves. Fig. 9 shows the separation of permanent gases at 50°C under isothermal conditions. At this temperature there is baseline resolution among carbon monoxide, methane and carbon dioxide.

Water is a problematic analysis on most GC column, but it can be achieved by using a porous polymer. Fig. 10 shows the separation of water from methanol at 130°C and Fig. 11 shows the separation of ammonia liquor at 100°C, detected with a micro thermal conductivity detector.

Owing to the basic pyridine functional group of the OPPLOT-S column, it can be applied to basic nitrogen compounds, such as ammonia, diethylamine and triethylamine (Figs. 11 and 12). These compounds cannot be analysed on other types of capillary column because of absorption.

4. Conclusions

The OPPLOT-S column can be prepared with good reproducibility. The method of in situ suspension copolymerization should be applicable to preparing different porous polymer PLOT columns in the future. The OPPLOT-S column performed very efficiently in analysing volatile compounds and gases. It provides good separations of NH_3–H_2O and CO–CH_4–CO_2 in a short time under general conditions. It was found that the content of 4VP affected the polarity and selectivity of the OPPLOT-S column. Electron micrographs of the columns showed that the size of the polymer beads decreased with increasing content of 4VP or decreasing content of DVB. The OPPLOT-S column is different from other porous polymer capillary columns as basic nitrogen compounds can be separated with high resolution.

Acknowledgement

This work was supported by the National Natural Science Foundation of China.

References

[1] O.L. Hollis, *Anal. Chem.*, 38 (1966) 309.
[2] O.L. Hollis and W.V. Hayes, *J. Gas Chromatogr.*, 4 (1966) 235.
[3] O.L. Hollis, *J. Chromatogr. Sci.*, 11 (1973) 335.
[4] B.O. Jansson, K.C. Hallgren and G. Widmark, *J. Chromatogr. Sci.*, 8 (1970) 398.
[5] M. Novotny and J.M. Hayes, *Science*, 189 (1975) 215.
[6] R. Komers, H. Kopecky and M. Kraus, *J. Chromatogr.*, 148 (1978) 43.
[7] L.-R. Deng, *J. Chromatogr.*, 186 (1979) 317.
[8] J. de Zeeuw, R.C.M. de Nijs, J.C. Buÿten, J.A. Peene and M. Mohnke, *Am. Lab.*, 10 (1987) 83.
[9] J. de Zeeuw, R.C.M. de Nijs, J.C. Buijten, J.A. Peene and M. Mohnke, *J. High Resolut. Chromatogr. Chromatogr. Commun.*, 11 (1988) 162.

[10] K.K. Gaines, W.H. Chatham and S.O. Farwell, *J. High Resolut. Chromatogr.* 13 (1990) 585.
[11] J. de Zeeuw, R.C.M. de Nijs, D. Zwiep and J.A. Peene, *Am. Lab.*, 6 (1991) 51.
[12] T.C. Shen, *J. Chromatogr. Sci.*, 30 (1992) 239.
[13] Q.-S. Wang and H.-X. Liu, *FenXi HuaXue*, 21, No. 1 (1993) 16.
[14] T.C. Shen and M.M. Fong, *J. Chromatogr. Sci.*, 32 (1994) 36.
[15] G. Castello and G. D'Amato, *J. Chromatogr.*, 269 (1983) 153.
[16] G. Castello and G. D'Amato, *J. Chromatogr.*, 212 (1980) 261.

ELSEVIER

Journal of Chromatography A, 693 (1995) 89–99

JOURNAL OF CHROMATOGRAPHY A

Analysis of a mixture of linear and cyclic siloxanes by cryo-gas chromatography–Fourier transform infrared spectroscopy and gas chromatography–mass spectrometry

S. Wachholz[a,*], F. Keidel[a], U. Just[a], H. Geissler[a], K. Käppler[b]

[a]*Federal Institute for Materials Research and Testing, Unter den Eichen 87, D-12205 Berlin, Germany*

[b]*Technical University Dresden, Mommsenstrasse 13, D-01069 Dresden, Germany*

First received 18 July 1994; revised manuscript received 1 November 1994; accepted 11 November 1994

Abstract

A mixture of linear and cyclic methylsiloxanes was analysed to characterize the different types of siloxane structures using gas chromatography (GC), mass spectrometry (MS) and Fourier transform infrared (FT-IR) spectroscopy. Siloxane structures are formed by hydrolysis of dimethyldichlorosilane under controlled conditions in technical applications. In the presence of methyltrichlorosilane or even trimethylchlorosilane, linear polydimethylsiloxanes and mono-, bi- or polycyclic methylsiloxanes are synthesized depending on the reaction conditions. The main structural units are $(CH_3)_3SiO_{1/2}$, $(CH_3)_2SiO$ and $(CH_3)SiO_{3/2}$. GC–MS may provide molecular mass information, but it is not able to identify isomeric structures, which are also formed in lower quantities by the mentioned reactions. Coupling GC with FT-IR enables the determination of group frequencies to assign specific structures. Thus, combination of GC with MS and FT-IR may be used in elucidating complex cyclosiloxane compounds. FT-IR measurements were performed with a Tracer unit.

1. Introduction

Hydrolysis and following condensation reactions of $(CH_3)_2SiCl_2$ in the presence of small amounts of CH_3SiCl_3 lead to the formation of monocyclic polydimethylsiloxanes (PDMSs); a greater amount of the latter component is the reason for the formation of also bicyclic or even polycyclic methylsiloxanes with ladder or cage structures [1–3]. Mixtures of $(CH_3)_2SiCl_2$ and $(CH_3)_3SiCl$ lead to mainly linear PDMSs, $(CH_3)_3SiCl$ acting as a chain stopper in forming siloxanes with the general formula M_2D_n [where $D = (CH_3)_2SiO$].

Cyclic methylsiloxanes were analysed as products of the pyrolysis of silicone resins to reveal the mechanisms of thermal rearrangements [4]; also structural investigations were made considering the additivity of retention index values in GC [5].

The identification of a complex siloxane mix-

* Corresponding author.

0021-9673/95/$09.50
SSDI 0021-9673(94)01115-X

ture should be possible using the coupling of GC with MS and Fourier transform (FT) IR.

2. Experimental

2.1. Samples

A mixture of cyclic $\{[(CH_3)_2SiO]_m$, D_m, $m = 5–12\}$ and linear $\{(CH_3)_3SiO–[(CH_3)_2SiO]_n–Si(CH_3)_3$, MD_nM, $n = 3–10$; $M = (CH_3)_3SiO_{1/2}\}$ PMDSs was obtained by hydrolysis of a mixture of 400 g dimethyldichlorosiloxane (from Chemiewerk Nünchritz, containing approximately 100 ppm methyltrichlorosilane) and 100 g trimethylchlorosilane (Chemiewerk Nünchritz) in 1300 g water. The organic phase was separated, then washed neutrally with a saturated solution of $NaHCO_3$ in water and distilled over a 1 m Vigreux column under reduced pressure (20 Torr; 1 Torr = 133.322 Pa) up to 200°C. The fraction from 100 to 180°C (approximately 50 g) was used for our investigations.

2.2. GC–FT-IR

The measurements were made with a Bio-Rad Digilab FTS-45A spectrometer equipped with a liquid nitrogen-cooled narrow-band MCT detector and a Tracer connected with the gas chromatograph. Using a Fisons gas chromatograph GC 8130 the sample was separated on an HP Ultra 2 column (5% phenyl methylsilicone, 25 m × 0.2 mm, 0.33 μm film thickness). The helium (5.6) gas flow was 0.6 ml/min (24 cm/s). A 1-μl volume of the siloxane mixture, diluted 1:2.5 with dichloromethane, was injected with a split ratio of 1:30. The GC oven temperature was initially 80°C (1 min isothermal), then increased at 12°C/min to 250°C, with 20 min isothermal at 250°C for removing the last components from the column. A heated transfer line connects the column with evacuated Tracer chamber. The GC eluates are deposited onto a liquid nitrogen-cooled ZnSe window, which is computer-controlled moved by stepper motors. The deposition tip and the transfer line temperatures were 250°C in each case. The diameter of the deposited spots is about 0.1 mm. Recent studies have shown the advantages of using of the Tracer compared with the light-pipe interface for providing IR spectra of low-molecular-mass substances [6,7]. The window accommodates chromatographic separations of nearly 30 h, before a cleaning of the crystal of previous depositions at room temperature will be necessary. The function of the Tracer is depicted in Fig. 1.

The focused IR beam transmits the frozen eluate spots. After passing a microscope optic the beam enters the MCT detector. Therefore the recorded spectra show sharp bands by using the Tracer, which may be compared with those measured in condensed phase, and the sensitivity was improved significantly contrary to the light-pipe interface and for that reason GC–FT-IR is comparable to GC–MS. The advantages are described in, e.g., Ref. [8]. Absorbance spectra were recorded in the 4000–700 cm^{-1} region with a spectral resolution of 8 cm^{-1}. Four scans/s were coadded by a MCT frequency of 20 kHz. The data collection time was 20 min.

2.3. GC–MS

The GC equipment was a HP 5890 series II (Hewlett-Packard, Waldbronn, Germany), the carrier gas helium (5.0), the column inlet pressure was 70 kPa, the gas flow 0.7 ml/min. The column used for separation was a DB-5, 30 m × 0.25 mm, 0.25 μm film thickness; the temperature was initially 80°C (1 min), then increased at 12°C/min to 250°C, and 25 min isothermal at 250°C. The injector temperature was 250°C; splitless injection mode; samples were diluted in chloroform. The temperature of the transfer line to MS was held at 280°C.

The single-stage quadrupole mass spectrometer SSQ700 (Finnigan MAT, Bremen, Germany) was used in the mass range 80–1000 u in the electron impact (EI)/chemical ionization (CI) mode (CI with isobutane), tuning automatically with perfluorotributylamine (FC43), scan time 0.75 s. The manifold heater temperature was 70°C. The ion source temperature was held at 150°C in the EI mode, at 170°C in the CI mode.

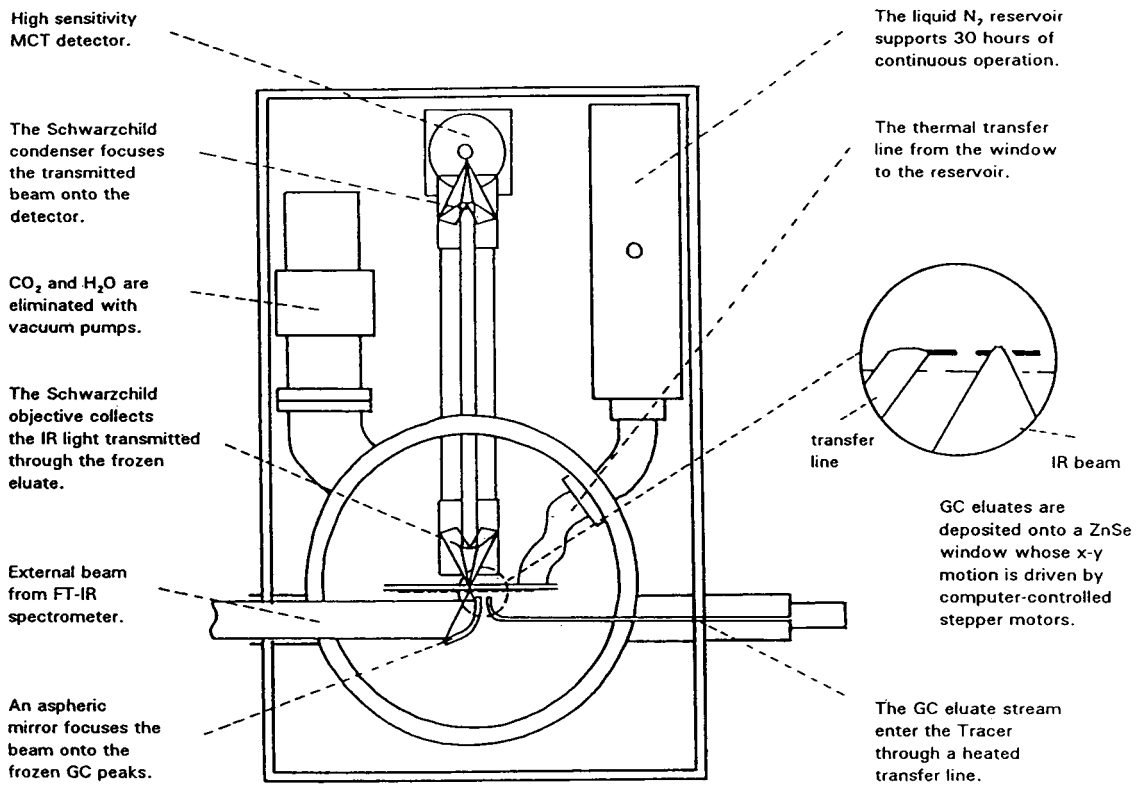

Fig. 1. Structure and function of the Tracer of the FTS-45A (Bio-Rad Digilab).

The ion source pressure in the CI mode was 6500 mTorr.

3. Results and discussion

3.1. GC–MS

Linear PDMSs

Fig. 2 shows the reconstructed ion chromatogram of the mixture containing linear and cyclic components. The mass spectra of all peaks were recorded in the EI and CI mode, where isobutane as reagent gas leads to the determination of MH^+ peaks. All spectra in the CI mode show the expected MH^+ peaks and also the cleavage of CH_4 from the quasi-molecular ion. All linear PDMSs (M_2D_n between M_2D_3 ($MH^+ = 385$) and M_2D_{11} ($MH^+ = 979$) are determined unambiguously. Polycyclic compounds were mainly expected eluting in the range between M_2D_3 and M_2D_5. In fact, the amounts of polycyclic compounds should be very low compared with linear and monocyclic methylsiloxanes.

Monocyclic methylsiloxanes

The cyclic compounds D_m were determined in the range of D_5 to D_{13} considering the MH^+ ions and the cleavage of methane using chemical ionization. Isobutane is useful as a reagent gas in obtaining MH^+ ions because of the capability to generate quasi-molecular ions without following fragmentation reactions.

Bicyclic methylsiloxanes

In the range between M_2D_3 ($M^+ = 384$) and M_2D_5 ($M^+ = 532$) several bicyclic siloxane structures are expected. These components will contain 6 or 7 silicon atoms, and very different structures are theoretically possible. The com-

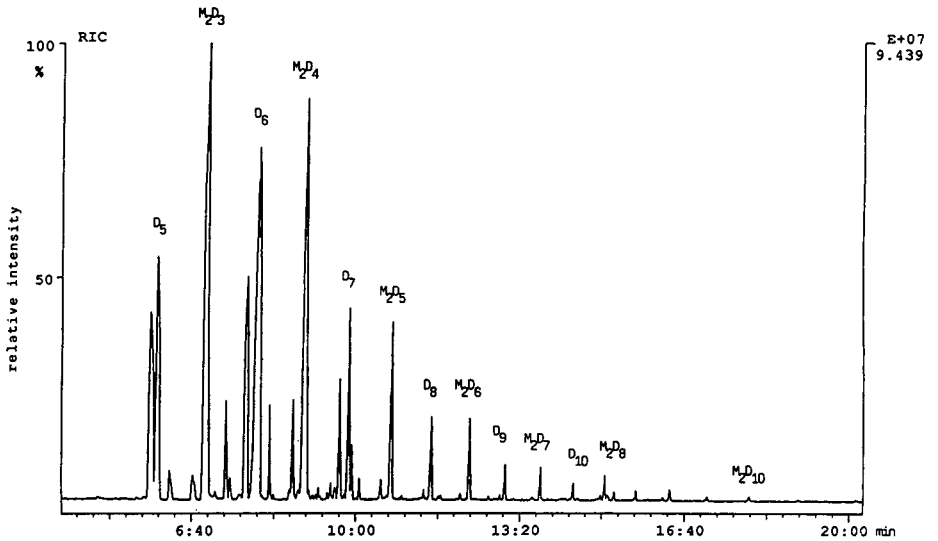

Fig. 2. Reconstructed ion chromatogram of siloxane mixture.

pound at 7.3 min in the GC–MS chromatogram shows a mass spectrum with $MH^+ = 431$ and is correlated to a siloxane with a bicyclic structure containing 6 silicon atoms (Fig. 3). This is to be concluded from the difference of 14 u to the molar mass of monocyclic D_6. FT-IR verifies this conclusion, and it is able to elucidate this compound to the bicyclic siloxane structure of T_2D_4 [$T = (CH_3)SiO_{3/2}$], as described later.

3.2. GC–FT-IR

Using GC–FT-IR real-time information about the cryotrapped components is available by calculating the Gram–Schmidt (GS) or functional group chromatograms [14]. The GS chromatogram shows the total absorbance of the detected peaks (Fig. 4).

By comparing the GS chromatogram with the

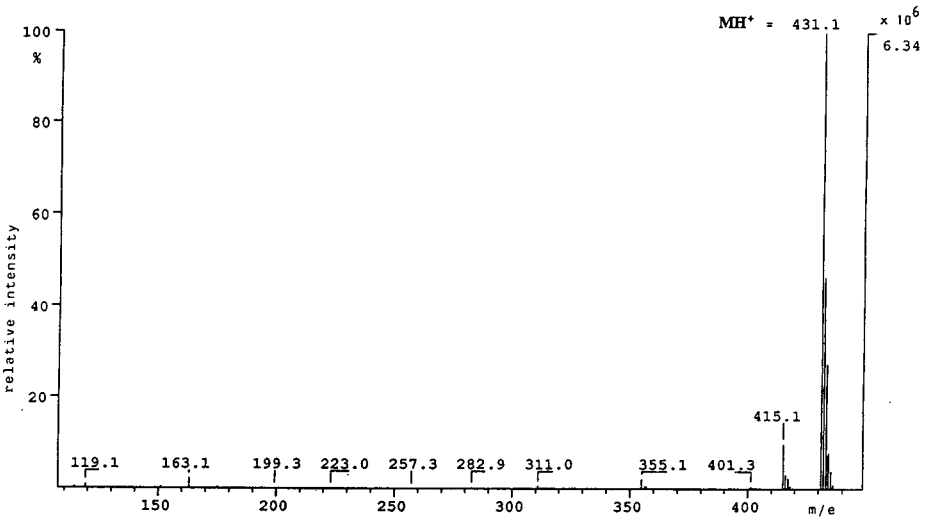

Fig. 3. Mass spectrum of the peak at 7.3 min of the ion chromatogram (CI mode).

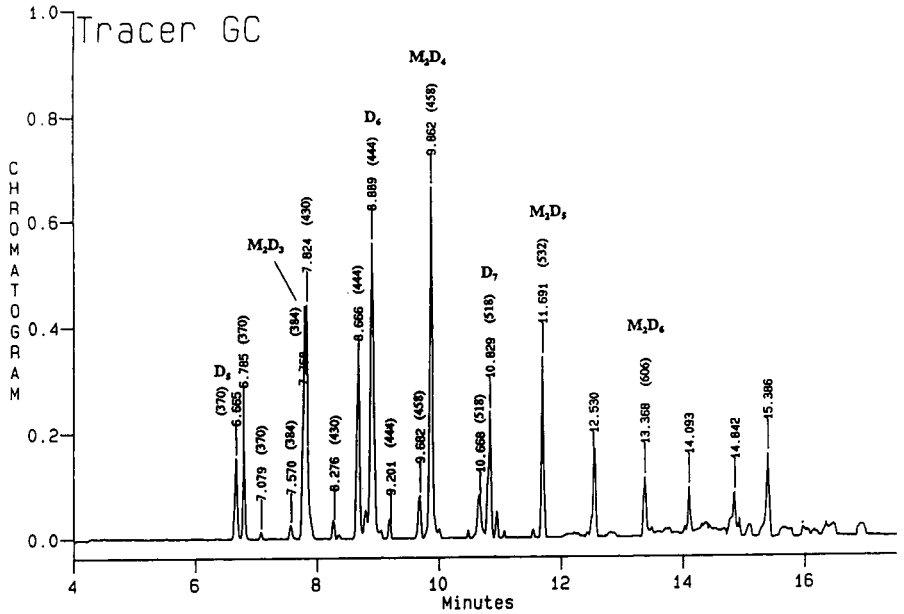

Fig. 4. Gram–Schmidt trace of siloxane mixture. Peaks are labeled (in parentheses) with values of molecular masses determined by GC–MS.

chromatogram of the GC–MS measurement a very good agreement is observed with regard to the retention of eluted compounds. Therefore some of the peaks detected by FT-IR were labeled with their molecular masses found by MS. The knowledge of the masses is very important for further identification.

In addition, the integrated absorptions of spectra created from each interferogram by Fourier transformation with reduced resolution give the special information with respect to characteristic Si–O, Si–CH_3 and CH groups of the sample components in this case, as shown in Fig. 5.

By means of IR spectra it is in principle possible to distinguish between linear chains, rings, branchings or networks in the siloxane framework. While the CH_3 stretching and bending frequencies are nearly the same in all compounds, the CH_3 rocking vibrations as well as the Si–O and Si–C frequencies are influenced by the structure of the molecule; therefore they are very helpful for interpretation of structural units [9]. The identification of the separated siloxane mixture is performed by assigning of the absorption bands and by comparing of the retention times with those from the GC–MS experiments. The GC–MS and GC–FT-IR results were confirmed by comparing the spectra and retention times with those from standards specially synthesized for this purpose. Because of the good agreement of the GS chromatogram with MS chromatogram (compare Fig. 4 with Fig. 1) the molecular masses (M_r) were adopted from the GC–MS experiment. Peaks with the same masses could be assigned to various structural groups for further identification using FT-IR: chains, monocyclic siloxanes, e.g. D_5 (M_r 370), D_6 (M_r 444) and D_7 (M_r 518) with their isomeric structures, or bicyclic siloxanes, e.g. D_4T_2 (M_r 430). GC–MS gives essential information about molecular masses, but cannot usually identify specific isomeric structures. The assignment of some of the separated compounds is suggested in this paper.

Linear PDMSs

Compounds with linear structures such as M_2D_3, M_2D_4, M_2D_5 and M_2D_6 were assigned to the peaks at retention times of 7.8, 9.9, 11.7 and

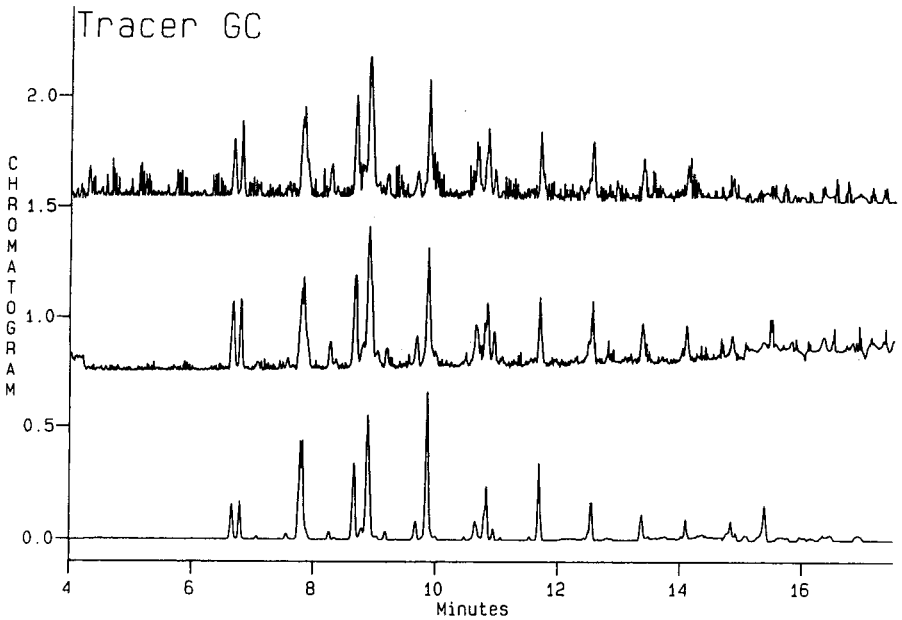

Fig. 5. IR chromatograms representing the integrated absorption of three selected spectral regions: lower trace: 2800–3000 cm^{-1}; middle: 780–900 cm^{-1}; upper: 990–1180 cm^{-1}.

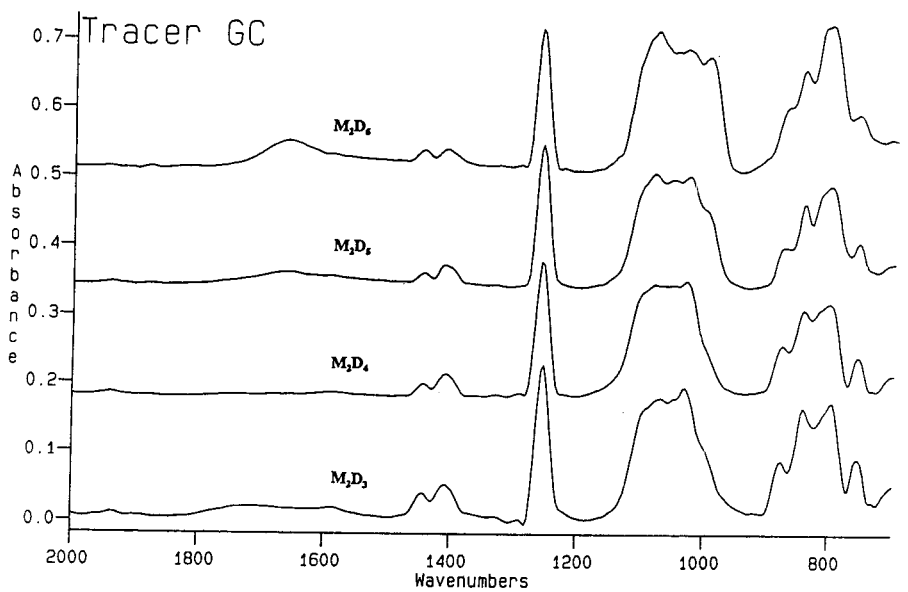

Fig. 6. Spectra of linear PDMSs ($n = 3$–6). Retention times: M_2D_3 = 7.76 min; M_2D_4 = 9.86 min; M_2D_5 = 11.69 min; M_2D_6 = 13.37 min.

13.4 min by means of the GC–MS results. The recorded subfile spectra are depicted in Fig. 6.

The spectra show the asymmetric Si–O–Si stretching vibrations split in several bands. In the spectra of M_2D_5 an additional band is formed as shoulder (near 1000 cm^{-1}), which is more structured and stronger in the M_2D_6 spectrum. Table 1 shows the frequencies of the spectra of Fig. 6. The assignments correspond to Refs. [9] and [10].

Monocyclic methylsiloxanes

D_6 is the main component of the analysed sample, but siloxanes with more D units and isomeric compounds were formed, too. In the case of D_5 (M_r 370) the GS chromatogram and the reconstructed ion chromatogram (RIC) show three peaks of the same mass. For D_6 and isomeric monocyclic siloxanes (M_r 444), too, three peaks were edited for interpretation, for D_7 (M_r 518) two peaks, for D_8 and also for D_9 one peak. For the higher siloxanes a lot of isomeric structures are possible, and the identification becomes more and more difficult. Fig. 7 shows the spectra of the peaks (M_r 370) at retention times 6.7, 6.8 and 7.1 min.

Some of characteristic vibrations of these compounds shifted by inductive, mechanical or steric effects, are listed in Table 2.

Especially the high absorption band at 1100 cm^{-1} in the spectrum of the peak eluted at 7.1 min points out a branched siloxane with a T unit, whereas the band at 1022 cm^{-1} is characteristic for a cyclotrisiloxane. The siloxane framework is constrained by well defined bond angles and the stretching vibration decreases to 1020 cm^{-1} [11]. M units in straight chains show absorption bands near 1055 cm^{-1}. The rocking vibration near 843 cm^{-1} is missing in cyclic siloxanes. The recorded spectra of the isomeric monocyclic structures (M_r 444) are given in Figs. 8–10. The defined structures are labeled in the figures.

The spectrum in Fig. 8 fully agrees with the spectrum of the cyclic tetramer siloxane MD_4T described by Smith [12] using the GC–FT-IR coupling technique (light-pipe device). The spectrum of the biggest peak of the GC chromatogram with M_r 444 is to be seen in Fig. 9. It consists of two components confirmed by GC–

Table 1
Assignment of stretching, bending and rocking vibrations of linear siloxanes (peaks are labeled in GS chromatogram in Fig. 4)

	M_2D_3, vibration $\tilde{\nu}$ (cm^{-1})	M_2D_4, vibration $\tilde{\nu}$ (cm^{-1})	M_2D_5, vibration $\tilde{\nu}$ (cm^{-1})	M_2D_6, vibration $\tilde{\nu}$ (cm^{-1})
$\nu_{as}CH_3$	2959	2960	2960	2962
ν_sCH_3	2901	2902	2903	2906
ν_{as}Si–O–Si	1075	1079	1081	1080
	1047	1054	1053	1036
	1031	1029	1027	1029
			1000 (sh)	996
$\delta_{as}CH_3$	1444	1444	1444	1444
δ_sCH_3	1255	1256	1258	1260
	1408	1408	1412	1410
ρSi–$(CH_3)_2$	876	875	874	872
ρ_{as}Si–$(CH_3)_3$	841	843	843	844
ρSi–CH3 and νSi–C	796, 754	801, 755	802, 755	803, 759

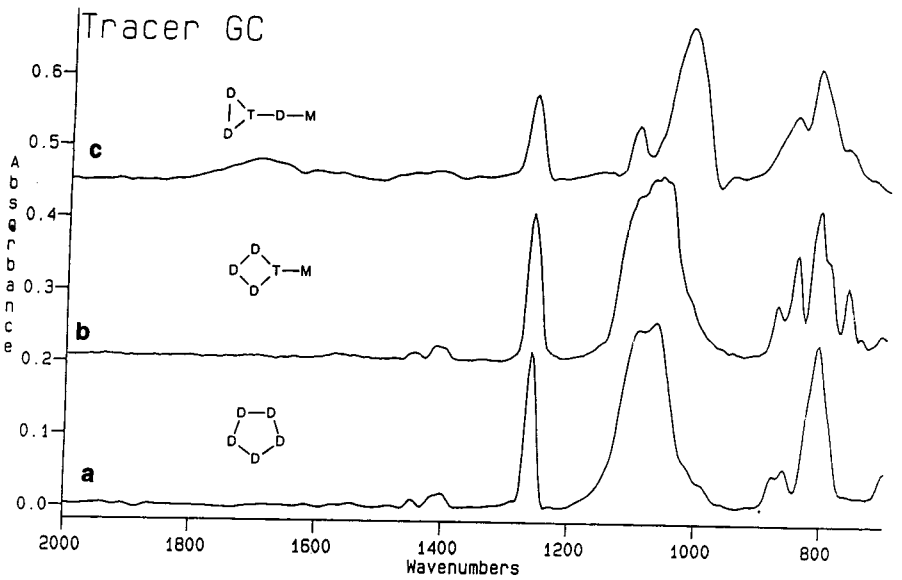

Fig. 7. Spectra of the compounds corresponding to the peaks at (a) 6.7 (6.67), (b) 6.8 (6.78) and (c) 7.1 (7.08) min in the GS chromatogram (M_r 370).

MS results. Therefore a superposed spectrum was observed. The band at 1091 cm^{-1} suggests a cyclic pentamer siloxane, the band at 1080 cm^{-1} a cyclic hexamer siloxane. The methyl rocking vibration band of $(CH_3)_2Si–O$ groups at 858 cm^{-1} represents D units. The 843 cm^{-1} band indicates M units. Together with the band at about 1050 cm^{-1} a linear siloxane structure coupled with the pentamer ring is concluded.

The spectrum in Fig. 10, corresponding to the peak at the retention time of 9.2 min, suggests a cyclotrisiloxane because of the very low Si–O–Si band at 1018 cm^{-1}. Linear parts are indicated by the bands at 847 and 1055 cm^{-1}. The additional band above 1100 cm^{-1} indicates a branched structure (T unit) [9].

Bicyclic methylsiloxanes

As described before, during the synthesis of dimethyldichlorosilanes other chlorosilanes are formed, mainly CH_3SiCl_3. The traces of CH_3SiCl_3 could cause the presence of compounds with molecular masses of $M_r(D_n) - 14$, because T units resulting from the hydrolysis/condensation process can be fitted into the cyclic siloxanes. From D_6, e.g., several T_2D_4 molecules [M_r 430 = $M_r(D_6) - 14$] with different isomeric structures are formed [13], see Fig. 11.

Table 2
Assignment of the IR bands (corresponding to Refs. [9] and [11]) for compounds with M_r 370

Retention time (min)	$\tilde{\nu}_{as}$Si–O–Si (cm^{-1})	Rocking vibrations (cm^{-1})	Structure
6.7	1091, 1065	864, 807	D_5
6.8	1096, 1072, 1060	872, 842, 808, 760	M
7.1	1100, 1055sh, 1020	845, 815	+chain

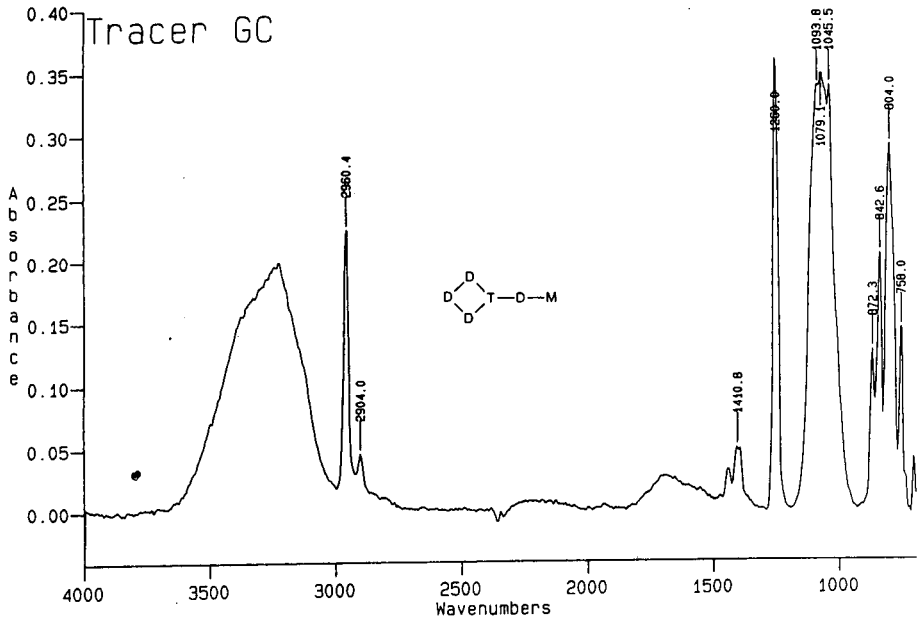

Fig. 8. Spectrum of cyclotetramer siloxane MD_4T (M_r 444).

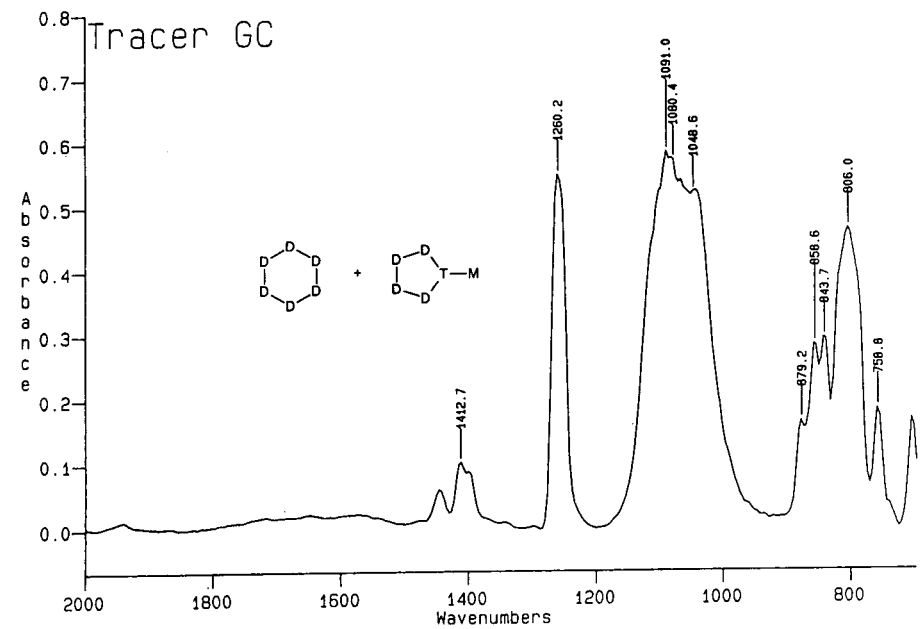

Fig. 9. Spectrum of the compounds corresponding to the unresolved peak at the retention time of 8.9 min in the GS chromatogram, assigned to D_6 and cyclopentamer siloxane MD_4T (M_r 444).

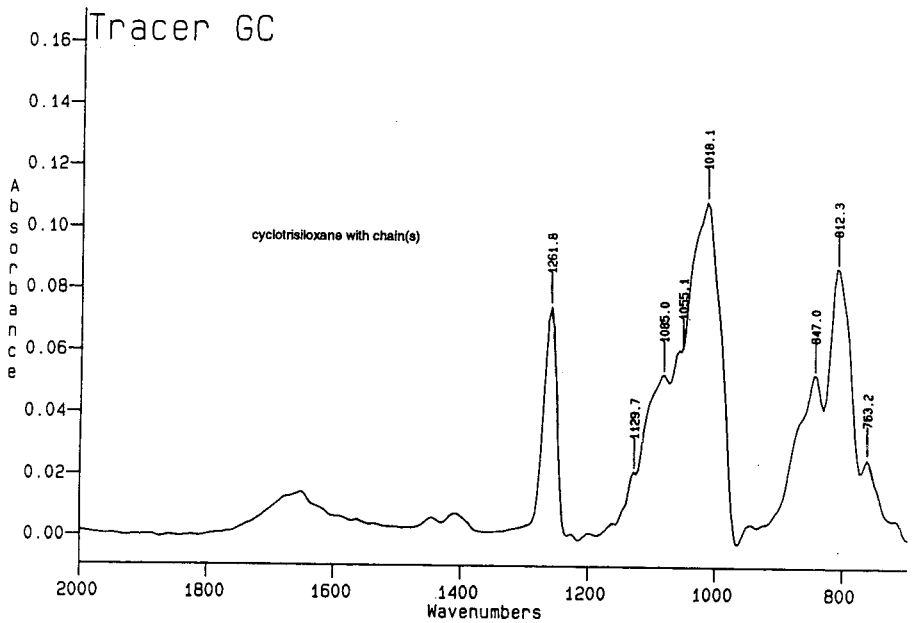

Fig. 10. Spectrum of the compound corresponding to the peak at the retention time of 9.2 min in the GS chromatogram, assigned to cyclotrimeric siloxane (M_r 444).

Fig. 12 shows the spectrum of the compound corresponding to the peak at 8.26 min and the suggested structure 2 of Fig. 11 as a bicyclic siloxane. The bands at 1072 and 1107 cm^{-1} indicate a cyclic tetramer siloxane with T units of a branched siloxane. The structures 1, 3 and 4 for T_2D_4 can be excluded in this case, because the characteristic bands for cyclic trimer siloxanes near 1020 cm^{-1} and for cyclic pentamer siloxanes near 1090 cm^{-1} are missing. Also a linear structure is excluded, because the bands at 843 and 1055 cm^{-1} are not to be seen in the spectrum.

4. Conclusions

Cryo-GC–FT-IR combined with GC–MS is a powerful tool in the elucidation of siloxane structure. Both techniques are supplementary in identifying cyclosiloxane compounds, especially isomers. A mixture of linear and cyclic siloxanes

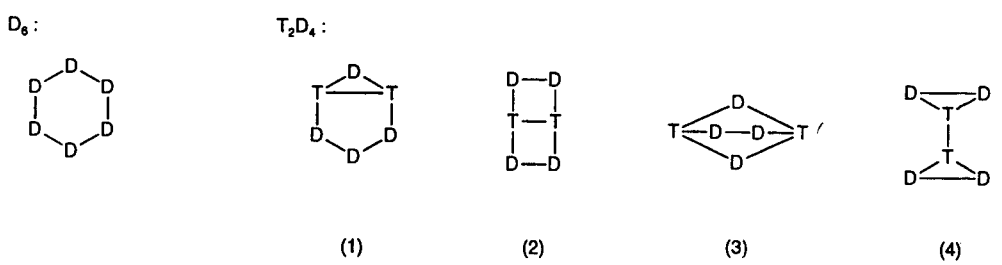

Fig. 11. Symbolic representation of D_6 and of geometric isomers of T_2D_4.

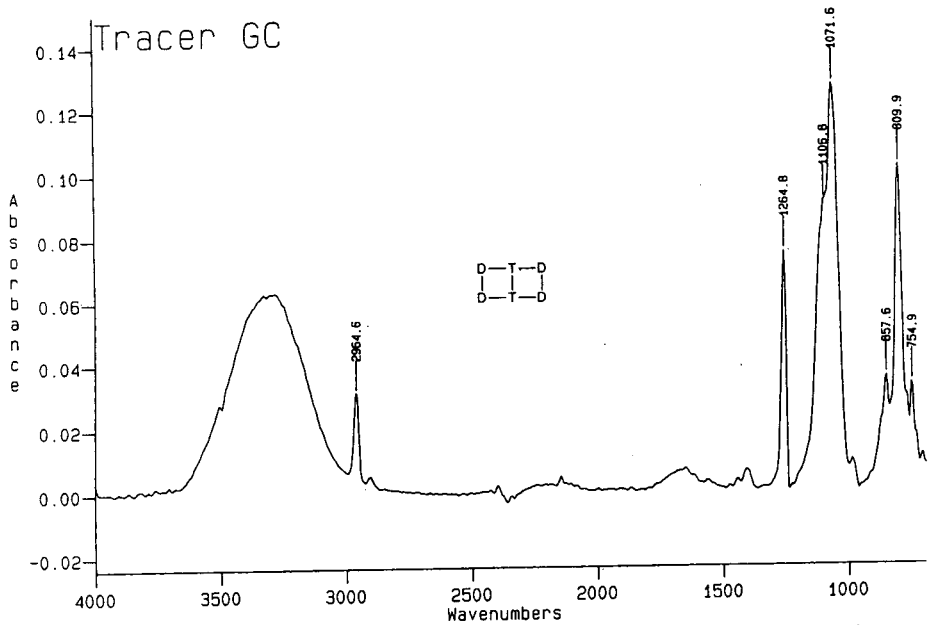

Fig. 12. Spectrum of the compound corresponding to the peak at the retention time of 8.3 min in the GS chromatogram, assigned to T_2D_4 (M_r 430).

assigned by these both techniques may be used as reference material for identifying low-molecular-mass siloxanes.

References

[1] D.W. Scott, *J. Am. Chem. Soc.*, 68 (1946) 356.
[2] W. Patnode and D.F. Wilcock, *J. Am. Chem. Soc.*, 68 (1946) 358.
[3] C.B. Hurd, *J. Am. Chem. Soc.*, 68 (1946) 364.
[4] G. Garzó, J. Tamás, T. Székely and K. Ujszászi, *Acta Chim. (Budapest)*, 69 (1971) 273.
[5] G. Alexander and G. Garzó, *Chromatographia*, 7 (1974) 190.
[6] J. Powell and S. Compton, *Tech. Quart.*, 3 (1991) 123.
[7] N.R. Smyrl, D.H. Hembree, Jr., W.E. Davis, D.M. Williams and J.C. Vance, *Appl. Spectros.*, 46 (1992) 2, 277.
[8] S. Bourne, A.M. Haefner, K.L. Norton and P.R. Griffiths, *Anal. Chem.*, 62 (1990) 2448.
[9] H. Kriegsmann, *Advances in Molecular Spectroscopy*, Pergamon Press, Oxford, 1962, pp. 999–1014.
[10] H. Kriegsmann, *Z. Anorg. Allg. Chem.*, 298 (1959) 232.
[11] E.D. Lipp and A.L. Smith, in A.L. Smith (Editor), *The Analytical Chemistry of Silicones*, Wiley, New York, 1991, p. 323.
[12] A.L. Smith, in J.R. Durig (Editor), *Chemical, Biological and Industrial Applications of Infrared Spectroscopy*, Wiley, New York, 1985, p. 73.
[13] H. Jancke, G. Engelhardt, M. Mägi and E. Lippmaa, *Z. Chem.*, 13 (1973) 392.
[14] G.M. Brissey, D.E. Henry, G.N. Giss, P.W. Yang, P.R. Griffiths and C.L. Wilkins, *Anal. Chem.*, 56 (1984) 2002.

ELSEVIER

Journal of Chromatography A, 693 (1995) 101–111

JOURNAL OF CHROMATOGRAPHY A

Influence of ageing on the supercritical fluid extraction of pollutants in soils

V. Camel[a], A. Tambuté[b], M. Caude[a,*]

[a]*Laboratoire de Chimie Analytique de l'Ecole Supérieure de Physique et Chimie Industrielles de Paris, 10 Rue Vauquelin, 75231 Paris Cedex 05, France*

[b]*Direction des Recherches et Etudes Techniques, Centre d'Etudes du Bouchet, BP No. 3, Le Bouchet, 91710 Vert-le-Petit, France*

First received 31 May 1994; revised manuscript received 30 September 1994; accepted 10 October 1994

Abstract

Soil samples were contaminated with several solutes, two means of contamination being evaluated to obtain homogeneous samples, in order to simulate real samples. The soils were allowed to age and periodically sampled. Letting the samples dry in a hood for less than 1 day resulted in a dramatic decrease in the recoveries, owing to evaporation of the spiking solvent. The extraction became generally more difficult as the ageing time increased, but the nature of both the solute and the soil had a strong influence on the results. Hence, a phosphonate and a phosphate were always quantitatively extracted, whereas aromatics were strongly retained in a very organic soil. Increasing the temperature, at constant pressure, greatly enhanced the extraction of all the investigated solutes. Similar results were obtained by adding methanol (10%, v/v) to the supercritical carbon dioxide; however, in that event, the dynamic time must be chosen with care, otherwise part of the extracted solutes is eluted from the trap by the polar modifier.

1. Introduction

For several years, considerable applications of supercritical fluid extraction (SFE) have been reported. Owing to the unique properties of supercritical fluids, this new technique has many advantages over classical extraction methods such as liquid–liquid extraction, namely speed of extraction, selectivity, safety, the possibility of direct coupling to chromatographic techniques [1–3] and mainly reduce the volumes of hazardous solvents. Indeed, the need for alternative extraction methods is emphasized by current efforts by the US Environmental Protection Agency to reduce by 95% the use of methylene chloride as an extraction fluid for environmental sample preparation in the next few years [4].

Supercritical carbon dioxide (CO_2) has proved to be efficient in removing selected pollutants from different environmental matrices [5], e.g., herbicides from soils [6,7], polychlorinated biphenyls (PCBs) from river sediments [8,9], polycyclic aromatic hydrocarbons (PAHs) from urban air particulate matter or soil [8,10] and total petroleum hydrocarbons (TPHs) from soils [11]. Unfortunately, supercritical CO_2 behaves as a non-polar extractant; so its extraction strength is insufficient for the quantitative recovery of many

* Corresponding author.

0021-9673/95/$09.50
SSDI 0021-9673(94)00972-4

polar analytes from adsorptive samples. As an example, phosphonates and phosphates in soil were not quantitatively extracted with pure CO_2 [12]. This problem may be partially overcome by the addition of a polar solvent (modifier) to the supercritical CO_2, either directly to the matrix itself or to the fluid via an additional pump. Thus, methanol-modified supercritical CO_2 gives much better recoveries for phosphonates and phosphates [12]. Methanol was also a good modifier during the SFE of organochlorine and organophosphorous pesticides from soils [13].

In some particular cases, a reactive modifier can be added to the matrix prior to the SFE. Some applications reported the in situ chemical derivatization of herbicides in soil and sediment using either trimethylphenylammonium hydroxide and boron trifluoride in methanol [14], or a mixture of tetrabutylammonium hydroxide and methyl iodide [15]. Also, the extraction of PAHs from urban dust and a marine sediment was greatly enhanced by the addition of a mixture of hexamethyldisilane and trimethylchlorosilane (2:1) to the CO_2, due to derivatization of the matrix [16].

Occasionally, other supercritical fluids have been preferred to CO_2 because of their higher solvation power. For example, N_2O gave better recoveries than CO_2 during the extraction of chlorinated dibenzofurans in municipal fly ash [17] or the extraction of amines from contaminated soils [18]; also, using $CHClF_2$ (Freon-22) or N_2O as the extractant greatly improved the recoveries of PCBs from sediment material, PAHs from petroleum waste sludge and PAHs from railroad bed soil [19]. However, the use of these fluids is not always possible. N_2O can oxidize some organic matrices, so we must take care with this supercritical fluid in order to avoid explosion hazards [20]. Despite its higher polarity, the use of $CHClF_2$ is also not recommended because of the negative environmental effects of Freons, particularly with ozone. For these reasons, CO_2 remains the most widely used extraction fluid.

The nature of the matrix to be extracted is of prime importance. For example, soils with a high organic content are known to usually retain polar solutes more strongly [21]. Numerous interactions may exist simultaneously between a solute molecule and a complex matrix. Spiking analytes on to heterogeneous matrices, such as soils, may not be a reliable means of representing the extraction behaviour of native analytes.

The purpose of this study was to investigate the reliability of employing SFE to extract pollutants from soil samples. The investigated solutes were two irritants (*o*-chlorobenzylidenemalonitrile and dibenzo[*b*,*f*]-1,4-oxazepin), and products related to toxic compounds, tributyl phosphate {a simulant, for the volatility, of a chemical warfare agent [O-ethyl,S-(2-diisopropylaminoethyl) methylphosphonothiolate or VX]}, pinacolyl ethyl methylphosphonate [a derivative of a chemical warfare agent (pinacolyl methylphosphonofluoridate or soman)], benzophenone (a final degradation product of the 3-quinuclidinyl benzylate or BZ) and methyl salicylate {a simulant, for the volatility, of a chemical warfare agent [bis(2-chloroethyl) sulfide or yperite]}. We also investigated two derivatives of the latter compound in order to determine the influence of the hydroxyl group on the retention.

We studied the effect of ageing (up to 60 days) for soil samples spiked using two techniques. The nature of the soil was also taken into account. The extraction conditions (pressure, temperature, addition of methanol to the CO_2) were changed to improve the recoveries.

2. Experimental

2.1. Reagents and chemicals

Ethyl salicylate (ES) and methyl 2-methoxybenzoate (MMYB) were obtained from Aldrich (Strasbourg, France) (purity 99%). Methyl salicylate (MS), methyl 2-methyl benzoate (MMB), tributyl phosphate (TBP), *o*-chlorobenzylidenemalonitrile (CB), dibenzo[*b*,*f*]-1,4-oxazepin (CR), 2-cyanodibenzo[*b*,*f*]-1,4-oxazepin (CR-CN), pinacolyl ethyl methylphosphonate (PEMP) and 2-methylcyclohexyl ethyl methylphosphonate (MCEMP) were synthesized

in our laboratory. Trimethyl phosphate (TMP) was obtained from Janssen Chimica (Noisy le Grand, France) (purity 97%). Benzophenone (B) was obtained from Prolabo (Paris, France) (purity 99%) and 2-chloro-5-nitrobenzophenone (ClNB) from Leune (Paris, France) (purity 99%). The structures and normal boiling temperatures of all the solutes and their related toxic compounds are illustrated in Fig. 1. Some of them were solids (CB, CR, CR-CN, B, ClNB) and others liquids (ES, MMYB, MS, MMB, PEMP, MCEMP, TBP, TMP) at room temperature.

Individual stock solutions of each solute at 1000 or 5000 ppm (μl l^{-1} for liquids, mg l^{-1} for solids) were prepared either in methanol (HPLC grade) or in diethyl ether (extra-pure grade) in order to spike the soil samples. They were kept in a refrigerator to avoid any degradation. However, as chemical degradation has been observed

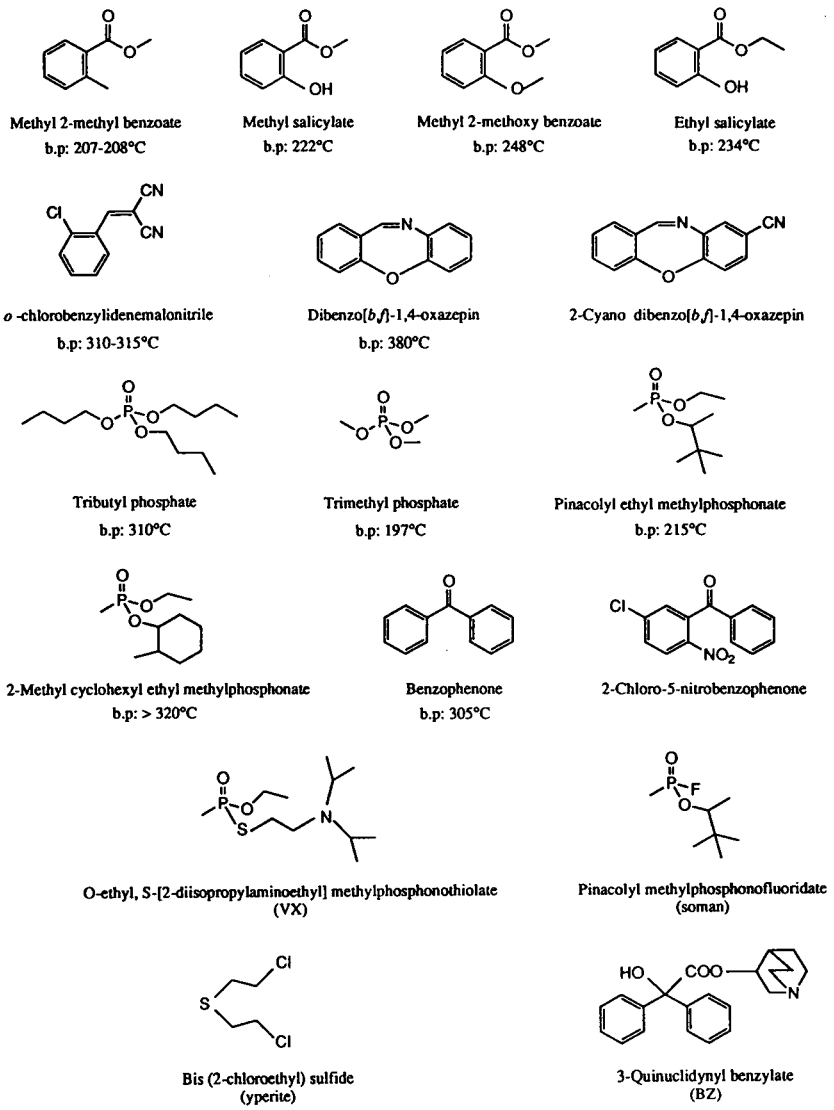

Fig. 1. Structures of the investigated compounds and of their related toxic compounds (b.p. = normal boiling temperature).

for CB in methanol, acetonitrile (gradient grade) was used as the solvent for the three related compounds CB, CR and CR-CN.

SFC-grade carbon dioxide (purity N 48; Alphagaz, Saint Quentin en Yvelines, France) was used as the supercritical fluid.

2.2. Soil samples

Three types of soil were used: a sand (a sandy loam soil: 83.4% sand, 13.7% silt, 2.9% clay, 0.4% moisture, 0.98% organic matter, surface area 1.6 $m^2 g^{-1}$); a podzol (91.9% sand, 5.4% silt, 2.7% clay, 1.1% moisture, 6.93% organic matter, surface area 0.4 $m^2 g^{-1}$) obtained from the French National Institute of Agronomic Research (INRA, Olivet, France); and an organic soil (9.6% sand, 59.6% silt, 30.8% clay, 25.8% organic matter) collected next to our laboratory (fine gravels were removed, then the soil was allowed to dry at room temperature for 1 week and sieved). For the sand and the podzol, the surface area was determined by the adsorption of liquid nitrogen at −195°C, using the Brunauer–Emmett–Teller (BET) method.

Contamination of the soil samples was performed using two different spiking methods.

In the "spot" method, approximately 5.5 g of soil were weighed in a cupel; 0.2 or 0.5 μl (for liquids) or 0.2 or 0.5 mg (for solids) of the solute(s) to be extracted (0.2 ml of the 1000 ppm solution or 0.1 ml of the 5000 ppm solution) were added directly to the soil and mixed with a spatula. This resulted in a contamination level of either 36 or 91 ppm. Then the sample was kept for an appropriate period of time (ageing time) in a hood at room temperature before its extraction.

In the "slurry" method, 300 g of dry soil were weighed into a flask; 10 μl (for liquids) or 10 mg (for solids) of each solute were mixed with 50 ml of diethyl ether, and the solution obtained was added to the soil. Then the flask was placed in a rotary evaporator for 1 h at 60°C in order to remove the diethyl ether gently. Assuming that the contamination was homogeneous, the contamination level was 33 ppm for each solute. The contaminated soils obtained were kept at room temperature and aliquots (5.5 g) were periodically sampled and extracted.

2.3. Supercritical fluid extraction

All SFE experiments were carried out using an HP 7680A supercritical fluid extractor (Hewlett-Packard France, Les Ulis, France). Approximately 5.5 g of soil were placed in the 7-ml thimble. The sample was typically extracted with CO_2 at 200 bar, 40°C (density 0.84 g ml^{-1}), and 1 ml min^{-1} of liquid CO_2 as the flow-rate in the dynamic mode. The nozzle was maintained at 45°C to prevent plugging. Extracted solutes were usually trapped on an octadecylsilica (ODS, 30–40 μm particle diameter) column maintained at 30°C. After the extraction, the trap was rinsed with 0.9 ml of methanol to elute the extracted solutes (one rinse was sufficient).

Each experiment was done in triplicate to give an average extraction recovery and a relative standard deviation (R.S.D.). In addition, blank extractions of the empty vessel were conducted between two experiments to clean the system. No memory effect was observed.

If insufficient recoveries were obtained after a typical dynamic extraction of 15 min with supercritical CO_2 (40°C, 200 bar, 1 ml min^{-1}), additional extractions were usually performed with methanol–supercritical CO_2 mixtures. Addition of methanol was made either directly to the sample (the soil was put back in the cupel and mixed with methanol; the sample was placed in the cell again and another extraction was performed), or continuously using an auxiliary pump (Hewlett-Packard Model 1050).

In some experiments, the gaseous CO_2 leaving the trap was collected in methanol using two successive vials, in order to dissolve the solutes that might be entrained out of the trap. Each vial contained 5 ml of solvent maintained at −14°C using a cryostat. After the extraction, the solutions were sonicated for a few minutes to remove the dissolved carbon dioxide, then 1.5 μl of each

vial content was analysed using gas chromatography, after the addition of an internal standard.

2.4. Gas chromatographic analysis

The extracts were analysed by gas chromatography with flame ionization detection (GC–FID) using a Varian Model 3400 instrument equipped with a Varian Model 8200 autosampler, a split–splitless injector and a 25 m × 0.25 mm I.D. fused-silica capillary column (CP-Sil-5 CB, 0.25 μm film thickness; Chrompack). Helium was used as the carrier gas (1 ml min^{-1}) and as the FID make-up gas (30 ml min^{-1}). The injector and detector temperatures were 250 and 300°C, respectively. Samples (1.5 μl) were injected with a splitting ratio of 1:25 using the solvent flush technique (methanol was used as the rinse solvent). A good separation of all the solutes was achieved using the following column temperature programme: 80°C for 4 min, ramped at 5°C min^{-1} to 120°C (maintained for 2 min) and at 5°C min^{-1} to 180°C (maintained for 15 min). The elution order of analytes was: trimethyl phosphate, methyl 2-methylbenzoate, methyl salicylate, pinacolyl ethyl methylphosphonate, ethyl salicylate, methyl 2-methoxybenzoate, 2-methylcyclohexyl ethyl methylphosphonate, *o*-chlorobenzylidenemalonitrile, benzophenone, tributyl phosphate, dibenzo[*b*,*f*]-1,4-oxazepin, 2-cyanodibenzo[*b*,*f*]-1,4-oxazepin and 2-chloro-5-nitrobenzophenone.

Quantification was based on the addition of an appropriate internal standard directly to the trap rinse solution: trimethyl phosphate for tributyl phosphate; ethyl salicylate for methyl salicylate, methyl 2-methylbenzoate and methyl 2-methoxybenzoate; 2-cyanodibenzo[*b*,*f*]-1,4-oxazepin for *o*-chlorobenzylidenemalonitrile and dibenzo[*b*,*f*]-1,4-oxazepin; 2-methylcyclohexyl ethyl methylphosphonate for pinacolyl ethyl methylphosphonate; and 2-chloro-5-nitrobenzophenone for benzophenone. Calibration graphs were obtained using a Shimadzu Model C-R5A integrator. Excellent correlation coefficients were obtained ($R > 0.9992$).

3. Results and discussion

A preliminary study was first conducted to check the efficiency of the collection step. Freshly contaminated samples were extracted at 40°C, 200 bar and 1 ml min^{-1} CO_2. After only 15 min (30 min for pinacolyl ethyl methylphosphonate), quantitative recoveries were obtained for all the solutes. Indeed, we expected the extraction to be easy, because the spiking solvent was initially present in the cell, and also the solutes did not have time to diffuse inside the matrix. In fact, these results underline the efficiency of the collection on an octadecylsilica column maintained at 30°C.

However, we noticed an entrainment effect with the more volatile solutes, methyl salicylate and methyl 2-methylbenzoate, for extraction times longer than 20–30 min (this was confirmed by collecting the CO_2 leaving the trap in methanol using two successive vials maintained at −14°C). Additional experiments showed that losses could be avoided by using a silica gel column, owing to hydrogen bonding between the solutes and the silanol groups of the silica.

3.1. Extraction of soil samples contaminated using the "spot" method

After their contamination, soil samples were kept in the hood at room temperature for a certain period of time. Several experiments were conducted to investigate the effect of the spiking solvent on the recovery. Because the nature of either the matrix, the solute or the solvent can have a strong influence on the results, several combinations were studied.

Sand–CB or CR–acetonitrile

Firstly, sand samples were contaminated with 0.5 mg of *o*-chlorobenzylidenemalonitrile or dibenzo[*b*,*f*]-1,4-oxazepin dissolved in acetonitrile, and allowed to dry in the hood at room temperature for about 1–3 days. Mean recoveries vs. extraction time are illustrated in Fig. 2. A 30-min extraction with pure CO_2 gave recoveries of only 30% for *o*-chlorobenzyl-

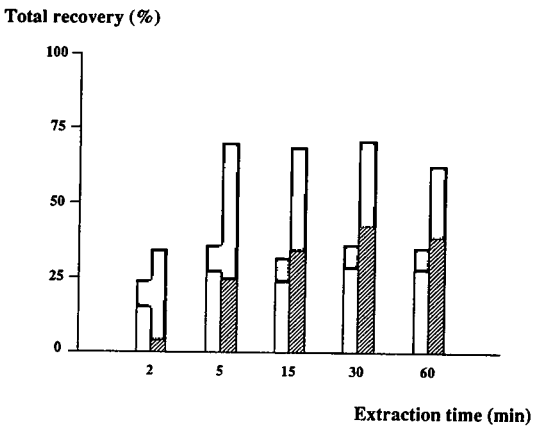

Fig. 2. Recoveries for *o*-chlorobenzylidenemalonitrile (CB) and dibenzo[*b*,*f*]-1,4-oxazepin (CR) from aged spiked sand samples (1–3 days) for several extraction times. CB: (▭) 1st extraction; (▭) 2nd extraction (addition of 0.2 ml methanol). CR: (▨) 1st extraction; (▭) 2nd extraction (addition of 0.2 ml methanol). Extraction conditions: $T_{cell} = 40°C$, $P = 200$ bar, 1 ml min^{-1} of liquid CO_2, $T_{nozzle} = 45°C$, $T_{trap} = 30°C$ (ODS), 0.2 min static followed by the dynamic period specified, spiking of 0.5 mg of each solute in acetonitrile.

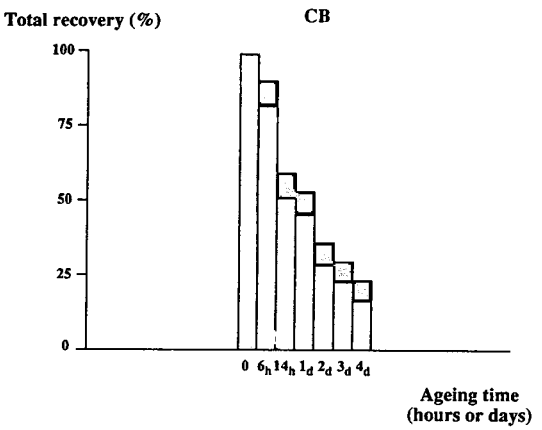

Fig. 3. Influence of the ageing time (up to 4 days) on the recovery of *o*-chlorobenzylidenemalonitrile (CB) added to sand samples using the "spot" method. (▭) 1st extraction; (▭) 2nd extraction (addition of 0.2 ml of methanol). Extraction conditions: $T_{cell} = 40°C$, $P = 200$ bar, 1 ml min^{-1} of liquid CO_2, $T_{nozzle} = 45°C$, $T_{trap} = 30°C$ (ODS), 0.2 min static followed by 15 min dynamic, spiking of 0.5 mg of CB in acetonitrile.

idenemalonitrile and 43% for dibenzo[*b*,*f*]-1,4-oxazepin. Apparently, no more solute could be extracted with longer extraction times (60 min) under these conditions (40°C, 200 bar, 0.84 g ml^{-1}). Extracting the samples at a higher temperature or pressure (density) would certainly result in improved recoveries, but the purpose of this study was simply to determine the role of the spiking solvent.

Each sample was re-extracted under the same conditions after the addition of methanol (0.2 ml) directly to the soil. As can be observed in Fig. 2, this solvent enhanced the extraction, especially for dibenzo[*b*,*f*]-1,4-oxazepin. This could result from hydrogen bonds between dibenzo[*b*,*f*]-1,4-oxazepin molecules and methanol. However, high relative standard deviations were obtained: 5–12% for dibenzo[*b*,*f*]-1,4-oxazepin and ca. 25% for *o*-chlorobenzylidenemalonitrile, probably because of differences in ageing times between triplicate samples (1–3 days). This was confirmed by performing 15-min extractions of aged samples (up to 4 days) contaminated with *o*-chlorobenzylidenemalonitrile (Fig. 3). The recoveries decreased after 6 h, but this time better relative standard deviations were obtained between the triplicate samples (2.4–18.5%). As no trace of any degradation product was detected by gas chromatography, part of the *o*-chlorobenzylidenemalonitrile may be either strongly bound to the matrix or, more probably, transformed into polar compound(s) that is (are) either difficult to extract or to determine using gas chromatography (as the normal boiling temperature of *o*-chlorobenzylidenemalonitrile is 310–315°C, the decrease in recoveries cannot be attributed to evaporation losses).

Organic soil–MMB, MS and MMYB–methanol

The next study was conducted to investigate the effect of ageing for other solutes. This time, organic soil samples were contaminated with methyl 2-methylbenzoate, methyl salicylate and methyl 2-methoxybenzoate using the "spot" method (methanol was used as the spiking solvent), and kept at room temperature in the hood for a given time (up to 4 days) before their extraction. As can be observed in Fig. 4, quan-

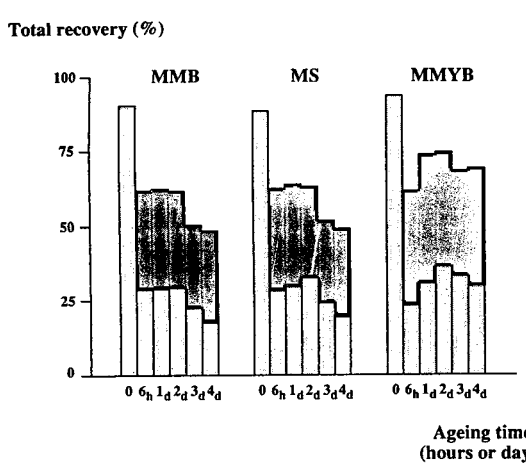

Fig. 4. Influence of the ageing time (up to 4 days) on the recovery of methyl 2-methylbenzoate (MMB), methyl salicylate (MS) and methyl 2-methoxybenzoate (MMYB) added to organic soil samples using the "spot" method. (□) 1st extraction; (■) 2nd extraction (addition of 0.2 ml of methanol). Extraction conditions: $T_{cell} = 40°C$, $P = 200$ bar, 1 ml min^{-1} of liquid CO_2, $T_{nozzle} = 45°C$, $T_{trap} = 30°C$ (ODS), 0.2 min static followed by 15 min dynamic, spiking of 0.2 μl of each solute in methanol.

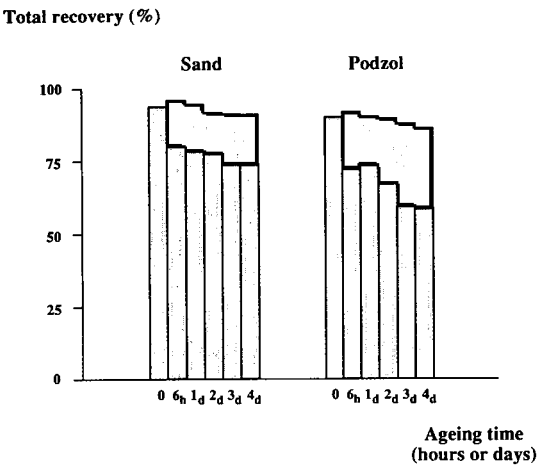

Fig. 5. Influence of the ageing time on the recovery of benzophenone (B) added to sand or podzol samples using the "spot" method. (□) 1st extraction; (■) 2nd extraction (addition of 0.2 ml of methanol). Extraction conditions: $T_{cell} = 40°C$, $P = 200$ bar, 1 ml min^{-1} of liquid CO_2, $T_{nozzle} = 45°C$, $T_{trap} = 30°C$ (ODS), 0.2 min static followed by 15 min dynamic, spiking of 0.2 μl in methanol.

titative extractions could be obtained for the three solutes immediately after their spiking. However, letting the samples dry in the hood (even for only 6 h) led to lower recoveries. This phenomenon can be explained either by the strong adsorption of the solutes molecules on the active sites of the matrix (the partitioning of the solutes is controlled by the "chemistry of the system"), or by the evaporation of methanol (methanol enhances the solute extraction).

Improved recoveries could be obtained after the addition of 0.2 ml of methanol directly to the soil samples and the performance of another extraction. Hence the low recoveries observed after the first extraction are mainly attributable to the absence of methanol.

Sand or podzol–B–methanol

In a similar study, we contaminated sand and podzol samples with 0.5 mg of benzophenone (methanol as the spiking solvent) and allowed them to dry in the hood (up to 4 days). Once extracted with pure CO_2 for 15 min, each sample was re-extracted after the addition of methanol (0.2 ml) directly to the soil. As illustrated in Fig. 5, benzophenone was easily extracted. Quantitative recoveries (around 90%) were obtained for freshly contaminated samples. Letting the samples dry resulted in slightly lower values, especially for podzol. However, 15-min extractions with pure CO_2 under moderate conditions (40°C, 200 bar, 1 ml min^{-1}) gave better results than for the solutes we studied earlier: 73% for sand and 58% for podzol after 4 days of ageing. In addition, high recoveries could be obtained after the second extraction, 91% and 86%, respectively. All the above results underline the fact that the spiking solvent enhances the extraction. Letting the solvent evaporate leads to two cases, depending on the solute nature. For non-polar compounds (i.e., highly soluble in pure supercritical carbon dioxide), quantitative extractions will still be obtained under the same conditions. In contrast, for the others, lower recoveries will be obtained. In fact, the latter case seems more frequent. To overcome the solute retention inside the matrix, a modifier can be added; however, a large solvent volume will lead to losses if

small columns are used to trap the analytes (owing to an elution effect inside the trap).

In order to simulate real soil samples, we further contaminated larger amounts of soil (300 g) according to the "slurry" method described earlier.

3.2. Extraction of soil samples contaminated using the "slurry" method

Influence of ageing time on the recoveries

Organic soil–MS and TBP–diethyl ether. Similar experiments were conducted with organic soil samples contaminated using the "slurry" method with methyl salicylate and tributyl phosphate (organic soil A). Extraction conditions were the same as above (Table 1). The results are illustrated in Fig. 6a. Whereas tributyl phosphate was still quantitatively extracted, methyl salicylate remained strongly retained on the matrix. Good relative standard deviations could be obtained between samples, showing the homogeneity of the contamination.

Organic soil–all investigated solutes–diethyl ether. Finally, the same protocol was used to contaminate the organic soil with all eight solutes investigated. Two kinds of soil samples were obtained (organic soils D_1 and D_2). Assuming the contamination was homogeneous, soil D_1 would contain 33 ppm of each solute. Soil D_2 would differ from soil D_1 in that benzophenone was ten times more concentrated (330 ppm) (we wanted to see if, with such a high concentration, the ODS trap would be overloaded, thus leading to inefficient collection).

The results obtained for D_1 are illustrated in Fig. 6b. Whereas pinacolyl ethyl methylphosphonate and tributyl phosphate could be quantitatively extracted for all samples, the mean recoveries decreased with ageing time for the other solutes, showing the progressive retention of the solute molecules on less accessible active sites. The fact that only aromatics were retained in the organic soil was probably due to $\pi-\pi$ interactions between these solutes and the organic matter of the soil [22]. Pinacolyl ethyl methylphosphonate and tributyl phosphate have neither a polar group nor an aromatic ring; as a consequence, they were easily extracted from the organic soil.

No trace of *o*-chlorobenzylidenemalonitrile could be detected in the extracts. Instead, one of its retro-synthesis product (*o*-chlorobenzaldehyde or CB*) was found. As this compound could not be detected for soil samples previously contaminated using the "spot" method, we believe that the higher temperature (60°C) used during the "slurry" contamination method enhanced the degradation of *o*-chlorobenzylidenemalonitrile. Thus, the following reaction seemed to take place:

Table 1
Experimental conditions for successive extractions

Successive extraction	Static period (min)	Dynamic period (min)	Volume of modifier added to the soil (μl)	Modifier added to the CO_2
1st	0.2	15	0	None
2nd	0.2	15	0	3% CH_3OH
3rd	0.2	15	0	5% CH_3OH
4th	5	15	500	None
5th	0.2	15	0	20% CH_3OH

$T_{cell} = 40°C$, $P = 200$ bar, 1 ml min^{-1} CO_2 liquid, $T_{trap} = 30°C$, $T_{nozzle} = 45°C$.

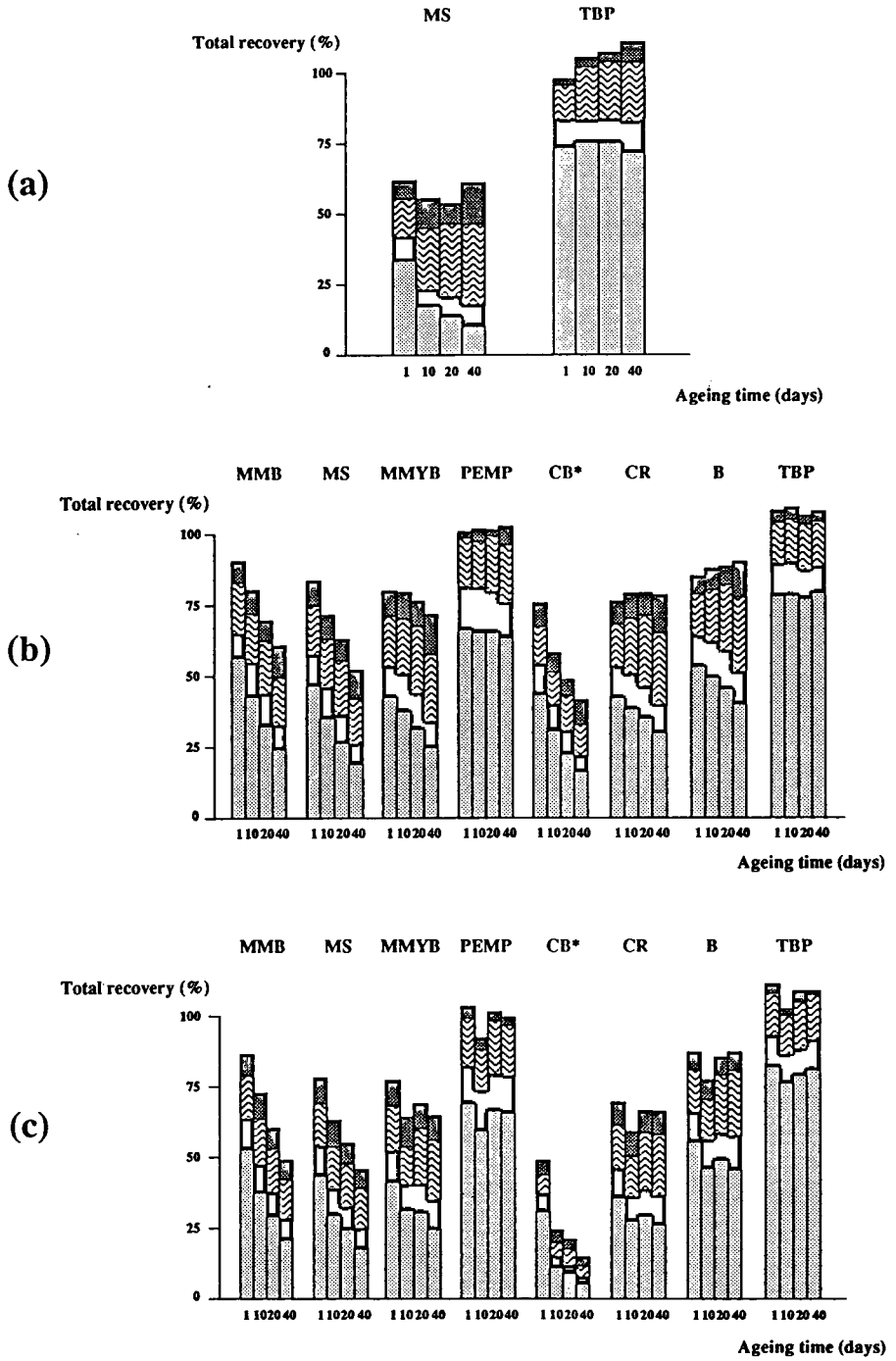

Fig. 6. Influence of the ageing time on the recovery of solutes added to organic samples using the "slurry" method. (a) Organic soil A; (b) organic soil D_1; (c) organic soil D_2. (▭) 1st extraction; (▭) 2nd extraction; (▭) 3rd extraction; (▭) 4th extraction. Extraction conditions: as in Table 1.

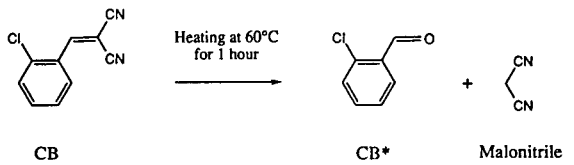

However, we cannot be certain that all the *o*-chlorobenzylidenemalonitrile was degraded, because no quantitative recoveries of *o*-chlorobenzaldehyde could be obtained. The other degradation product, malonitrile, was not present in the extracts; this might be due to its strong adsorption on the active sites of the matrix.

Similar results were obtained for D_2 (Fig. 6c), showing that the contamination level of B was still acceptable for the trap. Lower recoveries were observed for *o*-chlorobenzaldehyde, perhaps because less *o*-chlorobenzylidenemalonitrile had been degraded or because a stronger retention in the matrix took place.

The above results underline the homogeneity and the reproducibility obtained with such a contamination method.

A visual observation could be made whenever 0.5 ml of methanol was added directly to the organic soil samples: the extracts became yellow (for sand samples the colour was also visible, but it was less pronounced). This indicates that the addition of a modifier may entail the co-extraction of solutes and materials from the matrix (this could lead to a lower solubility of the investigated solutes in the supercritical fluid). Fortunately, in our study, they did not interfere with the solutes during the gas chromatographic analysis.

Effect of extraction conditions on recoveries

In order to improve the extraction recoveries of all the solutes from D_1 (ageing time ca. 55–60 days for the following experiments), we investigated the effect of changing either the density, the temperature or the nature of the fluid. The results are illustrated in Fig. 7.

Increasing the density at 40°C (0.95 instead of 0.84 g ml^{-1}) had no significant influence on the recoveries. On the other hand, elevating the temperature from 40° to 100°C resulted in enhanced recoveries, despite the fact that the density was lowered (0.74 g ml^{-1}). This positive effect of the temperature has already been observed during the extraction of native PAHs [10,23] and PCBs from sediments [8,9]. It probably results from an increase of the analytes' volatility (for the volatile compounds) or/and an easier desorption of the solute molecules from the active sites of the matrix. The distribution constant of a solute between the matrix and the fluid is defined as the ratio

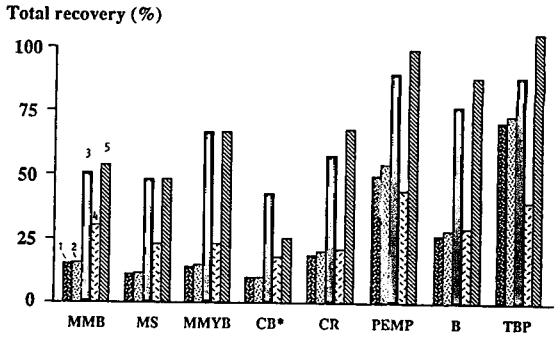

Fig. 7. Influence of the extraction conditions on the recovery of solutes added to organic soil samples using the "slurry" method (ageing time 55–60 days). (1) CO_2, 40°C, 200 bar, 0.84 g ml^{-1}, 15 min; (2) CO_2, 40°C, 383 bar, 0.95 g ml^{-1}, 15 min; (3) CO_2, 100°C, 379 bar, 0.74 g ml^{-1}, 15 min; (4) CO_2 + 10% CH_3OH, 40°C, 200 bar, 15 min; (5) CO_2 + 10% CH_3OH, 40°C, 200 bar, 3 × 5 min. Extraction conditions: 1 ml min^{-1} of liquid CO_2, T_{nozzle} = 45°C, T_{trap} = 30°C (ODS), 0.2 min static.

$$K = C^M / C^{SF}$$

where C^M and C^{SF} are the concentrations in the matrix and in the supercritical fluid, respectively. It is well known that K depends strongly on the temperature T, according to

$$\log K = -\Delta G / RT$$

where ΔG is the free energy and R the gas constant. As a consequence, an increase in temperature would lead to a decrease in K and, thus, to a higher solute concentration in the fluid.

Finally, adding 10% methanol (with a second pump) to the supercritical carbon dioxide slightly improved the recoveries of most of the solutes, compared with the results obtained with pure

CO_2 under the same conditions (Fig. 7). For benzophenone, similar results were observed; this was expected because this solute is non-polar. However, the observed recoveries of pinacolyl ethyl methylphosphonate and tributyl phosphate were reduced. This was surprising, as the addition of a modifier is known to have either a positive influence or no effect. We therefore suspected elution of the solutes by the modifier inside the trap during the extraction. To check this assumption, we conducted the same experiments but, this time, we performed three successive 5-min extractions. The gaseous CO_2 was collected using two successive vials filled with 5 ml of methanol at −14°C; they were changed and analysed after each 5-min extraction. The total recoveries for the three successive extractions are illustrated in Fig. 7. Much better values were obtained with this method than after a single 15-min extraction. This clearly demonstrates that during the 15-min extraction, the extracted solutes were partially eluted from the trap by methanol.

Again, employing methanol-modified CO_2 resulted in yellow extracts, because some matrix materials were co-extracted.

4. Conclusions

The supercritical carbon dioxide extraction of several solutes has been investigated. The spiking solvent, whatever its nature (methanol, acetonitrile or diethyl ether), enhanced the extraction. The retention depended on the nature of the soil–solute system. Whereas pinacolyl ethyl methylphosphonate and tributyl phosphate were quantitatively extracted, aromatics remained strongly bound to the matrix (probably owing to $\pi-\pi$ interactions between aromatics and the organic matter).

The addition of methanol to the CO_2 resulted in higher recoveries; however, care must be taken to avoid elution of the extracts by the modifier inside the solid trap. In addition, yellow extracts were obtained because of the co-extraction of soil materials. These two drawbacks can be avoided by increasing the extraction temperature instead of adding modifier to the fluid. This much easier way of obtaining high extraction recoveries should give acceptable results for real samples.

References

[1] L. Myer, J. Tehrani, C. Thrall and M. Gurkin, *Int. Labmate*, 15, No. 7 (1991) 15–19.
[2] J.L. Guinamant, *Analusis*, 20 (1992) m36–m38.
[3] V. Camel, A. Tambuté and M. Caude, *Analusis*, 20 (1992) 503–528.
[4] S.B. Hawthorne, in S.A. Westwood (Editor), *Supercritical Fluid Extraction and its Use in Chromatographic Sample Preparation*, Blackie, Glasgow, 1993, p 39.
[5] V. Camel, A. Tambuté and M. Caude, *J. Chromatogr.*, 642 (1993) 263–281.
[6] S. Ashraf, K.D. Bartle, A.A. Clifford, R. Moulder, M.W. Raynor and G.F. Shilstone, *Analyst*, 117 (1992) 1697–1700.
[7] T.R. Steinheimer, R.L. Pfeiffer and K.D. Scoggin, *Anal. Chem.*, 66 (1994) 645–650.
[8] J.J. Langenfeld, S.B. Hawthorne, D.J. Miller and J. Pawliszyn, *Anal. Chem.*, 65 (1993) 338–344.
[9] H.-B. Lee and T.E. Peart, *J. Chromatogr. A*, 663 (1994) 87–95.
[10] J.M. Levy, L.A. Dolata and R.M. Ravey, *J. Chromatogr. Sci.*, 31 (1993) 349–352.
[11] V. Lopez-Avila, J. Benedicto, N.S. Dodhiwala, R. Young and W.F. Beckert, *J. Chromatogr. Sci.*, 30 (1992) 335–343.
[12] W.H. Griest, R.S. Ramsey, C.-H. Ho and W.M. Caldwell, *J. Chromatogr.*, 600 (1992) 273–277.
[13] J.L. Snyder, R.L. Grob, M.E. McNally and T.S. Oostdyk, *Anal. Chem.*, 64 (1992) 1940–1946.
[14] S.B. Hawthorne, D.J. Miller, D.E. Nivens and D.C. White, *Anal. Chem.*, 64 (1992) 405–412.
[15] V. Lopez-Avila and N.S. Dodhiwala, *J. Agric. Food Chem.*, 41 (1993) 2038–2044.
[16] J.W. Hills and H.H. Hill, *J. Chromatogr. Sci.*, 31 (1993) 6–12.
[17] F.I. Onuska, K.A. Terry and R.J. Wilkinson, *J. High Resolut. Chromatogr.*, 16 (1993) 407–412.
[18] M. Ashraf-Khorassani, L.T. Taylor and P. Zimmerman, *Anal. Chem.*, 62 (1990) 1177–1180.
[19] S.B. Hawthorne, J.J. Langenfeld, D.J. Miller and M.D. Burford, *Anal. Chem.*, 64 (1992) 1614–1622.
[20] D.E. Raynie, *Anal. Chem.*, 65 (1993) 3127–3128.
[21] M.D. Burford, S.B. Hawthorne and D.J. Miller, *Anal. Chem.*, 65 (1993) 1497–1505.
[22] M.H.B. Hayes, in B. Yaron, G. Dagan and J. Goldshmid (Editors), *Pollutants in Porous Media. The Unsaturated Zone Between Soil Surface and Groundwater*, Springer, Berlin, 1984, pp. 126–142.
[23] H.-B. Lee, T.E. Peart, R.L. Hong-You and D.R. Gere, *J. Chromatogr. A*, 653 (1993) 83–91.

ELSEVIER

Journal of Chromatography A, 693 (1995) 113–130

JOURNAL OF CHROMATOGRAPHY A

Combined effects of non-linear electrophoresis and non-linear chromatography on concentration profiles in capillary electrophoresis

Michael S. Bello[1], Michael Yu. Zhukov[2], Pier Giorgio Righetti*

Faculty of Pharmacy and Department of Biomedical Sciences and Technologies, University of Milan, Via G. Celoria 2, 20133 Milan, Italy

First received 25 April 1994; revised manuscript received 26 July 1994; accepted 7 October 1994

Abstract

A theory of peak evolution in a column under the combined action of electromigration dispersion and equilibrium adsorption–desorption is presented. The basic equations for mass transport in zone electrophoresis are combined with those for non-linear chromatography. Langmuir's isotherm is assumed for describing the analyte interaction with the column wall (capillary electrophoresis in thin capillaries) or a sorbent (electrokinetic chromatography). The transport equation thus obtained is analysed and three specific cases determining the peak evolution are found: (A) the concentration velocity as a function of concentration is non-monotonous; (B) the velocity increases with analyte concentration; and (C) the velocity decreases with increments of concentration. Solutions to the transport equation for all three cases, describing the evolution of disperse boundary and discontinuities are derived. By assuming a "rectangular pulse" initial profile, a variety of peak shapes are generated. In the case of a non-monotonous velocity dependence on concentration, the initial concentration is shown to be an important parameter determining the peak shape and its transformations while moving along the column axis. A possibility of a counterbalance of the electromigration and adsorption mechanisms of the peak broadening, leading to a decay of the peak evolution into a "triangle" is found.

1. Introduction

Since the early 1980s [1], narrow-bore capillaries, down to 10 μm, have been used for electrophoretic separations. The main advantage of these capillaries is well known: they allow for significant decrease in the Joule heating and, thus, for an increase in the applied voltage leading to short separation times. Peak broadening mechanisms in these capillaries were found to be mostly the same as those in relatively wide capillaries (of about 2 mm I.D.) for which they were extensively studied many years ago [2,3].

Among others, these effects include electro-

* Corresponding author.

[1] Present address: Dionex Corp., 1228 Titan Way, Sunnyvale, CA 94088-3603 (USA).

[2] Permanent address: Department of Mechanics and Mathematics, Rostov State University, Zorge ul 5, Rostov-na-Donu 344104, Russian Federation.

0021-9673/95/$09.50
SSDI 0021-9673(94)00965-1

migration dispersion [4], i.e., an asymmetric peak broadening, caused by a mismatch between the electric conductivity of the analyte and the background electrolyte. The mass transport in electrophoresis is determined by the electric field. The presence of the analyte in the solution influences the electric conductivity of the solution and, therefore, the axial electric field in the column. This effect is expressed by a set of non-linear transport equations governing species concentrations in the solution.

It was understood by Virtanen [3] that interactions of an analyte with the capillary surface may affect the peak shape and electromigration time. However, these interactions were assumed to be negligible for large-bore capillaries. With narrow-bore capillaries, the analyte interactions with the capillary wall become important [5]. They even may be considered as one of the main obstacles to the progress of capillary electrophoresis (CE) and generated a great deal of research on surface coatings [6]. Such coatings should prevent analytes from being adsorbed on the wall, although it is doubtful that a universal coating that does not interact with all analytes exists.

The most elaborate method used to account for interactions of an analyte moving down a column with a solid phase is that developed in non-linear chromatography [7–9]. The transport equation governing analyte concentration in chromatography is derived by combination of the mass balance equation in the moving phase and the balance between solid and liquid phases. In the case of equilibrium between phases, the phase balance is described by Langmuir's isotherm, which leads to a non-linear transport equation.

This paper presents a novel theory uniting both mechanisms of peak broadening: electromigration dispersion and peak broadening due to adsorption. A brief review of electromigration and adsorption mechanisms of peak broadening is followed by derivation of the basic equation for the equilibrium mass transport in thin capillaries. Detailed analysis of this equation predicts various scenarios of the peak evolution.

2. Equations for zone electrophoresis and chromatography

This section presents known concepts from the theory of electrophoresis and non-linear chromatography.

2.1. Electrophoresis

Electrophoretic mass transport is modelled in a non-diffusion approximation by the following set of equations [10–12]:

$$\frac{\partial c}{\partial t} + \frac{\partial i_e}{\partial x} = 0 \tag{1}$$

$$i_e = \mu c E \tag{2}$$

$$\sigma = \sigma_0(1 + \alpha c), \quad j = \sigma E \tag{3}$$

where c is the concentration of an analyte, i_e is the electrophoretic mass flux, t is the time, x is the axial coordinate, μ is the electrophoretic mobility, E is the electric field strength, σ is the electric conductivity of the solution, σ_0 is the electric conductivity of the pure buffer, α is the concentration coefficient of the electric conductivity of the solution and j is the density of the electric current.

The dependence of the electric conductivity on the analyte concentration given by Eq. 3 is valid only for dilute solutions.

Excluding electric field strength from Eqs. 1–3, one finds

$$\frac{\partial c}{\partial t} + \frac{\partial}{\partial x}\left(\frac{\mu E_0 c}{1 + \alpha c}\right) = 0, \quad E_0 = \frac{j}{\sigma_0} \tag{4}$$

The solution for Eq. 4 with initial conditions in the form of a "rectangular pulse",

$$c(x, t)|_{t=0} = \begin{cases} c_0, & 0 \leq x \leq x_0 \\ 0, & x < 0, \quad x_0 < x \end{cases} \tag{5}$$

is well known [10,13]. It is shown in Fig. 1 (1.1 and 1.2) for positive and negative values of the parameter α.

For $\alpha > 0$ transformations of the initial profile are shown in Fig. 1 (1.1). The initial profile (A) evolves, after the motion starts, into the profile (B) with a rear discontinuity, having a coordi-

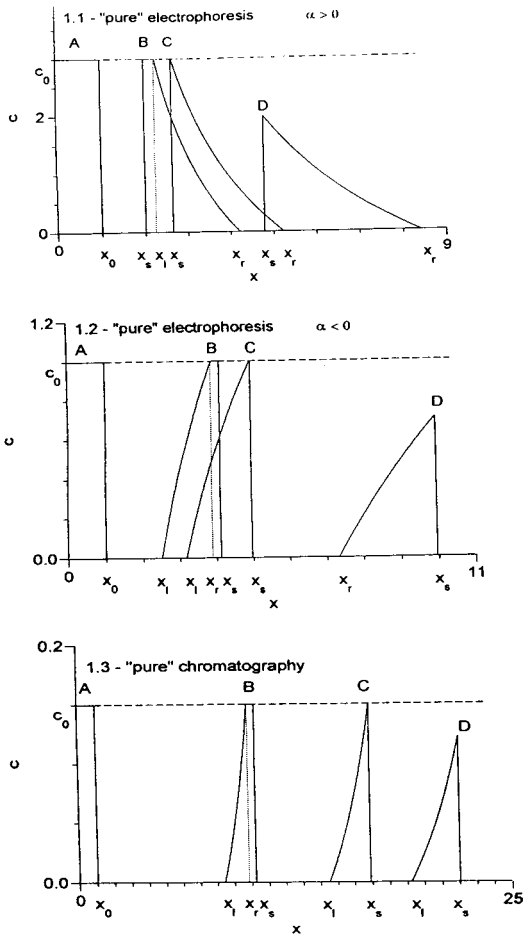

Fig. 1. Here and in all subsequent, relevant figures, patterns A–D represent the concentration profiles taken at different time moments along the column axis. The dashed vertical line is located at the point $x_l(t)$, called the left edge of the dispersed boundary, with which the rear discontinuity (vertical solid line) will merge at a certain time moment (here represented by profile C). In all relevant figures, x represents the column length. (1.1) Peak evolution in electrophoresis in the case $\alpha > 0$, $\alpha = 0.2$; (1.2) peak evolution in electrophoresis in the case $\alpha < 0$, $\alpha = -0.2$; (1.3) peak evolution in non-linear chromatography, $k_1 = 0.3$, $k_2 = 4$.

nate $x_s(t)$ at a time moment t, a region of the constant concentration and front disperse boundary. The front disperse boundary is bounded by a point $x_l(t)$ and a point $x_r(t)$ which we shall call the left edge and the right edge of the disperse boundary, respectively. The rear discontinuity moves faster than the left edge of the front disperse boundary and after a certain time catches it, eliminating the region of the constant concentration (C). After this moment the peak becomes "triangle"-like (D) with a rear discontinuity and a front disperse boundary. In the case of $\alpha < 0$ [Fig. 1 (1.2)], the initial profile (A) is subjected to similar transformations (B), (C) and (D). In both instances the peak evolution is characterized by the formation of a moving discontinuity, the coordinate of which is denoted by x_s, a disperse boundary with left edge x_l and right edge x_r.

Here a remark on the terminology is appropriate. The reader has probably realized that this paper deals with the phenomena called "non-linear waves", the mathematical theory of which was developed by Lax [14–16] and for electrophoresis [11]. Works on non-linear waves in chromatography have been recently reviewed by Helffrich [7] and Helffrich and Carr [8]. It was pointed out [7,8] that non-linear waves have been studied in mathematics, fixed-bed engineering and chromatography (we now add electrophoresis to this list) and it led to different terminologies used in different fields but describing the same phenomena. The most precise terminology has been developed in mathematics, but for chemists it might be rather unusual. We tried to find a compromise in this paper between rigorousness of definitions and intuition. The terminology used to describe the patterns shown in Fig. 1 (1.1 and 1.2) will be used in subsequent figures, where applicable. Therefore, we reserve the word *discontinuity* for what is also called "shock" or "abrupt transition" and denote its coordinate by x_s, $\bar{x}_s$ or $\tilde{x}_s$. A region in space where the concentration monotonously increases or decreases is called a *disperse boundary*. It is bounded by its *left edge* x_l and the *right edge* x_r. A region where the substance concentration is not zero will be called a *peak* or *zone*. The region of the peak where the concentration increases along the space coordinate, even discontinuously, will be called the *peak rear* and

that where it decreases will be called the *peak front* (see [8]).

2.2. Non-linear chromatography

Non-linear, non-equilibrium chromatography of a single analyte is governed by the following set of equations [17,18]:

$$\frac{\partial c}{\partial t} + \frac{\partial i_c}{\partial x} + \frac{\partial q}{\partial t} = 0\,, \quad i_c = Vc \tag{6}$$

$$\frac{\partial q}{\partial t} = k_a(S - q)c - k_d q \tag{7}$$

where c is the concentration of the analyte in the liquid phase, i_c is the chromatographic mass flux, q is the analyte concentration in the immobile phase, V is the velocity of the liquid, k_a and k_d are coefficients of the adsorption and desorption, respectively, and S is the concentration of the binding sites in the immobile phase (we assume the porosity of the medium to be included in the coefficients k_a and k_d).

In the case of equilibrium chromatography, the concentration q in the immobile phase may be expressed through c. By neglecting fast processes in the establishment of the phase equilibrium, one can simplify Eqs. 6 and 7 to

$$\frac{\partial c}{\partial t} + \frac{\partial (Vc)}{\partial x} + \frac{\partial}{\partial t}\left(\frac{k_a S c}{k_a c + k_d}\right) = 0\,, \quad q = \frac{k_a S c}{k_a c + k_d} \tag{8}$$

The second expression for q in Eqs. 8 is known as the Langmuir isotherm.

The evolution of the "rectangular-pulse" initial profile predicted by Eqs. 8 is shown in Fig. 1 (1.3). The non-linear chromatographic peak evolution resembles that of zone electrophoresis when $\alpha < 0$ but the curvature of the rear disperse boundary is different.

In order to model mass transport in capillary zonal electrophoresis (CZE), we suggest combining the equation for the electrophoretic peak evolution (Eq. 4) with those of non-linear chromatography (Eqs. 8). These combined equations govern both the specific electrophoretic interaction of the sample with the buffer and mass exchange with the capillary wall, i.e., the immobile phase. These equations are also valid for electrokinetic chromatography [19,20].

3. Equations for zone electrophoresis in thin capillaries

The following combined equation is suggested for the modeling of the electrophoretic transport in thin capillaries where mass exchange with the capillary wall becomes significant:

$$\frac{\partial}{\partial t}\left(c + \frac{k_a S c}{k_a c + k_d}\right) + \frac{\partial}{\partial x}\left(Vc + \frac{\mu c E_0}{1 + \alpha c}\right) = 0 \tag{9}$$

where c is the analyte concentration in the buffer, k_a and k_d are the adsorption and desorption constants, respectively, μ is the electrophoretic mobility, E_0 is the electric field strength which would exist in the capillary in the absence of the sample and α is the concentration coefficient of the electric conductivity.

The term Vc in Eq. 9 describes, in particular, electroosmotic transport in the capillary. In this case the velocity V should be related to the electric field strength:

$$V = \mu_{os} E_{eff} \tag{10}$$

where μ_{os} is the effective electroosmotic mobility and E_{eff} is the effective electric field strength, proportional to the intensity of the external electric field. The effective electroosmotic mobility and the electric field strength may depend on the concentration of the analyte in the mobile and immobile phases, buffer pH, etc. As a rough approximation, they could be set at μ_{os} = constant and $E_{eff} = E_0$. In this paper we neglect effects of the electroosmotic transport and forced fluid flow, assuming

$$V = 0 \tag{11}$$

In order to transform Eq. 9 in a convenient form, the following dimensionless variables and characteristic values are introduced:

$$x = x' L_*\,, \quad t = t' \tau_*\,, \quad c = c' c_*\,,$$

$$k_1' = \frac{k_a}{k_d} \cdot S\,, \quad k_2' = \frac{k_a}{k_d} \cdot c_*\,, \tag{12}$$

$$\alpha' = \alpha c_*\,, \quad \tau_* = \frac{L_*}{\mu E_0}$$

where L_*, τ_*, c_* are the characteristic values (scales) of the length, time and concentration, respectively. Dimensionless variables and parameters in Eq. 12 are those primed. However, in order to make the following treatment more readable, we omit primes and assume all variables to be dimensionless.

A possible choice of the scales in Eq. 12 is the length of the capillary or the width of the initial peak x_0 as the length scale L_* and the buffer concentration as the concentration scale c_*.

Eq. 9 may be rewritten in the following form:

$$\frac{\partial \psi}{\partial t} + \frac{\partial \phi}{\partial x} = 0 \tag{13}$$

$$\psi = \psi(c) = c + \frac{k_1 c}{1 + k_2 c}, \quad \phi = \phi(c) = \frac{c}{1 + \alpha c} \tag{14}$$

where ϕ is the dimensionless density of the mass flux and ψ is the sum of the dimensionless concentrations in the liquid and immobile phases.

Evidently, Eq. 4 is a particular case of Eqs. 13 and 14 describing "pure" electrophoresis when $k_1 = 0$ (and $k_2 = 0$). Eqs. 8 for "pure" chromatography are another particular case of the same equations at $\alpha = 0$ (formally, in this case $V = 1$).

Eqs. 13 and 14 and also Eqs. 4 and 8 are not applicable to discontinuities. Solutions of these equations represent only disperse boundaries or regions of constant concentration. However, the usual approach is to study the evolution of the initial peak in the form of a "rectangular pulse", i.e., a discontinuous profile (see Fig. 1). In this case Eq. 13 should be supplemented with a condition relating fluxes and concentrations at both sides of the discontinuity:

$$D_{c_l,c_r}\{\psi(c_l) - \psi(c_r)\} = \phi(c_l) - \phi(c_r),$$

$$\frac{dx_s(t)}{dt} = D_{c_l,c_r} \tag{15}$$

where c_l and c_r are the concentrations at a close vicinity to the left and right sides of the discontinuity, respectively; D_{c_l,c_r} denotes the velocity of the discontinuity motion along the capillary and $x_s(t)$ is the axial coordinate of the discontinuity. We shall also use another notation for the velocity of the discontinuity: $D\{c_l, c_r\}$ explicitly showing its functional dependence on c_l and c_r (see [14–16]).

An explanation to Eq. 15 is the following. Assume that at the left side of the discontinuity the analyte concentration in the mobile and immobile phases is $\psi = \psi(c_l)$ and the flux density is $\phi = \phi(c_l)$. At the right side of the discontinuity $\psi = \psi(c_r)$ and $\phi = \phi(c_r)$. The mass flux due to the motion of the discontinuity is equal to $D_{c_l,c_r}\{\psi(c_r) - \psi(c_l)\}$. According to the law of mass conservation it should be balanced by the difference of the fluxes $\phi(c_r) - \phi(c_l)$ as it is expressed by Eq. 15.

Eqs. 13 and 14 are subjected to the following physical constraints: concentration c is positive or zero, coefficients k_1 and k_2 are positive or zero (see Eqs. 16) and electric conductivity is positive (see Eq. 17):

$$c(x,t) \geq 0, \quad k_1 \geq 0, \quad k_2 \geq 0 \tag{16}$$

$$1 + \alpha c(x,t) > 0 \tag{17}$$

The concentration coefficient of conductivity α is supposed to have both signs and, in particular, to be zero.

The initial conditions for Eqs. 13–17 are Eq. 5.

The set of equations Eqs. 13–17 and 5 represents the simplest non-linear mathematical model taking into account effects of the electrodispersion and interaction with the capillary wall (or the sorbent, in electrokinetic chromatography). Solutions to this kind of equations are known to exhibit "non-uniqueness", i.e., they can give several values of concentration for one space point. In order to have a physically meaningful solution, additional conditions, further specified, should be added to Eqs. 13–17 and 5.

4. Dependence of velocity on concentration

The concentration dependence of the concentration velocity is of decisive importance for a peak profile. This section studies possible dependences of the concentration velocity on con-

centration and relates them to the shape of the peak.

Eqn. 13 may be represented in the form

$$\frac{d\psi}{dc}\cdot\frac{\partial c}{\partial t}+\frac{d\phi}{dc}\cdot\frac{\partial c}{\partial x}=0$$

which transforms to the well known transport equations for concentration c [8,11,14–16]:

$$\frac{\partial c}{\partial t}+v(c)\frac{\partial c}{\partial x}=0 \qquad (18)$$

where $v(c)$ is the concentration velocity. By comparing Eq. 18 with the previous one, we derive

$$v(c)=\frac{\phi'(c)}{\psi'(c)} \qquad (19)$$

Taking into account Eq. 14 one obtains an explicit expression for $v(c)$:

$$v(c)=\frac{1}{(1+\alpha c)^2}\cdot\frac{(1+k_2c)^2}{k_1+(1+k_2c)^2} \qquad (20)$$

Analysing the dependence of the concentration velocity $v(c)$ on the parameters k_1, k_2 and α, one can distinguish three cases: (i) the velocity is non-monotonous (Fig. 2A-i); (ii) the velocity increases with increasing concentration (Fig. 2A-ii); (iii) the velocity decreases with an increase in concentration (Fig. 2A-iii). The following relationships determine the three cases:

$$\text{(i)}\quad k_1(k_2-\alpha)>\alpha\,,\quad \alpha>0 \qquad (21)$$

$$\text{(ii)}\quad \alpha<0\,,\quad (1+\alpha c)>0 \qquad (22)$$

$$\text{(iii)}\quad k_1(k_2-\alpha)<\alpha\,,\quad \alpha>0 \qquad (23)$$

The maximum velocity v_m and the concentration c_m corresponding to it in Fig. 2A-i are given by

$$c_m=\frac{1}{k_2}\left\{\left[\frac{k_1(k_2-\alpha)}{\alpha}\right]^{1/3}-1\right\},$$

$$v_m=\max_{c\geq 0}v(c)=v(c_m) \qquad (24)$$

Let us consider the evolution of the initial peak rear. The initial distribution of the concentration is given by Eq. 5. At the initial moment the analyte concentration c at $x=0$ lies within the range $0\leq c\leq c_0$.

When the electric field is applied, each point on the analyte moves with the velocity given by Eq. 20 (Figs. 2A-i, 2A-ii and 2A-iii) and in the time moment close to $t=+0$, transforms to the shapes shown in Figs. 2B-i, 2B-ii and 2B-iii. The arrows in Figs. 2B indicate the velocities of the points having different concentrations. The graphs in Figs. 2B were obtained from those in Figs. 2A by a reflection relative to the bisector of the coordinate angle. Figs. 2B illustrate that for a peak rear the points of the initial concentration profile move according to

$x=v(c)t$ or, in another form,

$$v(c)=z\,,\quad z=\frac{x}{t} \qquad (25)$$

For a peak front the points of the initial concentration profile move according to

$x=x_0+v(c)t$ or, in another form,

$$v(c)=z\,,\quad z=\frac{x-x_0}{t} \qquad (26)$$

where z is the variable proportional to the coordinate x at any time moment t.

Eq. 25 determines in an implicit fashion a dependence of the analyte concentration on x and t.

Unfortunately, an explicit equation for $c(z)$ is difficult to obtain. However, for a qualitative analysis, the explicit equation is not necessary. In fact, the function $c(z)$ is already shown in Figs. 2B.

Not all of the peaks shown in Figs. 2B may exist. Thus, at a time moment t_1 there are three different values of concentration corresponding to one space point $x_1=z_1t_1$ in Fig. 2B-i and two different concentration values in Fig. 2B-iii (see the vertical dashed lines). This situation, obviously, cannot exist. Only in Fig. 2B-ii does the transformed profile have the necessary property of uniqueness and, thus, is compatible with real experimental conditions. In order to avoid non-uniqueness of the profiles shown in Figs. 2B-i and 2B-iii, a discontinuous profile should be realized. Its motion is determined by Eq. 15. Additionally, only one of the two branches of the profile in Fig. 2B-i can exist. A solution to

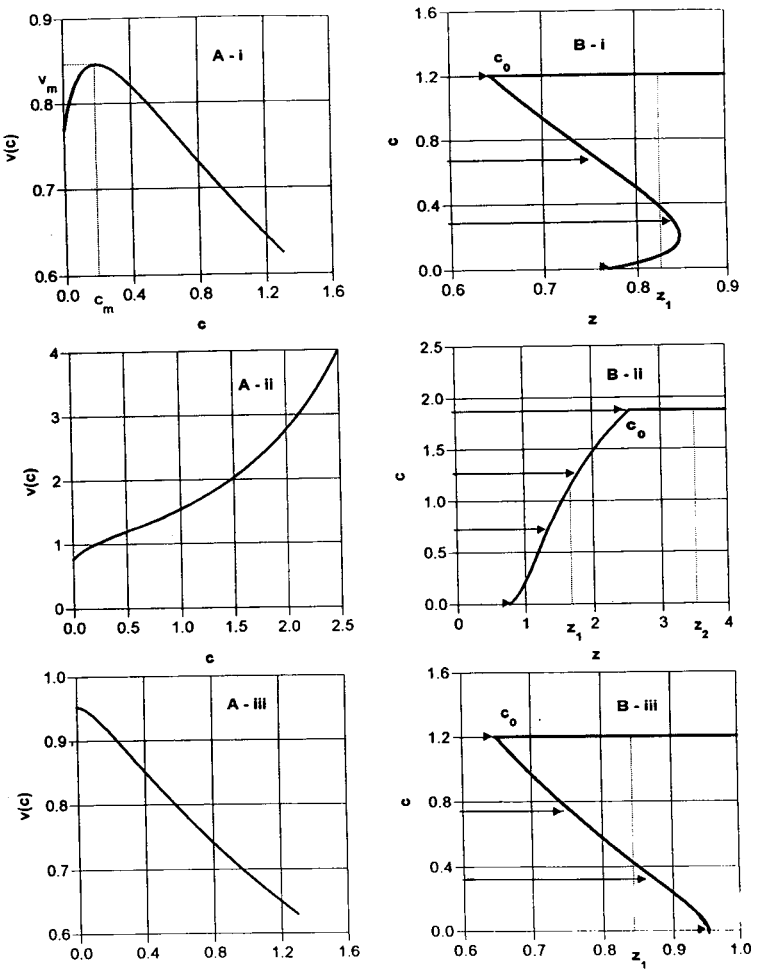

Fig. 2. Dependence of the concentration velocity on the concentration (A) and a transformation of the edges of the initial "rectangular pulse" (B). (A-i, B-i) Non-monotonous dependence of the concentration velocity on the concentration. $k_1(k_2-\alpha)>\alpha$, $\alpha=0.2>0$, $k_1=0.3$, $k_2=4$, $c_0=1.2$. (A-ii, B-ii) Monotonously increasing dependence of the concentration velocity on the concentration. $1+\alpha c>0$, $\alpha=-0.2<0$, $k_1=0.3$, $k_2=4$, $c_0=1.8$. (A-iii, B-iii) Monotonously decreasing dependence of the concentration velocity on the concentration. $k_1(k_2-\alpha)<\alpha$, $\alpha=0.2>0$, $k_1=0.05$, $k_2=4$, $c_0=1.2$.

Eq. 25 or 26 for case (i), corresponding to Fig. 2B-i, can be represented in the following form:

$$c(z)=\begin{cases}c_1(z), & \text{for } 0\leq c\leq c_m, \quad z=v(c_1)\\ c_2(z), & \text{for } c_m<c\leq c_0, \quad z=v(c_2)\end{cases} \tag{27}$$

where $c_1(z)$ and $c_2(z)$ are two branches of the inverse function $c=v^{-1}(z)$.

The requirement of the uniqueness of the concentration at any space point makes impossible the existence of disperse boundaries in Fig. 2B-ii and for $0\leq c\leq c_m$ (Fig. 2B-i) at the peak front. Analogously, the existence of the disperse boundary in Fig. 2B-iii and for $c_m\leq c\leq c_0$ 2B-i at the peak rear is impossible.

Fig. 3 illustrates an evolution of the whole initial peak in case (i), Eq. 21, when the concentration velocity is non-monotonous. Lines (a, b) and (c, d) show the lines of discontinuities in the profile. Evidently, the upper branch of the profile should be rejected at the rear and the lower branch should be rejected at the front of

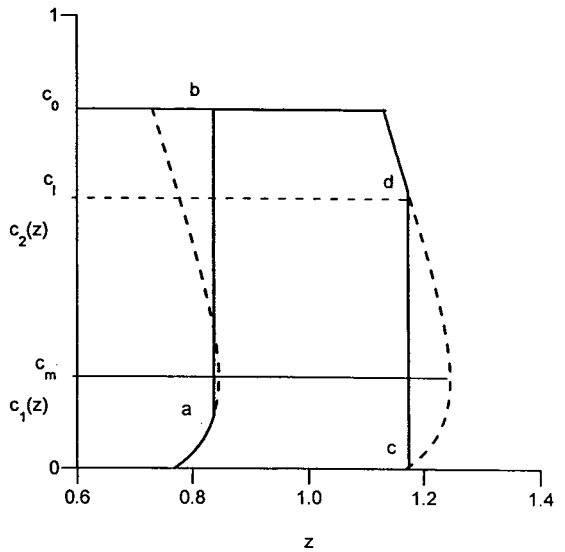

Fig. 3. Scheme of the "rectangular pulse" transformation when the concentration velocity is not monotonous. c_m is the concentration corresponding to the maximum velocity; a, b and c, d are the lines of discontinuities imposed to obtain uniqueness of the concentration. Dashed curves indicate non-existent solutions.

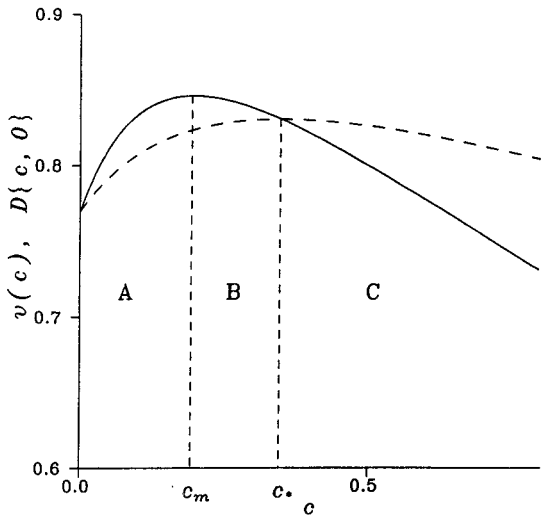

Fig. 4. Dependence of the concentration velocity $v(c)$ (solid curve) and the velocity of the discontinuity $D\{c, 0\}$ (dashed curve) on concentration. $\alpha = 0.2$, $k_1 = 0.3$, $k_2 = 4$.

the peak (dashed lines). These two dashed lines would again violate the principle of concentration uniqueness at some given space points and, thus, have to be rejected. Locations of the discontinuities are regulated by Eq. 15.

It may occur that a discontinuity is not stable, i.e. it also cannot exist. Thus, consider a discontinuity at the peak front, line (c, d) in Fig. 3. The concentration at the left side of the discontinuity is c_l and at the right side $c_r = 0$. As $\psi(0) = 0$ and $\phi(0) = 0$ (see Eq. 14), the velocity of the discontinuity found according to Eq. 15 is

$$D_{c_l,0} = \frac{\phi(c_l)}{\psi(c_l)} = \frac{1 + k_2 c_l}{(1 + k_1 + k_2 c_l)(1 + \alpha c_l)} \qquad (28)$$

Fig. 4 shows the dependence of the discontinuity velocity $D_{c,0}$ on the concentration c. The concentration velocity $v(c)$ is shown by a dashed line. The two curves have an intersection point at concentration c_*, i.e.,

$$v(c_*) = D_{c_*,0} = D\{c_*, 0\}$$

$$c_* = \frac{1}{k_2}\{(1 + k_2 c_m)^{3/2} - 1\}$$

$$= \frac{1}{k_2}\left\{\left[\frac{k_1(k_2 - \alpha)}{\alpha}\right]^{1/2} - 1\right\} > c_m \qquad (29)$$

It is seen from Fig. 4 that

$$v(c) \geq D_{c,0}, \quad 0 \leq c \leq c_* \qquad (30)$$

$$v(c) \leq D_{c,0}, \quad c_* \leq c \leq c_0 \qquad (31)$$

When the concentration velocity is less than the velocity of the discontinuity, Eq. 31, the discontinuity cannot exist, as the concentration at the left side of the discontinuity lags behind it and thus destroys the discontinuity. In contrast, in the case given by Eq. 30, the concentration at the left side of the discontinuity moves faster than the discontinuity. This leads to non-uniqueness of the concentration profile and, thus, to the necessity for the discontinuity.

In particular, for $c_0 \geq c_*$, the discontinuous profile of the left edge shown in Fig. 3 exists only if $c_l \geq c_*$.

A general condition of the discontinuity stability is given by

$$v(c_l) \geq D_{c_l,c_r} \geq v(c_r) \quad (32)$$

A concentration profile giving a solution to the problem in Eqs. 13–17 is found by combining solutions of Eq. 27 and introducing discontinuities where the solutions of Eq. 27 are not unique. The discontinuities should satisfy Eqs. 15 and 32. All stages of the peak evolution for the cases (i)–(iii) (as illustrated in Figs. 2) are described in the following section.

5. Peak evolution

This section deals with evolutions of the initial profile for the three types of the velocity dependence on the concentration (Eqs. 21–23).

The most interesting case, generating a variety of peak shapes, is when the dependence of the velocity on concentration has a maximum. A condition for the existence of the maximum is given by Eq. 21.

5.1. Case (i). Peak evolution with non-monotonous velocity; $k_1(k_2 - \alpha) > \alpha$, $\alpha > 0$

The concentration c_m, corresponding to the maximum of the concentration velocity, and the concentration c_*, corresponding to the equality of the concentration velocity to the velocity of the discontinuity, divide the whole range of the initial concentration c_0 into three intervals (see Fig. 4):

(A) $c_0 < c_m$, the interval of low initial concentration;

(B) $c_m < c_0 < c_*$, the interval of intermediate initial concentration;

(C) $c_* < c_0$, the interval of high initial concentration.

The behaviour of the concentration profile depends on the interval to which the initial concentration belongs. It is analysed successively below for all three intervals.

(A) Interval of low initial concentration, $c_0 < c_m$ (see Fig. 4)

Under the condition in which the initial concentration is less than the concentration c_m corresponding to the maximum of $v(c)$, only the first branch of the function $c = c_1(z)$ exists, Eq. 27. Successive stages of the initial profile evolution are shown in Figs. 5 and 6. Fig. 5 presents patterns at different time moments as they move along the capillary axis in the same length scale. The structure of the peaks is shown on a larger scale in Fig. 6. At the time moment $t = +0$ the initial profile (Fig. 6A) transforms into the peak shown in Fig. 6B. The left edge of the rear disperse boundary x_l moves along the x-axis with constant velocity $v(0)$:

$$x_l(t) = v(0)t \quad (33)$$

The concentration in the rear disperse boundary between x_l and x_r is given by the function $c_1(z)$, Eq. 27. The right edge of the rear disperse boundary $x_r(t)$ also moves with constant velocity $v(c_0)$:

$$x_r(t) = v(c_0)t \quad (34)$$

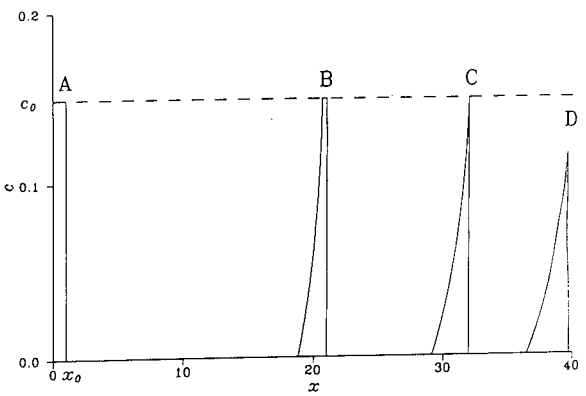

Fig. 5. Peak evolution for non-monotonous velocity and low initial concentration $c_0 < c_m$. (A), (B), (C) and (D) are the peak shapes at dimensionless time moments $t = 0$, 24.5, 36.45 and 38.3, respectively. Parameters: $\alpha = 0.2$, $k_1 = 0.3$, $k_2 = 4$, $c_0 = 0.15$. Values of $c_m = 0.1966$ and $c_* = 0.3470$. $v(0) = 0.7692$, $v(c_0) = 0.8437$, $D_{c_0,0} = 0.8176$.

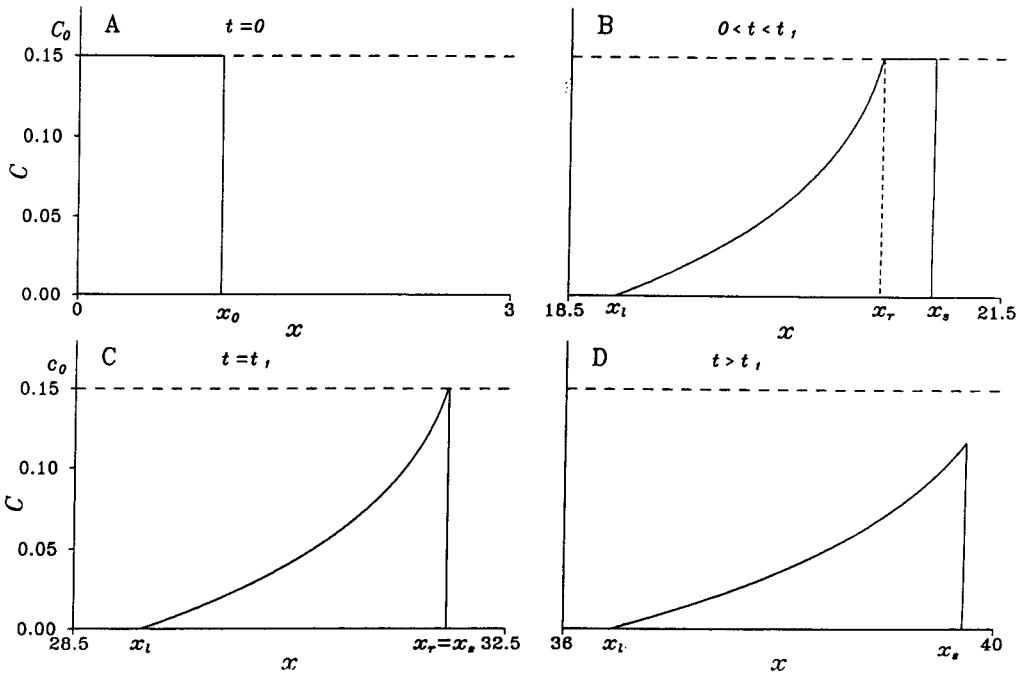

Fig. 6. Structure of the peaks shown in Fig. 5. Peaks A and B are plotted in the same scale (on the x-axis), which is, however, different from the scale used for peaks C and D. (A) Initial "rectangular pulse" distribution at $t = 0$, $x_0 = 1$. (B) A peak with a developed disperse rear boundary, a region of constant initial concentration and a sharp discontinuity at the front. (C) A peak at the time moment $t = t_1 = 38.3$ when the disperse boundary reaches the front. The concentration of the peak maximum is still the initial concentration. (D) A "triangle"-like peak at $t = 47.4$. Note that, in this last instance, the peak maximum has decreased.

As the velocity corresponding to the initial concentration c_0 is higher than the velocity corresponding to the zero concentration $v(c_0) > v(0)$, the width of the rear disperse boundary $x_r - x_l = \{v(c_0) - v(0)\}t$ increases linearly with time. The peak front is a sharp discontinuity which moves along the x-axis with constant velocity $D_{c_0,0}$:

$$x_s(t) = x_0 + D_{c_0,0}t \tag{35}$$

It is seen from Fig. 4 that the stability condition of the discontinuity, Eq. 32, is satisfied, i.e., $v(c_0) > D_{c_0,0} > v(0)$. It follows from this inequality that the edge $x_r(t)$ will catch up the front discontinuity $x_s(t)$ at the time moment t_1 (Fig. 6C):

$$x_r(t_1) = x_s(t_1), \quad t_1 = \frac{x_0}{v(c_0) - D_{c_0,0}} \tag{36}$$

Further development of the peak is determined by the velocity of the discontinuous front, Eq. 28, which is not algebraic in this case, but an ordinary differential equation:

$$\frac{d\bar{x}_s(t)}{dt} = D\{c_1, 0\} = \frac{1 + k_2c_1(\bar{x}_s/t)}{[1 + k_1 + k_2c_1(\bar{x}_s/t)][1 + \alpha c_1(\bar{x}_s/t)]} \tag{37}$$

with the initial condition

$$\bar{x}_s(t_1) = x_s(t_1) = x_r(t_1) = \frac{v(c_0)x_0}{v(c_0) - D_{c_0,0}} \tag{38}$$

where $\bar{x}_s(t)$ is a new function describing a position of the peak front after the time t_1 given by Eq. 36.

A general case, like the Gauche problem in Eqs. 37 and 38, can be solved only by computer

methods. However, the peak behaviour in the final stage can be easily analysed in an asymptotic form.

The final stage of the peak evolution is shown in Fig. 6D. A "triangle"-like peak moves along the x-axis, keeping its shape. The concentration in the peak maximum decreases with time.

Asymptotic solution. Let us assume that after a relatively long time the concentration becomes small and later verify that. In this case it is easy to find an asymptotic solution to the problem in Eqs. 37 and 38. By expanding functions $\psi(c)$, $v(c)$ and $D_{c,0}$ (Eqs. 14, 20 and 28) in power series of c, and neglecting terms proportional to powers of c higher than two, one derives

$$\psi(c) \approx (1 + k_1)c\,, \quad v(c) \approx v(0) + v_c'(0)c\,,$$

$$D_{c,0} \approx v(0) + \frac{1}{2} v_c'(0)c$$

Then, it follows from Eq. 25 that

$$c_1(z) = \frac{z - v(0)}{v_c'(0)}\,, \quad z = \frac{x(t)}{t}\,, \quad x_1(t) \leq x \leq \bar{x}_s(t) \tag{39}$$

Eq. 37 simplifies to

$$\frac{d\bar{x}_s(t)}{dt} \approx \frac{1}{2}\left[\frac{\bar{x}_s(t)}{t} + v(0)\right] \tag{40}$$

A solution to Eq. 40 is given by

$$\bar{x}_s(t) = v(0)t + b\sqrt{(t)} \tag{41}$$

where b is the integration constant.

Constant b cannot be found from the initial condition, Eq. 38, as this equation does not assume small concentration values. For this purpose, the mass concentration law is applied. As ψ is the mass concentration in the mobile and immobile phases, the mass conservation law implies that

$$\int_{x_1(t)}^{\bar{x}_s(t)} \psi[c_1(y/t)]\,dy = m_0\,, \quad m_0 = x_0\psi(c_0)$$

where m_0 is the mass of the substance introduced in the column. By evaluating the integral with the approximated expression for $\psi(c)$, the following expression is found:

$$m_0 \approx \frac{1 + k_1}{2v'(0)} \cdot b^2$$

and, finally, the constant b is found as

$$b = \sqrt{\frac{2\psi(c_0)v'(0)x_0}{1 + k_1}} > 0 \tag{42}$$

The concentration at the point of discontinuity, which is the maximum concentration of the peak in this instance, is given by

$$c_s = c_1[\bar{x}_s(t)/t] \approx \frac{b}{v'(0)\sqrt{(t)}} \tag{43}$$

where c_s is the concentration at the discontinuity point.

The width of the peak Δx is given by

$$\Delta x(t) = \bar{x}_s(t) - x_1(t) = b\sqrt{(t)} \tag{44}$$

Therefore, the peak width increases with time proportionally to the square root of time. This is the same law that governs the peak width of a Gaussian peak, but the mechanism of the broadening and the peak shape are different. In contrast to a Gaussian peak, the peak we analyse here is asymmetric and its concentration grows linearly from zero at $x = x_1$, Eq. 33, to c_s at the point $x = \bar{x}_s$, given by Eqs. 41 and 43. The value of the function ψ at the discontinuity point is $\psi(c_s)$ and the total mass of the substance in the column may be found as the area of the triangle

$$m_0 = \frac{1}{2}\Delta x\,\psi(c_s) \tag{45}$$

Of course, Δx and c_s, as given by Eqs. 43 and 44, satisfy Eq. 45. The latter can be used as a simple way to determine the constant b.

Concluding the analysis of the peak evolution in the case of low initial concentration, the following scenario can be presented. At the initial stage of the peak evolution the left and right edges of the rear disperse boundary and the front discontinuity move with constant but different velocities (Fig. 6B). The velocity of the discontinuity is less than the velocity of the right edge of the rear disperse boundary (see Fig. 4).

After the time moment $t = t_1$, when the peak transformation occurs, i.e., when the disperse boundary reaches the front discontinuity (Fig. 6C), the velocity of the front decreases approaching the velocity of the left edge of the rear disperse boundary (Fig. 6D).

(B) Interval of intermediate initial concentration, $c_m < c_0 < c_*$ (see Fig. 4)

A specific feature of this interval of the initial concentration is that both branches $c_1(z)$ and $c_2(z)$ could exist (see Fig. 3 and Eq. 27). However, the branch $c_2(z)$, as was discussed above (Eqs. 30–32), exists only for initial concentrations higher than c_*.

The peak rear for the case in which the initial concentration c_0 is higher than the concentration c_m cannot be represented by a disperse boundary given by $c_1(z)$ and continuously matching the region of the constant initial concentration, as we have seen in the previous subcase of low initial concentration [the branch $c_1(z)$ exists only for $c < c_m$, Eq. 27]. However, it is possible to combine a solution $c_1(z)$ with a discontinuity (Fig. 3). The front of the peak can be represented as a discontinuity, since $c_0 < c_*$, and, therefore, the concentration velocity is higher than the velocity of the discontinuity (Fig. 4). The latter is required by Eq. 32.

Successive stages of the peak evolution are shown in Figs. 7 and 8. Fig. 7 presents all patterns in the same scale, whereas in Fig. 8 they are shown on an enlarged scale in order to describe their peculiarities. The initial rectangular profile (Figs. 7A and 8A) transforms at the time moment $t = +0$ into the peaks shown in Figs. 7B and 8B. The edges $x_1(t)$ and $x_s(t)$ move along the x-axis with the constant velocities $v(0)$ and $D_{c_0,0}$, respectively:

$$x_1(t) = v(0)t \tag{46}$$

$$x_s(t) = x_0 + D_{c_0,0}t \tag{47}$$

It is slightly more complex to determine the velocity and law of motion of the right edge of the rear disperse boundary. In order to find this velocity, Eq. 37 should be used. It has the following form in the present case:

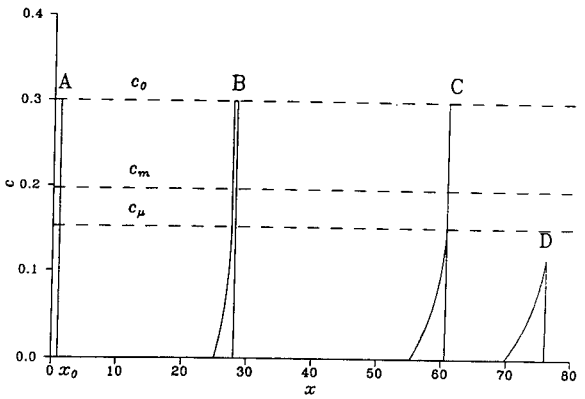

Fig. 7. Peak evolution for non-monotonous velocity and intermediate initial concentration $c_m < c_0 < c_*$. (A), (B), (C) and (D) are the peak shapes at dimensionless time moments $t = 0$, 32.62, 72.41 and 90.6, respectively. Parameters: α, k_1 and k_2 as in Figs. 5 and 6. $c_0 = 0.3$. Values of c_m, c_* and $v(0)$ as in Figs. 5 and 6. $\mu = 0.844$, $D_{c_0,0} = 0.83$, $c_1(\mu) = 0.152$.

$$\frac{dx_r}{dt} = D\{c_1(x_r/t), c_0\} \tag{48}$$

with the initial condition

$$x_r(0) = 0 \tag{49}$$

The value of $x_r(t)/t$ is indeterminate at $t = 0$. By using the L'Hospital rule for revealing indeterminacy, one finds

$$\lim_{t\to 0} \frac{x_r}{t} = \left.\frac{dx_r(t)}{dt}\right|_{t=0} = v_r(0) \equiv \mu_1$$

where μ_1 denotes the velocity of the right edge $v_r(0)$, still unknown at the initial time moment $t = 0$.

Eq. 48 at time $t = 0$ may be represented as follows:

$$\mu_1 = D\{c_1(\mu_1), c_0\} \tag{50}$$

Eq. 50 allows one to determine the velocity μ_1. We can easily solve it by noting that the velocity μ_1 is at the same time the concentration velocity, corresponding to a certain concentration c_{μ_1}, and the velocity of the discontinuity, having a concentration c_{μ_1} at the left and a concentration c_0 at the right. In order to find an approximate value of c_{μ_1}, one plots two functions, $y = D\{c, c_0\}$ and $y = v(c)$, and finds the

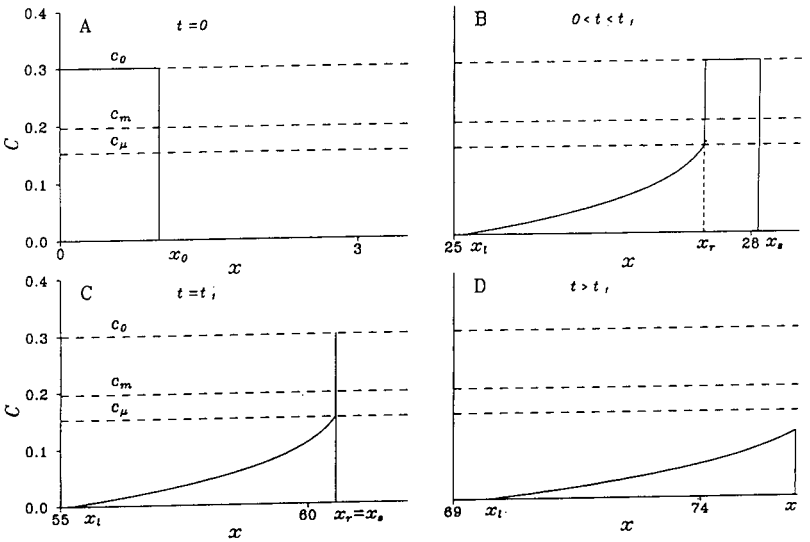

Fig. 8. Structure of the peaks shown in Fig. 7. Peaks A and B are plotted on the same scale (on the x-axis), which is, however, different from the scale used for peaks C and D. (A) Initial "rectangular pulse" distribution at $t = 0$, $x_0 = 1$. (B) A peak with a developed disperse rear boundary, right discontinuity, a region of constant initial concentration and a front discontinuity, $t = 32.62$. (C) A peak at the time moment $t = t_1 = 72.41$ when the disperse boundary reaches the front. The concentration of the peak maximum is still the initial concentration. (D) A "triangle"-like peak at $t = 90.6$.

point of their intersection having coordinates (c_{μ_1}, μ_1) (Fig. 9).

The solution to Eq. 48 is found in the following simple form:

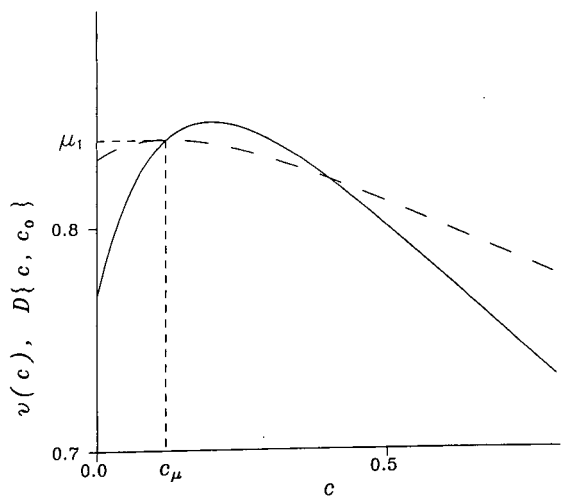

Fig. 9. Dependences of the concentration velocity and the velocity of the discontinuity D_{c,c_0} on concentration for $\alpha = 0.2$, $k_1 = 0.3$, $k_2 = 4$ and $c_0 = 0.4$.

$$x_r(t) = \mu_1 t \tag{51}$$

In order to verify this, it is sufficient to note that substituting $x_r(t)$ from Eq. 51 into Eq. 48 transforms the latter into an equation like Eq. 50 and the initial condition, Eq. 49, is also satisfied. It follows from Eq. 51 that the right edge of the disperse boundary x_r moves along the x-axis with a constant velocity μ_1. Concentration $c_1(\mu_1)$, corresponding to the concentration at the right edge of the rear disperse boundary, is the peak tail height. It is worth noting that this concentration is a constant until the time moment t_1 when the rear discontinuity reaches the front discontinuity.

At the time moment t_1, determined from the condition $x_r(t_1) = x_s(t_1)$, the right edge of the disperse boundary reaches the sharp front $x_s(t)$ (Figs. 7C and 8C). After this moment the peak shape becomes "triangle"-like (Figs. 7D and 8D), and the peak evolves analogously to the case considered above (Eqs. 41 and 43).

Summarizing the analysis presented above, the following scenario of the peak evolution in the

case of an intermediate initial concentration might be suggested. Similarly to the previous case of low initial concentration, the rear disperse boundary, the width of which grows linearly with time, and the discontinuity at the front are formed. However, another discontinuity at the right edge of the rear disperse boundary distinguishes this case from the previous one (compare Figs. 6B and 8B). A very interesting characteristic of the peak evolution shown in Figs. 7 and 8 is that the peak height falls abruptly from c_0 to c_{μ_1} at $t = t_1$. It is also worth noting that the time moment t_1 when the rear disperse boundary reaches the front and the location of this event at the x-axis are almost twice as long in comparison with the case of low concentration. This means that one observes either a triangle or a peak having a rectangular region depending on the initial concentration of the analyte.

(C) Interval of high initial concentration, $c_m < c_* < c_0$ (see Fig. 4)

The initial peak transformations are shown in Figs. 10 and 11. The development of the rear disperse boundary combined with the discontinuity is essentially the same as in the previous case. However, the front region of the peak cannot be represented as a pure discontinuity as

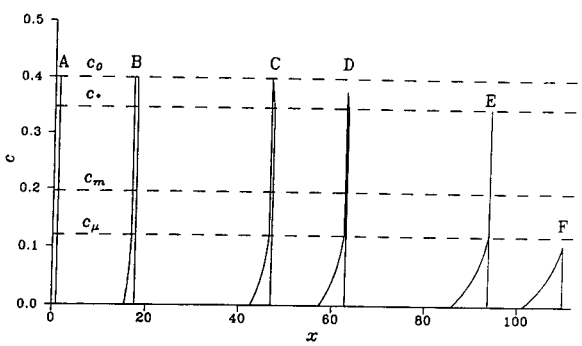

Fig. 10. Peak evolution for the non-monotonous velocity and high initial concentration $c_m < c_* < c_0$. (A), (B), (C), (D), (E) and (F) are the peak shapes at dimensionless time moments $t = 0$, 20.1, 55.3, 74.5, 111.5 and 131.5, respectively. Parameters α, k_1 and k_2 and the values of c_m, c_* and $v(0)$ as in Figs. 5–8. $c_0 = 0.4$, $\mu_1 = 0.839$, $c_1(\mu_1) = 0.12$, $\mu_2 = 0.831$, $c_2(\mu_2) = c_*$.

the stability condition for the discontinuity is not satisfied there (the velocity of the discontinuity is higher than the concentration velocity at the left from the discontinuity, see Fig. 4, $c > c_*$). Therefore, the concentration profile at the front boundary of the peak should be a combination of the profile $c_2(z)$ and a discontinuity, in analogy with that found in the previous case for the rear disperse boundary.

The right and left edges of the rear disperse boundary move along the x-axis with constant velocities:

$$x_l(t) = v(0)t\,, \quad x_r(t) = \mu_1 t \tag{52}$$

where μ_1 is the velocity found from Eq. 50.

The motion of the left edge of the front disperse boundary is governed by

$$\bar{x}_l(t) = v(c_0)t + x_0 \tag{53}$$

where $\bar{x}_l(t)$ is the coordinate of the left edge of the front disperse boundary.

The equations for the right edge of the front disperse boundary will then be similar to Eqs. 48 and 49:

$$\frac{d\bar{x}_r}{dt} = D\left\{c_2\left(\frac{\bar{x}_r - x_0}{t}\right), 0\right\} \tag{54}$$

$$\bar{x}_r(0) = x_0 \tag{55}$$

Again, as in the previous case of intermediate initial concentration,

$$\lim_{t\to 0}\frac{\bar{x}_r - x_0}{t} = \left.\frac{d(\bar{x}_r(t) - x_0)}{dt}\right|_{t=0} \equiv \mu_2 \tag{56}$$

where μ_2 is the velocity of the right edge of the front disperse boundary. This velocity can be found from the following equation, which is similar to Eq. 50:

$$\mu_2 = D\{c_2(\mu_2), 0\} \tag{57}$$

Then, for the right edge of the front disperse boundary, we find

$$\bar{x}_r(t) = \mu_2 t + x_0 \tag{58}$$

It is important to note that, since μ_2 satisfies Eq. 57 and at the same time is the concentration velocity, the velocity μ_2 is the velocity $v(c_*)$

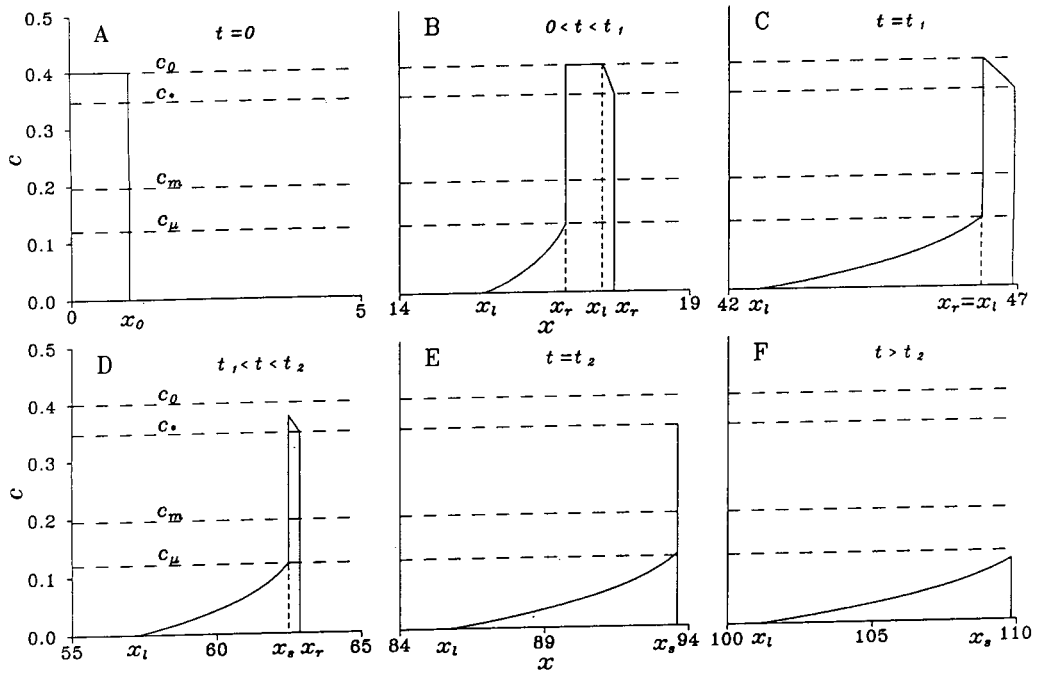

Fig. 11. Structure of the peaks shown in Fig. 10. Peaks A–C are plotted on the same scale (on the x-axis), which is, however, different from the scale used for peaks D–F. (A) Initial "rectangular pulse" distribution at $t = 0$, $x_0 = 1$. (B) A peak with a disperse rear boundary, right discontinuity, a region of constant initial concentration, a front disperse boundary and a front discontinuity, $t = 20.1$. (C) A peak at the time moment $t = t_1 = 55.3$ when the rear disperse boundary reaches the front disperse boundary. (D) A peak with a rear disperse boundary, a discontinuity, a front disperse boundary and a front discontinuity. The concentration at the peak maximum decreasing as the peak moves along the capillary, $t = 74.5$. (E) The second peak transformation: the right edge of the rear disperse boundary reaches the right edge of the front disperse boundary, $t = t_2 = 111.5$. (F) The final stage of the peak evolution, $t = 131.5$.

corresponding to the intercept of the concentration velocity and the discontinuity velocity curves. Therefore, the concentration corresponding to the amplitude of the front discontinuity is $c_{\mu_2} = c_*$, given by Eq. 29 and illustrated in Fig. 4.

At a time t_1 the right edge of the rear disperse boundary x_r reaches the left edge of the front disperse boundary $\bar{x}_1$ (Figs. 10C and 11C). The time t_1 is found from the following equation:

$$t_1 = \frac{x_0}{\mu_1 - v(c_0)} \tag{59}$$

The motion of the new right edge of the rear disperse boundary is found from the following equation:

$$\frac{d\bar{x}_s}{dt} = D_{c_1,c_2} \equiv D\left\{c_1\left(\frac{\bar{x}_s}{t}\right), c_2\left(\frac{\bar{x}_s - x_0}{t}\right)\right\} \tag{60}$$

with the initial condition

$$\bar{x}_s(t_1) = \frac{\mu_1 x_0}{\mu_1 - v(c_0)} \tag{61}$$

The problem in Eqs. 60 and 61 can be solved numerically.

The next transformation of the peak occurs when the boundary $\bar{x}_s$ reaches the right edge of the front disperse boundary $\bar{x}_r$ (Figs. 10C and 11C). The time moment t_2 when this event occurs is calculated from

$$\bar{x}_s(t_2) = \bar{x}_r(t_2) \tag{62}$$

After that the peak becomes "triangle"-like and

its further evolution is described again by Eqs. 41 and 43.

It is interesting that the time t_2 of the second transformation after which the peak becomes "triangle"-like is longer than in previous cases of lower initial concentration. This makes it possible to observe experimentally all stages of the peak evolution. The analysis presented above fully settles the case of the non-monotonous dependence of the concentration velocity on concentration. This type of velocity dependence on concentration reflects the fact that the electromigration and chromatographic mechanisms of the peak dispersion are comparable and act in opposite directions. We have seen in Fig. 1 (1.1) that electromigration in the case of $\alpha > 0$, corresponding to a decreasing dependence of the concentration velocity on concentration, leads to the development of a peak with a front disperse boundary. Chromatography, characterized by an increasing concentration dependence of the concentration velocity, in contrast, produces peaks with a rear disperse boundary. Combination of both, as shown above, is able to delay peak transformation significantly and thus preserve a narrow peak of the analyte.

We proceed to the following two cases of the concentration velocity monotonously increasing with concentration [case (ii), Eq. 22] and of the concentration velocity monotonously decreasing with concentration [case (iii), Eq. 23]. The analysis of the peak transformations is similar to that presented above, although there are qualitative differences in the peak behaviour.

5.2. Case (ii) Peak evolution with monotonously increasing velocity $\alpha < 0$, $(1 + \alpha c) > 0$

The initial concentration cannot be arbitrary high, otherwise the electric conductivity will become negative for high values of concentration. It is assumed below that the concentration is limited by the inequality $c < -1/\alpha$. The evolution of a concentration profile is shown in Fig. 12 (12.1).

The initial pulse (A) transforms into the peak (B) with a disperse rear boundary and a front discontinuity. The disperse boundary reaches the discontinuity (C) and the peak becomes "triangle"-like (D). The motion of the edges x_l, x_r and boundaries x_s, $\bar{x}_s$ is given by Eqs. 33–37. The asymptotic Eqs. 39–45 are also valid. A qualitative difference of the peaks shown in Fig. 12 (12.1) from those shown in Figs. 1 (1.1) and 5 is in the shape of the disperse boundary. In contrast to the peaks in Figs. 1 (1.1) and 5, the concentration profiles B, C, D in Fig. 12 (12.1) have an inflection point. In practice, a concentration profile with an inflection point might be misinterpreted as a diffusional boundary.

5.3. Case (iii). Peak evolution with monotonously decreasing velocity $\alpha > 0$, $k_1(k_2 - \alpha) < \alpha$

The peak evolution for this case is illustrated in Fig. 12 (12.2). It passes the following stages. The initial "rectangular pulse" (A) keeps a discontinuity at the rear and develops a disperse boundary at the front (B). The coordinates of the discontinuity and the edges of the disperse boundary are given by

$$x_s(t) = D_{c_0,0}t\,, \quad x_l(t) = v(c_0)t + x_0\,,$$
$$x_r(t) = v(0)t + x_0 \tag{63}$$

At the time moment t_1,

$$t_1 = \frac{x_0}{D_{c_0,0} - v(c_0)} \tag{64}$$

the discontinuity reaches the left edge of the disperse boundary (C) and after that the amplitude of the peak decreases and generates again the "triangle"-like shape (D). The coordinates of the discontinuity and the maximum concentration are found from a numerical solution of the equation

$$\frac{d\bar{x}_s}{dt} = D\left\{0, c_1\left(\frac{\bar{x}_s - x_0}{t}\right)\right\} \tag{65}$$

with the initial condition

$$\bar{x}_s(t_1) = x_0 \cdot \frac{D_{0,c_0}}{D_{c_0,0} - v(c_0)} \tag{66}$$

The asymptotic solution for the peak is also found analogously to Eqs. 39–45. However, the sign of the constant b in Eq. 43 is negative:

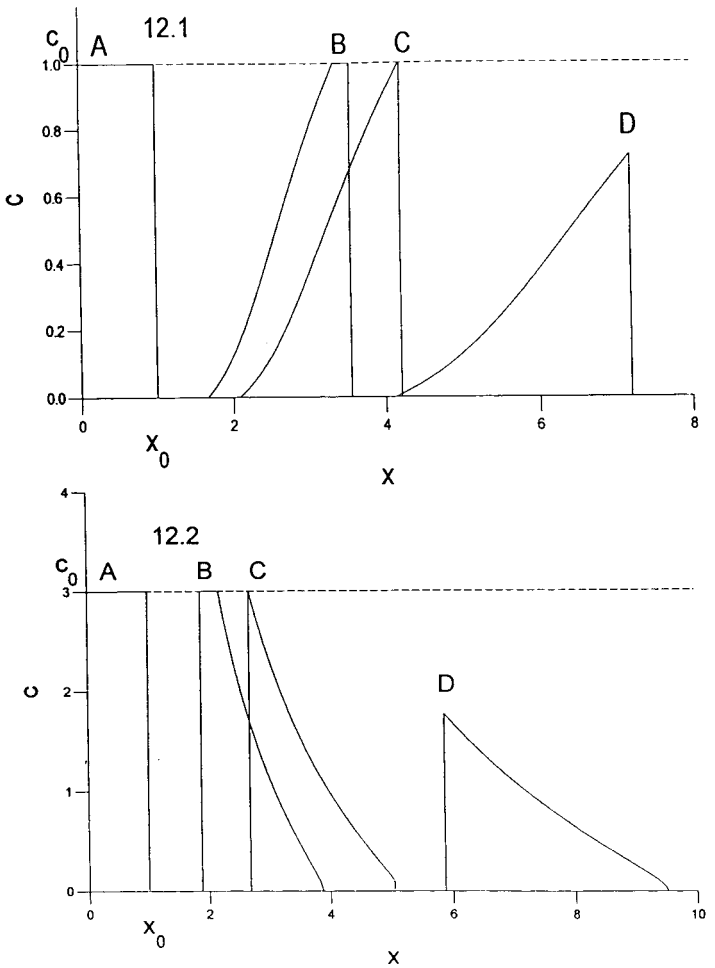

Fig. 12. (12.1) Peak evolution in the case of monotonously increasing concentration velocity. $\alpha = -0.2$, $k_1 = 0.3$, $k_2 = 4$, $c_0 = 1$. $v(0) = 0.7692$, $v(c_0) = 1.544$, $D_{c_0,0} = 1.179$. (A) Initial distribution $t = 0$, $x_0 = 1$. (B) A peak with a disperse rear boundary, a region of constant initial concentration and a discontinuity at the front. (C) The moment of the peak transformation into a "triangle", $t_1 = 2.74$. (D) The final stage of the peak evolution. (12.2) Peak evolution in the case of monotonously decreasing concentration velocity. $\alpha = 0.2$, $k_1 = 0.05$, $k_2 = 4$, $c_0 = 3$. $v(0) = 0.952$, $v(c_0) = 0.391$, $D_{c_0,0} = 0.6223$. (A) Initial distribution, $t = 0$, $x_0 = 1$. (B) A peak with a discontinuity at the rear, a region of constant initial concentration and disperse front. (C) The moment of the peak transformation into a "triangle", $t_1 = 4.3$. (D) The final stage of the peak evolution.

$$b = -\sqrt{-\frac{2\psi(c_0)v'(0)x_0}{1+k_1}} \tag{67}$$

6. Conclusions

In chromatography and electrophoresis, the concentration velocity is a monotonously increasing (non-linear chromatography and electrophoresis $\alpha < 0$) or a monotonously decreasing (electrophoresis $\alpha > 0$) function of the concentration. This leads to relatively simple and fast transformations of the initial "rectangular pulse" to a "triangle"-like peak. Combination of electrophoresis and non-linear adsorption can lead to a non-monotonous dependence of the concentration velocity on concentration and, as a result, to variety of peak shapes and scenarios of peak evolution.

The mechanisms of electromigration peak dis-

persion and non-linear chromatographic peak broadening are shown to be able partially to counterbalance each other. This is expressed in the long time required for transformation of the initial distribution into a "triangle"-like peak.

One of the most interesting findings, from a practical point of view, presented in this paper is that, depending on the initial concentration of an analyte, one may observe a peak as a "triangle"-like peak or as a peak with sharp discontinuities at its front and/or rear.

Variations of the capillary length, applied voltage or amount of the injected analyte may also lead to the appearance of all the kinds of peaks shown in this paper.

Acknowledgements

This work was supported in part by a grant from the European Community, Biomed I (No. Gene-93-0018) and by the Comitati di Biologia e Medicina e Chimica (CNR, Rome) to P.G.R.

References

[1] J.N. Jorgenson and K.D. Lukacs, *Science*, 222 (1983) 266–272.
[2] S. Hjértén, *Chromatogr. Rev.*, 9 (1967) 122–219.
[3] R. Virtanen, *Acta Polytech. Scand.*, 123 (1974) 1–67.
[4] S. Hjértén, *Electrophoresis*, 11 (1991) 665–690.
[5] F.M. Everaerts, T.A. van de Goor, Th.P.E.M. Verheggen and J.L. Beckers, *J. High Resolut. Chromatogr.*, 12 (1989) 28–31.
[6] S.F.Y. Li, *Capillary Electrophoresis—Principles, Practice and Applications*, Elsevier, Amsterdam, 1992, pp. 155–198.
[7] F.G. Helffrich, *J. Chromatogr.*, 629 (1993) 95–96.
[8] F.G. Helffrich and P.W. Carr, *J. Chromatogr.*, 629 (1993) 97–122.
[9] G. Klein, *AIChE Symp. Ser.*, 81, No. 242 (1985) 28.
[10] F.E.P. Mikkers, F.M. Everaerts and Th.P.E.M. Verheggen, *J. Chromatogr.*, 169 (1979) 1–10.
[11] V.G. Babskii, M.Yu. Zhukov and V.I. Yudovich, *Mathematical Theory of Electrophoresis*, Consultants Bureau, New York, 1989.
[12] R.A. Mosher, D.A. Saville and W. Thormann, *The Dynamics of Electrophoresis*, VCH, Weinheim, 1992.
[13] V. Sustacek, F. Foret and P. Boček, *J. Chromatogr.*, 545 (1991) 239–248.
[14] P.D. Lax, *Commun. Pure Appl. Math.*, 10 (1957) 537–566.
[15] G.B. Withem, *Linear and Non-Linear Waves*, Wiley, New York, 1974.
[16] B.L. Rozdestvenskii and N.N. Yanenko, *The Systems of Quasilinear Equation*, Nauka, Moscow, 1978 (in Russian).
[17] J.L. Wade, A.L. Bergold and P.W. Carr, *Anal. Chem.*, 59 (1987) 1286–1295.
[18] S. Golshan-Shirazi and G. Guiochon, in F. Dondi and G. Guiochon (Editors), *Theoretical Advancement in Chromatography and Related Separation Techniques*, Kluwer, Dordrecht, 1992, pp. 1–33.
[19] T. Tsuda, *Anal. Chem.*, 59 (1987) 521–523.
[20] W.D. Pfeffer and E.S. Yeung, *J. Chromatogr.*, 557 (1991) 125–136.

ELSEVIER

Journal of Chromatography A, 693 (1995) 131–143

JOURNAL OF CHROMATOGRAPHY A

Enhancement of selectivity and concentration sensitivity in capillary zone electrophoresis by on-line coupling with column liquid chromatography and utilizing a double stacking procedure allowing for microliter injections

S. Pálmarsdóttir[a], L.-E. Edholm[b]*

[a] *Analytical Chemistry, University of Lund, P.O. Box 124, S-221 00 Lund, Sweden*
[b] *Bioanalytical Chemistry, Astra Draco AB, P.O. Box 34, S-221 00 Lund, Sweden*

First received 8 August 1994; revised manuscript received 25 October 1994

Abstract

A double stacking procedure based on field enhancement is described as a means to increase the concentration sensitivity in capillary electrophoresis. Microliter volumes of sample are concentrated directly in the electrophoresis capillary without significant loss of separation performance. The whole procedure can be performed with a high degree of precision. A sensitivity gain of ca. 400 can easily be obtained by concentration of a 3-μl sample as compared with a 7-nl sample. The effect of experimental parameters on the final separation was studied for the enantiomers of *rac*-terbutaline, using alkyl substituted β-cyclodextrins as chiral selectors. Other enantiomers of chiral drugs can also be separated using the same procedure. Column liquid chromatography was used on-line with capillary electrophoresis for sample pre-treatment and concentration of the sample which allowed for injection of microliter volumes into the electrophoresis capillary. The selectivity and sensitivity gain of combining column liquid chromatography with capillary electrophoresis for determination of low concentrations of drugs in biosamples is exemplified.

1. Introduction

Although very high mass sensitivity detection is obtained in capillary zone electrophoresis (CZE), concentration sensitivity is poor. This is because the small diameter of the capillary only allows for small injection volumes (nanoliters). Thus determination of analytes at low concentrations e.g. drugs in biosamples, where concentrations in the range nmol–pmol/l are common [1], is hampered. Improved concentration sensitivity in CZE is therefore crucial in order to fully utilize the inherent potential of this technique.

There are a number of ways to increase the concentration sensitivity. For example by using more sensitive detection methods such as laser based fluorescence detection [2], electrochemical detection [3] and mass spectrometry [4]. UV–VIS detection is commonly employed in CZE but the concentration sensitivity which can be

* Corresponding author.

0021-9673/95/$09.50
SSDI 0021-9673(94)01047-1

obtained by conventional approaches is poor, commonly μmoles/l. Several ways have been tried to improve on sensitivity using UV–VIS detection for example by using "z" cells [5] and other methods that increase the optical path length [6].

Another possibility to increase sensitivity is to utilize a sample pre-treatment step, preceding capillary electrophoresis. In this way selectivity can be gained as well as concentration of the sample from a larger sample volume and thereby more sample can be injected in the CZE capillary.

This will be of special importance when samples in complicated matrices are concentrated for further analysis by CZE.

Sample pre-treatment and pre-concentration can be performed either on- or off-line with CZE or directly in the CZE capillary. Several procedures have been proposed in the literature; some examples are the following.

1.1. On-line coupling with column liquid chromatography

Bushey and Jorgenson [7] showed that by combining CLC and CZE on-line, the combined system had a much greater resolving power and peak capacity than either of the two systems used independently of each other. Although not discussed by the authors, enhancement of concentration sensitivity could in principle also be obtained with their approach for example by injection of a preconcentrated sample before injection into the first column.

1.2. Solid-phase extraction

Solid-phase extraction is a commonly employed technique for sample pre-treatment of crude samples in order to isolate the analyte from matrix components. The technique allows for pre-concentration on-column [8,9] or either on- [10] or off-line [11] with CZE. Under favourable conditions up to 250-fold enrichment has been obtained for standard samples with the in-line plug extraction approach [8].

1.3. Isotachophoretic pre-concentration

Isotachophoresis (ITP), which is another mode of electrophoresis [12], has been used by several groups for on-line sample concentration with CE [13–15]. A part of the ITP zone is injected into the CE capillary and up to a 1000-fold enrichment has been reported [14]. Apart from the possibility of large volume injection using ITP, a gain in selectivity could also be obtained. A complication with ITP is that optimum analyte focusing demands that the electrolytes are properly chosen with respect to mobilities and pK values of the constituents and length of the stacking zones. Irreproducibility of the electroosmotic flow can also give rise to poor enrichment performance.

Recently several groups performed ITP-CE in a single capillary [16–19]. An increase in sensitivity by a factor 50 to 100 was obtained. This procedure can be carried out easily in commercially available instruments but still suffers from the difficulties in finding the right combination of buffer components. In one approach [17] a procedure was introduced that allowed for removal of all sample ions with mobilities below that of the analyte ion from the capillary column. The increased detectability and gain in selectivity makes this a promising method when dealing with e.g. biosamples. However, for trace analysis, sample pre-treatment might also be necessary in order to obtain sufficient selectivity [17].

1.4. Field enhanced pre-concentration (stacking)

An analyte dissolved in a sample matrix which has a lower conductivity than the background electrolyte will experience a locally increased field strength and higher electrophoretic mobility and will migrate with higher velocity than in the background electrolyte. When the analyte reaches the boundary between the sample matrix zone and the background electrolyte it will slow down again and stack into a zone much narrower

than the original sample zone. This field enhanced pre-concentration effect [20] can be utilized to increase the volume injected in CE [21]. The maximum volume (enrichment factor of about ten) at optimal conditions is restricted by the mismatch between the composition of the electrophoretic buffer and the sample plug [22]. A hydrostatic pressure (back-pressure) is created at both sides of the sample–background electrolyte boundary and the laminar back-flow causes additional band broadening.

Chien and Burgi showed that it is possible to increase the sample volume beyond the optimal conditions using both hydrodynamic [23] and electrokinetic injection [24]. In the first case they used the electroosmotic flow to remove the sample matrix zone during or after the enrichment step, before the start of the actual CE separation. The maximum sample volume which can be pre-concentrated without loss of any analytes out of the capillary end is shown to depend on the ratio of the electrophoretic mobility of the analytes to the electroosmotic mobility. For phenylthiohydantoin–aspartic acid anion, injection zones at least as long as 1/3 of the total capillary length could be injected without loss of analyte or much band broadening. In the second case Chien and Burgi utilized the field enhancement effect during electrokinetic injection. Enrichment factors up to several hundred could be obtained by replacing the buffer vial by sample vial during a reversed polarity step.

The performance of these field enhanced pre-concentration techniques as discussed by Chien and Burgi [25] was not investigated in detail. Recently Nielen [26] applied the techniques described by Burgi and Chien for pre-concentration of environmental samples. Nielen found that it was very difficult to obtain reproducible results utilizing the field enhanced electrokinetic injection procedure, but good reproducibility was obtained using field enhanced pre-concentration when 1/3 of the capillary was filled with weak buffer containing herbicides. As field enhanced pre-concentration require samples having a relatively low and reproducible conductivity it was necessary to pre-treat the environmental samples using membrane extraction disks.

1.5. Aim of present work

In earlier communications from this laboratory, results were presented from ongoing investigations on the use of CZE for bioanalytical work [27–29]. Apart from the need to increase sensitivity, it was emphasized that sample pre-treatment also will be necessary in order to get rid of matrix components which would allow for higher selectivity, to get a better match with the composition of the sample and the electrophoresis buffer, and to avoid contamination of the capillary. The approach we have taken to cope with the above needs is to use column liquid chromatography (CLC) for sample pre-treatment and pre-concentration on-line with CZE [29]. An analyte in a large sample volume e.g., one milliliter of plasma is concentrated into a smaller volume by for example solid-phase extraction and thereafter injected into a micro-CLC system (see Fig. 4). When the analyte elutes from the micro-CLC column (μl volumes), the whole volume is transferred to the CE capillary which can be partially or completely filled with sample. A double stacking procedure was then used for in-line concentration of the injected sample [28]. By using the double stacking procedure described below, almost complete filling of the electrophoresis capillary is possible without significant loss of CZE separation performance. In this way sample pre-treatment with a gain in selectivity, as well as a tremendous increase in sensitivity can be obtained. In our first investigations [29] we evaluated reversed-phase liquid chromatography using methanol as organic modifier because of the versatility of this separation mode for many compounds of biological interest.

In the present work the double stacking procedure was further evaluated for several experimental parameters using the enantiomers of the β-agonist terbutaline (cations) as model substances. The experimental conditions for the CZE separation of the enantiomers using alkyl

substituted β-cyclodextrins were reported earlier in a communication from this laboratory [30]. The potential of our multidimensional approach for bioanalysis is also demonstrated.

2. Experimental

2.1. Chemicals and buffers

2-Hydroxypropyl-β-cyclodextrin with an average degree of substitution of 0.9 and 2,3,6-"di"-methyl-β-cyclodextrin having the 2-, 3- and 6-hydroxyl groups partially substituted with methoxyl groups, the average degree of substitution being 1.8 was obtained from Wacker-Chemie.(Burghausen, Germany). 2,6-Dimethyl-β-cyclodextrin, β-cyclodextrin, *rac*-brompheniramine (maleate) and *rac*-ephedrine (hydrochloride) were obtained from Sigma (St. Louis, MO, USA), mesityl oxide from Aldrich (Steinheim, Germany), *rac*-terbutaline (sulphate) and *rac*-bambuterol (hydrochloride) from Astra Draco (Lund, Sweden) and *rac*-propranolol (hydrochloride) from Astra Hässle (Mölndal, Sweden). All other chemicals were of analytical-reagent grade from Merck (Darmstadt, Germany).

Phosphate buffer pH 2.5 (0.1 *M*) was prepared by mixing appropriate concentrations of phosphoric acid and sodium dihydrogenphosphate solutions. Phosphate buffer pH 7.5 (0.005 *M*) was prepared by mixing appropriate concentrations of sodium dihydrogenphosphate and disodium hydrogenphosphate solution.

All water used was purified with a Milli-Q system (Millipore, Bedford, MA, USA). Mesityl oxide was used as neutral marker for measurement of electroosmotic flow.

Fig. 1 shows the structure of the analytes separated in this work.

2.2. Double stacking procedure

The CE separations were carried out using a Prince (Lauerlabs, Emmen, Netherlands) programmable injection and high voltage power supply system. A variable wavelength UV absorbance detector (Model Spectra 100, Spectra-Physics, San Jose, CA, USA) equipped with a deuterium lamp was used for detection and operated at 210 nm. The separations were performed in 70-cm effective length (81 cm total length) untreated fused-silica capillaries, 75 μm I.D. and 372 μm O.D. (Polymicro Technologies, Phoenix, AZ, USA). The separations were carried out at room temperature (ca. 23°C) and no forced cooling was applied to the capillary. Data analysis and collection were accomplished using System Gold software (Beckman, Palo Alto, CA, USA), version 712.

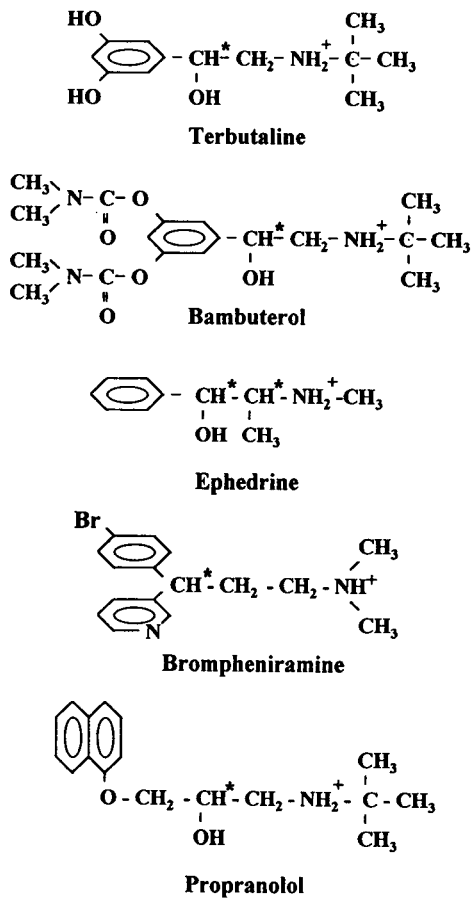

Fig. 1. Structures of chiral drugs separated in this work.

At the beginning of each working day the capillary was washed with 100 column volumes of 0.1 *M* NaOH solution. Before each run the capillary was washed with four column volumes each of 0.1 *M* NaOH, water and electrolyte

solution. After each working day the capillary was washed with ten volumes each of 0.1 *M* NaOH and water. The capillary was then dried with air.

Fig. 2 is a schematic representation of the different steps comprising the double stacking procedure. As the figure is only used to describe the different steps in the double stacking procedure mixing between zones during the procedure is not accounted for.

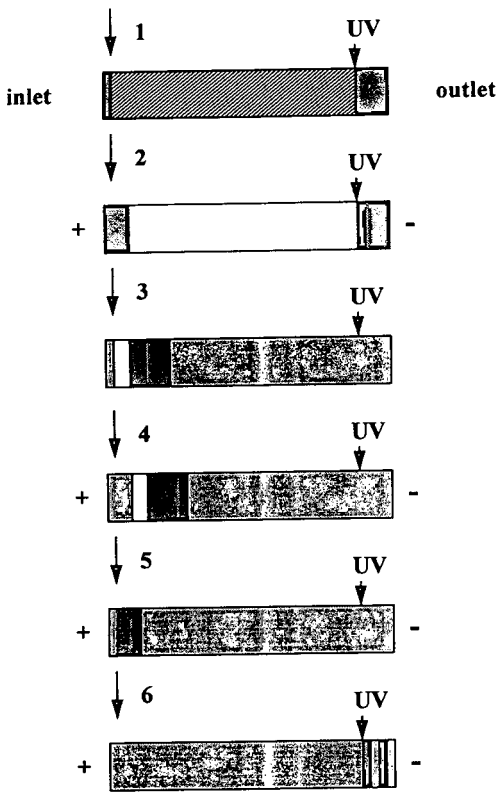

Fig. 2. A schematic presentation of the different steps comprising the double stacking procedure. Diagonal lines: 60% methanol–0.5 m*M* H_3PO_4–400 n*M* terbutaline; dark grey: 5 m*M* phosphate buffer pH 7.5; white: 60% methanol–phosphate buffer; black: terbutaline; light grey: 0.1 *M* phosphate buffer pH 2.5–10 m*M* dimethyl β-cyclodextrin. (1) Injection 200 mbar for 2.8 min; (2) stacking 30 kV for 6 min, back-pressure 44 mbar; (3) back-pressure 180 mbar for 1.8 min to move sample plug towards capillary inlet; (4) stacking 30 kV; (5) back-pressure 100 mbar to remove methanol plug, voltage lowered to 23 kV; (6) back-pressure off, final separation of terbutaline enantiomers.

During all stacking and separation steps a positive voltage was applied at the capillary inlet and the analyte cations migrated towards the cathode because of the net effect of the electrophoretic and electroosmotic mobilities.

The Prince system is equipped with a facility which allows for applying a back-pressure which is used in the different steps to either balance the electroosmotic flow or to pump the stacked band to the inlet part of the capillary.

In step one the capillary was filled (200 mbar for 2.8 min; 1 Bar = 10^5 Pa) almost to the detector window (3 μl) with sample solution (as marked by a distinctive change in the refractive index) exemplified here with a solution containing 400 n*M* *rac*-terbutaline (200 n*M* of each enantiomer), 0.5 m*M* H_3PO_4 and 60% methanol (pH 3.6). The bulk solution contained 5 m*M* phosphate buffer pH 7.5. The high pH of the bulk solution compared to the sample plug opposes the mismatch in electroosmotic flow at the boundary between the two zones reducing the laminar back-flow band broadening [22].

In step two the first stacking procedure was carried out by applying a voltage of 30 kV for 6 min, at the same time as a back-pressure of 44 mbar was applied. The back-pressure was used to prevent the stacking analyte from moving too fast towards the outlet of the capillary and allowing some of the first bulk electrolyte solution to remain in the capillary end. The back-pressure setting was judged to be right if the boundary between the methanol containing solution and the 5 m*M* phosphate buffer passed the detector at the end of the 6 min stacking (marked by a distinctive change in the refractive index as shown in Fig. 3). As almost all the field strength is dropped across the methanol containing solution, the electric field in the 5 m*M* phosphate buffer at the capillary outlet approaches zero. As a result the electrophoretic velocity of the ions in that buffer will approach zero and the ions will move only with the electroosmotic flow counteracted by the back-pressure of 44 mbar, thus no separation of the enantiomers will occur in this step.

In step three a separation buffer containing dimethyl-β-cyclodextrin as chiral selector was

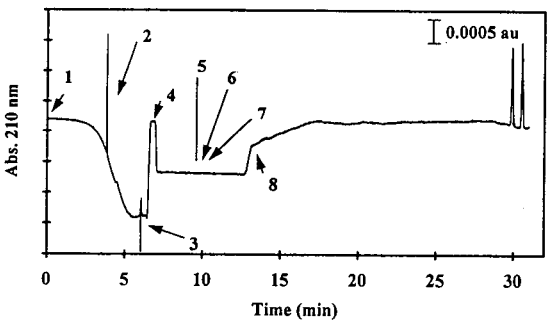

Fig. 3. Electropherogram obtained after using the double stacking procedure followed by CE enantiomer separation. 3 μl of 400 n*M* *rac*-terbutaline (200 n*M* of each enantiomer) was injected. Conditions as presented in Fig. 2. Arrows indicate the different events. (1) Stacking step one begins; (2) stacking peak of positive species; (3) voltage off, back-pressure on; (4) zone of 5 m*M* phosphate buffer pH 7.5; (5) back-pressure off; (6) voltage on, stacking step two at the inlet end of the capillary; (7) back-pressure on; (8) back-pressure off, final separation step begins.

introduced to allow for the separation of the terbutaline enantiomers [30]. At the same time as the 100 m*M* phosphate buffer pH 2.5 containing 10 m*M* dimethyl β-cyclodextrin was introduced the stacked peak was forced back to the injection end of the capillary. This was done by applying a back-pressure of 180 mbar to the system after turning off the high voltage. When about 3/4 of the original sample volume had been pushed out of the capillary which took 1.8 min (previously determined by injection of the 5 m*M* phosphate buffer) the back-pressure was stopped. The inlet end of the capillary was now filled with a mixture of the methanol solution, the stacked sample and buffer ions followed by a short band of the 5 m*M* phosphate buffer. The rest of the capillary was filled with the cyclodextrin separation electrolyte.

In steps four and five a second stacking procedure was carried out at 30 kV which compensated for the band broadening obtained after transportation of the previously stacked sample to the inlet part of the capillary. The positive species will now stack up at the concentration boundary between the 100 m*M* buffer containing cyclodextrin and the 5 m*M* buffer (mixed with methanol solution). The low pH of the cyclodextrin containing buffer (pH 2.5) compared to the 5 m*M* buffer (pH 7.5) will also increase the stacking effect in this step. At the same time as the stacking is in progress a back-pressure of 100 mbar is used to push the methanol containing band out of the capillary. After 2.5 min the separation voltage is lowered to 23 kV to prevent too much Joule heating in the system. The timing of this step was guided by the increase in current. During the first 2 to 3 min of the stacking the current in the system was low (1–3 μA) but it increased rapidly after that. When the current indicates that most of the high-resistant solution has been pushed out of the capillary (ca. 90 μA), the back-pressures was switched off. The final separation was obtained in step six.

Fig. 3 shows an electropherogram obtained with the double stacking procedure and enantiomer separation after injecting 3 μl of 400 n*M* *rac*-terbutaline (200 n*M* each enantiomer). Indicated in the figure is also the time for each event in the procedure. It is interesting to observe that the band broadening that has occurred after turning off the voltage and after pumping the sample back using back-pressure is compensated for in the second stacking step.

The information given above on experimental parameters that were used in the different steps are given as guidance. Differences from the experimental conditions given above are given in the text.

2.3. Micro-CLC on-line with CZE

In Fig. 4 the experimental set up is shown, which was used in this work to inject a sample corresponding to ca. 39 μl of plasma into the micro CLC column for further transfer (<3 μl) into the CE capillary. Before injection into the CLC column, the plasma sample (1 ml) was previously pre-treated and separated by coupled column liquid chromatography according to Edholm et al. [31]. After the last column [31], the fraction containing terbutaline was collected and transferred to a vial and evaporated to dryness and dissolved in 800 μl of water.

A pump (1) (Model 2150, Pharmacia LKB, Bromma, Sweden) was connected to an Acurate Microflow Processor (2) (LC Packings, Zurich,

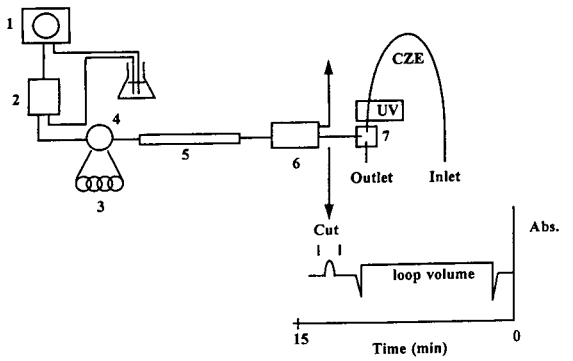

Fig. 4. Experimental set-up of micro-CLC coupled on line with CZE. (1) Pump; (2) flow processor; (3) loop; (4) valve; (5) analytical column; (6) μ-dumper interface; (7) Tee adapter. For details see the text.

Switzerland) resulting in a flow of 3 μl/min through the analytical column (5) which was made of steel (3.5 cm × 320 μm I.D.) and packed with Spherisorb ODS-2, 5 μm (LC Packings). A loop (3) with a volume of 31 μl connected to Valco valve (4) Model C6W KA 218 (Valco, Houston, TX, USA) was used for sample injection. To prevent bubble formation the mobile phase 80%, methanol–1 m*M* H_3PO_4, was degassed with helium.

The analyte fraction was transferred from the analytical column to the CZE capillary by switching of the μ-Dumper Interface (6) (LC Packings) a miniaturized switching device which was connected to the CZE capillary through a Fused Silica Tee Adapter (7) (Valco) having a inner diameter of 125 μm. The tee was positioned near the outlet of the CZE capillary which measured 90 cm from inlet to the detector, 95.5 cm from inlet to tee adaptor and 100.5 cm from inlet to outlet. While transferring the analyte fraction from the analytical column to the CZE capillary (previously filled with the CLC mobile phase) the outlet of the capillary was closed with a PVC stopper (manually operated).

Before starting the first step in the double stacking procedure the capillary was filled from the outlet to the detector (back-pressure 150 mbar for 0.9 min) with the 5 m*M* phosphate buffer (pH 7.5). Then the double stacking procedure was applied as described above.

3. Results and discussion

3.1. Performance of the double stacking procedure

In Fig. 5 the separation of *rac*-terbutaline (50 μM each enantiomer) after injection of 7 nl of a 100 μM solution in 100 m*M* phosphate buffer pH 2.5 containing 10 m*M* dimethyl β-CD is compared to the injection of about 3000 nl (200 mbar, 2.8 min) 400 n*M* *rac*-terbutaline (200 n*M* each enantiomer) after using the above procedure. No considerable loss in separation performance is observed and the increase in sensitivity is almost 400 times (step two Fig 2, stacking for 6 min).

It was observed that the time used for stacking in step two (Fig. 2) of the stacking procedure produced differences in the recovery. Fig. 6 shows the effect of the time of stacking on the peak areas obtained in the final enantiomer separation. Stacking for 1 min contributes to more than 60% of the peak area obtained after stacking for 10 min. After 10 min of stacking a maximum in peak area has been reached.

This behaviour is reproducible and seems to have no practical consequences, except for lowering the sensitivity. At present we have made the following observations. In the first stacking step, a sharp or a broad peak can be obtained

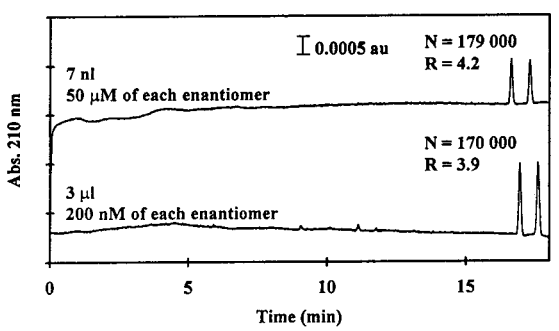

Fig. 5. Comparison of 7 nl injection versus 3000 nl injection. Conditions for 7 nl injection: 50 μM each terbutaline enantiomer, 0.10 *M* phosphate buffer (pH 2.5) electrolyte, 2,3,6-"di"methyl β-cyclodextrin concentration 10 m*M* and separation voltage 23 kV; for 3000 nl injection: 200 n*M* each terbutaline enantiomer other conditions as presented in Fig. 2.

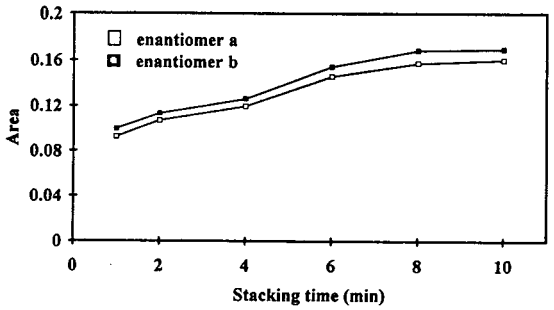

Fig. 6. The effect of the time of stacking on the peak areas obtained in the final separation. Conditions as presented in Fig. 2.

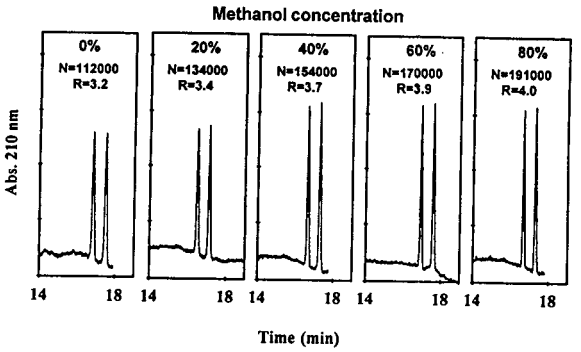

Fig. 7. Separation of terbutaline enantiomers using different methanol concentration (v/v) in the sample plug. Conditions as presented in Fig. 2 except for injection time, hydrodynamic back-pressure in the first stacking step and the time length of back-pressure in step 3 which were the following at each methanol concentration (v/v): 0% methanol: 2.1 min/ −76 mbar/1.3 min; 20% methanol: 2.6 min/ −68 mbar/1.7 min; 40% methanol: 2.8 min/ −60 mbar/1.8 min; 60% methanol: 2.8 min/ −44 mbar/1.8 min; 80% methanol: 2.4 min/ −40 mbar/1.5 min.

independently of the stacking time but with no effect on the overall reproducibility. The low recovery we expect is due to loss of analyte in the step were the analyte is transferred back to the inlet. The high field strength at the beginning of the stacking step contributes to more than 60% of the recovery. As the field strength is lowered with time, the recovery will reach a plateau.

3.2. Effect of methanol and electrolyte concentration

The methanol concentration in the sample plug (Fig. 2, step one) affects the final enantiomer separation observed after step six. Fig. 7 shows the enantiomer separations obtained after the final step when the methanol concentration in the sample plug was varied from 0% to 80% keeping the buffer concentration constant (0.5 m*M* H_3PO_4). The injection and back-pressure times for the different solutions were adjusted according to the principles described under Experimental. Higher efficiency and resolution was observed at increased methanol concentrations. The stacking effect obtained in step two (Fig. 2) depends on the methanol concentration in the sample plug. Fig. 8 shows the electropherograms obtained during the first stacking step when the methanol concentration in the sample plug was 80% and 40%. A very large stacking effect was obtained at 80% methanol concentration but when the methanol concentration was 40%, 20% and 0% (as indicated by absence of a sharp peak) less stacking effect was observed. The field strength in the capillary will vary with the conductivity of the background electrolyte [32].

The introduction of methanol in the sample solution will increase the resistivity of the sample solution compared to an aqueous solution and

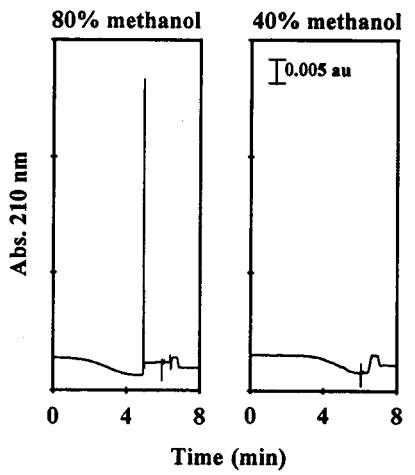

Fig. 8. Electropherograms showing the stacking effect in the first stacking step at methanol concentration (v/v) in the sample plug of 80% and 40%. Conditions as in Fig. 7.

thus the electric field strength in the sample zone will be raised further compared to the bulk solution and the stacking power increased, an effect which probably is the main reason why the efficiency and resolution is increased at higher concentrations of methanol. Fig. 7 demonstrates the importance of the second stacking step which compensates for the band broadening obtained in the preceding steps and thus makes it possible to handle large sample volumes. It can probably also be concluded, that the methanol concentration is of most importance in the second stacking step. The importance of the second stacking step is also clear from the fact that good reproducibility was obtained even though the effect of stacking varied from run to run in the first stacking step.

Fig. 9 shows the effect of ionic strength in the sample plug (Fig. 2, step one) on the final enantiomer separation at 60% and 80% methanol concentration when the double stacking procedure shown in Fig. 2 was followed (injection time and back-pressure times at 80% methanol were adapted to different viscosity). When the H_3PO_4 concentration in the sample plug is increased from 0.5 m*M* to 5 m*M* only a little loss of separation performance was observed at 80% methanol concentration, but at 60% methanol concentration the loss of separation performance was considerable. This observation also gives support to the above discussion on the importance of a high field strength. Higher methanol concentration in the sample plug thus allows for analysis of samples having higher ionic strength.

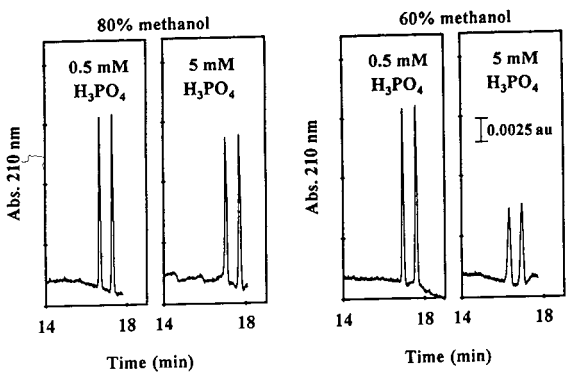

Fig. 9. Effect of electrolyte concentration in the sample plug on the final terbutaline enantiomer separation at 80% and 60% methanol concentration (v/v). Conditions as in Fig. 7 except for H_3PO_4 concentration.

In an untreated fused-silica capillary the electrophoretic migration and the bulk electroosmotic migration of ions depend linearly on the field strength.

Both the electrophoretic migration of sample ions and electroosmotic migration also depend on the composition, pH, concentration and viscosity of the background electrolyte. It has been observed that the mobility depends inversely on buffer concentration [33] and that organic solvents also affect the electroosmotic mobility dramatically [34,35].

Fig. 10 shows the effect of methanol concentration on the electroosmotic mobility in a fused-silica capillary, using mesityl oxide as neutral marker. The measurements were carried out in 0.5 m*M* phosphate buffer at pH around 3.5. It can be seen that the electroosmotic mobility starts to decrease with increased methanol concentration but reaches a minimum and starts to increase at higher concentrations. Also shown in the figure is the *relative* change in viscosity compared to pure aqueous buffer. The relative

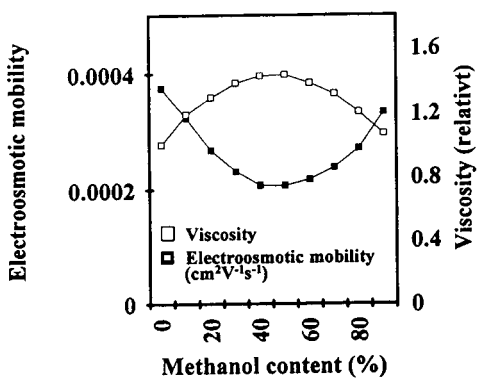

Fig. 10. Effect of methanol concentration (v/v) on electroosmotic mobility and relative viscosity of the electrolyte. Conditions; All solutions contained 0.5 m*M* H_3PO_4 giving the following pH values in the solutions. 0%, 10% and 20% methanol, pH 3.44; 30% methanol, pH 3.47; 40% methanol, pH 3.53; 50% methanol, pH 3.60; 60% methanol, pH 3.71; 70% methanol, pH 3.82; 80% and 90% methanol, pH 3.88. The neutral marker was mesityl oxide and voltage 30 kV.

viscosity was estimated from the time it took to fill 70 cm of 0.75 μm I.D. capillary to the detector window using 200 mbar hydrostatic pressure. The shape of the viscosity curve is in close resemblance, indicating the importance of the viscosity for the change of the electroosmotic flow at this low pH. As the charge at the silica surface is very much suppressed at this pH it would be plausible to conclude that the observed changes in electroosmotic flow are to a great extent due to the changes in viscosity. Other investigators [35] have shown that methanol suppresses the electroosmotic flow with increasing concentration (up to 80% methanol concentration). These observations were made at pH 9, so it is believed that the dependence found at pH around 3.5 as in this work will not be similar. At pH 9 the effect of viscosity will be less pronounced as compared to the effect on the charge on the wall of the capillary.

In order to obtain a good stacking effect in the first step it is important to reduce the laminar broadening due to mismatch in electroosmotic flow between sample zone and bulk solution [22]. As mentioned above, the high pH in the bulk solution compared to the sample plug (Fig. 2, step two) opposes the mismatch in electroosmotic flow. But the methanol concentration and ionic strength in the sample plug also affect the electroosmotic flow. At high compared to low methanol concentration the laminar broadening due to mismatch in electroosmotic flow seems to be more reduced. However any eventual mismatch in the first stacking step is compensated for in the second stacking step.

3.3. Linearity and reproducibility of the double stacking procedure

The linearity of the stacking procedure shown in Fig. 2 was studied for terbutaline enantiomer concentrations ranging from 12.5 n*M* to 500 n*M*. The calibration graph for peak areas is shown in Fig. 11. The results are the mean values from two runs. The correlation coefficient (r) for both enantiomers was 0.9998 and the intercept for enantiomer a was 0.0014 and for enantiomer b 0.0015.

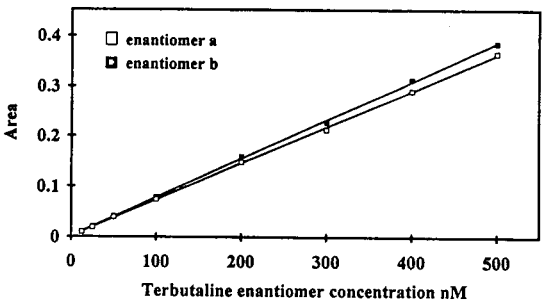

Fig. 11. Calibration graph at different concentrations of each enantiomer of *rac*-terbutaline. Conditions as presented in Fig. 2.

A study of the reproducibility of the double stacking procedure at different enantiomer concentrations is shown in Table 1. The results clearly indicate that sufficient performance can be obtained making the procedure most interesting for further evaluation in quantitative bioanalysis.

3.4. Application to other chiral analytes

Fig. 12 demonstrates the separation obtained after injection of 3 μl of sample solutions containing the enantiomers of some commonly used drugs, *rac*-bambuterol, *rac*-brompheniramine, *rac*-propranolol and *rac*-ephedrine in 80% methanol and 0.5 m*M* H_3PO_4.

After applying the double stacking procedure, the enantiomers were separated using the conditions previously described [30]. Baseline or almost baseline separation of all the enantiomers were obtained. Under the conditions used, all analytes were in their cationic form.

3.5. Column liquid chromatography on-line for sample pre-treatment and injection of microliter volumes into the CE capillary

For on-line coupling of CLC with CZE, micro columns were chosen because of the relative ruggedness of these columns and because μl-volumes of analyte eluting at reasonable reten-

Table 1
Reproducibility of the double stacking procedure at different concentrations

Parameter	Reproducibility (R.S.D., %)					
	Enantiomer a			Enantiomer b		
	1 μM ($n = 4$)	200 nM ($n = 7$)	62.5 nM ($n = 4$)	1 μM ($n = 4$)	200 nM ($n = 7$)	62.5 nM ($n = 4$)
Time	0.5	1.5	1.0	0.6	1.0	1.0
Peak area	0.7	1.2	2.4	1.0	0.9	3.5
Peak height	1.4	2.2	3.9	2.9	3.3	2.8
Resolution	1.9	1.7	1.1			
E (mean)	3.9	4.5	1.6			

tion times are compatible with the volume of an ordinary sized CZE column.

By connecting a micro CLC column directly to the CE capillary (Fig. 4), a cut [1] could be taken and transferred directly to the CE capillary. By this means sample pre-treatment as well as enhancement of concentration sensitivity can be obtained allowing for determination of low concentrations of analytes in biosamples. Fig. 13 shows an electropherogram, obtained after separation of a plasma sample containing the enantiomers of terbutaline at 5 nM concentration. The obtained electropherogram readily demonstrates the potential of the combined use of CLC for sample pre-treatment for enhancement of sensitivity and selectivity. Although terbutaline has a poor UV absorbance at λ 210 nm, nanomolar concentrations can still be reached.

The above results on the effect of methanol on the double stacking procedure shows that it

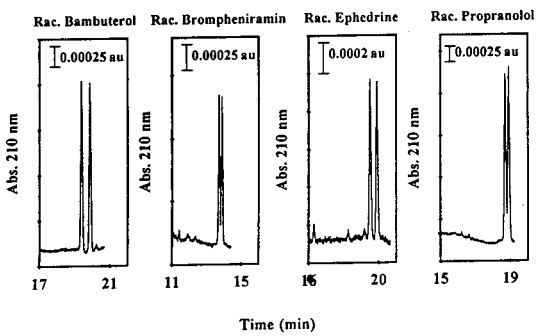

Fig. 12. Separation of the enantiomers of *rac*-bambuterol, *rac*-brompheniramine, *rac*-ephedrine and *rac*-propranolol after injection of ca. 3 μl sample. The sample plug contained 80% (v/v) methanol and conditions were as in Fig. 7 except for type and concentration of cyclodextrin in the final separation which were the following; *rac*-bambuterol–10 mM 2,6-dimethyl β-cyclodextrin, *rac*-brompheniramine–25 mM hydroxypropyl β-cyclodextrin, *rac*-ephedrine–25 mM 2,6-dimethyl β-cyclodextrin and *rac*-propranolol–10 mM hydroxypropyl β-cyclodextrin.

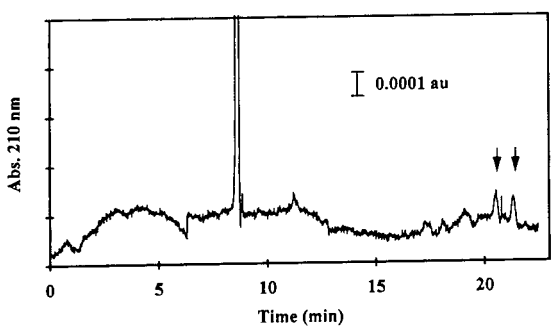

Fig. 13. Electropherogram obtained after the separation of a plasma sample containing the enantiomers of terbutaline at 5 nM concentration. The two arrows indicate both enantiomers. Conditions: CE capillary 90 cm to the detector, first stacking step 30 kV for 10 min using 51 mbar back-pressure, back-pressure in step three 180 mbar for 2.6 min, back-pressure in step five 150 mbar for 3 min then 100 mbar until current reached 90 μA. Second stacking step and the separation of terbutaline enantiomers were carried out at 30 kV. Other conditions see Fig. 2. For the experimental set-up see Fig. 4.

should be possible to use CLC mobile phases with high as well as low methanol content. Thus it should in principle be possible to apply the on-line approach to analytes of different lipophilicity.

4. Conclusion

The results presented in this work demonstrate that it is possible to concentrate μl-volumes of sample in a CZE capillary with mobile phase compositions commonly used in reversed-phase CLC without loss of separation performance which allows for an increase in concentration sensitivity. It is possible to carry out the double stacking procedure with good reproducibility by commercially available equipment. By combining CZE with CLC and sample preparation procedures like extraction using supported liquid membranes [36,37], large volumes (ml) of e.g. plasma can be pre-concentrated into microliter volumes which can be further concentrated by the double stacking procedure. The proposed procedure overcomes a significant problem in application of CZE to samples differing in composition and contamination of the CZE capillary is minimized.

Using different modes of liquid chromatography and other sample pre-treatment techniques, our approach should be investigated for application to other type of analytes in complicated matrixes. The concentration sensitivity which can be obtained is dramatic. Work is now in progress in our laboratory to explore our approach for quantitative analysis of drugs in biosamples using different combinations of sample pre-treatment techniques. Further work will also focus on more detailed investigations on the dependence of the double stacking procedure on experimental parameters.

Acknowledgement

We like to thank Mrs. Britt-Mary Kennedy for her help with the plasma sample preparations.

References

[1] L.-E. Edholm and L. Ögren, in I. Wainer (Editor), *Liquid Chromatography in Pharmaceutical Development*, Aster, Springfield, OR, 1986, pp. 345–373.
[2] P. Gozel, E. Gassmann, H. Michelsen and R.N. Zare, *Anal. Chem.*, 59 (1987) 44.
[3] R.A. Wallingford and A.G. Ewing, *Anal. Chem.*, 59 (1987) 1762.
[4] J.A. Olivares, N.T. Nguyen, C.R. Yonker and R.D. Smith, *Anal. Chem.*, 59 (1987) 1230.
[5] J.P. Chervet, R.E.J. van Soest and M. Ursem, *J. Chromatogr.*, 543 (1991) 439.
[6] S.F.Y. Li, *Capillary electrophoresis: Principles, Practice and Applications*, Elsevier, New York, 1992, pp. 55–154.
[7] M.M. Bushey, J.W. Jorgenson, *Anal. Chem.*, 62 (1990) 978.
[8] M. Merion, R.H. Aebersold and M. Fuchs, Poster presented at the *Third International Symposium on High Performance Capillary Electrophoresis*, San Diego, CA, February 3–6, 1991.
[9] I. Morita and J. Sawada, *J. Chromatogr.*, 641 (1993) 375.
[10] A.J.J. Debets, M. Mazereeuw, W.H. Voogt, D.J. Van Iperen, H. Lingeman, K.-P. Hupe and U.A.Th. Brinkman, *J. Chromatrogr.*, 608 (1992) 151.
[11] M.C. Roach, P. Gozel and R.N. Zare, *J. Chromatogr.*, 426 (1988) 129.
[12] A.T. Andrews, *Electrophoresis: Theory, Techniques and Biochemical and Clinical Applications*, Oxford University Press, New York, 1987, p. 289.
[13] F.M. Everaerts, T.P.E.M. Verheggen and F.E.P. Mikkers, *J. Chromatogr.*, 169 (1979) 21.
[14] D.S. Stegehuis, U.R. Tjaden and J. van der Greef, *J. Chromatogr.*, 591 (1992) 341.
[15] F. Foret, E. Szoko and B.L. Karger, *J. Chromatogr.*, 608 (1992) 3.
[16] S. Hjertén, K. Elenbring, F. Kilár, J.-L. Liao, A.J.C. Chen, C.J. Siebert and M.-D. Zhu, *J. Chromatogr.*, 403 (1987) 47.
[17] N.J. Reinhoud, U.R. Tjaden and J. van der Greef, *J. Chromatogr. A*, 653 (1993) 303.
[18] F. Foret, E. Szökö and B. Karger, *Electrophoresis*, 14 (1993) 417.
[19] C. Schwer, B. Gas, F. Lottspeich and E. Kenndler, *Anal. Chem.*, 65 (1993) 2108.
[20] S. Hjertén, S. Jerstedt and A. Tiselius, *Anal. Biochem.*, 11 (1965) 219.
[21] S.F.Y. Li, *Capillary electrophoresis: Principles, Practice and Applications*, Elsevier, New York, 1992, pp. 36–37.
[22] D.S. Burgi and R.-L. Chien, *Anal. Chem.*, 63 (1991) 2042.
[23] R.-L. Chien and D.S. Burgi, *Anal. Chem.*, 64 (1992) 1046.
[24] R.-L. Chien and D.S. Burgi, *J. Chromatogr.*, 559 (1991) 141.

[25] R.-L. Chien and D.S. Burgi, *Anal. Chem.*, 64 (1992) 489R.
[26] M.W.F. Nielen, *Trends Anal. Chem.*, 12 (1993) 345.
[27] S. Pálmarsdóttir and L.-E. Edholm, *Poster presented at the Fifth International Symposium on High Performance Capillary Electrophoresis, Orlando, Florida, January 25–28, 1993.*
[28] S. Pálmarsdóttir and L.-E. Edholm, Poster presented at the *13th Analytical Days, Lund, Sweden, June 14–18, 1993.*
[29] S. Pálmarsdóttir and L.-E. Edholm, Poster presented at the *Sixth International Symposium on High Performance Capillary Electrophoresis, San Diego, CA, January 31–February 3, 1994.*
[30] S. Pálmarsdóttir and L.-E. Edholm, *J. Chromatogr.*, 666 (1994) 337.
[31] L.-E. Edholm, B.-M. Kennedy and S. Bergquist, *Chromatographia*, 16 (1982) 341.
[32] M. Alonso and E.J. Finn, *Physics*, Addison-Wesley, Reading, MA, 1983, p. 478.
[33] H.J. Issaq, I.Z. Atamna, G.M. Muschik and G.M. Janini, *Chromatographia*, 32 (1991) 155.
[34] K. Salomon, D.S. Burgi and J.C. Helmer, *J. Chromatrogr.*, 559 (1991) 69.
[35] C. Schwer, and E. Kenndler, *Anal. Chem.*, 63 (1991) 1801.
[36] B. Lindegård, H. Björk, J.Å. Jönsson, L. Mathiasson and A.M. Olsson, *Anal. Chem.*, in press.
[37] B. Lindegård, S. Pálmarsdóttir, P. Deininger, L.-E. Edholm, L. Mathiasson and J.Å. Jönsson, in preparation.

ELSEVIER

Journal of Chromatography A, 693 (1995) 145–154

JOURNAL OF CHROMATOGRAPHY A

Monitoring of a conjugation reaction between fluorescein isothiocyanate and myoglobin by capillary zone electrophoresis

Peter R. Banks*, Donald. M. Paquette

Department of Chemistry and Biochemistry, Concordia University, 1455 De Maisonneuve Boulevard W., Montreal, Quebec H3G 1M8, Canada

First received 30 August 1994; revised manuscript received 1 November 1994; accepted 9 November 1994

Abstract

The conjugation reaction between the amine reactive fluorescent probe fluorescein isothiocyanate and the protein horse heart myoglobin was directly monitored as the reaction progressed by capillary zone electrophoresis with UV absorbance detection. Kinetic analysis of the data indicated that the order of the reaction was first with respect to myoglobin and 1.3 with respect to fluorescein isothiocyanate. The separation of peaks attributable to the incorporation of $n = 1, 2, \ldots 7$ fluorochrome labels into the protein has some significance for the generation of single-label protein probes, such as antibodies.

1. Introduction

Capillary electrophoresis (CE) is a relatively new analytical technique which is presently experiencing a rapid growth as increasing numbers of researchers discover the power of the technique for the separation of a wide range of molecules. Recently, a comprehensive review of the technique has been published which chronicles developments made in the fundamental understanding, instrumentation, and applications of the technique [1]. One area that has attracted much interest is the CE separation of proteins. It was originally supposed that exceptionally sharp zones would be achieved for protein separations since they possess relatively small diffusion coefficients [2]. However, capillary wall interactions lead to zone broadening and sometimes, to irreversible adsorption. Numerous methods have been developed to correct this problem [3], although no one method ensures satisfactory performance for all proteins.

Other problems exist with CE separations. The narrow bore of the capillary puts severe limitations on detector technology. When used as a detector for CE, the ubiquitous absorbance detector must be made to work with a path length which is typically at least two orders of magnitude shorter than that for standard spectrophotometers using 1 cm path lengths. This corresponds to relatively high limits of detection (10^{-5}–10^{-6} M). Furthermore, the dynamic range of the technique will be very narrow as the high concentration limit is controlled by the ionic strength of the run buffer. Typically, if the concentration of the run buffer is not significantly greater than the analyte concentration (i.e. [run buffer] > 100[analyte]), localized po-

* Corresponding author.

0021-9673/95/$09.50
SSDI 0021-9673(94)01110-9

tential gradients can be created leading to irregular peak shapes [3]. Therefore, for a 10 m*M* run buffer, the best possible dynamic range is 1 to 2 orders of magnitude. For this reason, other detection methods have been investigated which can lower the detection limit and thereby broaden the dynamic range for the technique.

Fluorescent methods are attractive for this purpose. Amine-reactive fluorescent probes can be used to create fluorescent derivatives of non-fluorescent analytes to allow for their sensitive detection. Cheng and Dovichi [4] have demonstrated sub-attomole (10^{-18} mol) mass detection limits for fluorescein isothiocyanate (FITC) derivatives of amino acids. This performance has subsequently been improved to the zeptomole range with picomolar (10^{-12} *M*) concentration detection limits [5]. This effectively drops the detection limit by approximately six orders of magnitude and increases the dynamic range of the technique to at least five orders of magnitude.

However, if the analyte of interest contains more than one reactive site, a complex mixture of products is typically obtained in a conjugation. This is due to the fact that the reactive fluorescent probes are quite bulky and the reaction process does not go to completion. Thus numerous products are produced differing in the number and spatial orientation of the conjugated probe [6]. It has been shown that for a molecule with n primary amino groups, $2^n - 1$ reaction products are possible [7]. The separation power of CE is capable of partially resolving this complex mixture leading to complex electropherograms with one analyte and indecipherable electropherograms with more than one. For the CE analysis of proteins, which contain numerous possible conjugation sites, this becomes catastrophic for practical analyses.

For amine-reactive fluorescent probes like FITC, conjugation to proteins occurs almost exclusively through nucleophilic attack by the ϵ-amino group of lysine residues and the N-terminal α-amino group [8]. Although the reaction is quite specific, proteins typically contain numerous lysine residues. Myoglobin, for example, contains 19 lysine residues and 1 N-terminal amino group[1]. Thus $2^{20} - 1 = 1\,048\,575$ different products are possible from a conjugation reaction. Somewhat fortunately, this formidable number is not fully realized, but one would still expect numerous products in a conjugation reaction with FITC.

In this study, we have monitored the conjugation reaction between myoglobin and FITC with time to obtain kinetic data and better understand the conjugation process. If the reaction proves to be second order overall, then FITC is incorporated into the protein in a stepwise fashion. Therefore, there should presumably be a point early in the conjugation reaction where a single, unique product with one FITC molecule incorporated is yielded. This would be of significant interest to CE separations that rely on fluorescence detection.

2. Experimental

2.1. Apparatus

CE separations were performed on a ATI-Unicam (Mississauga, Canada) Model Crystal 310 system with a 48-position peltier-cooled autosampler. Injection reproducibility of 0.40% R.S.D. based on peak area for 42 replicate dynamic compression injections is claimed for cytosine using this instrumentation [9]. In this study, dynamic compression injections of 10 mbar for 0.1 min were used. The sample tray in the Crystal 310 system could be temperature controlled from 4 to 40°C with a stability of ± 1° C. All conjugations were performed at 20 ± 1°C. Conjugation solutions were contained in glass vials sealed with Starburst caps to prevent evaporation, but allow periodic sampling by the Crystal 310 system. Detection was provided using a Unicam (Mississauga, Canada) 4225 UV-absorbance $^2H_2$ lamp-based detector operating at 200 nm. Absorbance signals where collected at 10 Hz using a National Instruments (Austin, TX, USA) NB-MIO-16X-H (16 bit resolution) data acquisi-

[1] Data from the Swiss Protein Data Base at the European Molecular Biology Labs.

tion board and stored as binary files on the hard disk of an Apple Computer (Cupertino, CA, USA) Model Macintosh Quadra 650 personal computer using an application developed in the National Instruments graphical programming language, LabView 3.0. The binary files were then read into the application program, Igor (WaveMetrics; Lake Oswego, OR, USA) where the data could be presented in graphical form.

2.2. Conjugations

Myoglobin was selected as the model protein for this study since excellent CE separation efficiencies have been demonstrated for this protein by simply using a run buffer with a pH that is significantly higher that the isoelectric point (p*I*) of the analyte. Lauer and McManigill [10] used this method to achieve theoretical plate counts of over 200 000 for both horse and sperm whale myoglobin. Myoglobin conjugations with FITC were achieved using molar ratios of 5:1 and 10:1, dye to protein. Typically, 5 mg/ml solutions of myoglobin in run buffer (0.1 *M* borate, pH 9.2) were used. Conjugation was initiated by adding an aliquot, which was 10% of the volume of the myoglobin solution, of FITC in N,N-dimethylformamide (DMF). The addition of the cosolvent DMF resulted in an increase in pH by about 0.3 pH units in the conjugation solution, which was deemed insufficient to effect the conjugation. Indeed, DMF is compatible with most aqueous protein solutions even at up to 30% (v/v) ratios [8].

2.3. Separations

All separations were performed with Polymicro (Phoenix, AZ, USA) 60 cm × 50 μm I.D. × 350 μm O.D. fused-silica capillaries. A small window was burned in the polyimide coating of the capillary 10 cm from the grounded outlet buffer vial. Capillaries were treated before use by flushing them with 0.1 *M* KOH for approximately 5 min, followed by HPLC-grade water, then run buffer, 0.1 *M* borate, pH 9.28, for similar durations. The capillary was then left in run buffer overnight. All separations followed a similar methodology that could be programmed into the Crystal 310 system. Initially, the outside of the capillary was rinsed by immersing it in a vial of run buffer for 0.01 min, then a sample was injected for 0.1 min, followed by another rinse in the same initial vial, then the capillary was immersed in a separate vial containing run buffer used for the separation. Separations were initiated by applying positive potential (24 kV) to the inlet buffer vial through a Pt–Ir (80/20) wire. Current flow in the capillary was approximately 44 μA. After separation, the capillary was purged using 2300 mbar of pressure for 0.5 min, making it ready for the next analysis.

2.4. Molar ratios of conjugated FITC to myoglobin

The molar ratio of conjugated FITC to myoglobin (F/P) was obtained by two methods. Both methods relied on stopping the conjugation reaction by the addition of at least a 50-fold molar excess of hydroxylamine (pH adjusted to 8.5 with 5 *M* NaOH) relative to the initial FITC concentration. The conjugation reaction solution was then passed through a Sephadex G-25 column equilibrated with run buffer to remove the hydroxylamine–FITC conjugate. In the first method, the electropherogram of the purified solution was obtained and areas of the individual peaks attributable to successive numbers of FITC conjugated to myoglobin were integrated using the application program, Igor. This peak area is due to the sum absorbance from myoglobin and the FITC labels, however. Therefore the relative extinction coefficient for FITC to myoglobin was determined at 200 nm using pure standard solutions of the two compounds. This was determined to be 0.022. The individual peak areas then had to be corrected for the contribution from FITC absorbance. For example, the peak area attributable to M + 1F was subtracted by 0.022(peak area), M + 2F by 2(0.022)(peak area) and so on. The average number of FITC labels incorporated into the myoglobin was then computed according to the equation:

$$\text{Average F/P} = \frac{\sum_{n=0}^{8} nM_n(1-c)}{\sum M_n} \quad (1)$$

where c refers to the relative extinction coefficient for FITC to myoglobin, n to the number of FITC peaks incorporated into myoglobin ($n = 0$–8) and M_n to the area of each peak attributable to a separated M + nF component.

In the second method, the absorbances of the purified conjugation reaction mixture were measured at 409 and 490 nm using an Hewlett-Packard (Palo Alto, CA, USA) Model 8451A diode array spectrophotometer. As the extinction coefficient (ϵ) of FITC is reduced approximately 10% on protein conjugation, the extinction coefficient for FITC incorporated into myoglobin was taken to be 68 000 cm^{-1} M^{-1} [11]. The extinction coefficient for Fe(III) in the heme group of myoglobin which absorbs at 409 nm was taken to be 188 000 cm^{-1} M^{-1} according to Tamura et al. [12] The F/P was then calculated according to the following equation:

$$\text{Average F/P} = \frac{A_F \epsilon_P}{A_P \epsilon_F} \quad (2)$$

Spectra obtained for a pure FITC solution in run buffer demonstrated insignificant levels of absorbance at 409 nm so that the absorbance measurement at 409 nm for the protein conjugate was assumed to be totally due to the heme group of myoglobin.

2.5. Chemicals

Myoglobin from horse heart (95–100%), Sigma-grade borax (approx. 99%) and Sephadex G-25 fine, were purchased from Sigma (St. Louis, MO, USA). HPLC-grade DMF was purchased from Aldrich (Milwaukee, WI, USA). Fluorescein-5-isothiocyanate, Isomer I (FITC) was purchased from Molecular Probes (Eugene, OR, USA). Hydroxylamine hydrochloride (99% purity) was obtained from ICN Biochemicals (St. Laurent, Canada).

3. Results

Fig. 1 contains an electropherogram of horse heart myoglobin at a concentration of 5 mg/ml. DMF has been added to the solution to conform to the reaction conditions used for conjugation. There are two well separated peaks for myoglobin which is expected from the reported dual isoelectric points [13]. Lauer and McManigill's technique separates according to pI, with the higher pI protein eluting first due to less associated negative charge [10], therefore the larger peak eluting first is due to that portion of myoglobin with a pI of 7.3. The smaller peak due to myoglobin (pI 6.8) is at a sufficiently low concentration (peak height is $>10\times$ smaller than that for pI 7.3) that it is not a detectable participant in the conjugation. The theoretical plate count for myoglobin (pI 7.3) is approximately 200 000 based on calculations using peak widths at half maximum.

Fig. 2 contains a number of electropherograms of conjugation reactions occurring between myoglobin and FITC at dye-to-protein molar ratio of 5:1. Each electropherogram serves as a snapshot of the reaction's progress. In examining the electropherograms, an obvious development as the time coordinate of the conjugation reaction increases is the appearance of an increasing number of peaks in the electropherograms while the myoglobin peak height decreases. These peaks are due to an increasing number of fluorescent probes being conjugated per protein molecule. As the fluorochrome is incorporated into the protein through lysine residues, a positive charge associated with the protein is replaced by a negative charge since at the pH of the conjugation/run buffer, the ϵ-amino group of lysine is positively charged ($pK_{R\ group}$ 10.5 for lysine amino acid [14]), whereas fluorescein is negatively charged. It is realized that the $pK_{R\ group}$ can be altered through conjugation to proteins and is dependent on the spatial environment of the residue in the protein's quaternary structure, but the pH of the run buffer is sufficiently lower than 10.5 that all lysine residues in the myoglobin are positively charged in the run

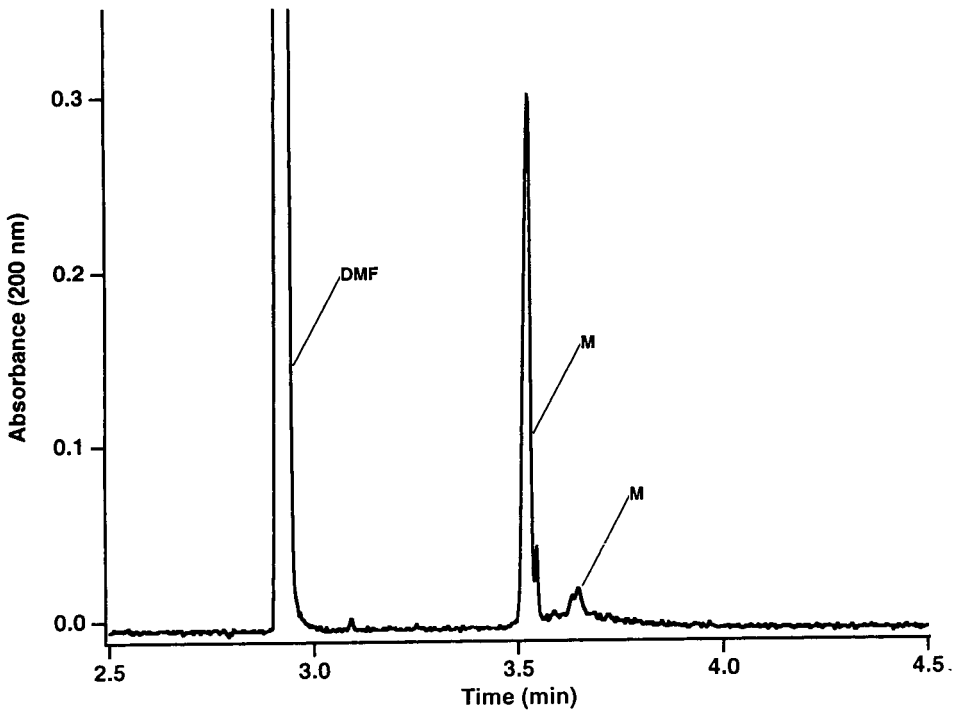

Fig. 1. Electropherogram of 5 mg/ml horse heart myoglobin in run buffer, 0.1 *M* borate, pH 9.28, with 10% DMF. Peaks labelled with an M are attributable to myoglobin.

buffer. Therefore, conjugation with a fluorescein reactive probe effectively changes the p*I* of the protein, which can be resolved from the pure protein. In all there are individual peaks in the electropherograms due to myoglobin being conjugated with from 1 to 7 FITC molecules. The relatively equal spacing between these peaks supports this hypothesis. Furthermore, myoglobin from horse heart muscle contains 19 lysine residues[2], therefore there are certainly enough conjugation sites for this degree of conjugation.

This hypothesis was verified by comparing the molar ratios of conjugated dye to protein estimated by the peak areas in the electropherograms and the more conventional spectrophotometric methods using absorbance measurements and extinction coefficients. Fig. 3 contains the electropherogram for a 10:1 FITC-to-myoglobin conjugation that was stopped by the addition of 50-fold excess of hydroxylamine relative to the initial FITC concentration after approximately 1 h of reaction time has elapsed. The mean of this distribution, computed using Eq. 1, equal to the average F/P, is 4.6. The F/P was spectrophotometrically determined to be 4.1 which demonstrates an acceptable agreement with that obtained from the electropherogram and tends to confirm the peak assignment used in Figs. 2 and 3. The spectrophotometric determination of F/P appears to be more accurate than that acquired from the peak integration method since the peak area of the FITC peak for a 10:1 conjugation reaction is approximately 40% smaller after 1 h conjugation reaction time compared to a blank. An improved performance would be obtained for the peak integration method if a Vis detector were available since absorbance measurements

[2] Data from the Swiss Protein Data Base at the European Molecular Biology Labs.

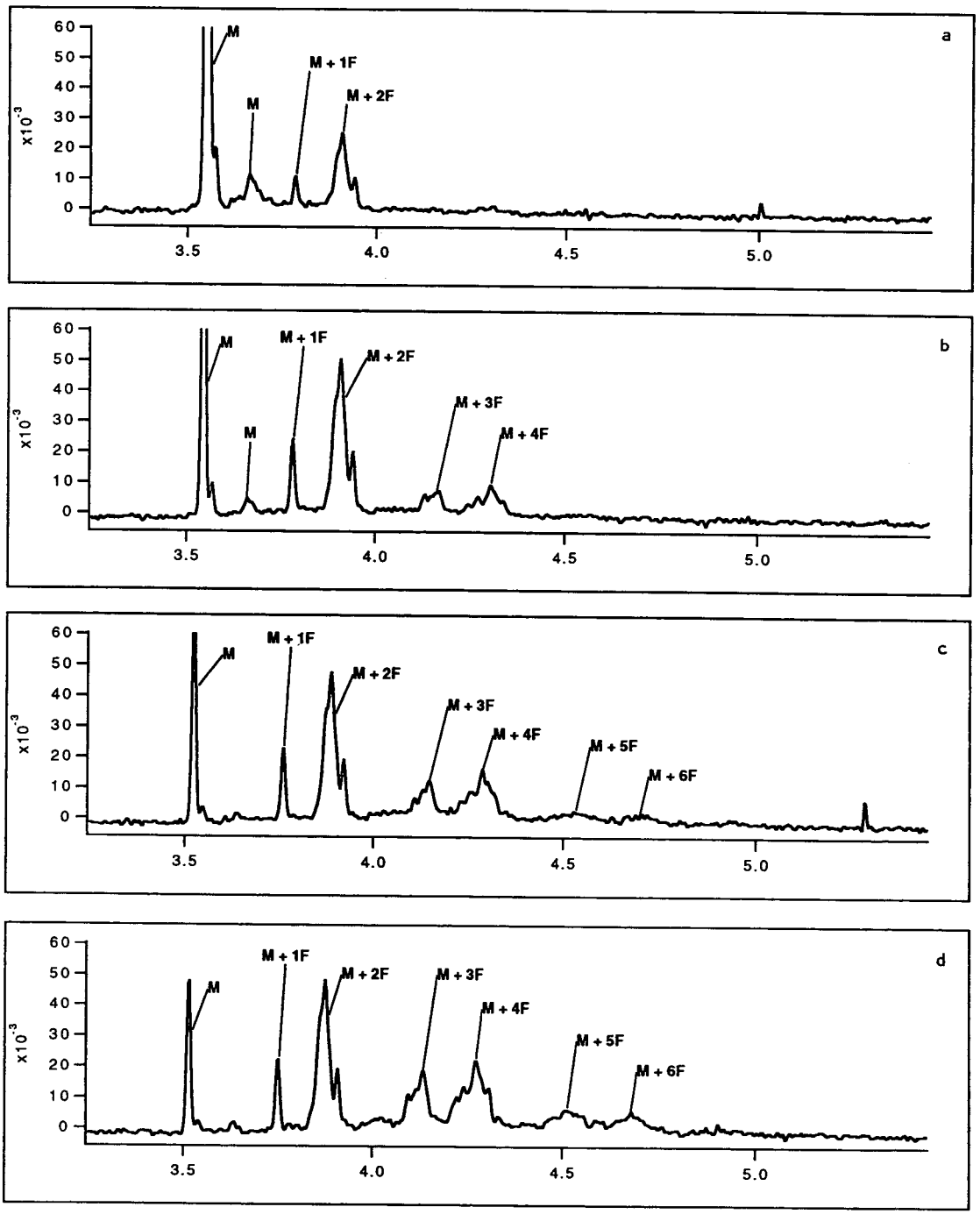
a
M
M
M + 1F
M + 2F
x10^-3
60
50
40
30
20
10
0
3.5
4.0
4.5
5.0
b
M
M
M + 1F
M + 2F
M + 3F
M + 4F
c
M
M + 1F
M + 2F
M + 3F
M + 4F
M + 5F
M + 6F
d
M
M + 1F
M + 2F
M + 3F
M + 4F
M + 5F
M + 6F

Fig. 2.

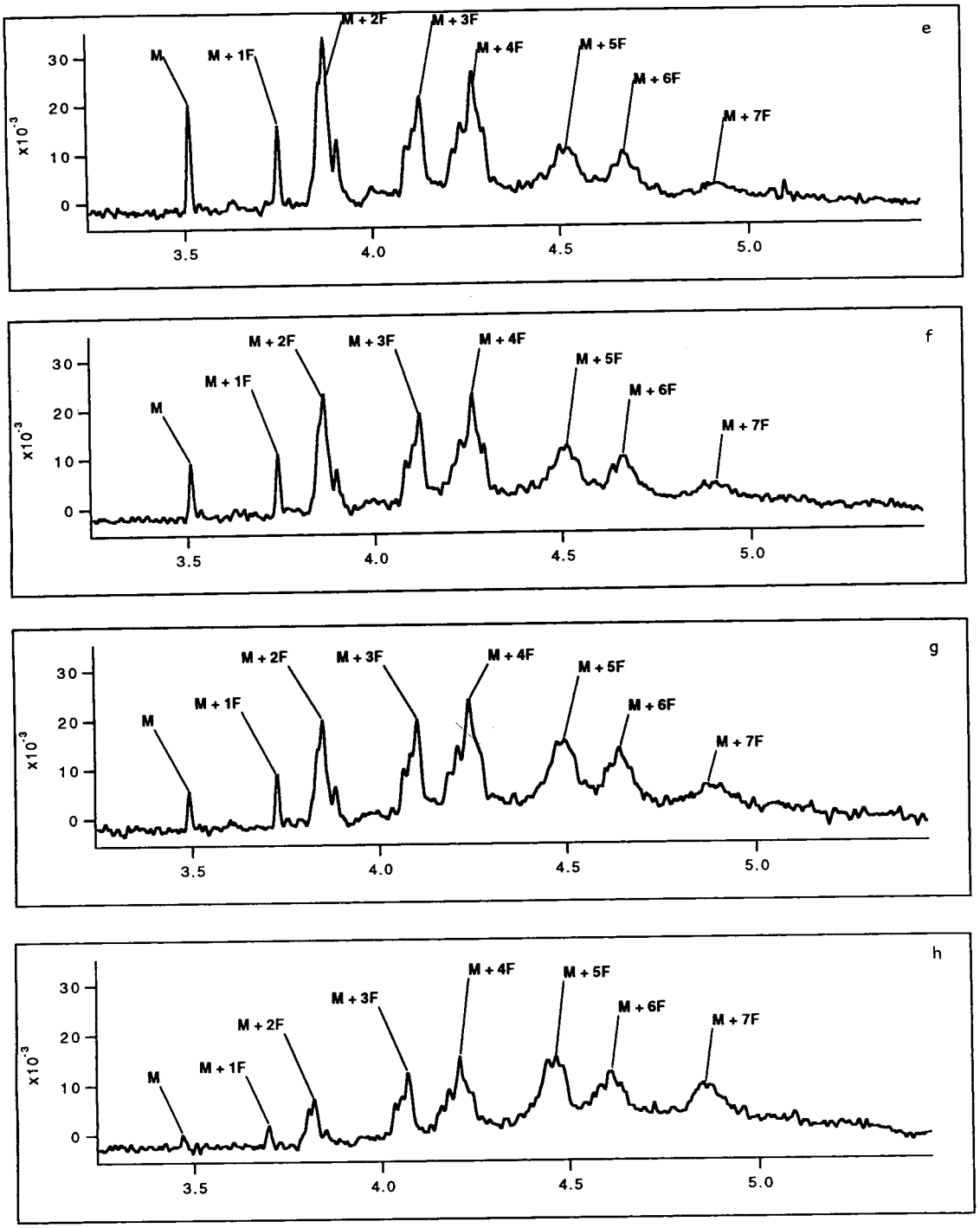

Fig. 2. Electropherograms for a 5:1 molar ratio conjugation of FITC to myoglobin at various times after the initiation of the conjugation reaction: (a) 2 min; (b) 19 min; (c) 36 min; (d) 52 min; (e) 85 min; (f) 110 min; (g) 135 min; (h) 218 min. Peaks labelled with M are attributable to myoglobin; M + 1F to myoglobin with one FITC molecule conjugated; M + 2F to myoglobin with two FITC molecules conjugated; . . . ; M + 7F to myoglobin with seven FITC molecules conjugated.

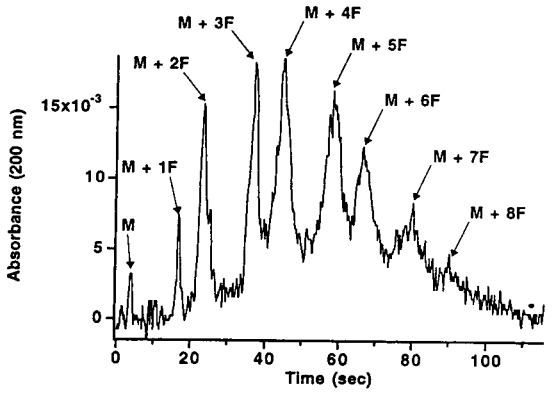

Fig. 3. Electropherogram for a 10:1 molar ratio conjugation of FITC to myoglobin which has been stopped by the addition of hydroxylamine after 1 h and the conjugation mixture passed through a G-25 column. Peak assignments as in Fig. 2.

at 409 nm would be directly attributable to the heme group of myoglobin with no significant interference from FITC.

Fig. 4 shows time profiles for some of the peaks evident in the electropherograms for the 5:1 molar ratio. Since peak height is directly proportional to concentration according to Beer's Law, kinetic analysis of the data can be made. The myoglobin peak follows an exponential decline described by pseudo-first order kinetics due to the excess concentration of FITC. An effective rate constant of 0.023 min^{-1} was obtained from the slope of a plot of the natural logarithm of the myoglobin peak height versus conjugation reaction time from 0 to 170 min. The straight line correlation for the plot was 0.996. The peak height of the myoglobin + 1 fluorochrome (M + 1F) peak experiences a doubling in peak height within 20 min of its first appearance. This is followed by a gradual decline in peak height throughout the remainder of the conjugation reaction. The apex of the M + 1F peak coincides with the time where the myoglobin's peak height is 1/e that of its initial height. This seems appropriate since the production of M + 1F should slow as the myoglobin is consumed and the M + 1F fraction reacts further with FITC to produce M + ($n > 1$)F peaks. The production of peaks with greater degrees of conjugation is evident by examining the M + 5F peak which slowly grows with increasing conjugation reaction time. However, approximately 40 min of reaction time is needed before the M + 5F peak is produced in detectable amounts.

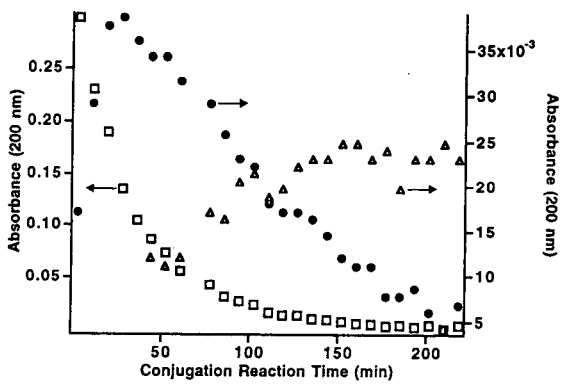

Fig. 4. Conjugation reaction time profiles for myoglobin, M, peak height absorbance (□); M + 1F peak height absorbance (○); and M + 5F peak height absorbance (△).

In general, from the analysis of the electropherograms, it is evident that the higher conjugated myoglobin fractions grow as the conjugation reaction proceeds at the expense of the lower conjugated myoglobin fractions. After nearly 4 h of reaction in the 5:1 molar ratio, no peak attributable to myoglobin is evident and little M + 1F or M + 2F. Even the peak heights of M + 3F and M + 4F have begun to diminish.

Another interesting aspect in the electropherograms is that lower conjugated protein peaks display sharper zones. Numerous peaks appear to be underlayed by the M + nF envelopes. Upon expansion of the peaks along the time axis, the M + 2F peak seems to be comprised of perhaps four individual peaks, M + 4F of five peaks and M + 7F of eight peaks. This indicates that separation is based not only on pI changes induced by the degree of conjugation, but also to the relative position of the dye labels in the protein conformation, albeit to a lesser extent. Also evident in the electropherograms is the development of a broad background with time, on which the peaks are superimposed. If the reaction is allowed to continue for 24 h, the broad background increases further and shifts to

longer migration times indicative of multi-conjugation of the protein.

If the ratio of FITC to myoglobin is increased to 10:1, little difference is seen except for an approximate tripling of the effective rate constant to 0.060 min^{-1} due to the doubling of the FITC concentration. The straight line correlation for this plot is 0.998, which is marginally better than that for the 5:1 ratio conjugation as one would expect as the pseudo-first order kinetics are more closely approximated. The broad background noted in the 5:1 conjugation ratio electropherograms appears earlier in the 10:1 ratio conjugation, as expected.

An interesting conclusion can be made from this kinetic analysis. The tripling of the effective rate constant with an increase in FITC concentration by two suggests that the overall order of the reaction is not second. The effective rate constant is related to the product of the true rate constant of the reaction and the concentration of the FITC to whatever order (α) it participates in the reaction (see Eq. 3).

$$k_{eff} = k[\text{FITC}]^{\alpha} \quad (3)$$

where k_{eff} is the effective rate constant, k is the true rate constant and [FITC] is the initial concentration of FITC, assumed to remain unchanged throughout the conjugation reaction. For α to equal 1 and the conjugation reaction be described by second-order kinetics, the doubling in concentration of FITC should result in a like doubling in the effective rate constant. However, k_{eff} appears to triple. If the initial FITC concentration in the conjugation reaction is tripled and quadrupled relative to the 5:1 conjugation, the effective rate constant was evaluated to be 0.11 and 0.14 min^{-1}, respectively. If the natural logarithm is taken of both sides of Eq. 3, α can be obtained from the slope of the straight line from a plot of ln k_{eff} versus ln [FITC]. This was found to be 1.3. Therefore the rate equation for the conjugation of FITC to myoglobin may be written:

$$-\frac{\text{d[myoglobin]}}{dt} = k[\text{myoglobin}][\text{FITC}]^{1.3} \quad (4)$$

This hypothesis could have been verified by fully applying the Ostwald isolation method (see [15]) and monitoring a conjugation reaction with a large excess of myoglobin relative to FITC to accurately determine if FITC is a first-order participant in the conjugation reaction. This was not practical with the current methodology, however, as large amounts of injected protein tended to influence the electrophoretic performance and yield irreproducible results.

4. Discussion

From the "snap shot" electropherograms of the myoglobin–FITC conjugation, it is evident that at no point in the conjugation is there a single, unique peak attributable to a fluorescent protein conjugate. After 2 min of conjugation for the 5:1 conjugation, there are two peaks, attributable to 1 and 2 FITC molecules conjugated to the protein. Furthermore, if areas are computed for these peaks, the M + 1F peak represents only 3% of the total protein concentration in the conjugation reaction mixture; the M + 2F peak only 18% in the 5:1 conjugation. Thus, only approximately 20% of the myoglobin has been conjugated. By the time these peaks have become more significant, M + 3F and M + 4F peaks have further complicated the electropherogram. In addition, the kinetic analysis indicates that FITC is not incorporated into myoglobin in a stepwise manner, therefore it is improbable that a single, unique peak can be obtained. An improved performance could possibly be obtained with other fluorescent reactive probes and will be the subject of further study in this research group.

On a brighter note, the complete separation of the M + 1F peak from both myoglobin and the M + 2F peak suggests a means for generating single-label antibody probes which may be used for analyses demonstrated by Shimura and Karger [16] group recently. Using rather complex chemical techniques, they were able to generate μg amounts of single-label antibody directed against methionyl recombinant human growth hormone, which were sufficient to perform several thousand assays.

In the 5:1 conjugation reaction after 19 min, the M + 1F peak represents approximately 7% of the total protein peak area. The injection plug is about 6 nl, so for the 5 mg/ml sample, the M + 1F peak represents 2 ng of protein, or enough for several assays if the protein in question was an antibody. So if a similar separation of the conjugation reaction could be made using an antibody as the protein, presumably one could collect a single-label product using fraction collection techniques.

Cheng et al. [17] have recently demonstrated the utility of poly(vinylidene difluoride) membranes for efficient fraction collection from a CE apparatus without significant sample loss or dilution while maintaining good spatial resolution. The authors where able to separate and collect a protein mixture of myoglobin and β-lactoglobulin. The amount of myoglobin collected on the membrane was 28 pmol, or about 500 ng. Although this is two orders of magnitude higher than the amount of M + 1F detected in our system, presumably the fraction collection system would function satisfactorily for smaller fractions. Furthermore, consecutive CE membrane fraction collections were demonstrated of the separated protein mixture so that successive M + 1F fractions could be harvested from the conjugation reaction mixture. The M + 1F peak is present throughout the first 2 h of the conjugation, therefore at least six successive harvests could be made yielding a total of about 10 ng of product. This method for producing a single label antibody will be investigated by this group in the future.

Acknowledgements

This work was funded by the Natural Sciences and Engineering Research Council and by Concordia University through an FRDP grant. We thank Dr. D.Y. Chen for developing the LabView application program used for collecting absorbance data and Dr. N.J. Dovichi for the provision of a connector box allowing the interface of the detector to the NB-MIO board.

References

[1] C.A Monnig and R.T. Kennedy, *Anal. Chem.*, 66 (1994) 280R–314R.
[2] J.W. Jorgenson and K.D. Lukacs, *Science*, 222 (1983) 266–272.
[3] R.A. Wallingford and A.G. Ewing, *Adv. Chromatogr.*, 29 (1989) 1–76.
[4] Y.F. Cheng and N.J. Dovichi, *Science*, 242 (1988) 562–564.
[5] S. Wu and N.J. Dovichi, *J. Chromatogr.*, 480 (1989) 141–155.
[6] J. Liu, Y.Z. Hsieh, D. Wiesler and M. Novotny, *Anal. Chem.*, 63 (1991) 408.
[7] J.Y. Zhao, K.C. Waldron, J. Miller, J.Z. Zhang, H.R. Harke and N.J. Dovichi, *J. Chromatogr.*, 608 (1992) 239–242.
[8] M. Brinkley, *Bioconjugate Chem.*, 3 (1992) 2–13.
[9] *Technical Report; Capillary Electrophoresis 1: Dynamic Compression Injection;* Unicam Analytical Systems, Madison, WI.
[10] H.H. Lauer and D. McManigill, *Anal. Chem.*, 58 (1986) 166–170.
[11] R.P. Haugland, in K.D. Larison (Editor), *Handbook of Fluorescent Probes and Research Chemicals*, Molecular Probes, Eugene, OR, 5th ed., 1992–1994, p. 22.
[12] M. Tamura, T. Asakura and T. Yonetani, *Biochim. Biophys. Acta*, 295 (1973) 467–479.
[13] B.J. Radola, *Biochem. Biophys. Acta*, 295 (1973) 412–428.
[14] A.L. Lehninger, D.L. Nelson and M.M. Cox, *Principles of Biochemistry*, Worth Publishers, New York, 2nd ed., 1993, p. 113.
[15] P.W. Atkins, *Physical Chemistry*, W.H. Freeman, New York, 3rd ed., 1986, p. 696.
[16] K. Shimura and B.L. Karger, *Anal. Chem.*, 66 (1994) 9–15.
[17] Y.F. Cheng, M. Fuchs, D. Andrews and W. Carson, *J. Chromatogr.*, 608 (1992) 109–116.

ELSEVIER

Journal of Chromatography A, 693 (1995) 155–161

JOURNAL OF CHROMATOGRAPHY A

Analysis of oxalate in Bayer liquors: a comparison of ion chromatography and capillary electrophoresis

P.E. Jackson

Waters Australia, Pty. Ltd., Private Bag 18, Lane Cove, N.S.W. 2066, Australia

First received 16 September 1994; revised manuscript received 2 November 1994; accepted 9 November 1994

Abstract

The performances of ion chromatography (IC) and capillary electrophoresis (CE) are compared for the quantitative analysis of oxalate in Bayer liquor, an industrial process solution used in the extraction and precipitation of alumina from bauxite. CE has a number of advantages over IC for this particular application. The most important difference between the two techniques was the fact that the selectivity of CE allowed for complete resolution of oxalate from the matrix components in Bayer liquor. However, oxalate results obtained by IC were consistently higher than those for CE due to the presence of chromatographic interferences. Chloride and sulfate could also be determined with oxalate in the same separation using CE, however the simultaneous determination of oxalate, chloride and sulfate in Bayer liquors was not possible by IC due to significant chromatographic interferences. CE gave improved precision for the replicate analysis of oxalate in liquor samples, with an overall average of 1.71% R.S.D., compared to an average of 2.85% R.S.D. when using IC. A further advantage of CE was the fact that it also allowed the simultaneous determination of oxalate, chloride and sulfate in liquor samples which had been stabilised with tartaric acid.

1. Introduction

The Bayer process involves the extraction (and precipitation) of alumina from bauxite using hot sodium hydroxide. The process is cyclic and soluble impurities, mostly organic and inorganic ions, accumulate in the process liquor stream [1]. Of these ions, oxalate is of prime importance as its stability and removal controls refinery productivity [2]. A typical liquor contains approximately 3.5 *M* sodium hydroxide, 0.5 *M* sodium carbonate, 1.0 *M* sodium aluminate [$NaAl(OH_4)$], 0.4 *M* sodium chloride, 0.25 *M* sodium sulfate, 2–3.5 g/l sodium oxalate and 20–30 g/l total organic carbon present as organic acid anions [1]. These amounts vary from refinery to refinery and also depend upon the source of the bauxite. The high ionic strength and pH, coupled with the fact that aluminium hydroxide is insoluble in the pH range of approximately 5–10, makes the routine analysis of oxalate in Bayer liquor a difficult task.

Oxalate is typically analysed in such a matrix using either gas chromatography (GC), after methylation, or ion chromatography (IC). Both techniques suffer significant drawbacks; in terms of either lengthy sample preparation time for GC, or organic acid interferences and short column (and suppressor) lifetime with IC. The selectivity of capillary electrophoresis (CE) appears to be particularly advantageous for the analysis of mixtures of inorganic anions and

0021-9673/95/$09.50
SSDI 0021-9673(94)01104-4

organic acids [3,4] and the feasibility of this technique for the analysis of oxalate in Bayer liquor has been demonstrated previously [1]. In this paper, the performances of IC and CE are compared for the quantitative analysis of oxalate in Bayer liquor. The advantages and disadvantages of both techniques for this particular analysis will be presented. The feasibility of performing simultaneous chloride, sulfate and oxalate analysis, using both IC and CE, will also be discussed.

2. Experimental

2.1. Ion chromatography system

The ion chromatograph consisted of a Waters (Milford, MA, USA) 510 solvent-delivery system, a 717 autosampler, a 431 conductivity detector, a 486 variable-wavelength UV detector operated at 214 nm and a Millennium 2010 chromatography management system. Data were collected at 1 point/s for IC. Two methacrylate-based anion exchangers were used, a Waters IC Pak Anion high-resolution (HR) column (75 × 4.6 mm I.D.) and a Waters IC Pak Anion high-capacity (HC) column (150 × 4.6 mm ID). The borate–gluconate eluent consisted of 1.6 m*M* sodium tetraborate, 7.3 m*M* boric acid, 1.6 m*M* sodium gluconate, 5 g/l glycerin, 120 ml/l acetonitrile and 20 ml/l *n*-butanol at pH 8.5.

2.2. Capillary electrophoresis system

The CE instrument used was a Waters Quanta 4000E with a Millennium 2010 chromatography management system. Data were collected at 10 points/s for CE. The separations were performed on a conventional (60 cm × 75 μm I.D.) fused-silica capillary from Waters. An electrolyte of 5 m*M* chromate with an osmotic flow modifier, Waters CIA-Pak OFM anion-BT, at pH 8.0 was used at an operational voltage of −20 kV. Isomigration mode, value 3, was used for all separations. Detection was carried out using indirect photometry at 254 nm with a time constant of 0.1 s. The capillary and the sample cabinet were maintained at a constant temperature of 25°C.

2.3. Reagents and procedures

Millipore (Bedford, MA, USA) Milli-Q 18 MΩ water was used for all electrolyte, eluent, sample and standard preparations. Sodium tetraborate, boric acid, sodium chloride, sodium sulfate (analytical-reagent grade) and glycerin (laboratory-reagent grade) were obtained from Ajax (Sydney, Australia). HPLC-grade acetonitrile and *n*-butanol were also obtained from Ajax. Sodium gluconate (laboratory-reagent grade) was obtained from Fluka (Buchs, Switzerland) and oxalic acid dihydrate (guaranteed-reagent grade) was obtained from Merck (Darmstadt, Germany). Sodium chromate tetrahydrate was obtained from Aldrich (Milwaukee, WI, USA). Electrolytes and eluents were prepared daily, filtered through a Millipore 0.45-μm HV filter and degassed in an ultrasonic bath before use. Samples were injected after dilution with Milli-Q water and filtration through a Millipore 0.45-μm Millex HV syringe filter.

3. Results and discussion

Having previously established the feasibility of the determination of oxalate in Bayer liquor by CE [1], the objective of this work was to compare CE results to those obtained by the more commonly used technique of IC. A further objective of the work was to investigate the possibility of performing simultaneous chloride, sulfate and oxalate analysis, using both CE and IC, as the analysis of these two inorganic anions in Bayer liquor is also of importance.

3.1. Ion chromatography

The IC analysis of Bayer liquor is complicated by the high ionic strength and pH of the sample; along with the fact that aluminium hydroxide is insoluble in the pH range of approximately 5–10. This then restricts the choice of eluents to those which are of low pH, high pH or those which

keep alumina soluble through complex formation [2]. Tartrate–borate at pH 4.5 has been used to determine both chloride and sulfate in Bayer liquors; however, this eluent does not permit resolution of organic acid solutes, such as oxalate [1]. Carbonate–hydrogencarbonate with suppressed conductivity detection has previously been used for oxalate analysis in liquors [5], however the main disadvantage of this approach is that alumina has limited solubility in the suppressor, which reduces suppressor efficiency and lifetime [2].

Borate–gluconate is a complexing mobile phase which permits good resolution and sensitivity for chloride, sulfate and oxalate. Fig. 1 shows the chromatograms obtained from a 100-μl injection of a standard solution containing chloride, sulfate and oxalate obtained using a borate–gluconate eluent and the Anion HR column with dual conductivity (a) and direct UV detection at 214 nm (b). Fig. 2 shows chromatograms of a typical Bayer liquor, after 200 × dilution, again using conductivity (a) and direct UV detection (b). The combination of conductivity and direct UV detection, which is widely used for the analysis of complex samples by IC [6], proved useful in order to determine the presence of organic acid interferences in this case. The conductivity chromatogram showed that chloride was not fully resolved from an adjacent unknown peak and that a non-interfering system peak, eluting at approximately 5.5 min, was present under the mobile phase conditions used [7]. The UV chromatogram indicated oxalate was not completely resolved from the other organic acids present in the sample;

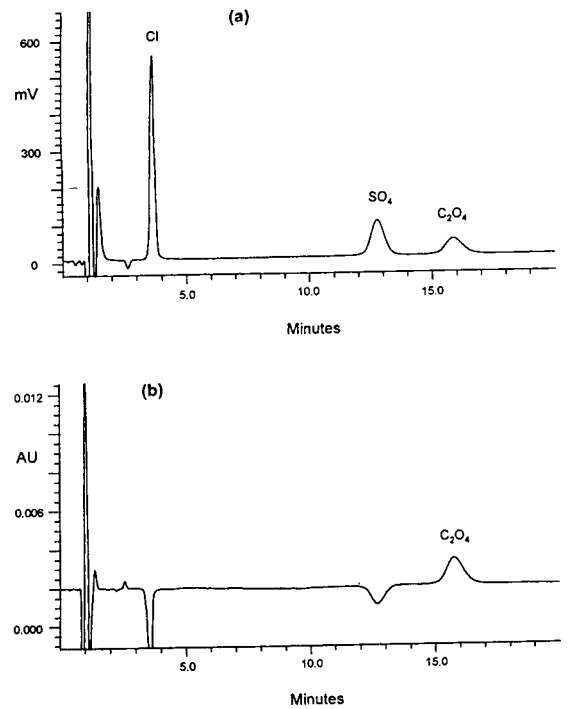

Fig. 1. Chromatogram of chloride, sulfate and oxalate standard obtained using IC with dual conductivity and direct UV detection. Conditions: column, Waters IC Pak Anion HR; eluent, borate–gluconate at 1.0 ml/min; injection volume, 100 μl; detection, conductivity (a) and direct UV detection at 214 nm (b); solutes: chloride (10 ppm), sulfate (8 ppm), oxalate (5 ppm).

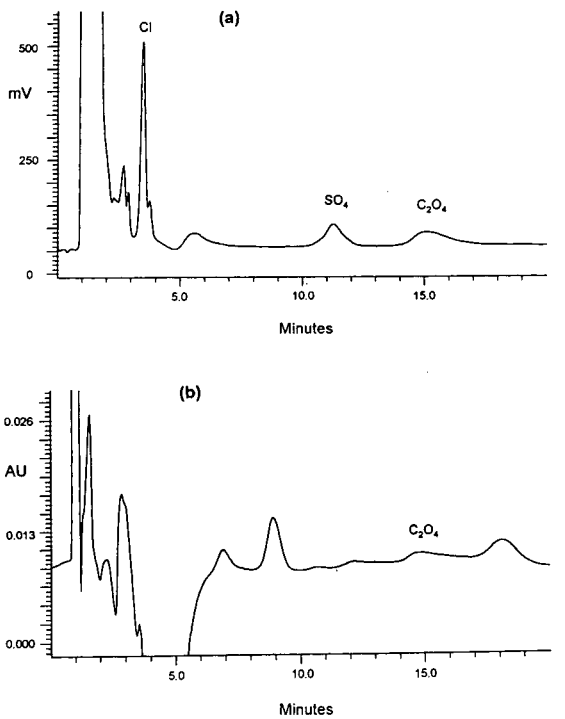

Fig. 2. Chromatogram of a typical Bayer liquor obtained using IC with dual conductivity and direct UV detection. Conditions as for Fig. 1, except: injection volume, 50 μl; sample preparation, 200 × dilution with water; solutes (injected concentrations): chloride (20.6 ppm), sulfate (11.1 ppm), oxalate (15.1 ppm).

however, the total peak area of the interferences was negligible compared to that of oxalate with conductivity detection. The UV detector also showed the (negative) system peak and a number of additional organic acids, including succinic acid at a retention time of approximately 12 min, which co-eluted with the sulfate peak.

Variation of the eluent ionic strength and the use of a higher-capacity column, the IC Pak Anion HC, resulted in increased separation for the oxalate peak and somewhat improved resolution for both the chloride and sulfate peaks, although at the expense of increased chromatographic run time. The addition of up to 20% acetonitrile to the mobile phase also allowed for some minor selectivity changes, however these were not sufficient to completely resolve sulfate and oxalate from the other interferences. Generally, most anion exchangers have very similar selectivity and organic acids, such as succinate and tartrate, typically interfere with divalent inorganic anions, such as sulfate, when using a mobile phase in the pH range of 7–11. Lowering the mobile phase pH results in protonation, hence decreased retention, of the organic acids, although this results in the oxalate quantitation being significantly affected as a result of interference by other organic acids. Consequently, efforts to simultaneously determine chloride, sulfate and oxalate by IC are typically carried out using an anion-exchange separation, with the mobile phase conditions optimised to achieve maximum resolution of oxalate, which is the most important assay. Table 1 shows the results for chloride, sulfate and oxalate (reported conventionally as g/l disodium oxalate) in a number of Bayer liquor samples, obtained using the HC column, a borate–gluconate eluent and conductivity detection.

3.2. Capillary electrophoresis

The selectivity of CE is particularly advantageous for the analysis of oxalate as the ion's electrophoretic mobility is intermediate between the very mobile inorganic anions, such as chloride and sulfate, and the less mobile organic acids, such as tartrate, succinate and acetate, which are present in Bayer liquor. A chromate-based electrolyte was used with indirect UV detection as this combination permits good peak shape and sensitive detection [8]. A variety of separation conditions and electrolyte modifiers, including the addition of calcium, methanol and Z1-Methyl, were investigated in order to optimise the separation and precision of the CE analysis. A relatively simple electrolyte of 5.0 m*M* chromate with 0.5 m*M* CIA-Pak OFM anion-BT at pH 8.0, when used with an automated purge routine of 0.1 *M* sodium hydroxide, water and electrolyte for 1.0/1.0/2.0 min, respectively, proved to be the most appropriate for the determination of chloride, sulfate and oxalate in Bayer liquor samples.

The use of the purge routine proved to be crucial in attaining reproducible migration times, hence reproducible peak areas and amounts. The manner in which the current and voltage were applied to the separation also had a significant effect on the oxalate migration time reproduci-

Table 1
Oxalate (g/l disodium oxalate), chloride and sulfate (ppm) results for five Bayer liquor samples obtained using IC and CE

Sample[a]	Ion chromatography			Capillary electrophoresis		
	C_2O_4	Cl	SO_4	C_2O_4	Cl	SO_4
431	1.96	3369	1917	1.98	3320	494
432	4.66	1964	1012	4.15	1420	257
433	12.8	780	478	12.5	874	177
434	13.4	339	239	12.9	383	112
435	3.10	434	313	3.33	385	318

IC results obtained using HC column and borate–gluconate eluent.
[a]Bayer liquor samples diluted 200 × prior to analysis.

bility. The CE instrument allowed the application of either constant voltage, constant current or a patented combination of constant current/voltage termed "isomigration mode" [9]. The average migration time variation (% R.S.D.) for the oxalate peak, obtained from five replicates of a set of five liquor samples, was 3.690, 4.352, 2.242, 1.726 and 1.512 using constant-voltage, constant-current and isomigration settings of 1, 2 and 3, respectively. An isomigration value of 3 was used for all further work as this resulted in the least migration time variation. Fig. 3 shows an electropherogram of a 20-s hydrostatic injection of the standard solution containing chloride, sulfate and oxalate, while Fig. 4 shows an electropherogram of the same Bayer liquor sample shown in Fig. 2, again after a 200 × dilution. Table 1 also shows the results for chloride, sulfate and oxalate (reported as g/l disodium oxalate) in five Bayer liquor samples, obtained using the chromate electrolyte and indirect photometric detection at 254 nm.

3.3. Comparison of results

CE and IC can be considered complimentary analytical techniques for the determination of ionic solutes [3]. CE offers the advantages of increased separation efficiency with a selectivity

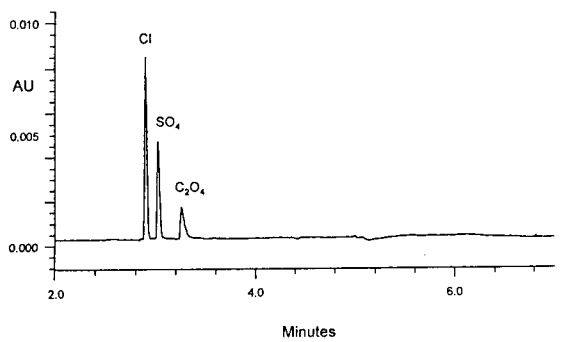

Fig. 3. Electropherogram of chloride, sulfate and oxalate standard obtained using CE with indirect photometric detection. Conditions: capillary, 60 cm × 75 μm fused silica; power supply, negative at 20 kV using isomigration value of 3; electrolyte, 5 m*M* chromate with 0.5 m*M* CIA-Pak OFM anion-BT at pH 8.0; injection, hydrostatic for 20 s; detection, indirect UV at 254 nm; solutes: chloride (10 ppm), sulfate (8 ppm), oxalate (5 ppm).

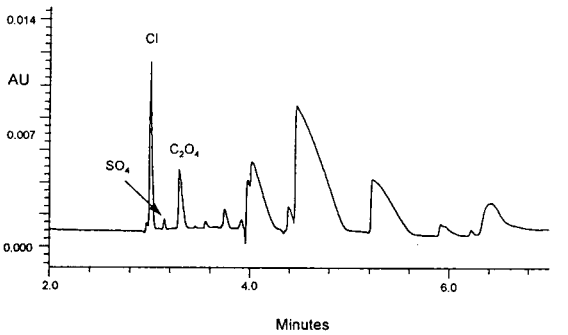

Fig. 4. Chromatogram of a typical Bayer liquor obtained using CE with indirect photometric detection. Conditions as for Fig. 3, except: sample preparation, 200 × dilution with water; solutes (injected concentrations): chloride (14.2 ppm), sulfate (0.8 ppm), oxalate (12.2 ppm).

which differs from IC. This selectivity proved to be particularly advantageous for the determination of oxalate, chloride and sulfate in Bayer liquors as all three peaks of interest were completely resolved from the matrix components. However, IC permits more stable retention times which subsequently makes automated peak identification and quantitation less prone to error. The absolute magnitude of the signal generated by IC was also significantly greater than that for CE, as shown by a comparison of the *y* axis scales for Fig. 1a and Fig. 3. As a result, detection limits obtained by IC are typically an order of magnitude lower than for CE.

Table 1 indicates that the results obtained for oxalate by IC using conductivity detection correlated reasonably well to those obtained using CE, not as well for chloride and very poorly for sulfate. Chloride accuracy was compromised by the adjacent unknown peak in IC, while sulfate co-eluted with succinate under all the chromatographic conditions investigated, leading to appreciably higher values than those obtained using CE. Table 1 also shows that the oxalate results obtained using CE were typically lower than the IC results, indicating the effect of the chromatographic interference which occurred with IC.

The precision of both techniques was then compared by analysing five liquor samples, obtained from a different site, five times each using both IC and CE. The results are shown in Table 2. Once again, the IC results were consistently

Table 2
Oxalate (g/l disodium oxalate) precision results (% R.S.D.) obtained from five replicate injections of Bayer liquor samples using IC and CE

Sample[a]	IC		CE	
	C_2O_4	R.S.D. (%)	C_2O_4	R.S.D. (%)
Liquor 1	1.78	3.13	1.62	0.97
Liquor 2	1.99	2.86	1.78	1.06
Liquor 6	2.49	2.33	2.29	1.78
Liquor 7	3.32	2.71	3.09	2.97
Liquor 8	4.61	3.13	3.72	1.76

IC results obtained using HR column and borate–gluconate eluent.
[a]Bayer liquor samples diluted 200 × prior to analysis.

higher than those obtained by CE, indicating the effect of the chromatographic interference with oxalate. Attempts to increase the separation of oxalate from the interferences by using an eluent of 1.2 m*M* carbonate–1.2 m*M* hydrogencarbonate with the HR column proved to be unsuccessful as the oxalate results were still consistently high. The CE gave improved precision, with an overall average of 1.71% R.S.D., compared to an overall average of 2.85% R.S.D. for IC. The precision of the IC results were perhaps not as good as would be expected for conventional HPLC, largely due to the difficulties associated with integrating the poorly shaped oxalate peak.

Perhaps the final advantage of CE for this analysis is the fact that the technique is also equally able to determine oxalate (plus chloride and sulfate) in "stabilised" liquor samples. Bayer liquors are frequently stabilised by the addition of ca. 3 m*M* tartaric acid [1]; however, this leads to a large peak which completely masks sulfate and significantly interferes with oxalate when using IC. All three solutes are completely resolved in the tartrate-stabilised liquor samples using CE.

4. Conclusions

The determination of oxalate in Bayer liquors appears to one of the few ion analysis applications where CE is clearly preferable to IC. Oxalate results obtained by IC were consistently higher than those for CE due to the presence of minor chromatographic interferences. The chloride and (particularly) sulfate results obtained by IC were subject to more severe chromatographic interferences, hence the simultaneous determination of oxalate, chloride and sulfate in Bayer liquors was not possible when using an anion-exchange separation with a borate–gluconate eluent and conductivity detection. Chloride and sulfate can be accurately determined in Bayer liquors by IC using a tartrate–boric acid eluent which discriminates against organic acid retention; however, this eluent does not permit oxalate analysis. Alternatively, the different selectivity of CE allowed for complete resolution of chloride, sulfate and oxalate from the matrix components in Bayer liquor using a relatively simple electrolyte, in a run time of less than 6 min. The electrophoretic technique gave improved precision for oxalate, with an overall average of 1.71% R.S.D., compared to an average of 2.85% R.S.D. for IC. A further advantage of CE is that it also allows the simultaneous determination of all three anions in tartaric acid-stabilised liquor samples.

References

[1] S.C. Grocott, L.P. Jefferies, T. Bowser, J. Carnevale and P.E. Jackson, *J. Chromatogr.*, 602 (1992) 257.
[2] T. Bowser and S.C. Grocott, *Proceedings of the 2nd International Alumina Quality Workshop, Perth, 1990*, p. 310.

[3] P.E. Jackson and P.R. Haddad, *Trends Anal. Chem.*, 12 (1993) 231.
[4] J.P. Romano, P. Jandik, W.R. Jones and P.E. Jackson, *J. Chromatogr.*, 546 (1991) 411.
[5] K. The and R. Roussel, *Light Met.*, (1984) 115.
[6] P.E. Jackson and T. Bowser, *J. Chromatogr.*, 602 (1992) 33.
[7] C. Erkelens, H.A.H. Billiet, L. de Galan and E.W.B. de Leer, *J. Chromatogr.*, 404 (1987) 67.
[8] P. Jandik and W.R. Jones, *J. Chromatogr.*, 546 (1991) 431.
[9] *Capillary Ion Analysis Brochure*, Millipore, Bedford, MA, 1993.

ELSEVIER

Journal of Chromatography A, 693 (1995) 162–166

JOURNAL OF CHROMATOGRAPHY A

Short communication

Simultaneous structure–activity determination of disulfiram photolysis products by on-line continuous-flow liquid secondary ion mass spectrometry and enzyme inhibition assay

Linda M. Benson[a,b], Karen A. Veverka[a,d], Dennis C. Mays[c,d], Albert N. Nelson[c,d], Zachary H. Shriver[c,d], James J. Lipsky[c,d,e], Stephen Naylor[a,b,c,d,*]

[a]*Biomedical Mass Spectrometry Facility, Mayo Clinic, Guggenheim C009B, 200 First Street SW, Rochester, MN 55905, USA*
[b]*Department of Biochemistry and Molecular Biology, Mayo Clinic, Guggenheim Building, Rochester, MN 55905, USA*
[c]*Clinical Pharmacology Unit, Mayo Clinic, Guggenheim Building, Rochester, MN 55905, USA*
[d]*Department of Pharmacology, Mayo Clinic, Guggenheim Building, Rochester, MN 55905, USA*
[e]*Department of Internal Medicine, Mayo Clinic, Guggenheim Building, Rochester, MN 55905, USA*

First received 4 August 1994; revised manuscript received 1 November 1994; accepted 8 November 1994

Abstract

Disulfiram (DSF) is used in the treatment of recovering alcoholics and exerts its effect by inhibiting the enzyme aldehyde dehydrogenase (ALDH). We analyzed a mixture of products derived photochemically from DSF with on-line microbore HPLC–continuous-flow liquid secondary ion mass spectrometry (HPLC–CF-LSI-MS). By utilizing the post-HPLC column split of solvent flow, a small proportion (ca. 5%) was sent directly into the mass spectrometer, and the remainder was collected. Simultaneous MS analysis and enzyme inhibition studies on ALDH were then possible. Furthermore, using HPLC–CF-LSI-MS–MS, we were able to structurally characterize an interesting sulfine compound that inhibited ALDH.

1. Introduction

The dithiocarbamate disulfiram (DSF) is the only commercially available therapeutic agent (trade name Antabuse) used in the treatment of recovering alcoholics [1]. The ethanol-sensitizing effect of DSF is due to its irreversible inhibition of the enzyme aldehyde dehydrogenase (ALDH). Inhibition of ALDH leads to elevated levels of acetaldehyde in the bloodstream, which results in nausea, vomiting, flushing and tachycardia in individuals after ingestion of ethanol [1]. We have demonstrated recently that the dithiocarbamate, sulfiram, is unstable in solution [2] and is readily photoconverted to products, including DSF, that inhibit ALDH [3]. We undertook this investigation to determine if DSF, which is structurally similar to sulfiram, is also photoconverted to products that inhibit ALDH.

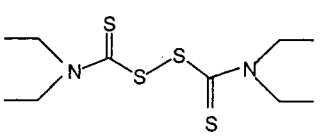

(DSF)

* Corresponding author.

0021-9673/95/$09.50
SSDI 0021-9673(94)01101-X

Continuous-flow liquid secondary ion mass spectrometry (CF-LSI-MS) is a useful and sensitive technique for the analysis of mixtures when coupled to microbore HPLC [4]. However, it is necessary to split the HPLC flow in order to accommodate the vacuum constraints of the mass spectrometer. Typically the sample splitting allows only a small portion of the analyte (ca. 5%) into the MS system while sending a majority to waste (ca. 95%). Traditionally, CF-LSI-MS has been thought of as "limited" by such low flow-rates (ca. 1–3 μl/min into MS), but we have found that the splitting of sample can be useful for another application. By recovering the HPLC eluent of a mixture derived from photochemically treated DSF destined for "waste", and subjecting fractions to bioassay, it was possible to ascertain the inhibitory activity of specific compounds against ALDH. Combining this information with the structural analysis provided by HPLC–MS and HPLC–tandem mass spectrometry (HPLC–MS–MS), it was possible to characterize on-line the structure–activity relationship of DSF and photolytically produced products.

2. Experimental

2.1. Reagents and materials

DSF was purchased from Sigma (St. Louis, MO, USA) and recrystallized twice in ethanol before use (m.p. 71–72°C). Aldehyde dehydrogenase [aldehyde: NAD(P) oxidoreductase, EC 1.2.1.5; specific activity: 51 units/mg enzyme protein], isolated from *Saccharomyces cerevisiae*, NAD (grade 1 free acid, 100%), Tris · HCl and Tris base were purchased from Boehringer Mannheim (Mannheim, Germany). Acetaldehyde and KCl were obtained from Aldrich (St. Louis, MO, USA). Acetonitrile and ethanol (redistilled before use) were obtained from Baxter (McGaw Park, IL, USA).

2.2. Photolysis of DSF

DSF was dissolved in acetonitrile under subdued light to afford an 85 m*M* solution and subsequently subjected to photolysis. Dark control solutions of DSF in glass vials with PTFE-lined screw caps were wrapped in foil and stored at room temperature. Other solutions of DSF were irradiated at 254 nm for 4 h at 31°C in a Rayonet Photochemical Reactor (Model RMR-600; Southern New England Ultraviolet, Branford, CT, USA). Light intensity at the center of the photochemical reactor was 12.8 μW/cm^2.

2.3. HPLC–CF-LSI-MS

HPLC separations were performed on an ultrafast microprotein analyzer (UMA) system (Michrome Bioresources, Pleasanton, CA, USA). Samples of the DSF photolysis reaction mixture (2-μl aliquots in acetonitrile) were injected directly into the HPLC system and analytes were separated on a Michrome UMA microbore column (150 mm × 1 mm I.D.) with Reliasil C_{18} (100 Å, 3 μm) packing material. Separations were achieved using a mobile phase of acetonitrile–water–glycerol (50:48:2, v/v) delivered isocratically for 15 min followed by a 10-min linear gradient to acetonitrile–water–glycerol (80:18:2, v/v) at a flow-rate of 59 μl/min. Absorbance at 225 nm was continuously monitored. A post-column split of 1:20 allowed ca. 3 μl/min of eluent to enter into the mass spectrometer and the remainder was sent to "waste" (56 μl/min) and recovered and subjected to bioassay for ALDH inhibitory activity as shown schematically in Fig. 1. Prior to bioassay, the recovered material was lyophilized to remove excess solvent.

All HPLC–CF-LSI-MS and HPLC–CF-LSI-MS–MS experiments were performed on a Finnigan MAT 95Q mass spectrometer (Bremen, Germany) of BE Q_1Q_2 configuration, where B is the magnet, E is the electrostatic analyzer, Q_1 is a radio frequency (rf)-only octapole collision cell and Q_2 is a mass filter quadrupole. Samples were ionized by CF-LSI-MS in positive mode using cesium as a source of primary ions at an ion voltage of 20 kV (Cs^+ ions). The CF-LSI-MS probe consisted of a silica capillary (50 μm I.D. × 200 μm O.D.) connected directly to the HPLC. The ion source was maintained at 60°C

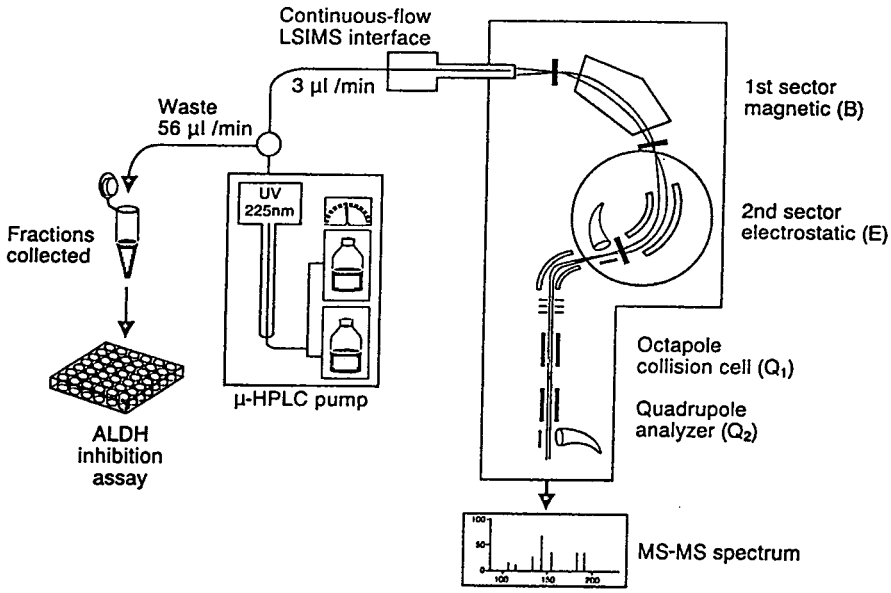

Fig. 1. Schematic of the instrumentation used in the simultaneous structure–activity determination of disulfiram photolysis products employing a CF-LSI-MS interface connected to a MAT 95Q hybrid mass spectrometer.

with an operating resolution of ca. 1200, scanning over a mass range of 50–300 u at 3 s/decade.

2.4. Tandem mass spectrometry

Molecular ions (also referred to as precursor ions) of standards and photolysis products of DSF were selected with a resolution of ca. 1000 using BE (MS1) and subjected to collision-induced dissociation (CID) in the octapole collision cell Q1 using argon as the collision gas. Collision energies of ca. 20–ca. 30 eV with an argon gas pressure of ca. $6 \cdot 10^{-6}$ mbar were used to induce CID of precursor ions. The product (fragment) ions were mass analyzed in Q_2 (MS2) and product ion spectra acquired by scanning Q2 over the mass range of 40 to 350 with 10 to 20 scans acquired and averaged to afford a composite product ion spectrum.

2.5. ALDH assay

The activity of yeast ALDH was assayed with a microplate reader (Molecular Devices, Menlo Park, CA, USA) at 22°C by following the formation of NADH spectrophotometrically at 340 nm. All reagents were prepared in 50 m*M* sodium pyrophosphate buffer, pH 8.8. The assay mixture in a final volume of 200 µl contained the following: sodium pyrophosphate (pH 8.8):1.5 m*M* NAD; 0.03 units yeast ALDH; 2.4 m*M* acetaldehyde; and DSF or DSF photolysis products (collected from HPLC) in 1.75 µl of ethanol (0.88%, v/v, final concentration of ethanol). An equal volume of ethanol or mobile phase was added to control assays without inhibitor. The order of addition of reagents was sodium pyrophosphate, yeast ALDH, NAD and inhibitor. The solutions were mixed by gently tapping the microtiter plate, and the substrate acetaldehyde (2.4 m*M* final concentration) was added to start the reaction. The solutions were again mixed and the initial rates obtained by following the absorbance at 340 nm for 3 min at 22°C.

3. Results and discussion

Fractions from the HPLC "waste" eluent containing individual components were assayed for inhibition of ALDH. Substantial inhibition

was observed for a number of compounds that eluted in the solvent front, as well as late eluting components at retention times of ca. 27, 29.5 and 39.5 min (see Fig. 2). However, complete (100%) inhibition of ALDH was detected for individual compounds at retention times of ca. 7.5, 9.5 and 19.5 min (Fig. 2). The compound eluting at ca. 13 min, based on relative retention time compared to authentic standard, was determined to be unphotolyzed and/or regenerated DSF, and this was subsequently confirmed by MS analysis. However, due to the high concentration of DSF in this fraction, precipitation occurred which adversely affected the enzyme inhibition assay. We have determined previously that the IC_{50} of DSF on yeast ALDH is ca. 2 μM [3].

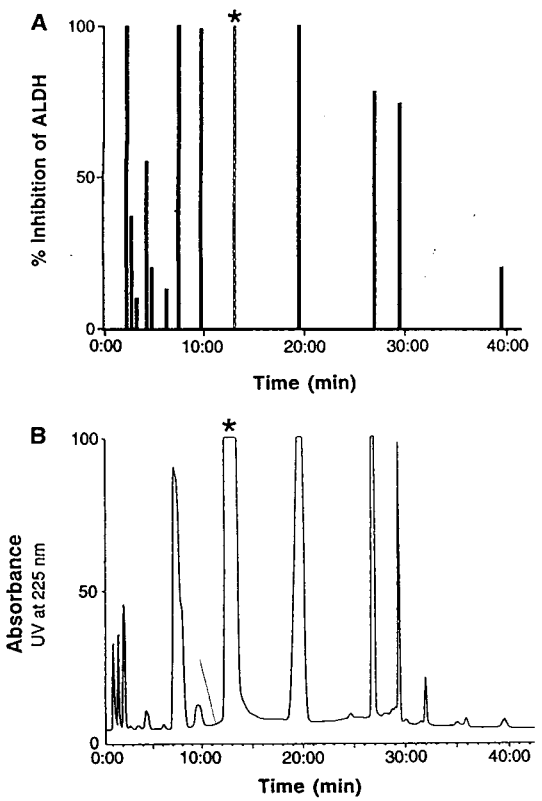

Fig. 2. Inhibitory activity of DSF photolysis products against the enzyme ALDH after reversed-phase HPLC separation. (A) Enzyme inhibition (%) of photolysis products of ALDH; (B) HPLC chromatogram with UV detection of photolysis products of disulfiram (at 225 nm). (*) This peak corresponds to DSF which, because of its high concentration, precipitated and interfered with the enzyme inhibition assay.

Concomitant HPLC–CF-LSI-MS analysis of the photolysis mixture revealed molecular ions at $MH^+ = 281$ [retention time (t_R) 7.5 min]; $MH^+ = 313$ ($t_R = 9.5$ min); $MH^+ = 297$ ($t_R = 13$ min) corresponding to unphotolyzed DSF; and $MH^+ = 212$ ($t_R = 27$ min) as shown in Fig. 3. No clearly discernible molecular ions were detected for solvent front components ($t_R = 0$–5 min) nor for late-eluting active components ($t_R = 19.5$, 29.5 and 39.5 min) (Fig. 3).

In order to determine structures of the components at m/z 281, 313, 297 and 212, the precursor ions were subjected to MS–MS via collision induced dissociation with the target gas argon contained in an rf-only octapole collision cell. The details of this work will be reported elsewhere. However, of major interest was the

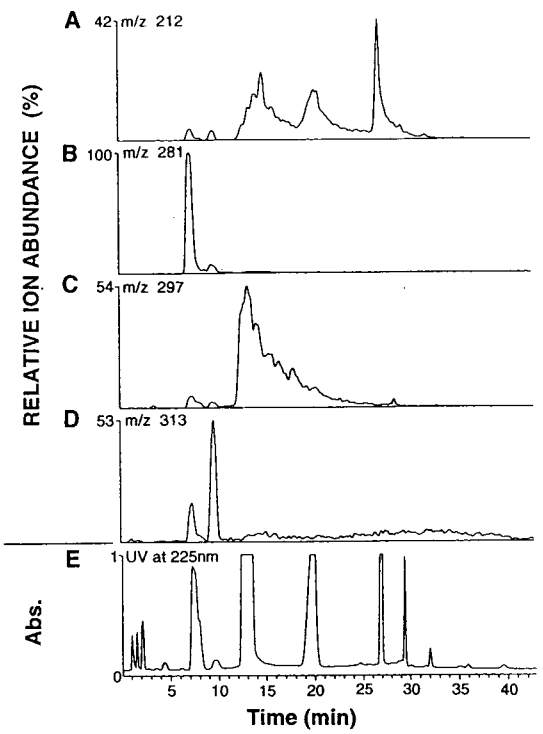

Fig. 3. On-line HPLC–CF-LSI-MS analysis of disulfiram photolysis products. Ion current; (A) m/z 212; (B) m/z 281; (C) m/z 297 and (D) m/z 313. (E) HPLC chromatogram of the mixture of photolysis products (UV detection at 225 nm).

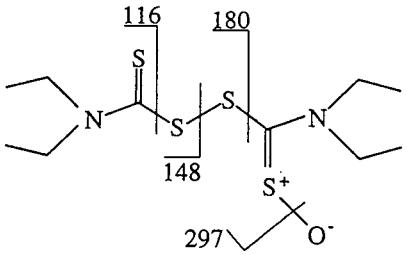

Fig. 4. Proposed structure of the sulfine photolysis product at a HPLC retention time of 9.5 min with assignment of product ions produced after collision induced dissociation of the precursor ion $MH^+ = 313$.

ion at m/z 313 which constituted $<5\%$ of unphotolyzed DSF (as determined by UV) yet completely inhibited ALDH. The molecular ion value indicated addition of a single oxygen to the parent compound DSF without concomitant loss of a hydrogen atom. The product ion spectrum revealed ions at m/z 297 (10%), 180 (55%), 148 (15%) and 116 (10%) (values in parenthesis represent product ion abundance as a percentage of the MH^+ ion). The product ion spectrum strongly indicated the formation of a sulfine derivative of DSF had been formed, as shown in Fig. 4, and further studies are underway to confirm this structure. It is noteworthy that a structurally similar sulfine, which is also an inhibitor of ALDH, has been identified recently as a novel metabolite of DSF [5].

4. Conclusions

HPLC–LSI-MS–MS is a profitable technique for performing on-line structure–activity analysis. While HPLC–LSI-MS is typically considered to be limited by the splitting of sample and limited sample flow, we have found this feature to be useful for probing structure–activity relationships using an on-line analytical technique. By recovering the "waste" eluent from the HPLC–CF-LSI-MS interface, it is possible to closely couple the mass spectral identification of potentially labile photolysis products of DSF with their inhibitory activity against ALDH in vitro.

Acknowledgements

We would like to thank Mrs. Diana Ayerhart for all her contributions in putting this manuscript together. This work was supported by grants NIH RO1-AA09543 and HHS FD-T-000886-02.

References

[1] P.K. Gessner and T. Gessner, *Disulfiram and its Metabolite Diethyldiothiocarbamate: Pharmacology and Status in the Treatment of Alcoholism, HIV Infections, AIDS and Heavy Metal Toxicity*, Chapman & Hall, London, 1992.
[2] E.C. Kathman, A.N. Nelson and J.J. Lipsky, *Pharm. Sci. Commun.*, 4 (1994) 103.
[3] D. Mays, A.N. Nelson, L.M. Benson, K.L. Johnson, S. Naylor and J.J. Lipsky, *Biochem. Pharmacol.*, 48 (1994) 1917.
[4] R.M. Caprioli (Editor), *Continuous-Flow Fast Atom Bombardment Mass Spectrometry*, Wiley, Chichester, 1990, p. 189.
[5] A. Madan and M.D. Faiman, *Drug Metabol. Dispos.*, 22 (1994) 324.

ELSEVIER

Journal of Chromatography A, 693 (1995) 167–175

JOURNAL OF CHROMATOGRAPHY A

Short communication

Use of narrow-bore high-performance liquid chromatography–diode array detection for the analysis of intermediates of the biological degradation of 2,4,6-trinitrotoluene

F. Ahmad, D.J. Roberts*

Department of Civil and Environmental Engineering, University of Houston, Houston, TX, USA

First received 17 December 1993; revised manuscript received 4 November 1994; accepted 8 November 1994

Abstract

A single method was developed for the separation and quantitation of hexahydro-1,3,5-trinitro-1,3,5-triazine, 2,4,6-trinitrotoluene (TNT), and most of the known and suspected biodegradation intermediates of TNT by RP-HPLC and diode array detection. The known biodegradation intermediates of TNT analyzed were 2-amino-4,6-dinitrotoluene, 4-amino-2,6-dinitrotoluene, 2,6-diamino-4-nitrotoluene, 2,4-diamino-6-nitrotoluene, 2,4,6-triaminotoluene, 2,2′,6,6′-tetranitro-4,4′-azoxytoluene, and 4,4′,6,6′-tetranitro-2,2′-azoxytoluene. The suspected biodegradation intermediates of TNT included 1,2,3-benzenetriol (pyrogallol), 1,3,5-benzenetriol (phloroglucinol), 2-methyl-1,3,5-benzenetriol (methyl phloroglucinol) and 4-methylphenol (*p*-cresol). Mobile phases consisting of aqueous buffers adjusted to three different pH values in a gradient with acetonitrile were examined for their efficiency in separating the intermediate compounds and for the minimization of speciation of the ionizable intermediates (e.g. 2,4,6-triaminotoluene). A final aqueous buffer pH of 3.2 was selected to minimize the interference to the separation caused by 2,4,6-triaminotoluene speciation. Solvent consumption was minimized by the use of a narrow-bore column. All of the known reduction products as well as *p*-cresol and methylphloroglucinol were identified in culture supernatants from TNT-degrading cultures while pyrogallol and phloroglucinol were not.

1. Introduction

Nitro-substituted munitions compounds such as 2,4,6-trinitrotoluene (TNT) have been found to contaminate soils [1] and could also contaminate groundwater [2] because of past disposal practices at explosives manufacturing, loading and packing facilities. The toxicological effects of TNT on various organisms are well documented [3–6]; in humans, these effects may result in toxic hepatitis and aplastic anemia [7]. TNT has also been found to be mutagenic by the Ames bacterial assay [8]. Concern over the environmental fate of these compounds has intensified research into safe and economical treatment options like biodegradation. However, the degradation of TNT does not necessarily mean a removal of its deleterious characteristics; the primary biotransformation products of TNT, 2-amino-4,6-dinitrotoluene (2ADNT) and 4-amino-2,6-dinitrotoluene (4ADNT), have also been shown to have toxic [9] and mutagenic [10] effects on certain biological species. The toxicity and mutagenicity of secondary and subsequent

* Corresponding author.

0021-9673/95/$09.50
SSDI 0021-9673(94)01095-1

biodegradation intermediates of TNT, such as 2,6-diamino-4-nitrotoluene (DA4NT), 2,4-diamino-6-nitrotoluene (DA6NT) and 2,4,6-triaminotoluene (TAT), have yet to be explored. Therefore, a simple and accurate method for the identification and quantitation of TNT and its biotransformation products is needed so that acceptable mass balances can be established during biodegradation.

A separation step must precede identification and quantitation in the selected method owing to the functional similarities of many of the intermediates. Separation of the intermediates by gas chromatography can result in the coelution of aminodinitrotoluenes (ADNTs) and diaminonitrotoluenes (DANTs) [11]. In addition, some of the analytes are thermally unstable [1], making gas chromatography an unfavorable separation option. Past work has favored reversed-phase high-performance liquid chromatography (RP-HPLC) as the method of choice for the separation of munitions compounds. Most of this work involved isocratic elution [12–14] of compounds with either a water–methanol or a water–methanol–acetonitrile mobile phase. Unfortunately, isocratic elution poses a problem when separating analytes of a wide range of polarities, such as the ones presented in this paper; there is a tradeoff between eluting the less polar tetranitroazoxytoluene (TNAZT) compounds [2,2′,6,6′-tetranitro-4,4′-azoxytoluene (4,4′-Az) and 4,4′,6,6′-tetranitro-2,2′-azoxytoluene (2,2′-Az)] within reasonable time and achieving a separation between the more polar compounds (DA4NT and DA6NT) because significantly different organic fractions in the mobile phase are required for each of these tasks. Kaplan and Kaplan [15] demonstrated this problem when they did isocratic elutions with 20 and 75% methanol to separate DANTs and TNAZTs, respectively. The answer to this problem lies in using gradient elution. Gradient elutions were performed by Kaplan and Kaplan [15] and Schuster and Gratfeld-Huesgen [16] using a water–methanol mobile phase.

In earlier work, only Yinon and Hwang [17], Jenkins and Grant [14] and Schuster and Gratfeld-Huesgen [16] included a post-LC identification/confirmation step. Yinon and Hwang used mass spectral identification, whereas Jenkins and Grant used an LC-CN (cyanopropylmethylsilyl bonded phase) column to confirm the identity of the analytes by an inversion of their retention time sequence. Schuster and Gratfeld-Huesgen used diode array detection (DAD), the same method as the one used in this study, for the UV–visible spectral identification of compounds. This study expands on Schuster and Gratfeld-Huesgen's work with DAD to include most of the known and suspected intermediates of TNT biodegradation.

This paper presents a single method for the separation, identification and quantitation of hexahydro-1,3,5-trinitro-1,3,5-triazine (RDX), TNT, and most of the known and suspected biodegradation intermediates of TNT by RP-HPLC and DAD. The known biodegradation intermediates of TNT analyzed were 2ADNT, 4ADNT, DA4NT, DA6NT, TAT, 4,4′-Az and 2,2′-Az [18,19]. The suspected biodegradation intermediates of TNT included 1,2,3-benzenetriol (pyrogallol), 1,3,5-benzenetriol (phloroglucinol), 2-methyl-1,3,5-benzenetriol (MPG) and 4-methylphenol (*p*-cresol) [20,21]. RDX was included in this study because many munitions contaminated soils are contaminated with appreciable concentrations of RDX as well as TNT [14]. Mobile phases consisting of aqueous buffers adjusted to three different pH values in a gradient with acetonitrile were examined for their efficiency in separating the intermediate compounds and for the minimization of speciation of the ionizable intermediates. Solvent consumption was minimized by the use of a narrow-bore column (2.1 mm I.D.).

2. Experimental

Samples of 2ADNT, 4ADNT, DA6NT, 2,2′-Az and 4,4′-Az were obtained through the generosity of Dr. R.J. Spanggord of SRI International, Menlo Park, CA, USA. Standards for

RDX, pyrogallol, phloroglucinol, MPG and *p*-cresol were acquired from Mr. S. Funk at the University of Idaho, Moscow, ID, USA. TNT and TAT were obtained from Chem Service of Westchester, PA, USA, and DA4NT was obtained from Aldrich, Milwaukee, WI, USA. Stock standards in the 100 mg/l range were prepared. All water used in the preparation of standards and mobile phase was type 1 reagent-grade water obtained from the Barnstead NANOpure II water purification system.

TNT was dried to a constant mass, crushed and made into a 100 mg/l stock standard in water using a method outlined by Ruchhoft and Meckler [22]. Stock standards of DA6NT, *p*-cresol, pyrogallol, phloroglucinol and MPG were made in water. RDX was obtained as a 10000 mg/l stock standard made in methanol. DA4NT, 2ADNT and 4ADNT were made in methanol–water (50:50, v/v). The TNAZT compounds were prepared in acetonitrile–methanol (50:50, v/v), as they were not soluble in the methanol–water mix. Stock standards for TAT were prepared in the aqueous mobile phase with which they were to be analyzed or in methanol or acetonitrile–methanol (50:50) to test TAT's stability in these solvents. For calibration purposes five additional diluted standards were prepared from each stock standard in the same solvent as the given stock standard. Diluted standards showed less than 4% decrease in area over a period of three months and stock standards showed less than 2% decrease over the same period of time.

Two mixed standards were prepared, one in pH 3.2 phosphate buffer and the other in acetonitrile–methanol (50:50). TAT (90 mg/l), phloroglucinol (35 mg/l), pyrogallol (9.4 mg/l) and MPG (24 mg/l) were prepared in pH 3.2 buffer because they showed less peak dispersion in this solvent than in any organic solvents. The second mixture contained 19.8 mg/l DA4NT, 21.3 mg/l DA6NT, 103 mg/l *p*-cresol, 59 mg/l RDX, 29 mg/l 2ADNT, 32 mg/l 4ADNT, 80 mg/l TNT, 30.6 mg/l 2,2′-Az and 37.2 mg/l 4,4′-Az, and was made up in methanol–acetonitrile (50:50).

Samples of the supernatant from TNT biodegradation studies were centrifuged at 14 000 rpm for approximately 15 min (16 000 *g*) and were stored and analyzed under the same conditions as the standards.

Acetonitrile was selected as the organic component of the mobile phase after observing that the TNAZT compounds were not completely soluble in methanol. The acetonitrile used in the mobile phase and the preparation of standards was Fisher Scientific HPLC-grade acetonitrile (UV cutoff 190 nm). Mallinckrodt HPLC-grade methanol was also used in standard preparation. Phosphate-buffered aqueous mobile phase components at pH 3.2 and pH 4.0 were prepared by first adding 50 μl of concentrated phosphoric acid/l water and then adding K_2HPO_4 to adjust to the desired pH. The approximate molarity of these buffers was 11 m*M*. Type 1 reagent-grade water, without any pH change, was used as the third aqueous phase component. The pH of the reagent-grade water was found to be 6.4. All aqueous mobile phase components were vacuum filtered through a 0.2-μm Gelman Sciences (Ann Arbor, MI, USA) membrane filter.

The LC analyses were performed with a Hewlett-Packard HP 1090 Series II/M liquid chromatograph with a DR 5 ternary solvent-delivery system, variable-volume auto-injector, temperature controlled autosampler (TCAS), thermostatically controlled column compartment and a built-in DAD system. Hewlett-Packard ^{3D}Chemstation was used for instrument control and data analysis. The column used for the separation was an Alltech Alltima RP-HPLC C_{18} column that contained 5-μm particles. Column dimensions were 250 mm × 2.1 mm I.D. An Alltech direct-connect refillable guard column packed with the same material was used to protect the analytical column.

Temperatures for the TCAS and the column compartment were maintained at 8 and 45°C, respectively, during analyses. The auto-injector was set to inject 10 μl of each sample. DAD was used for dual-wavelength detection at 210 and 254 nm. Peaks were scanned from 200 to 600 nm for compound characterization. The mobile

phase flow-rate was set at 0.4 ml/min. The initial method employed a 2-min equilibration at 10% acetonitrile, followed by a linear gradient from 2 to 20 min varying acetonitrile from 10 to 100%. The initial method was used to study pH effects on individual compounds. This method was then optimized so that maximum separation could be achieved between the analytes. The final optimized method varied acetonitrile in the following way: 10 to 55% from 0 to 14 min, 55 to 100% from 14 to 18 min, held at 100% from 18 to 19 min and 100 back to 10% from 19 to 22 min.

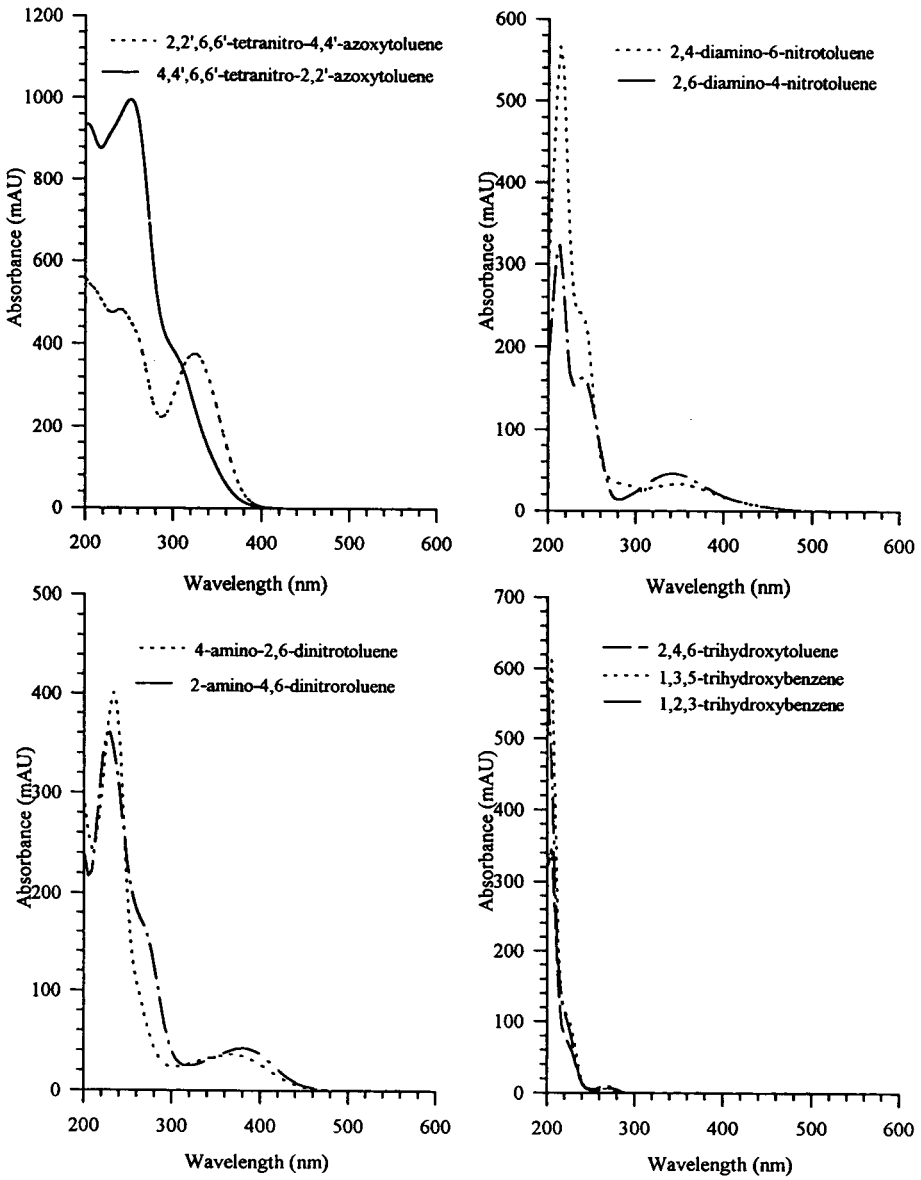

Fig. 1. The UV–Vis spectra of nine of the intermediates or suspected intermediates of TNT degradation. Spectra were obtained by scanning from 210 to 600 nm using the diode array detector.

3. Results

3.1. Effects of aqueous phase pH

No significant changes in retention times or response factors were observed with a variation in aqueous phase pH. There was no change in compound spectra, either; spectral matches of greater than 990 (on a scale of 1000) were obtained for compounds eluted at different pH values. The spectra obtained for most of the analytes are shown in Fig. 1.

The most significant effect of pH was seen on the stability of TAT. At pH 6.4, TAT eluted as five different peaks, causing an interference to the separation of the early eluting alcohols. The number of TAT peaks was reduced to four with a pH 4.0 aqueous phase. A drastic change occurred at pH 3.2 when TAT eluted as only two peaks with greater than 84% of the area in a single, possibly solvent, peak at a retention time of 1.55 min. TAT standards made in methanol and acetonitrile–methanol (50:50) and analyzed at pH 3.2 showed further improvements. TAT in methanol eluted as two peaks with greater than 85% of the area in a single peak. TAT in acetonitrile–methanol (50:50) eluted as a single identifiable peak. Based on these results pH 3.2 aqueous phase was selected for the final optimization of the separation.

3.2. Optimization of separation

The final gradient method selected varied acetonitrile in the following way: 10 to 55% from 0 to 14 min, 55 to 100% from 14 to 18 min, held at 100% from 18 to 19 min and 100 back to 10% from 19 to 22 min. The total analysis time was 22 min with 3 min of re-equilibration allowed between samples. The retention times, response factors and detection limits obtained for the analytes with this gradient are shown in Table 1. Changing the initial composition of the mobile phase to less than 10% acetonitrile resulted in the binding of the TNAZT compounds to the column and lengthening the retention times to extremes, making the method impractical for these compounds. Since the detection of these compounds is very important to the mass balance of TNT metabolism, it was decided that the at least 10% acetonitrile was necessary.

Decreasing the slope of the gradient caused increased interference between the early-eluting compounds and it did not improve separation between the non-baseline-separated pairs. Baseline separation could not be achieved be-

Table 1
Summary of chromatographic characteristics for the compounds studied

Compound	Retention time (min)	Response factor (mAU s mg^{-1} l^{-1})[a]	Detection limit (ng/injection)[b]	Signal-to-noise ratio at detection limit
Phloroglucinol	2.15	145.3 ± 1.6	10	22
Pyrogallol	2.88	110.3 ± 5.5	10	14
MPG	3.13	129.3 ± 2.3	10	26
DA4NT	6.11	144.2 ± 1.0	10	35
DA6NT	6.68	152.6 ± 9.8	10	33
p-Cresol	10.3	35 ± 1.8	10	114
RDX	10.4	53.2 ± 1.5	5	61
2ADNT	13.3	52.3 ± 0.5	10	26
4ADNT	13.4	56.4 ± 1.1	10	27
TNT	14.7	51.7 ± 0.9	1.1	2.7
2,2′-Az	18.2	54.1	0.66	5.6
4,4′-Az	18.5	52.1	0.58	0.6

[a] Results are average and 1 standard deviation ($n = 4$).
[b] Results indicate the lowest standard tested, detection of smaller amounts of material may be possible, but was not tested.

tween *p*-cresol and RDX and between 2ADNT and 4ADNT. However, separations were sufficient to allow spectral identification and integration of the different peaks. Increasing the slope of the gradient reduced the separation between the ADNTs and between *p*-cresol and RDX. Chromatograms at 210 and 254 nm are shown in Fig. 2. As it can be seen from Fig. 2, all of the

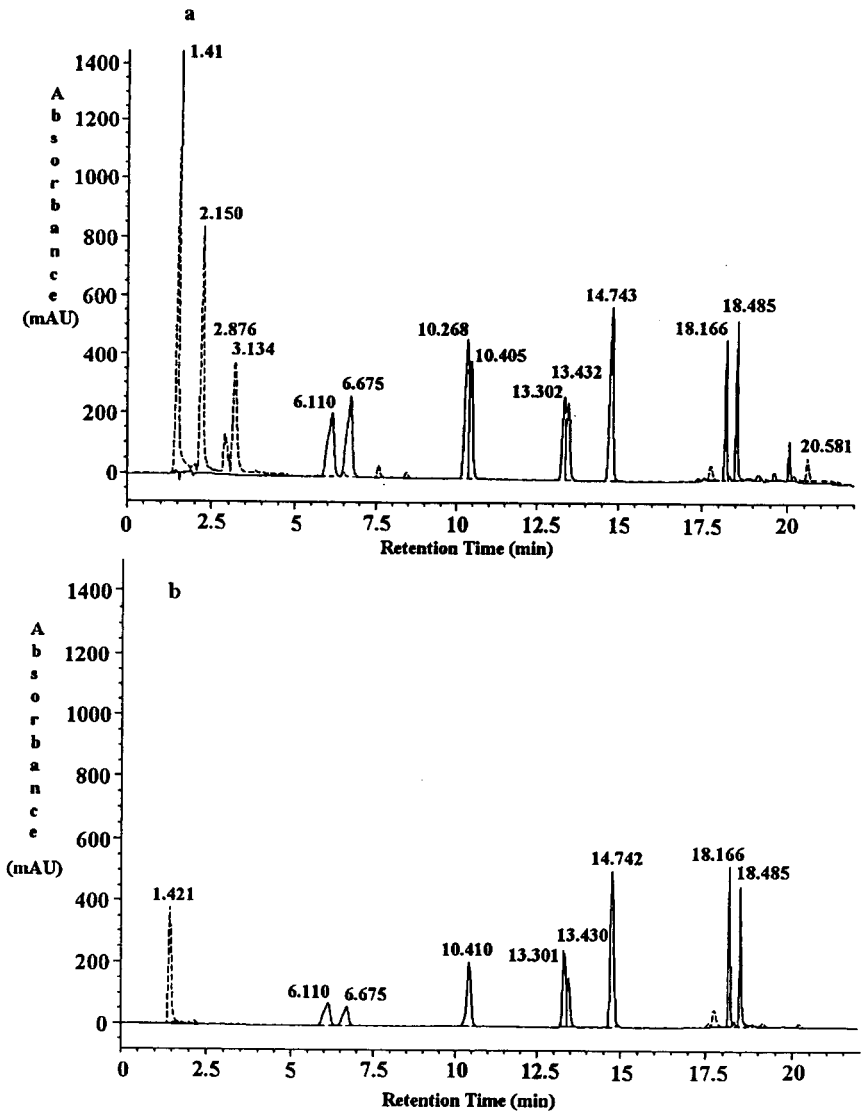

Fig. 2. The chromatographs of compound separation for the mixed standards containing all of the test compounds from signals saved at (a) 210 and (b) 254 nm. Dotted lines, standards of TAT (1.4 min, 90 mg/l), phloroglucinol (2.15 min, 35 mg/l), pyrogallol (2.88 min, 9.4 mg/l) and methylphloroglucinol (3.13 min, 24 mg/l) made up in pH 3.2 buffer. Solid lines, standards of DA4NT (6.11 min, 19.8 mg/l), DA6NT (6.68 min, 21.3 mg/l), *p*-cresol (10.27 min, 103 mg/l), RDX (10.4 min, 59 mg/l), 2ADNT (13.3 min, 29 mg/l), 4ADNT (13.4 min, 32 mg/l), TNT (14.74 min, 80 mg/l) 2,2′-Az (18.17 min, 30.6 mg/l) and 4,4′-Az (18.48 min, 37.2 mg/l) made up in methanol–acetonitrile (50:50).

suspected biodegradation intermediates of TNT showed no absorption in the 250–254 nm wavelength range.

Fig. 3 shows a chromatograph from a sample of a culture spiked with TNT. This culture has produced 4ADNT and DA6NT almost exclusively over the two other amino or diamino isomers. Low concentrations of *p*-cresol and MPG were detected and identified by comparing the spectra and retention times to the authentic standards. This culture was not inoculated under strictly anaerobic conditions but was allowed to create its own anaerobic conditions by the use of glucose by aerobic bacteria present in the culture. In such cases some of the TNAZT compounds are produced but do not remain in the culture for long. The presence of MPG and *p*-cresol indicates that the methyl group of the TNT molecule stays on the ring in its reduced form at least until *p*-cresol. There have been no indications of the presence of phloroglucinol or pyrogallol in our cultures. The peak at 1.9 min is seen occasionally in aqueous cultures spiked with TNT. This compound is as yet unidentified and may be methylresorcinol, resulting from the removal of one hydroxy group from the

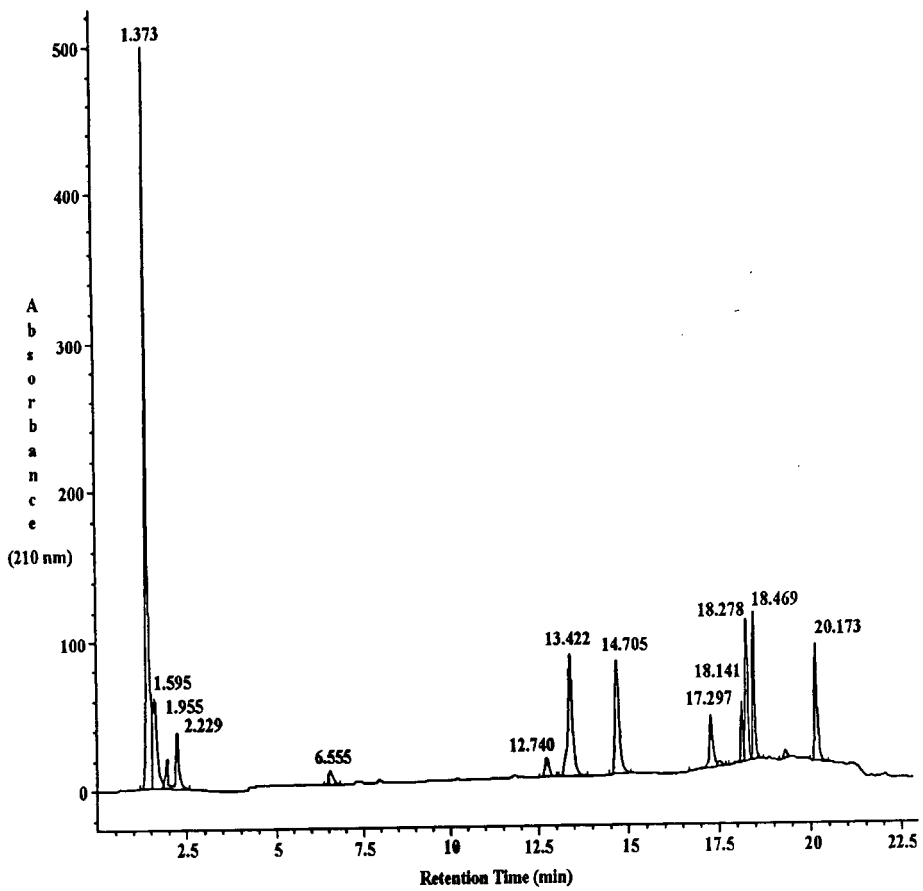

Fig. 3. A randomly selected chromatograph from analysis of the aqueous phase of TNT-degrading cultures. The retention times of some of the peaks have shifted due to column age but DAD analyses of the peak spectra confirm the identifications of methylphloroglucinol (2.229 min), DA6NT (6.555 min), 4ADNT (13.442 min), TNT (14.705 min), 2,2′-Az (18.141 min) and 4,4′-Az (18.469 min).

methylphloroglucinol or it may be an intermediate of *p*-cresol degradation.

4. Conclusions and discussion

The analysis of the intermediates of the biological degradation of TNT was accomplished using narrow bore HPLC with diode array detection. The aqueous phase of pH 3.2 was selected as the most suitable for the separation of the given compounds. This pH allowed the minimization of TAT speciation without causing any adverse changes in the chromatographic properties of the other analytes. Reduction of pH to 3.0 may further decrease the speciation of TAT. However, the operation a silica-based reversed-phase column below pH 3.0 is not recommended, as it can cause the cleavage of silanol groups connecting the alkyl chains to the silica particles. There are, however, several resin-based (e.g. styrene–divinylbenzene) reversed-phase columns available that have shown a wider range of pH tolerance than traditional silica-based reversed-phase columns. The low pH requirements also suggests that samples from TNT biodegradation studies should be acidified before analysis. The decrease in speciation of TAT is important in order to prevent its interference with the elution and quantitation of other compounds. TAT is very unstable and is not detected easily in biological samples due to its extreme sensitivity to oxygen. The sampling procedure used here, exposes the sample to oxygen while centrifuging, and so attempts made to quantitate TAT are done as specific experiments designed with minimized oxygen contact. The procedure developed here was for routine everyday analyses with TAT out of the way, and not for TAT analyses.

A detection wavelength of 250–254 nm is unsuitable for the detection of some of the suspected intermediates of TNT biodegradation. A wavelength in the range of 210–220 nm is more suitable for detection of these compounds. This also precludes the use of methanol as the organic component of the mobile phase, as methanol absorbs in this wavelength range. Prior to this work, only Yinon and Hwang [17] and Harvey et al. [23] have used acetonitrile as the sole organic phase.

Baseline separation of ADNTs could not be achieved using the method presented. In past literature this has only been accomplished by Walsh and Jenkins [24], who used an LC-CN column in series with an RP C_{18} column. Therefore, it is strongly suspected that baseline separation of the ADNTs cannot be achieved without the alteration of the stationary phase to one that is more selective for the ADNTs.

Acknowledgements

We thank Dr. Ronald J. Spanggord for his generous donation of chemical standards. This research was funded through a cooperative agreement with the US Environmental Protection Agency's Environmental Research Laboratory in Athens, GA, USA.

References

[1] T.F. Jenkins, M.E. Walsh, P.W. Schumacher, P.H. Miyares, C.F. Bauer and C.L. Grant, *J. Assoc. Off. Anal. Chem.*, 72 (1989) 890.
[2] W.E. Pereira, D.L. Short, D.B. Manigold and P.K. Roscio, *Bull. Environ. Contam. Toxicol.*, 21 (1979) 554.
[3] L.A. Smock, D.L. Stoneburner and J.R. Clark, *Water Res.*, 10 (1976) 537.
[4] A.J. Palazzo and D.C. Leggett, *J. Environ. Qual.*, 15 (1986) 49.
[5] W.D. Won, L.H. DiSalvo and J. Ng, *Appl. Environ. Microbiol.*, 31 (1976) 576.
[6] N.N. Amerikhanova and R.P. Naumova, *Estestv. Nauki (Biol. Khim.)*, (1975) 147.
[7] W.J. McConnel and R.H. Flinn, *J. Ind. Hyg. Tox.*, 28 (1945) 76.
[8] J.V. Dilley, C.A. Tyson and G.W. Newell, *Mammalian Toxicology Evaluation of TNT Wastewaters; Contract No. DAMD 17-76-C-6050*, Vol. III, Stanford Research Institute, Menlo Park, CA, 1978.
[9] N.N. Amerikhanova and R.P. Naumova, *Biol. Nauki.*, 2 (1979) 26.
[10] R.J. Spanggord, K.E. Mortelmans, A.F. Griffin and V.F. Simmon, *Environ. Mutagenesis*, 4 (1982) 163.
[11] D.J. Glover, J.C. Hoffsommer and D.A. Kubose, *Anal. Chim. Acta*, 88 (1977) 381.

[12] *Determination of Explosives in Water by HPLC; Method No. 8H*, US Army Toxic and Hazardous Materials Agency, Picatinny, NJ, 1982.
[13] R.T. Medary, *Anal. Chim. Acta.*, 258 (1992) 341.
[14] T.F. Jenkins and C.L. Grant, *Anal. Chem.*, 59 (1987) 1326.
[15] D.L. Kaplan and A.M. Kaplan, *Anal. Chim. Acta*, 136 (1982) 425.
[16] R. Schuster and A. Gratfeld-Huesgen, *HPLC Analysis of Explosive Constituents in Soil Samples; Publication No. 12-5091-7626E*, Hewlett-Packard, Avondale, PA, 1993.
[17] J. Yinon and D.-G. Hwang, *Biomed. Chromatogr.*, 1 (1986) 123.
[18] H.J. Channon, G.T. Mills and R.T. Williams, *Biochem. J.*, 38 (1943) 70.
[19] N.G. McCormick, F.E. Feeherry and H.S. Levinson, *Appl. Environ. Microbiol.*, 31 (1976) 949.
[20] R.P. Naumova, S.Y. Selivanovskaya and F.A. Mingatina, *Mikrobiologiya*, 57 (1988) 218.
[21] S.B. Funk, D.J. Roberts, D.L. Crawford and R.L. Crawford, *Appl. Environ. Microbiol.*, 59 (1993) 2171.
[22] C.C. Ruchhoft and W.G. Meckler, *Ind. Eng. Chem. (Anal. Ed.)*, 17 (1945) 430.
[23] S.D. Harvey, R.J. Fellows, D.A. Cataldo and R.M. Bean, *J. Chromatogr.*, 518 (1990) 361.
[24] M.E. Walsh and T.F. Jenkins, *Anal. Chim. Acta*, 231 (1990) 313.

ELSEVIER

Journal of Chromatography A, 693 (1995) 176–180

JOURNAL OF CHROMATOGRAPHY A

Short communication

Determination of chlorophylls by reversed-phase high-performance liquid chromatography with isocratic elution and the column-switching technique

Koichi Saitoh*, Izumi Awaka, Nobuo Suzuki

Department of Chemistry, Faculty of Science, Tohoku University, Sendai, 980-77, Japan

First received 22 April 1994; revised manuscript received 25 November 1994; accepted 25 November 1994

Abstract

A reversed-phase high-performance liquid chromatographic (HPLC) system was designed for the separation and determination of chlorophylls and their degradation products. Two separation columns packed with octadecyl-bonded silica gel (ODS) and octadecyl-bonded vinyl alcohol copolymer (ODP) were employed with the aid of a column-switching technique. The ODS column (1 cm) functioned for the separation of very hydrophobic compounds, such as chlorophyll *a*, chlorophyll *b*, pheophytin *a* and pheophytin *b*, and the ODP column (15 cm) for separating the compounds of low hydrophobicity, such as chlorophyll c_1, chlorophyll c_2, pheoporphyrin c_1, pheoporphyrin c_2, pheophorbide *a* and pheophorbide *b*. The HPLC system could cope with a variety of hydrophobicities of chlorophyll pigments by means of isocratic elution with methanol–phosphate buffer (pH 3) (92:8, v/v). Application to several seaweed samples was demonstrated.

1. Introduction

The determination of chlorophylls and their degradation products, such as pheophytins and pheophorbides, in natural samples from sea, lake, sediment and other sources gives valuable information about the biological processes occurring in these environments [1,2]. In oceanography, the chlorophyll abundance is an important measurement for estimating phytoplankton biomass [3]. The degradation products from chlorophylls found in a sediment are expected to act as paleoindicators of the nature of sedimentary input or living biomass composition [4].

Spectrophotometry and spectrofluorimetry, which are traditional and still popular methods for chlorophyll analysis [5], are not always effective with the complex range of chlorophylls and related compounds found in natural samples owing to the similarity of their spectral characteristics. Reversed-phase high-performance liquid chromatography (RP-HPLC) has become a promising means for the separation of chlorophylls, including chlorophyll-*a*, -*b* and -*c* (Chl-*a*, -*b* and -*c*), and also their demetallated forms, such as pheophytin-*a* and -*b* (Pheo-*a* and -*b*), and phytyl-free demetallated forms, such as pheophorbide-*a* and -*b* (Phor-*a* and -*b*) [6–8]. The successful resolution of Chl-*c* into Chl-c_1 and Chl-c_2 has been reported [9,10].

There are considerable differences in polarity (or hydrophobicity) among chlorophyll com-

* Corresponding author.

0021-9673/95/$09.50
SSDI 0021-9673(94)01175-3

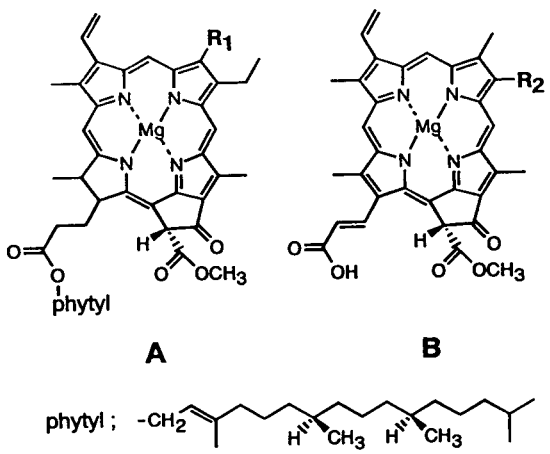

Fig. 1. Chlorophylls and its degradation products. Chl-*a* (A, R_1 = methyl); Chl-*b* (A, R_1 = formyl); Chl-c_1 (B, R_2 = ethyl); Chl-c_2 (B, R_2 = vinyl).

pounds owing to their molecular structures (see Fig. 1). Gradient elution is a popular and effective mode of HPLC to cope with a variety of compounds. However, it requires sophisticated instrumentation for changing the mobile phase composition in accordance with a preset programme. Isocratic elution is a convenient and desirable chromatographic mode from the viewpoint of the simplicity of the equipment. This paper describes the feasibility of a column-switching technique for the HPLC separation of chlorophylls with isocratic elution.

2. Experimental

2.1. Chlorophyll pigment standards

Chl-*a* and -*b* were extracted with acetone from fresh spinach and precipitated by adding dioxane and water [11]. The chlorophylls were purified by preparative RP-HPLC using an octadecyl-bonded silica gel (ODS) column (particle size 30–50 μm, 36 cm × 24 mm I.D.) (Fuji Gel RQ-2; Fuji, Tokyo, Japan) with methanol–acetone (70:30, v/v). Chl-c_1 and -c_2 were extracted with acetone from the fresh brown seaweed *Undaria pinnatifida* (Phaeophyceae) obtained at Onagawa Bay, Miyagi, Japan. After preliminary separation by liquid–liquid partitioning and then by preparative chromatography on an octadecyl-bonded silica gel column [10], Chl-c_1 and -c_2 were purified by HPLC on an ODP column (5 μm, 15 cm × 6 mm I.D.) (Asahipak ODP-50; Asahi Kasei, Kawasaki, Japan) with methanol–phosphate buffer (pH 3) (90:10, v/v).

Demetallated forms of chlorophylls were prepared by treatment of corresponding chlorophylls as detailed previously, for Pheo-*a* and -*b* and Phor-*a* [11] and pheoporphyrin c_1 and c_2 (Pheo-c_1 and -c_2) [10].

2.2. Chromatographic system

An isocratic elution HPLC system (Twincle; JASCO, Tokyo, Japan) equipped with a UV–visible absorption detector (SPD-6AV; Shimadzu, Kyoto, Japan) and a photodiode-array detector (modified Shimadzu SPD-M6A, wavelength range 300–800 nm) was used. Columns packed with ODS (Inertsil ODS-2; GL Science, Tokyo, Japan) (particle diameter 5 μm, 15 cm × 4.6 mm I.D.) and ODP (5 μm, 15 cm × 4.6 mm I.D.) (Asahipak ODP-50) were used for a preliminary retention study. A short ODS column (5 μm, 1 cm × 4.6 mm I.D.) was combined with the 15-cm ODP column in the HPLC system using a column-switching technique. The mobile phase was methanol–buffer solution (1.24 m*M* phosphoric acid–8.76 m*M* sodium dihydrogenphosphate, pH 3) (92:8, v/v) and the flow-rate was 1.0 ml/min. The detection wavelength was 450 nm unless indicated otherwise.

3. Results and discussion

3.1. Retention characteristics

It has been reported that Chl-*a* shows a longer retention than Chl-*b* on an ODS column working in the reversed-phase mode, and a similar retention trend held for the *a*–*b* pairs of pheophytins and pheophorbides [8,11]. There was almost no difference in the retention of Chl-c_1 and Chl-c_2 on an ODS column with a

methanol–water mobile phase, whereas a sharp difference appeared on an ODP column, Chl-c_1 showing a smaller retention than Chl-c_2 [11]. It was reasonable to use an ODP column for chlorophyll analysis with recognition of Chl-c_1 and -c_2. However, compounds possessing phytyl groups, such as Chl-*a* and -*b*, and also Pheo-*a* and -*b*, were retained so strongly on this column that they could not be eluted with the mobile phase effective for the resolution of Chl-*c* [e.g., methanol–buffer (pH 3) (92:8, v/v)]. The retention of each compound of interest on ODS was smaller than that on ODP with an identical composition of the mobile phase, as shown in Fig. 2a and b. Accordingly, ODS was regarded as being preferable to ODP, particularly for the separation of the phytylated compounds in a short time.

3.2. Column-switching technique

In order to permit the analysis of chlorophyll compounds in one run in a short time by isocratic elution, a selective decrease in retention times was required for hydrophobic compounds possessing phytyl groups. This problem was solved in this work by changing the effective separation column from the long ODP column (150 mm × 4.6 mm I.D.) to the short ODS column (10 mm × 4.6 mm I.D.) at a suitable time in each run by means of a column-switching technique. The mobile phase conditions remained identical throughout the analysis, i.e., methanol–phosphate buffer (pH 3) (92:8, v/v) at a flow-rate of 1.0 ml/min.

A sample solution was injected into the 1-cm ODS column that led to the 15-cm ODP column. Phytyl-free chlorophyll compounds, such as Chl-c_1, Chl-c_2, Pheo-c_2 and Phor-*a*, passed through the ODS column in short time without effective separation and flowed into the ODP column, whereas more hydrophobic compounds possessing phytyl groups, such as Chl-*a*, Pheo-*a*, Chl-*b* and Pheo-*b*, were retained on the former column. At this time (t_1), the column-switching valve was activated so as to bypass the ODS column and to allow the effective separation of the phytyl-free compounds in the ODP column. When the separation of these compounds was finished (at time t_2), the valve was driven so that the ODS column followed the ODP column, and phytylated compounds were resolved in the ODS column. After completion of an analysis, the order of connection of these columns was reset for subsequent analysis. The feasibility of the column-switching technique was demonstrated in the separation of several chlorophyll standards, as shown in Fig. 3a.

3.3. Application to seaweed samples

Green seaweeds (Chlorophyceae), *Monostroma nitidum* and *Bryopsis plumosa*, and brown seaweeds (Phaeophyceae), *Undaria pin-*

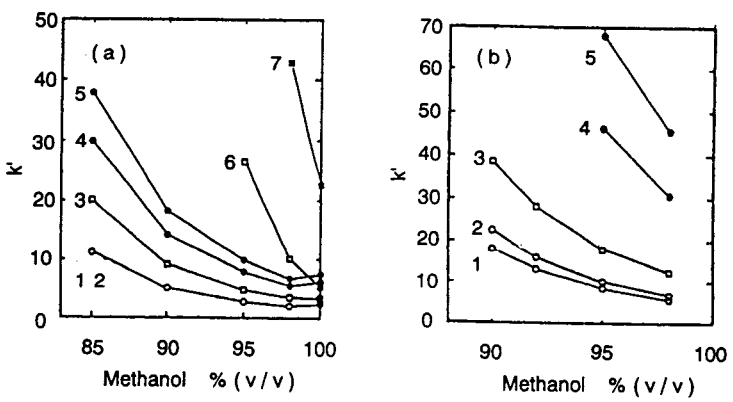

Fig. 2. Capacity factor (k') versus methanol content of the mobile phase on (a) ODS and (b) ODP. Compounds: 1 = Chl-c_1; 2 = Chl-c_2; 3 = Phor-*a*; 4 = Pheo-c_1; 5 = Pheo-c_2; 6 = Chl-*a*; 7 = Pheo-*a*.

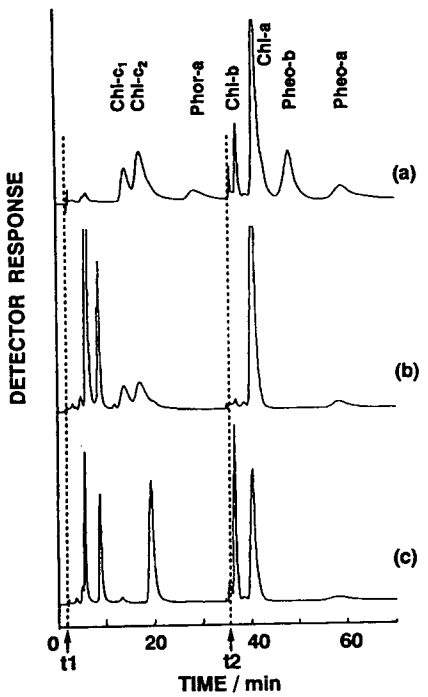

Fig. 3. Chromatograms for (a) chlorophyll standards, (b) extract from *Undaria pinnatifida* and (c) extract from *Monostroma nitidum*. Mobile phase, MeOH–buffer (pH 3) (92:8, v/v); flow-rate, 1.0 ml/min; detection wavelengths, 440 nm for Chl-*a* and -*b*, 450 nm for Chl-c_1 and -c_2 and 410 nm for Pheo-*a*, Pheo-*b* and Phor-*a*. t_1, t_2 = Timings of column switching.

natifida, *Laminaria religiosa* and *Sargassum sagamianum*, were sampled at Oshika (Pacific coast), Miyagi, Japan, and stored at −20°C until used. Chlorophyll pigments were extracted from a sample (0.2–3 g) with cold methanol (10 ml per gram of wet sample) in triplicate. The extract was passed through a PTFE membrane filter (0.5 μm), followed by dilution to the desired volume (10–100 ml) of test solution using the HPLC mobile phase. The extraction residue was dried at 85°C for 2 h and was then weighed.

A 10-μl aliquot of a test solution was applied to the HPLC system. In order to detect the compounds of interest with high sensitivity, the detection wavelength was changed automatically: 440 nm for Chl-*a* and Chl-*b*, 410 nm for Pheo-*a* and Phor-*a* and 450 nm for Chl-c_1, Chl-c_2, Pheo-c_1 and Pheo-c_2. The peak identification was supported by the UV–visible spectra obtained with the photodiode-array detector.

Chl-*a*, Chl-*b* and Pheo-*a* were detected in all green seaweed samples, and Chl-*a*, Pheo-*a*, Chl-c_1 and Chl-c_2 in brown seaweeds. Typical examples of chromatogram are shown in Fig. 3b and c. Several chlorophylls and related compounds were determined by comparing their peak areas with those measured for standards. The results for different seaweeds are given in Table 1. The values given in parentheses are the relative

Table 1
Determination of chlorophylls in seaweed samples collected at Oshika, Miyagi, Japan

Seaweed	Date	Mean (mg/g)[a]					
		Chl-*a*	Chl-*b*	Chl-c_1	Chl-c_2	Pheo-*a*	(c_1/c_2)[b]
Undaria pinnatifida	11 July 1991	8.4 (0.68)	ND[c] –	1.2 (1.7)	1.6 (11)	1.4 (4.4)	0.75
Laminaria religiosa	28 April 1990	4.0 (15)	ND –	0.41 (1.6)	0.99 (0.7)	2.6 (0.1)	0.42
Sargassum sagamianum	11 July 1991	4.5 (3.4)	ND –	0.53 (5.6)	1.1 (6.0)	1.7 (5.6)	0.50
Bryopsis plumosa	11 July 1991	6.0 (0.8)	5.6 (0.3)	ND –	ND –	0.49 (4.4)	–

[a] Mean of three determinations, based on dry mass of extraction residue, with R.S.D. (%) in parentheses.
[b] Ratio of Chl-c_1 to Chl-c_2.
[c] ND = Not detected.

standard deviations calculated from three measurements for each.

In conclusion, the column-switching technique has enabled HPLC to cope with the wide range of hydrophobicity of chlorophyll compounds even using the isocratic elution mode. The distinctive measurements of Chl-c_1 and -c_2 are expected to give useful information similarly to those for Chl-*a* and -*b* for determining biomass and pollution in the environment and also for the determination of biological activity.

References

[1] S.W. Wright and J.D. Shearer, *J. Chromatogr.*, 294 (1984) 281.
[2] I.D. Giraudiere, P. Laborde and J.C. Romano, *Mar. Chem.*, 26 (1989) 189.
[3] A.P. Murray, C.F. Gibbs, A.R. Longmore and D.J. Flett, *Mar. Chem.*, 19 (1986) 211.
[4] F.T. Gillan, *Mar. Chem.*, 9 (1980) 243.
[5] C.C. Trees, M.C. Kennicutt, II, and J.M. Brooks, *Mar. Chem.*, 17 (1985) 1.
[6] S. Roy, *J. Chromatogr.*, 391 (1987) 19.
[7] R.F.C. Mantoura and C.A. Llewellyn, *Anal. Chim. Acta*, 151 (1983) 297.
[8] K. Adachi, K. Saitoh and N. Suzuki, *J. Chromatogr.*, 457 (1988) 99.
[9] S.W. Jeffrey, *Biochim. Biophys. Acta*, 279 (1972) 15.
[10] K. Saitoh, I. Awaka and N. Suzuki, *J. Chromatogr. A*, 653 (1993) 247.
[11] N. Suzuki, K. Saitoh and K. Adachi, *J. Chromatogr.*, 408 (1987) 181.

ELSEVIER

Journal of Chromatography A, 693 (1995) 181–185

JOURNAL OF CHROMATOGRAPHY A

Short communication

Prediction of gas chromatographic retention indices of 2,4-dinitrophenylhydrazones

Miklós Görgényi[a,*], Herman Van Langenhove[b], Zoltán Király[a]

[a]*Institute of Physical Chemistry, University of Szeged, Rerrich B. tér 1, 6720 Szeged, Hungary*

[b]*Department of Organic Chemistry, University of Ghent, Coupure Links 653, 9000 Ghent, Belgium*

Received 16 August 1994; accepted 19 October 1994

Abstract

Kováts retention indices (I) of C_1–C_8 aldehydes and ketones and their 2,4-dinitrophenylhydrazones (DNPHs) were determined. The temperature gradient of the retention indices of keto hydrazones is higher than that of aldehyde hydrazones, hence the separation of certain co-eluting hydrazones is possible by changing the elution temperature. The retention index difference between the E- and Z-isomers increases with increasing asymmetry in the groups attached to the hydrazo carbon atom. The slope a in the equation $I_{DNPH} = aI_{oxo} + b$ is near unity for not heavily branched aldehyde DNPHs, whereas for keto E-isomers it is less than unity and changes with the structure.

Introduction

As volatile aldehydes and ketones are present in low concentrations in some matrices (e.g., automobile exhaust, foods and beverages, atmospheric air), their preconcentration is necessary before analysis. Derivatization to 2,4-dinitrophenylhydrazones (DNPHs) and subsequent determination by GC [1–5] and HPLC [6–10] is a generally used method.

The DNPHs of aldehydes and asymmetric ketones have E and Z stereoisomeric forms. The E-isomer is the form in which atoms or groups attached to the two ends of the C=N double bond and preferred to the sequence rule are on the opposite sides [11] (Fig. 1). The R_1 is a group preferred over R_2; R_1 = H in aldehydes. For DNPH isomers, R_3 = H and R_4 = $C_6H_3(NO_2)_2$. The DNPHs are generally, synthesized in acidic medium [12–15] with the formation of both E and Z-isomers.

Kováts retention indices of DNPHs were measured on a slightly polar packed column [16], where, owing to the insufficient resolving power of the column, the E and Z-isomers could not be separated. On a more efficient capillary column, however, this separation problem was avoided [1–3, 17]. A retention index system using the *anti*

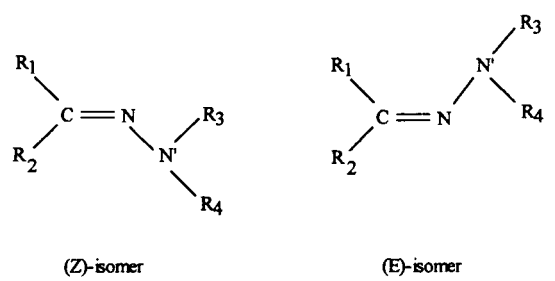

Fig. 1. Structural formulae of (Z)- and (E)-2,4-dinitrophenylhydrazone.

* Corresponding author.

0021-9673/95/$09.50
SSDI 0021-9673(94)01019-6

isomers of the DNPHs of linear alkanals as reference components has been proposed; the retention indices were determined on an SE-30 column [17].

Physico-chemical data, such as boiling point, refractive index, dipole moment and Van der Waals volume, and topological indices are generally used for the prediction of retention indices [18–20]. In this case, owing to the complicated nature of the molecule and the lack of physical data, the only attempt was a qualitative correlation of the retention indices of the DNPHs with the carbon numbers of the starting oxo compounds [16].

This paper reports the Kováts retention indices of some aldehydes and ketones and their DNPH isomers, together with the temperature gradients measured on an apolar column. We have made an attempt to estimate the retention indices of DNPHs from the experimental retention indices of the aldehydes and ketones via an empirical equation, i.e., to check the validity of an additivity rule, and to find an explanation for the difference in GC behaviour of the (*E*)- and (*Z*)-DNPH isomers.

2. Experimental

2.1. Materials

The DNPHs were synthetized by the literature method [21]. The aldehydes, ketones and reference C_{20}–C_{28} hydrocarbons were purchased from Fluka (Buchs, Switzerland) and Aldrich-Chemie (Steinheim, Germany).

2.2. Gas chromatography

The retention indices of DNPH isomers were determined on a 25 m × 0.32 mm I.D. dimethylpolysiloxane column (film thickness 0.25 μm, FSOT; Supelco), whereas those of aldehydes and ketones were determined on a 50 m × 0.32 mm I.D. column (0.52 μm, fused-silica open tubular; Hewlett-Packard). The retention indices were measured with a Hewlett-Packard Model 5890 Series II gas chromatograph with an HP 3365 Series II ChemStation. A flame ionization detector and nitrogen carrier gas were used. The injector temperature was 240°C and it was used in split mode, with a splitting ratio of 1:40.

The Kováts retention indices were calculated as described previously [22]; the fitting parameters and the statistics were calculated by means of PSI-PLOT (Polysoft International). The temperature gradients of the retention indices of the DNPHs were calculated from the data obtained in the range 180–230°C and those of oxo compounds from the data measured at 40–90°C (for some low-boiling compounds, 30–80°C). In both instances, measurements were made at 10°C intervals. The boiling points of aldehydes and ketones were taken from Ref. [23].

3. Results and discussion

The Kováts retention indices of the aldehydes and ketones studied and their DNPHs are listed together with their temperature gradients in Table 1.

At 200°C (a characteristic temperature for the separation of small- and medium-sized DNPHs), 2-propanone and 2-propanal were not separated, but, as a consequence of their different temperature gradients, a baseline separation was possible at 160°C.

The ketone DNPHs have higher temperature gradients (aldehyde DNPHs, 10.4 ± 0.7 i.u. (index unit) per 10°C, $n = 14$; ketone DNPHs, 11.7 ± 0.5 i.u. per 10°C, $n = 12$; the exceptionally high value of cyclohexane DNPH was not included in the calculations). This behaviour may give a possibility for the separation of closely eluting compounds.

The retention index of the (*Z*)-DNPH isomer was always lower than that of the *E*-isomer (Table 1). This behaviour was explained earlier by the more exposed nature of the *Z*-isomer [17,24].

The difference between the retention indices of the stereoisomers is largely dependent on the difference in the substitution patterns of the alkyl chains of R_1 and R_2, i.e., the greater the difference in the carbon numbers of R_2 and R_1

Table 1
Kováts retention indices (I) and their temperature gradients [$(dI/dT) \cdot 10$] for aldehydes and ketones and their DNPH derivatives

Compound	DNPH isomers			Oxo compounds		dI^c
	I^a	$(dI/dT) \cdot 10$	$I_E - I_Z$	I^b	$(dI/dT) \cdot 10$	
Formaldehyde	1905	10.5	–			
Acetaldehyde	2035	10.9	21	365.3	−0.3	1674
2-Propanone	2121	11.8	–	471.9	−0.4	1654
2-Propenal	2121	10.3	–	466.9	−0.2	1657
Propanal	2129	10.7	32	474.6	−0.3	1658
2-Methylpropanal	2173	9.8	33	542.2	0.1	1629
2,2-Dimethylpropanal	2202	9.2		584.6	0.6	1610
2-Butanone	2207	11.4	16	577.0	−0.1	1631
Butanal	2223	9.6	39	573.3	0.3	1646
3-Methyl-2-butanone	2260	11.8		642.3	0.3	1613
3-Methylbutanal	2275	10.2	39	637.1	0.7	1629
2-Methylbutanal	2277	11	60	647.6	0.6	1621
3-Pentanone	2279	12.1	–	676.9	0.1	1601
2-Butenal	2288	12.0	–	628.9	1.0	1647
2-Pentanone	2294	12.5	30	667.1	0.1	1624
Pentanal	2325	10.6	45	676.5	0.4	1643
4-Methyl-2-pentanone	2331	11.4	22	721.9	0.4	1604
3-Hexanone	2350	11.7	12	765.4	0.3	1581
2,4-Dimethyl-3-pentanone	2356	10.9	–	779.5	1.0	1563
2-Hexanone	2388	11.6	37	768.8	0.2	1616
3-Heptanone	2443	11.4	20	866.3	0.4	1572
5-Methyl-2-hexanone	2449	11.5	42	837.3	0.5	1604
2-Heptanone	2483	11.3	45	869.1	0.4	1609
Hexanal	2426	10.6	48	778.6	0.6	1640
2-Furancarboxaldehyde	2486	13.1	36	816.4	0.6	1661
Cyclohexanone	2545	18.4	–	868.0	3.5	1632
Octanal	2626	10.4	58	981.1	0.8	1634

[a] $I_{(E)\text{-DNPH}}$ at 200°C.
[b] Measured at 70°C.
[c] $I_{(E)\text{-DNPH}} - I$(analogous oxo compound, extrapolated) at 200°C.

(dC), the greater is the difference in the retention indices of the *E*- and *Z*-isomers (Fig. 2). Branching at the carbon atom next to the C = N double bond has the most significant effect on the retention behaviour and formation of the *Z*-isomer (see the great difference in the retention indices of (*E*)- and (*Z*)-2-methylbutanal DNPH; formation of the thermodynamically and kinetically unfavourable (*Z*)-2,2-dimethylpropanal, (*Z*)-2,2-dimethyl-3-butanone [17] and (*Z*)-3-methyl-2-butanone DNPHs was not observed).

In the *Z*-isomers, the larger group R_2 is *cis* to N-(R_3, R_4), so there may be a non-bonded interaction between these groups. This effect was observed for the *NN*-dimethylhydrazones [25] and N-methyl-N-phenylhydrazones [26] but not for the N-methylhydrazones [27] and hydrazones (R_1, R_2 = H) [28]. As a consequence, the aldehyde N,N-dimethyl- and N-methylhydrazones show no detectable isomerization around the C = N double bond [25,26]; they exist in the *E* form.

The predictability of retention indices of DNPHs from physical data is very limited as most of these data are not available but, as the compounds studied differ only in the "oxo part" of the molecules, the retention index of the whole molecule can be characterized:

(a) by the *boiling point* of the analogous

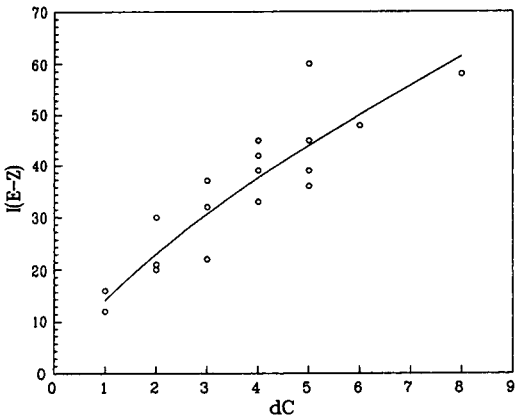

Fig. 2. Correlation between the retention index difference of the (*E*)- and (*Z*)-DNPH isomers and the difference in the carbon numbers of groups R_2 and R_1.

aldehyde or ketone as the generally best descriptor of dispersive forces:

$$I_{(E)\text{-DNPHs}} = (3.51 \pm 0.12)\text{b.p.(oxo)} + (1945 \pm 13)$$
$$n = 27; r = 0.9866; s = 27 \quad (1)$$

where n is the number of data involved in the calculations, r is the correlation coefficient and s is the standard error of estimation;

(b) by *the retention index of the aldehyde or ketone molecule* from which the DNPH was formed:

$$I_{(E)\text{-DNPHs}} = aI_{\text{oxo}} + b \quad (2)$$

where a and b are expected to be constant for a given class of compounds. This additivity rule was observed to hold when the retention indices of amides were correlated with those of the amines from which they were formed [29].

Eq. 1 is expected to hold when new types of interactions are not formed in any of the molecules studied or between some solute and the stationary phase.

The difference between the I values of DNPHs and the analogous oxo compounds is 1625 ± 28 at 200°C (Table 1). Substituting the measured retention indices into Eq. 2 (the I values of oxo compounds were extrapolated to 200°C), we obtain

$$I_{(E)\text{-DNPH}} = (0.91 \pm 0.03)I_{\text{oxo}} + (1688 \pm 22)$$
$$n = 26; r = 0.9864; s = 24 \quad (3)$$

Inspection of the calculated dI values (Table 1) and the deviation of the slope a in Eq. 3 from unity shows that the I_{DNPH} vs. I_{oxo} function has different slopes for the investigated ketones and aldehydes (Fig. 3). The dI value gradually decreases with increasing asymmetry and branching in R_1 and R_2 (e.g. 2-butanone →2-heptanone; pentanal →2,2-dimethylpropanal); a larger effect was observed for the ketone hydrazones.

The slope of Eq. 2 is near unity for aldehydes and their DNPHs:

$$I_{(E)\text{-DNPH}} = (0.97 \pm 0.03)I_{\text{ald}} + (1662 \pm 21)$$
$$n = 13; r = 0.9939; s = 19 \quad (4)$$

whereas for ketones (the behaviour of cyclohexanone DNPH is similar to that of aldehyde DNPHs) the additivity does not seem to hold:

$$I_{(E)\text{-DNPH}} = (0.84 \pm 0.04)I_{\text{ketone}} + (1718 \pm 32)$$
$$n = 12; r = 0.9870; s = 18 \quad (5)$$

We assume that the small anomaly in Eq. 2 (Fig. 3) may be explained by the interactions present in ketone hydrazones, which are not significant in aldehyde hydrazones.

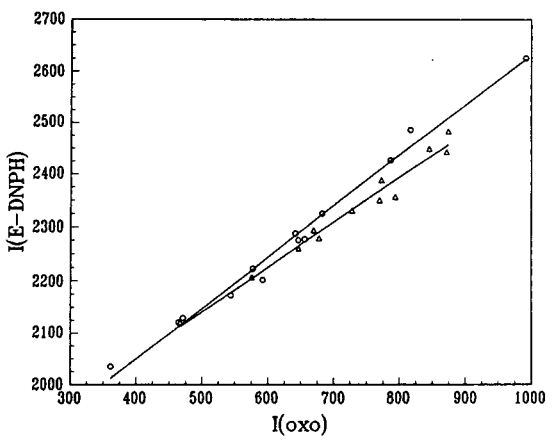

Fig. 3. Dependence of the retention indices of the (*E*)-DNPH (○) and the analogous aldehyde or ketone (△) at 200°C.

Acknowledgement

This work was supported by Grant No. 3064/91 from the Hungarian Science Foundation OTKA.

References

[1] Y. Hoshika and Y. Takata, *J. Chromatogr.*, 120 (1976) 379.
[2] R.R. Linko, H. Kallio and K. Rainio, *J. Chromatogr.*, 155 (1978) 191.
[3] G.A. Rutten, C.W.J. Burtner, H. Visser and J.A. Rijks, *Chromatographia*, 26 (1988) 274.
[4] M. Dalene, P. Persson and G. Skarping, *J. Chromatogr.*, 626 (1992) 284.
[5] R. Otson, P. Fellin, Q. Tran and R. Stoyanoff, *Analyst*, 118 (1993) 1253.
[6] H.R. Van Langenhove, M. VanAcker and N.M. Schamp, *Analyst*, 108 (1983) 329.
[7] J.-O. Levin, K. Anderson, R. Lindahl and C.-A. Nilsson, *Anal. Chem.*, 57 (1985) 1032.
[8] K.L. Olson and S.J. Swarin, *J. Chromatogr.*, 333 (1985) 337.
[9] J. Slemr, *Fresenius' J. Anal. Chem.*, 340 (1991) 672.
[10] C. Dye and M. Ohme, *J. High Resolut. Chromatogr.*, 15 (1992) 5.
[11] J. Rigaudy and S.P. Klesney (Editors), *Nomenclature of Organic Chemistry*, IUPAC Organic Chemistry Division, Pergamon Press, Oxford, 1976, p. 476.
[12] C.F.H. Allen, *J. Am. Chem. Soc.*, 52 (1930) 2955.
[12] C.F.H. Allen, *J. Am. Chem. Soc.*, 52 (1930) 2955.
[13] O.L.J. Brady, *J. Chem. Soc.*, 756 (1931).
[14] L.L. Braddock and M.L. Willard, *J. Org. Chem.*, 18 (1953) 313.
[15] J. Zhang, R.L. Hertzler and E.J. Eisenbraun, *J. Chem. Educ.*, 69 (1992) 1037.
[16] J.B. Pias and L. Gasco, *Chromatographia*, 8 (1975) 270.
[17] V.P. Uralets, J.A. Rijks and P.A. Leclercq, *J. Chromatogr.*, 194 (1980) 135.
[18] F.S. Calixto, A.G. Raso, *Chromatographia*, 15 (1982) 521.
[19] K. Héberger, *Anal. Chim. Acta*, 223 (1989) 161.
[20] N. Bosnjak, Z. Mihalic and N. Trinajstic, *J. Chromatogr.*, 540 (1991) 430.
[21] *Vogel's Textbook of Practical Organic Chemistry*, Longman, Harlow.
[22] M. Görgényi, Z. Fekete and L. Seres, *Chromatographia*, 27 (1989) 581.
[23] R.C. Weast (Editor), *Handbook of Chemistry and Physics*, CRC Press, Boca Raton, FL, 60th ed., 1979.
[24] H. Van Duin, *Ph.D. Thesis*, Free University of Amsterdam, Amsterdam, 1961.
[25] G.J. Karbatsos and R.A. Taller, *Tetrahedron*, 24 (1968) 3923.
[26] G.J. Karabatsos and K.L. Krumel, *Tetrahedron*, 23, (1967) 1097.
[27] G.J. Karbatsos and R.A. Taller, *Tetrahedron*, 24 (1968) 3557.
[28] G.J. Karabatsos and C.E. Osborne, *Tetrahedron*, 24 (1968) 3361.
[29] W. Krawczyk and G.T. Piotrowski, *J. Chromatogr.*, 463 (1989) 297.

PUBLICATION SCHEDULE FOR THE 1995 SUBSCRIPTION

Journal of Chromatography A and *Journal of Chromatography B: Biomedical Applications*

MONTH	1994	J 1995	F 1995	M 1995	
Journal of Chromatography A	Vols. 683–688	689/1 689/2 690/1 690/2	691/1 + 2 692/1 + 2 693/1 693/2	694/1 694/2	The publication schedule for further issues will be published later.
Bibliography Section				713/1	
Journal of Chromatography B: Biomedical Applications		663/1 663/2	664/1 664/2	665/1 665/2	

INFORMATION FOR AUTHORS

(Detailed *Instructions to Authors* were published in *J. Chromatogr. A*, Vol. 657, pp. 463–469. A free reprint can be obtained by application to the publisher, Elsevier Science B.V., P.O. Box 330, 1000 AH Amsterdam, Netherlands.)

Types of Contributions. The following types of papers are published: Regular research papers (full-length papers), Review articles, Short Communications and Discussions. Short Communications are usually descriptions of short investigations, or they can report minor technical improvements of previously published procedures; they reflect the same quality of research as full-length papers, but should preferably not exceed five printed pages. Discussions (one or two pages) should explain, amplify, correct or otherwise comment substantively upon an article recently published in the journal. For Review articles, see inside front cover under Submission of Papers.

Submission. Every paper must be accompanied by a letter from the senior author, stating that he/she is submitting the paper for publication in the *Journal of Chromatography A* or *B*.

Manuscripts. Manuscripts should be typed in **double spacing** on consecutively numbered pages of uniform size. The manuscript should be preceded by a sheet of manuscript paper carrying the title of the paper and the name and full postal address of the person to whom the proofs are to be sent. As a rule, papers should be divided into sections, headed by a caption (*e.g.*, Abstract, Introduction, Experimental, Results, Discussion, etc.). All illustrations, photographs, tables, etc., should be on separate sheets.

Abstract. All articles should have an abstract of 50–100 words which clearly and briefly indicates what is new, different and significant. No references should be given.

Introduction. Every paper must have a concise introduction mentioning what has been done before on the topic described, and stating clearly what is new in the paper now submitted.

Experimental conditions should preferably be given on a *separate* sheet, headed "Conditions". These conditions will, if appropriate, be printed in a block, directly following the heading "Experimental".

Illustrations. The figures should be submitted in a form suitable for reproduction, drawn in Indian ink on drawing or tracing paper. Each illustration should have a caption, all the *captions* being typed (with double spacing) together on a *separate sheet*. If structures are given in the text, the original drawings should be provided. Coloured illustrations are reproduced at the author's expense, the cost being determined by the number of pages and by the number of colours needed. The written permission of the author and publisher must be obtained for the use of any figure already published. Its source must be indicated in the legend.

References. References should be numbered in the order in which they are cited in the text, and listed in numerical sequence on a separate sheet at the end of the article. Please check a recent issue for the layout of the reference list. Abbreviations for the titles of journals should follow the system used by *Chemical Abstracts*. Articles not yet published should be given as "in press" (journal should be specified), "submitted for publication" (journal should be specified), "in preparation" or "personal communication".

Vols. 1–651 of the *Journal of Chromatography*; *Journal of Chromatography, Biomedical Applications* and *Journal of Chromatography, Symposium Volumes* should be cited as *J. Chromatogr.* From Vol. 652 on, *Journal of Chromatography A* (incl. Symposium Volumes) should be cited as *J. Chromatogr. A* and *Journal of Chromatography B: Biomedical Applications* as *J. Chromatogr. B.*

Dispatch. Before sending the manuscript to the Editor please check that the envelope contains four copies of the paper complete with references, captions and figures. One of the sets of figures must be the originals suitable for direct reproduction. Please also ensure that permission to publish has been obtained from your institute.

Proofs. One set of proofs will be sent to the author to be carefully checked for printer's errors. Corrections must be restricted to instances in which the proof is at variance with the manuscript.

Reprints. Fifty reprints will be supplied free of charge. Additional reprints can be ordered by the authors. An order form containing price quotations will be sent to the authors together with the proofs of their article.

New Tel. & Fax Nos. as of March 1, 1995:
Tel: (02421) 969-0; Fax: (02421) 969-199

FOR ADVERTISING INFORMATION PLEASE CONTACT OUR ADVERTISING REPRESENTATIVES

USA/CANADA

Weston Media Associates

Mr. Daniel S. Lipner
P.O. Box 1110, GREENS FARMS, CT 06436-1110
Tel: (203) 261-2500, Fax: (203) 261-0101

GREAT BRITAIN

T.G. Scott & Son Ltd.

Vanessa Bird
Portland House, 21 Narborough Road
COSBY, Leicestershire LE9 5TA
Tel: (0116) 2750.521, Fax: (0116) 2750-522

JAPAN

ES - Tokyo Branch

Ms. Noriko Kodama
20-12 Yushima, 3 chome, Bunkyo-Ku
TOKYO 113
Tel: (03) 3836 0810, Fax: (03) 3839-4344
Telex: 02657617

REST OF WORLD

ELSEVIER SCIENCE

Ms. W. van Cattenburch
Advertising Department
P.O.Box 211, 1000 AE AMSTERDAM
The Netherlands
Tel: (20) 485.3796, Fax: 485.3810